The Dissertation Committee for Robert Leo Fares
certifies that this is the approved version of the following dissertation:

A Framework to Model and Optimize the Operation of Lithium-Ion Energy Storage in Electricity Markets, and an Assessment of Lithium-Ion Energy Storage in Texas

Committee:

Michael E. Webber, Supervisor

Ross Baldick

James Eric Bickel

Dongmei (Maggie) Chen

Thomas F. Edgar

A Framework to Model and Optimize the Operation of Lithium-Ion Energy Storage in Electricity Markets, and an Assessment of Lithium-Ion Energy Storage in Texas

by

Robert Leo Fares, B.S.M.E.; M.S.E.

DISSERTATION

Presented to the Faculty of the Graduate School of

The University of Texas at Austin

in Partial Fulfillment

of the Requirements

for the Degree of

DOCTOR OF PHILOSOPHY

The University of Texas at Austin

August 2015

Acknowledgments

First and foremost, I would like to thank my advisor and research supervisor Dr. Michael E. Webber. He has provided me with an enormous number of opportunities that have helped me to develop as a scholar, a public speaker, an educator, a writer, and a citizen. His commitment to changing the way the world thinks about energy is clear in everything he does, and I can say without a doubt that he has made measurable progress toward that goal. No other person has made me feel more confident in my own ability to make a meaningful impact on the world.

I would also like to thank the other members of my doctoral committee, whose advice and guidance has been an integral part of my development as a scholar. In particular, I would like to thank Dr. Ross Baldick and Dr. Thomas F. Edgar, both of whom provided invaluable guidance and support during my tenure as a graduate student. Additionally, I would like to acknowledge my Masters Thesis advisor Dr. Jeremy P. Meyers, whose guidance helped to establish the foundation for this work.

I would like to give special thanks to my colleagues in the Webber Energy Group. Each of them has provided invaluable professional and personal support to me over the years. In particular, I would like to thank Dr. Chioke B. Harris for his friendship, leadership, and advice. I would also like to thank Dr. Jared B. Garrison, Dr. Kelly Twomey Sanders, and Dr. Ashlynn S. Stillwell for their leadership and guidance.

I owe a great deal of gratitude to the funding agencies whose resources provided me with the academic freedom to accomplish this work. I would like to thank Pecan Street Inc. and the U.S. Department of Energy Smart Grid Demonstration Program

for sponsoring this work. Additionally, I would like to thank Dr. Webber for providing resources that afforded me the privilege to travel nationally and internationally in order to disseminate my research to the academic community and the public.

Finally, I would like to acknowledge my family for their love and support over the years. My partner Stephanie Ruse has been my dogged ally, thoughtful counselor, and best friend throughout my time in graduate school. I cannot thank her enough. I would also like to thank my mother. Her love and kindness have been integral to my development into the man I am today. The more I pass into adulthood, the more I appreciate the immeasurable support she provided to me throughout my life.

A Framework to Model and Optimize the Operation of Lithium-Ion Energy Storage in Electricity Markets, and an Assessment of Lithium-Ion Energy Storage in Texas

Robert Leo Fares, Ph.D.
The University of Texas at Austin, 2015

Supervisor: Michael E. Webber

The lithium-ion (Li-ion) battery has become an established technology in portable electronics and electric vehicle applications. At the same time, there is rising interest in grid-based battery energy storage to improve the flexibility of the electric grid and integrate intermittent sources of renewable energy. To provide information for energy storage developers, battery system operators, state policymakers, and the general public, this research develops a framework to characterize, operate, and evaluate Li-ion battery energy storage that is connected to the electric grid and participates in a wholesale electricity market.

Methods are developed to characterize and model the voltage, temperature, and capacity degradation behavior of a Li-ion battery system. Then, an optimization program is developed to schedule Li-ion storage in an electricity market while modeling and controlling its operating state and rate of capacity loss. The optimization framework is used to simulate operation of Li-ion storage in Texas's Electric Reliability Council of Texas (ERCOT) electricity from 2002–2014, and the market revenue potential and operating lifetime of Li-ion storage are approximated. It is shown that controlling capacity degradation in operational management can extend the lifetime

of Li-ion battery modules by approximately 30–60% without significantly reducing market revenue potential.

To test the reliability impact of distributed Li-ion storage, residential electricity data are used to approximate how long a battery system could isolate downstream electricity customers during an outage. Thousands of outage events are simulated to show the expected islanding duration for outages occurring at different times of day. The potential reliability benefit from avoided residential electric outages is calculated and found to be much smaller than the revenue potential from the electricity market, indicating that market applications should be prioritized over residential reliability applications in siting and operating a battery system.

It is found that the net-present value (NPV) of a Li-ion battery system providing wholesale energy arbitrage in the ERCOT market is negative across a range of cost and benefit parameters. However, controlling capacity degradation in operational management of the battery system is found to increase its value by approximately \$100/kWh of rated energy capacity. The NPV of a battery system providing a combination of energy and Fast Responding Regulation Service (FRRS) is found to be positive across a wide range of cost and benefit parameters, indicating a Li-ion battery system could most likely provide a combination of energy and FRRS service to the ERCOT electricity market at a profit. Controlling capacity degradation in operational management of the battery system for energy and FRRS is found to have little impact on its NPV. However, controlling capacity loss makes the NPV less sensitive to variation in the lifetime of the battery modules, reducing the risks associated with premature battery cell failure.

Table of Contents

List of Tables

List of Figures

Chapter 1

Introduction

In 2010, U.S. electric providers sold over 3.7 trillion kWh of electrical energy, generating nearly $369 billion in revenue [1]. Despite the enormity of the electricity industry, the U.S. electric grid has very little capacity to store electricity. In 2011, the U.S. grid had only 22 GW of electric energy storage capacity, compared with over 1000 GW of generation capacity [1, 2]. Due to the cost, scale, and environmental impact of conventional pumped-hydro energy storage (PHES) [3], the most common form of large-scale storage, it has typically been more economical to produce electricity on demand, generating and then delivering it to the end user in real time. To reliably deliver electricity on demand, generation, transmission, and distribution equipment must have the capacity to serve peak electric load, which only occurs for a small portion of the year. Furthermore, electric generators must set aside reserve capacity for grid ancillary services to ensure electric supply consistently equals demand, even in the case of a contingency. These two aspects of today's electric grid represent a non-trivial component of the cost of electricity. At the same time, concerns about air pollution, sustainability, and anthropogenic climate change have driven an increase in the amount of intermittent renewable energy resources connected to the grid. Because of the grid's on-demand design, more flexible capabilities or resources are required as the penetration of intermittent resources increases [4, 5].

Grid energy storage is an appealing technology because it temporally decouples electricity supply from demand, adding new flexibility to grid operations with

the potential to reduce grid capital expenditures, integrate intermittent renewable energy, and increase electric reliability. For these reasons, recent advances in battery technology have driven renewed interest in grid-based battery energy storage. A leading technology candidate is lithium-ion (Li-ion) batteries, which have become an established technology in portable electronic and electric vehicle applications due to their high energy density and long life. Today, Li-ion batteries are the most commonly used battery energy storage technology on the U.S. grid, comprising 137 of the 259 MW of operational battery energy storage capacity as of April 2015 [6]. The market for grid-based Li-ion batteries is expected to grow significantly over the coming years. Analysts predict approximately 28,000 MW of Li-ion storage will be installed globally between 2014 and 2024, comprising the greatest share (35%) of total new grid energy storage capacity [7]. Li-ion storage is followed by PHES (14%), advanced lead-acid batteries (11%), and compressed-air energy storage (CAES) (10%) [7].

Li-ion batteries are expected to take on a larger role on the electric grid due to a combination of technical, economic, and policy factors. Unlike other emerging grid battery technologies, such as sodium-sulphur (NaS) and redox-flow batteries, Li-ion technology benefits from an established existing market in both consumer electronics and electric vehicle applications [8]. This fact not only gives Li-ion storage a greater present and anticipated production scale, but also shields Li-ion battery manufacturers from risks associated with the emerging grid energy storage market.

At the same time, a number of existing and proposed U.S. policies are expected to increase the market for Li-ion storage over the coming years. In 2013, the California Public Utilities Commission established the first U.S. energy storage capacity mandate, requiring 700 MW of new transmission-level bulk storage capacity and 625 MW of new distributed energy storage capacity by 2024 [9]. Note that the

mandate specifically prohibits PHES over 50 MW to promote emerging storage technologies [9]. Additionally, Consolidated Edison, the regulated utility for New York City, has significantly increased incentives for distributed energy storage and other demand-reducing technologies [10], and New York State is expected to consider additional incentives for energy storage and other distributed energy resources as part of its Reforming the Energy Vision (REV) initiative announced in 2014 [11]. Over the coming years, the state of Texas might also consider new policies to enable wider use of distributed grid energy storage. In November 2014, the regulated investor-owned utility Oncor announced a proposal to install up to 5,000 MW of new distributed energy storage capacity in Texas [12]. The proposal would require a change to Texas electricity policy, which forbids regulated transmission and distribution utilities from owning electricity resources that participate in market.

To provide information for energy storage developers, battery system operators, state policymakers, and the general public, this work develops a framework to characterize, operate, and evaluate Li-ion battery energy storage that is connected to the electric grid and participates in the wholesale electricity market.

A framework is developed to characterize the performance and lifetime of a Li-ion battery, and then optimally operate the battery in an electricity market. Models are selected to describe the battery's current, voltage, state of charge, temperature, and capacity degradation during operation. Then, the models are discretized and implemented within a nonlinear optimization program, which decides how the battery should operate in an electricity market to maximize its value. It is shown that the proposed optimization program can effectively plan the operation of Li-ion storage while dynamically predicting and controlling battery voltage, current, state of charge, temperature, and capacity degradation.

To demonstrate the application of the proposed operational framework, it is applied to the case of Li-ion storage operating in Texas's restructured electricity market, which is administered by the Electric Reliability Council of Texas (ERCOT). Historic price data from 2002–2014 are used to model the operation of Li-ion storage in the ERCOT energy and ancillary services markets. Then, results from this analysis are used to assess the revenue potential of first-entry Li-ion energy storage and test how factors such as end-of-life battery capacity, thermal conditions, and price foresight affect battery revenue and lifetime.

Once the market revenue potential of Li-ion storage has been evaluated, the potential for distributed Li-ion storage to provide backup power to downstream loads during an electric outage is investigated. Residential electricity use and rooftop solar electricity production data collected from an Austin, Texas smart grid test bed are used to assess how long Li-ion storage installed at the electricity distribution transformer could isolate downstream residences after an outage occurring at various times of day and various times of the year. The observed variation in how long Li-ion storage could power downstream customers is shown for different operational scenarios and compared to system reliability metrics reported by U.S. electric utilities.

Following the investigations into the market and reliability benefits of Li-ion storage operating in Texas, the installed cost of Li-ion storage is approximated using a bottom-up cost inventory for Li-ion battery modules and cost estimates for the power conditioning system, siting, and other energy storage system costs. Sensitivity analysis is used to show how various factors affect the cost of Li-ion storage, and then the net-present value (NPV) is approximated from the analysis of market and reliability benefits.

The remainder of this work is organized as follows: Chapter 2 provides relevant

background information on electricity markets, grid energy storage, battery modeling, and operation of energy storage in electricity markets. Chapter 3 introduces a framework to characterize Li-ion storage and optimally schedule its operation in an electricity market. Chapter 4 demonstrates the use of the framework by applying it to Li-ion storage operating in Texas's ERCOT electricity market, and then approximates the revenue potential and lifetime of Li-ion storage under different scenarios. Chapter 5 estimates how long distributed Li-ion storage could provide backup power to downstream customers in areas with and without solar panels available. Chapter 6 approximates the cost and NPV of Li-ion storage under different system cost, operation, and lifetime scenarios. Finally, Chapter 7 draws conclusions about the framework developed in this work and the potential value of Li-ion storage operating in Texas, and then discusses the potential for future research.

Chapter 2

Background

2.1 The Electric Grid and Electricity Markets

Today's electric grid has evolved around the paradigm of large, centrally controlled electricity generation located far away from electric customers. Electricity is typically produced in a central power station and delivered over high voltage transmission lines (electric "highways") and lower voltage distribution lines (electric "roads") to end-use customers. Because storing electric energy has historically been prohibitively expensive, the grid has very little storage capacity, and operates in an energy-on-demand fashion. The amount of electric energy delivered from generators is carefully controlled so that it equals the total amount of electric demand at all times. In practice, this balance is maintained by monitoring and controlling the grid's electrical frequency [13].

Because electric energy is stored in such small quantities, electric generation must be scheduled based on the anticipated and actual level of electric demand, which has traditionally been very inflexible. Traditionally, the process of planning and operating electricity generation has been carried out by vertically integrated electric utilities, which own generation, transmission, and distribution assets, and sell electricity to retail customers [13–15]. On a local basis, these utilities are often treated as "natural monopolies," with exclusive access to customers and electricity rates regulated on a cost-of-service basis [13–15]. Under the vertically-integrated scheme, each utility carries out its own internal power plant scheduling process to

minimize their overall costs while also maintaining sufficient electric reliability for their customers [13].

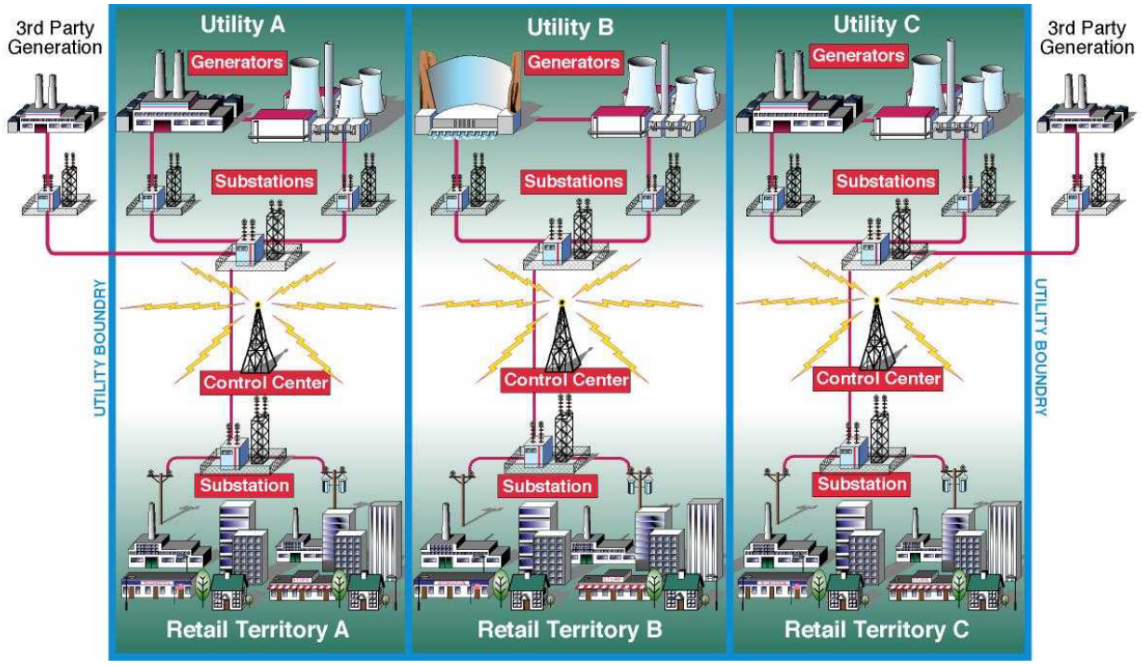

Figure 2.1: In the past, electricity generation, transmission, and distribution were wholly owned and operated by vertically-integrated electric utilities, which were often regulated as local monopolies [13, 14]. Figure from [13].

In recent years, there has been a shift away from the vertically-integrated scheme toward an unbundled scheme, which separates electricity generation, transmission/distribution, and retail industries into separate companies [13, 14]. Typically, transmission and distribution companies remain regulated monopolies, while electricity generation companies become competitive. Electricity retail companies are either regulated or competitive, depending on local regulations [14]. For transmission and distribution companies, an electric delivery rate is established on a cost-recovery basis and charged to all electricity customers in the system. In turn, the transmission and distribution company is typically obligated to provide electricity generation compa-

nies an equal level of access to the portion of the grid they operate [13, 14].

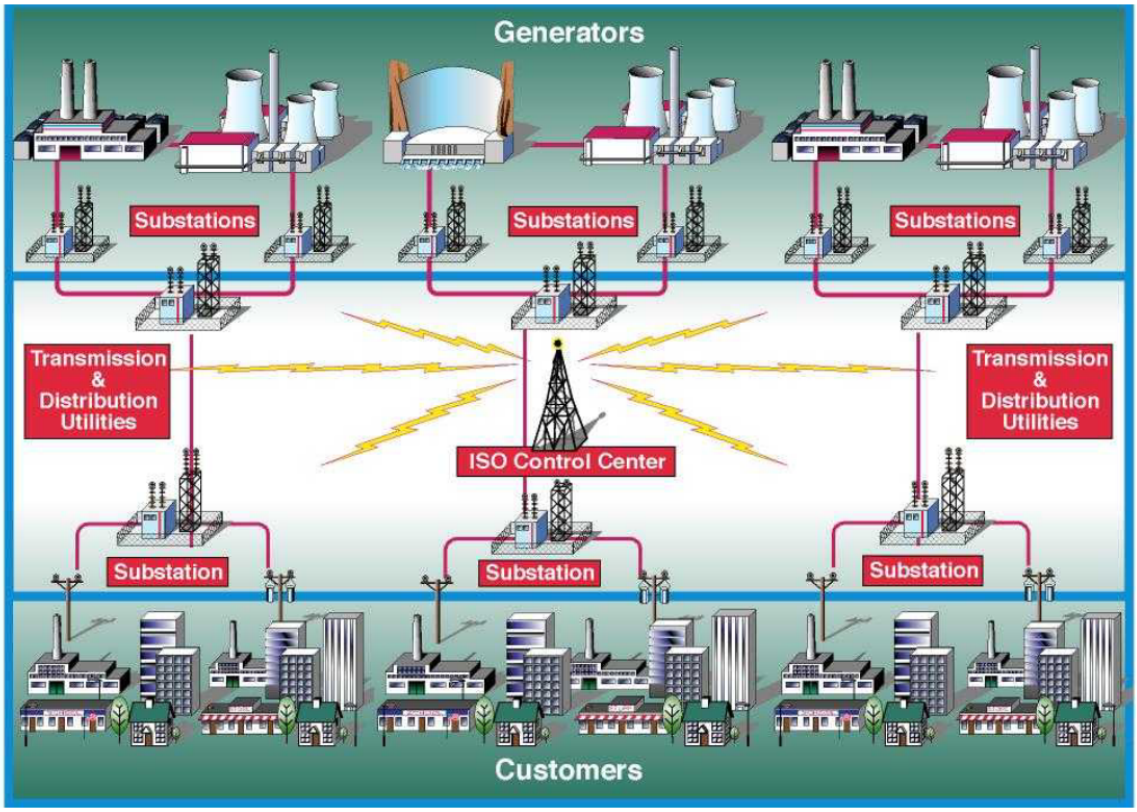

Figure 2.2: In an unbundled electricity system, generation, transmission/distribution, and retail industries are separated into different companies. An entity called the independent system operator (ISO) schedules electricity generation and operates the transmission system to minimize overall costs while maintaining reliability [13]. Figure from [13].

In an unbundled system, the function of operating the transmission system and scheduling electricity generation to maintain reliability and minimize cost is typically assigned to an entity called the independent system operator (ISO). The ISO also manages the electricity market, which is used to procure electricity generation from independent power producers. Each day, electricity resources submit information about their production costs to the ISO, and then the ISO executes an "economic dispatch" program to minimize overall electricity costs while maintaining electric

reliability [13, 16–19]. By doing so, the ISO clears the market and establishes an electricity price, which is equal to the marginal cost of providing an additional unit of generation at a particular time and place on the grid [17–19]. Fluctuations in electric demand over the day and the year can cause the price of electricity to vary significantly from one hour to the next. Furthermore, constraints in the transmission grid can cause the price of electricity to vary from one location to another.

To date, ISO's and competitive electricity markets have expanded to cover much of the continental United States, and a significant portion of total U.S. electric load. ISO's currently operate electricity markets in California, Texas, and much of the Midwest and Northeast. On the other hand, the Northwest and Southeast have not fully transitioned toward an ISO-organized central electricity market and open transmission network [13]. Rather, wholesale electricity generation transactions are accomplished through bilateral trades, and the transmission network is largely owned by vertically-integrated utilities [13]. However, Federal Energy Regulatory Commission (FERC)'s Open Access Transmission Tariff rule requires utilities to provide open third-party access to their transmission networks [13].

An advantage of competitive electricity markets is that they provide price transparency for both wholesale electric energy and ancillary services [17–19]. Wholesale electric energy is bulk electric power produced to meet electric demand, while ancillary services are load-following and reserve capabilities provided by power plants to maintain adequate voltage and frequency throughout the grid system at all times [13]. This aspect of electricity markets provides greater competition and access for alternative electricity technologies and strategies that might not have been preferred under a vertically-integrated scheme, such as demand response (incentivizing customers to reduce their electric demand) and energy storage. As the subject of this work is

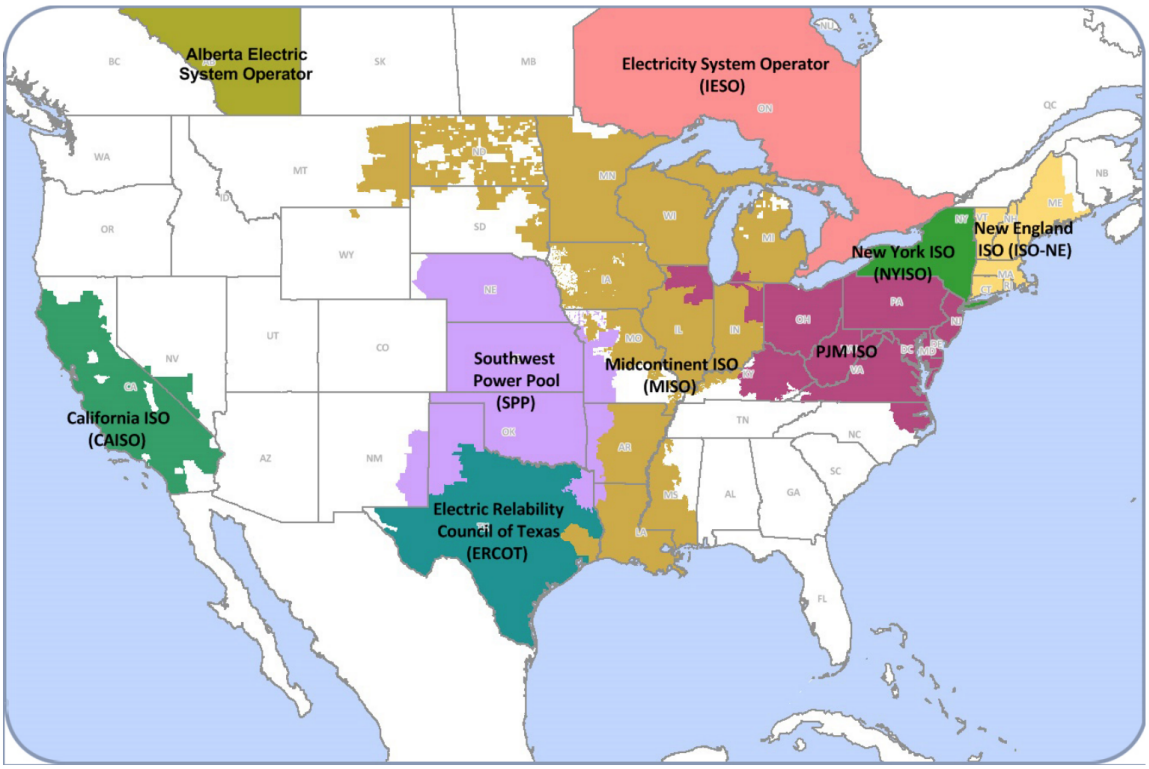

Figure 2.3: To date, ISO-organized electricity markets have expanded to cover much of the continental United States, and a significant portion of total U.S. electric load. Figure from [20].

the characterization, operation, and assessment of grid-connected lithium-ion (Li-ion) battery storage, the following sections will introduce grid energy storage technologies, and then applications both within and outside the electricity market.

2.2 Grid Energy Storage Technologies

A number of technologies exist with the capability to store electric energy in bulk quantities. These technologies have been reviewed and compared extensively in the literature [21–33]. Thus, rather than present a detailed discussion of established and emerging energy storage technologies, this section will broadly compare technologies and identify to what extent various technologies are in use today.

Grid energy storage technologies can be broadly divided into three categories: mechanical, electrical, and electrochemical storage. Mechanical energy storage uses a motor/generator to store electricity in the form of potential or kinetic mechanical energy. Existing forms of mechanical grid energy storage include pumped-hydro energy storage (PHES), compressed-air energy storage (CAES), and flywheel energy storage [21–26]. PHES and CAES are typically used for bulk energy shifting, while flywheels are used to provide rotational inertia to the grid [22, 25].

Pure electric energy storage stores energy in the potential created by electric charge separation. To achieve the energy and power density required for grid applications, charge separation is typically carried out in a supercapacitor, which uses materials with a high volumetric surface area and an electrochemical or electrostatic double layer to achieve a greater power and energy density than traditional capacitors [22,24,25]. In general, supercapacitors are used in high-power applications, where long-duration energy storage is less important than on-demand power generation or storage [22, 24, 25].

Electrochemical or battery energy storage stores energy in the electrochemical potential difference that exists between two materials, which make up the negative (anode) and positive (cathode) sides of the battery. During charge and discharge, the materials undergo reversible electrochemical reactions to produce or consume electrons, which flow between the negative and positive sides of the battery through an external circuit. A wide variety of battery technologies exist, ranging from high-power batteries with characteristics resembling those of a supercapacitor to liquid-based redox-flow batteries with characteristics more closely resembling PHES and other bulk energy storage technologies [21, 24, 29, 30].

Figure 2.4 compares common energy storage technologies according to their

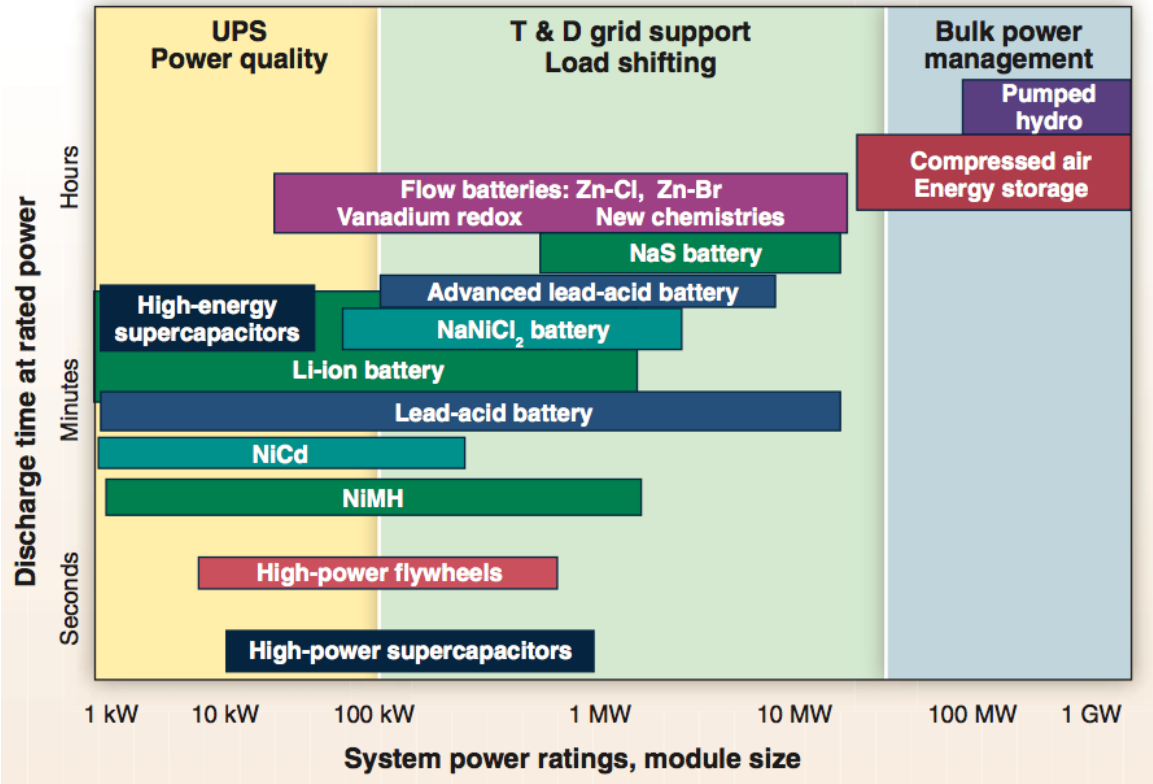

Figure 2.4: This figure compares various energy storage technologies based on their typical power and energy ratings, and candidate grid applications. Note that the ranges shown are only for typical systems, and do not represent strict technical limits on either energy or power capacity [27]. Figure from [27].

typical power capacity and energy capacity ratings. Regions are identified corresponding to different grid services that each technology could provide. Large-scale PHES and CAES systems typically have a power rating greater than 100 MW, and provide bulk management of electric power over long time scales [23, 27]. Battery technologies are the most flexible, with a typical power rating ranging from 1 kW to greater than 10 MW [27]. Thus, they can provide applications ranging from short-term power quality management to longer-term diurnal load shifting. Flywheels and supercapacitors can provide 1 kW to 1 MW of power for a period ranging from a few seconds to minutes [27]. Thus, they are typically used to mitigate frequency

and voltage fluctuations in the transmission system, or provide short-term backup power [23, 25, 27].

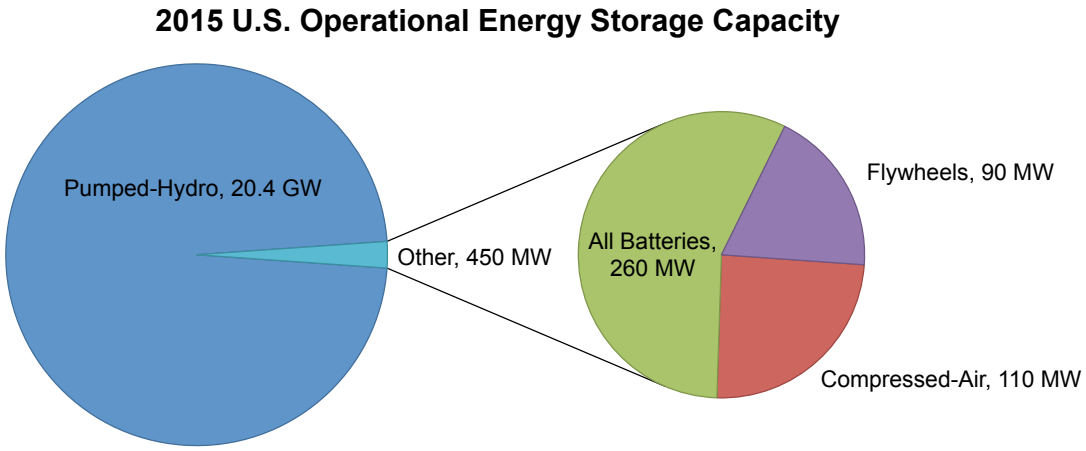

Figure 2.5: Today, PHES comprises the vast majority of operational U.S. grid energy storage capacity. Non-PHES capacity is divided amongst battery, compressed-air, and flywheel energy storage [6].

Figure 2.5 shows the technology share of operational U.S. energy storage capacity reported in the U.S. Department of Energy Global Energy Storage Database as of April 2015 [6]. PHES comprises the vast majority of existing U.S. grid energy storage capacity, with a cumulative installed capacity greater than 20 GW. Despite the fact that grid energy storage is not widely used today, PHES has been used on the U.S. grid for nearly a century, with the first plant commencing operation in 1930 [34]. The majority of additional PHES capacity was installed between the years of 1960 and 1990 [35]. Since then, no new U.S. PHES facilities have been constructed, mostly due to market uncertainty and environmental concerns [35].

In recent years, battery energy storage has seen increasing use on the electric grid, in part due to its advantages over PHES when it comes to siting, ecological impact, and modular scale. Between 2011 and 2015, installed U.S. battery energy

storage capacity nearly doubled from 136 MW to 259 MW [6, 36]. Figure 2.6 shows the technology share of operational U.S. battery energy storage capacity in 2015.

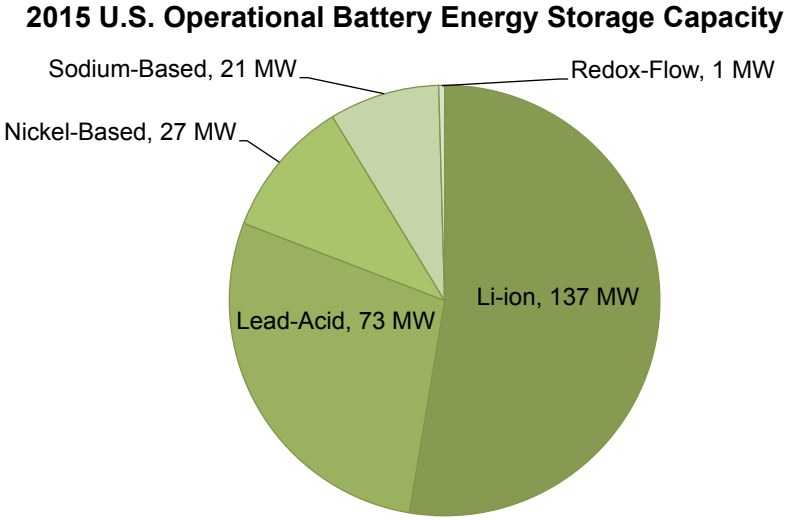

Figure 2.6: Today, Li-ion and lead-acid technologies comprise the vast majority of installed U.S. battery energy storage capacity, in part due to their greater technological maturity versus other emerging battery technologies [6].

Between 2011 and 2015, installed Li-ion capacity increased from 54 MW to 137 MW. Today, it comprises the majority of U.S. battery energy storage capacity, and is expected to increase significantly in the coming years [7,8,37]. This fact can be attributed to, 1) Li-ion's greater technological maturity versus redox-flow and other emerging grid battery technologies, 2) increasing production scale of Li-ion battery cells for consumer electronics and electric vehicles, 3) Li-ion's high efficiency, small footprint, and long lifetime, and 4) a number of existing and proposed policies meant to promote adoption of distributed grid energy storage [7–9, 11, 12, 27, 37, 38]. As Li-ion battery technology advances, the cost of Li-ion battery packs is expected to converge to approximately $230 per kWh of energy capacity by 2017–2018 [39].

The remainder of this work is devoted to characterization, operational man-

agement, and economic assessment of Li-ion storage used on the electric grid. The following section introduces applications for grid energy storage.

2.3 Grid Energy Storage Applications

All applications for grid energy storage stem from the fact that it can shift electric energy in time, and mitigate costs associated with producing or delivering energy on demand. These costs stem from a wide range of factors including: capital costs of required peaking generation, additional fuel costs for peaking generation relative to baseload generation, the cost of ancillary services to maintain adequate power system control, the capital cost of sufficient transmission and distribution infrastructure to serve peak electric demand, costs incurred by over or under predicting electric demand, and a number of other costs [21, 25, 40–42].

Table 2.1 provides a summary of typical grid energy storage applications. Applications are divided into electricity supply, transmission/distribution, and customer applications, mirroring the separation that exists in an unbundled utility market, as discussed in Section 2.1. In an unbundled context, electricity supply applications would be provided to an ISO-organized electricity market in exchange for payment, transmission and distribution applications would be provided to reduce electric delivery costs, and customer applications would be provided to reduce monthly utility bills.

One aspect of energy storage that differentiates it from conventional electricity generation technologies is that its value is wholly realized from storing and then discharging electric energy to mitigate external costs; i.e. energy storage does not produce any electric energy or other commodities itself. Thus, the value of grid energy storage is highly dependent on the conditions in the wider electric grid and

Table 2.1: Grid energy storage has applications ranging from bulk electricity supply to customer-side services. This table identifies and briefly describes common applications, and distinguishes them based on the division of electricity generation from transmission/distribution and retail sales in an unbundled electricity market context [21, 25, 40–42]

Application	Description
Category 1: Electricity Supply	Electric generation applications
Wholesale energy arbitrage	Store off-peak energy for sale during peak hours
Frequency regulation service	Balance electricity supply and demand to maintain a grid frequency of 60 Hz AC
Reserve capacity	Provide reserve power capability in case of an unexpected generation shortfall
Category 2: Transmission and Distribution	Electric delivery applications
Transmission voltage support	Provide active or reactive power to regulate transmission system voltage
Transmission congestion support	Mitigate transmission congestion to reduce congestion costs or defer new transmission investments
Distribution voltage support	Provide active or reactive power to regulate distribution system voltage
Electric reliability	Provide backup power to withstand a temporary distribution-system outage
Category 3: Electricity Customer	Utility retail customer applications
Time-of-use utility tariff management	Store off-peak energy for use during peak hours to avoid on-peak utility charges
Demand charge management	Reduce monthly peak electric demand to reduce utility demand charges
Power quality	Provide active or reactive power to ensure the quality of incoming grid power
Electric reliability	Provide backup power to the customer to withstand a temporary outage

market, and the profit maximization problem is considerably more difficult for a grid energy storage device than it is for a conventional power plant.

A number of researchers have sought to analyze the value of electricity storage in the context of restructured electricity markets. Early studies use simple assumptions about energy storage system performance, operating revenue, and cost to assess the value of electricity storage in a restructured electricity market from a largely qualitative perspective [42–44]. More recent studies utilize multiple years of dynamic electricity price data that have become available since restructured electricity markets opened to quantitatively assess the value of electricity storage [21, 40, 41, 45–55]. Typically, studies focus on assessing the techo-economic performance of one specific technology in a given market and system context using optimization and other techniques to reveal how energy storage could respond to external price signals.

A principle limitation of existing studies is that they typically assume a storage device has a constant roundtrip efficiency, energy capacity, and power capability, regardless of its instantaneous operating state or current state of capacity degradation. This assumption not only affects the overall economic assessment of a given energy storage device, but also makes it difficult to realize an economic operational strategy for a deployed grid battery system, which has performance characteristics that might differ significantly from those assumed.

To connect operational management and economic assessment of grid energy storage with real-time battery control, this work develops a framework to characterize and then manage the operation of Li-ion storage in restructured electricity markets. To do so, models are implemented to describe the dynamic performance and degradation of Li-ion battery storage in an optimization context. The following section reviews methods to model battery energy storage.

2.4 Battery Modeling

Researchers have developed a number of models to describe a battery. These models can be broadly classified into two major categories: first-principles electrochemical models and empirical behavioral models.

First-principles models use physical equations to describe the transport and reaction of active species inside a battery. Chemical and electrical equations are used to describe conservation of mass, conservation of charge, charge-transfer reaction kinetics, diffusion speed, and other fundamental physical mechanisms that affect the observed voltage and current behavior at a battery's terminals [56–61]. In the same way, electrochemical models can describe physical processes such as Li-ion battery solid electrolyte interphase (SEI) layer growth, which causes the amount of usable capacity available to fade [62–65]. While electrochemical models have the advantage of describing fundamental physical mechanisms, they are computationally intensive, typically requiring the battery cell geometry to be divided into finite elements so that conservation equations can be applied to approximate the concentration of active species at locations throughout the cell [56–61].

Empirical behavioral models use mathematical equations or physical analogs (e.g. electric circuits) to describe the system-level characteristics of a battery, such as capacity, efficiency and voltage. Peukert's law, which describes the relationship between rate of discharge and discharge capacity, is one of the earliest empirical models [66, 67]. Other models describe a battery's non-linear capacity/recovery effects [68–71], or energy efficiency [72]. Many empirical models use an electric circuit analog to describe the system-level behavior of a battery using a combination of variable voltage sources, resistors, and capacitors. A number of these models have been developed in the literature including Thévenin equivalent circuit models [73–75],

impedance-based models [76–78], and runtime-based models [79,80]. More recent electric circuit analog models combine the benefits of many of these models to empirically describe a number of complex battery characteristics [81, 82].

Empirical models are advantageous for real-time battery control because they can be designed to describe complex battery characteristics without significant computational complexity. In particular, electric circuit analog models have proven to be a flexible tool for empirically describing battery performance under diverse operating conditions, including temperature, state of charge, and charge-discharge rate [81–86]. These models describe a battery's open circuit voltage using a variable potential source, and then use a combination of series resistors and parallel resistor-capacitor couples to describe a battery's ohmic potential drop and dynamic voltage behavior at various time scales. Numerous studies have developed methods to experimentally extract the electrical parameters required to describe a battery's dynamic state using these models [81, 85–88].

At the same time, an inherent limitation of empirical models is that they require battery performance data collected at various current rates, temperatures, and states of charge to accurately describe a battery under diverse operating conditions [81,85,86]. Because battery manufacturers typically do not share extended performance data, battery performance must be measured under a variety of conditions to extract parameters for an empirical battery model. Once the model parameters have been established, empirical battery models provide a computationally lean and reasonably accurate way to describe battery performance within a real-time control or optimization framework.

The following chapters describe the development of a new framework to characterize, model, optimally schedule, and assess grid-connected Li-ion energy storage.

This framework modifies existing empirical battery models and then combines them with optimization to encapsulate a prediction of dynamic battery performance and degradation within a dynamic decision-making framework, so that energy storage participation in electricity markets can be optimally scheduled to not only maximize revenue, but also minimize capacity degradation during operation.

Chapter 3

A Framework to Characterize Lithium-Ion Storage and Schedule Its Operation in Electricity Markets[1]

It is not obvious how lithium-ion (Li-ion) energy storage should operate in an electricity market for primarily two reasons. First, because energy storage charges and discharges with electric energy only, its revenue potential is closely linked to the magnitude and volatility of the external price of electricity. This situation is distinct from the case of a conventional power plant that converts a fuel stock to electricity, because there is typically a consistent price difference between the cost of fuel (e.g. coal or natural gas) and the price of electric energy sold to the market. To generate revenue from the sale of electric energy, a grid battery operator must decide when their battery should charge and discharge to maximize the price difference between energy used for charging and energy sold to the market during discharging. The second reason it is not obvious how Li-ion storage should operate in electricity markets relates to the processes that are used to store energy. As a Li-ion battery operates, its materials undergo irreversible processes that cause the effective energy capacity of the battery to fade over time. The rate at which this capacity degradation occurs impacts the lifetime and total revenue of a battery energy storage system. Thus, a battery system operator would benefit from considering the relationship between battery cycling and capacity degradation in their operational decisions.

[1]Portions of this chapter were previously published in: Fares, R. L., and Webber, M. E. (2014). A flexible model for economic operational management of grid battery energy storage. *Energy*, 78, 768-776. Michael E. Webber contributed to the work as the research supervisor.

The goals of the work presented in this chapter are to 1) model a Li-ion battery's dynamic state during operation, 2) predict the impact that operation has on the rate of capacity loss, and 3) incorporate this information into the decision of how much capacity to offer to the electricity market for both energy and ancillary services using an optimization framework. The remainder of this chapter is organized as follows: Section 3.1 implements an electrochemical model of Li-ion storage to describe its performance and degradation, and then develops control-oriented empirical models suitable for describing battery state variables and capacity loss within a dynamic optimization framework. Section 3.2 introduces a nonlinear optimization program to schedule the participation of Li-ion storage in an independent system operator (ISO)-organized electricity market using information from the models. Section 3.3 summarizes this chapter and its key findings.

3.1 Lithium-Ion Battery Characterization and Modeling

Li-ion battery technologies encompass a wide variety of chemistries and formats, which can have significantly different voltage behavior, rate capabilities, thermal properties, and capacity degradation [37, 38, 89, 90]. Even Li-ion batteries using the same material in their anode and cathode but different electrolytes have been shown to exhibit varying capacity degradation behavior [90]. Thus, it is difficult to generalize performance and degradation for the entire family of Li-ion batteries, or even a particular Li-ion chemistry, because slight differences in design and chemistry that might only be known to the battery cell manufacturer can produce a large variation in observed system-level performance and degradation.

Therefore, the goal of this section is not to generalize the performance and degradation of all Li-ion batteries or even a particular Li-ion chemistry. Rather, this

section introduces a framework that a Li-ion battery system manufacturer or operator could use to experimentally characterize a particular battery system, and then extract empirical model parameters to describe dynamic voltage behavior, thermal properties, and capacity degradation within an optimization program to schedule the battery in an electricity market. This method would help operators with charge-discharge decisions in a competitive electricity market.

To illustrate the use of this empirical modeling framework, this work considers the case of Li-ion storage, which uses electric-vehicle type Li-ion battery cells with an $LiNi_{1/3}Mn_{1/3}Co_{1/3}O_2$ (NMC) cathode and a graphite anode. This type of system is selected for analysis because of the rapidly falling cost of electric-vehicle Li-ion batteries [39], and the fact that a Texas regulated transmission and distribution utility has proposed installing up to 5,000 MW of distributed battery storage [12].

To characterize the battery system, data are generated from a commercial electrochemical Li-ion battery model [62,91]. Electrochemical model data are used in lieu of experimental data because data about battery performance and degradation under diverse operating conditions can be generated much more quickly from an electrochemical model than could be obtained via experiment, allowing for tests of a wide range of operating conditions.

Section 3.1.1 provides specifications for the type of battery system considered, and then discusses the electrochemical model that is used to approximate its behavior. Sections 3.1.2–3.1.4 introduce control-oriented models to describe battery voltage, temperature, and capacity degradation, respectively.

3.1.1 Battery Specifications

A distributed Li-ion energy storage system similar to systems proposed by Electric Power Research Institute (EPRI), American Electric Power (AEP), and others is considered [12, 21, 92, 93]. Figure 3.1 shows a schematic of a system resembling the one considered in this work. The system uses Li-ion battery modules to store energy. The power conditioning system (PCS) converts the DC power from the battery packs to AC power with a voltage and frequency acceptable for the electric grid.

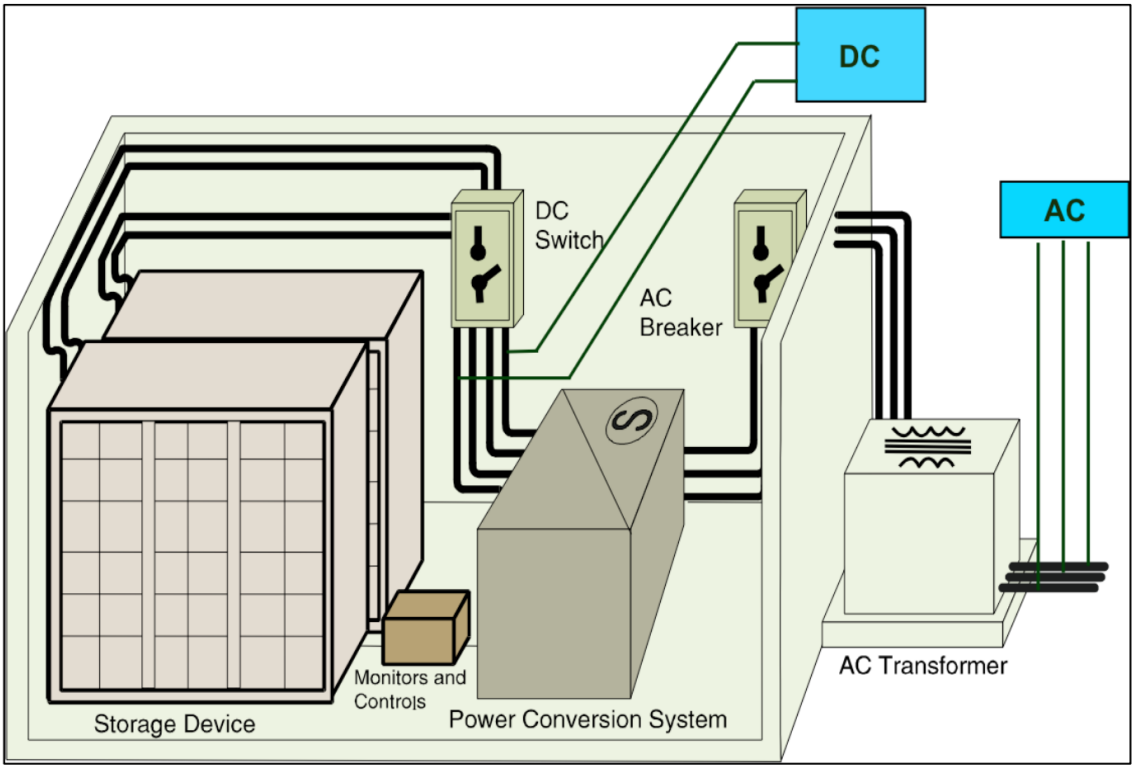

Figure 3.1: The system considered in this work uses Li-ion battery modules to store energy. The battery modules are contained in the storage device illustrated above, and the PCS equipment converts the DC power from the battery packs to AC power with a voltage and frequency acceptable for the electric grid.

The electrochemical behavior of the system considered depends on the chemistry and geometry of its Li-ion battery cells. Information about the chemistry and

geometry of the battery cells is collected from parameters provided by the U.S. Department of Energy [94–96], and specifications provided by General Motors in the literature [97, 98]. Table 3.1 provides specifications for the Li-ion battery cells considered, which represent those of a hypothetical generic NMC Li-ion cell.

To form a system with sufficient voltage, power, and energy capacity, a number of Li-ion battery cells are combined to form a battery pack. Figure 3.2 illustrates how cells are assembled to form a module, and how modules are interconnected and cooled within the battery pack.

A hypothetical 30 kWh Li-ion battery pack is considered. Larger battery systems could be constructed by connecting more than one battery pack in series or parallel. The specifications for the battery pack are approximated based on information provided by the U.S. Department of Energy and General Motors [94–98], and are given in Table 3.2. Note that the design power is designated based on the minimum battery pack power corresponding to a charge/discharge rate limit of 1 C or 15 A per cell. The maximum power capability of the battery pack is greater than the design power, because energy capacity is the determining design factor for the selected battery chemistry [94, 95]. However, the maximum power level could only be achieved for a period of 10 seconds or less without damaging the battery cell or imposing a greater safety risk [94, 95]. Thus, a charge/discharge limit of 1 C (15 A per cell) is selected for the battery pack.

To characterize the battery pack, the parameters given in Tables 3.1 and 3.2 are entered into AutoLion-ST, a thermally-coupled electrochemical Li-ion battery model capable of describing dynamic battery performance and degradation [62,64,91]. The software uses specifications of a battery pack's geometry, configuration, and cell chemistry with electrochemical parameters collected from experimental tests of over

Table 3.1: Specifications for a hypothetical generic $LiNi_{1/3}Mn_{1/3}Co_{1/3}O_2$ (NMC) Li-ion battery cell are developed based on information in the literature [94–98].

Parameter	Value
Cell Specifications	
Cell format	Stacked electrode prismatic pouch
Cell width	79 mm
Cell height	260 mm
Cell thickness	6.5 mm
Cell mass	268 g
Cell capacity	15 Ah
Positive Electrode Specifications	
Current collector material	Aluminum
Current collector thickness	20 μm
Active material	NMC
Conductive agent	Carbon
Binder	polyvinylidene difluoride (PVdF)
Electrode loading	3.8 mAh/cm^2
Electrode thickness	208 μm
Electrode porosity	0.32
Number of electrode layers	12
Negative Electrode Specifications	
Current collector material	Copper
Current collector thickness	12 μm
Active material	Graphite
Binder	PVdF
Electrode loading	5.1 mAh/cm^2
Electrode thickness	212 μm
Electrode porosity	0.34
Number of electrode layers	13
Electrolyte and Seaparator Specifications	
Separator type	Celgard microporous membrane
Separator thickness	20 μm
Electrolyte salt	Lithium hexafluorophosphate ($LiPF_6$)
Electrolyte solvent	EC-EMC-DMC
Electrolyte concentration	1.2 mol/L

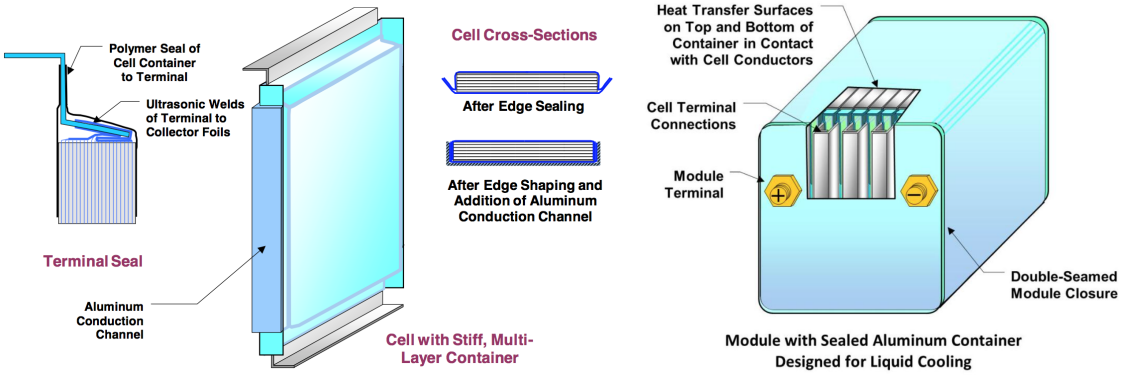

(a) Prismatic Li-ion Cell

(b) Module Consisting of Several Cells

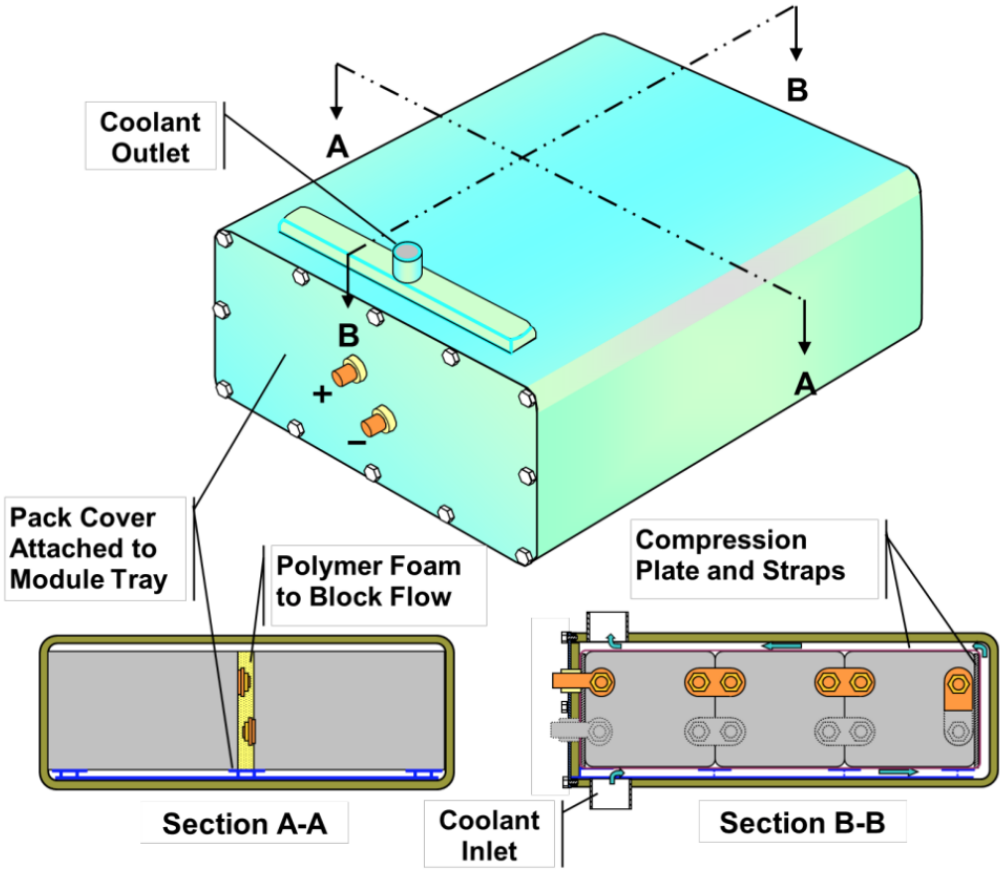

(c) Pack Consisting of Several Modules and Coolant Channels

Figure 3.2: A typical Li-ion battery pack consists of a number of interconnected battery modules, which themselves contain a number of interconnected battery cells. Coolant flows across the surface of the battery modules to regulate the battery's internal temperature. Figures from [94].

Table 3.2: Specifications for the battery pack are approximated based on parameters provided by the U.S. Department of Energy and General Motors [94–98].

Parameter	Value
Battery Pack Parameters	
Rated energy capacity	30 kWh
Maximum power capability (10-second pulse)	110 kW
Design power	25 kW
Mass	230 kg
Number of modules in series	8
Battery Module Parameters	
Number of cells per parallel group	3
Number of parallel groups in series	24
Total number of cells per module	72

100,000 coin cells operating at temperatures ranging from -30 to 60 °C to create a model of the battery that can be used to characterize its dynamic voltage behavior and capacity degradation [62, 64, 91]. The model uses Equations 3.1–3.6 to describe the reaction kinetics, charge transfer, species transport, and heat transfer inside a Li-ion battery [61,62,99]. The nomenclature for these equations is given in Table 3.3. Equations 3.1 and 3.2 represent conservation of charge in the solid phase and electrolyte phase, respectively. Similarly, Equations 3.3 and 3.4 represent conservation of species in the solid phase and electrolyte phase, respectively. Equation 3.5 represents the kinetics of the electrochemical reaction at the electrode surface. Finally, Equation 3.6 represents conservation of energy and heat transfer inside the battery.

$$\nabla \cdot (\sigma^{eff} \nabla \phi_s) = j^{Li} \tag{3.1}$$

$$\nabla \cdot (\kappa^{eff} \nabla \phi_e) + \nabla \cdot (\kappa_D^{eff} \nabla \ln c_e) = -j^{Li} \tag{3.2}$$

$$\text{where: } \kappa_D^{eff} = \frac{2RT\kappa_{eff}}{F}(t_+^0 - 1)\left(1 + \frac{d\ln f_\pm}{d\ln c_e}\right)$$

$$\frac{\partial c_s}{\partial t} = \frac{D_s}{r^2}\frac{\partial}{\partial r}\left(r^2\frac{\partial c_s}{\partial r}\right) \tag{3.3}$$

$$\frac{\partial(\varepsilon_e c_e)}{\partial t} = \nabla\cdot(D_e^{eff}\nabla c_e) + \frac{1-t_0^+}{F}j^{Li} \tag{3.4}$$

$$j^{Li} = a_s i_o\left\{\exp\left[\frac{\alpha_a F}{RT}\left(\eta - \frac{R_{SEI}}{a_s}j^{Li}\right)\right] - \exp\left[-\frac{\alpha_c F}{RT}\left(\eta - \frac{R_{SEI}}{a_s}j^{Li}\right)\right]\right\} \tag{3.5}$$

$$\frac{\partial(\rho c_p T)}{\partial t} = \nabla\cdot(k\nabla T) + q_r + q_j \tag{3.6}$$

$$\text{where: } q_r = j^{Li}\left(\phi_s - \phi_e - U_j + T\frac{\partial U_j}{\partial T}\right)$$

$$q_j = \sigma^{eff}\nabla\phi_s\nabla\phi_s + k^{eff}\nabla\phi_e\phi_e + k_D^{eff}\nabla\ln c_e\nabla\phi_e$$

To build an electrochemical model of the battery pack considered, the specifications for the battery cells and the battery pack given in Tables 3.1–3.2 are entered into the AutoLion-ST software. The resulting representation of the battery pack is used in Matlab/Simulink to simulate operation of the battery pack and experimentally characterize its dynamic voltage behavior and capacity degradation under different operating conditions, so that empirical models can be developed to describe these mechanisms within an optimization framework. Details about how a battery pack model is implemented in AutoLion-ST are available in the user manual [91]. The following sections present empirical models to describe the battery system, and demonstrate how model parameters could be extracted from experimental or simulated characterization tests.

Table 3.3: The nomenclature used in Equations 3.1–3.6 are defined as follows.

Symbol	Definition	Units
c_e	concentration of the electrolyte	mol/cm^3
c_s	surface concentration in spherical particle	mol/cm^3
c_p	specific heat	J/kg-K
D	diffusion coefficient	cm^2/s
$f_\pm$	electrolyte mean molar activity coefficient	
F	Faraday's constant	C/eq.
j^{Li}	current density	A/cm^2
k	thermal conductivity	W/cm-K
q	volumetric heat generation rate	W/cm^3
t_+^0	transference number of lithium ion	
T	temperature	K
U_j	equilibrium potential	V
r	radial coordinate along active material particle	cm
R	universal gas constant	J/mol-K
ε	volume fraction of a phase	
κ^{eff}	effective solution conductivity	Ω^{-1}cm^{-1}
ρ	lumped density	kg/cm^3
σ^{eff}	effective electrode conductivity	Ω^{-1}cm^{-1}

3.1.2 Voltage Model

A major objective of battery modeling is to describe the relationship between the current that is applied to a battery and the voltage that is observed at its terminals. In general, the voltage is nonlinear and hysteretic, i.e. it depends on the instantaneous current that is applied to the battery and the current that was applied in the past. The observed terminal voltage corresponds to the electrochemical potential of the battery's internal charge-transfer reactions, which behave dynamically due to reaction kinetics and mass transport [56, 100]. In a Li-ion battery, the operating voltage of a battery cell is typically constrained between 4.2 V (fully charged), and 2.75 V (fully discharged). Any operation outside this range might produce reactions

that damage the battery cell and introduce a greater safety risk [100].

To approximate the relationship between a battery's current, voltage, and state of charge, a dynamic electrical circuit model is used [81, 85, 86]. The model describes the state of a battery using two coupled electrical circuits, as shown in Figure 3.3. The "state of charge circuit" on the left-hand side of Figure 3.3 approximates a battery's state of charge based on the current input, I. The capacitor C_{c} integrates the charge flowing into and out of the battery to approximate state of charge. The circuit components combine to produce a voltage at node V_{SOC} corresponding to the battery's state of charge. The "voltage-current characteristics circuit" on the right-hand side of Figure 3.3 estimates the behavior of a battery's terminal voltage, V, based on the current input, I, and state of charge (V_{SOC} from the battery lifetime circuit). The variable potential source $V_{\mathrm{OC}}(V_{\mathrm{SOC}})$ models how open-circuit voltage changes with state of charge, and the series resistor R_s and two parallel RC networks consisting of $R_{t,s}$, $C_{t,s}$, $R_{t,\ell}$, and $C_{t,\ell}$ model how the battery's terminal voltage dynamically changes under a variable applied current, I, due to the ohmic potential drop and short- and long-term transient reaction dynamics inside the battery. Each of these circuit components has parameters defined by a variable function determined from experimental performance data [81, 85, 86].

Researchers have extracted the parameters required to describe the performance of a number of different batteries using this model. Chen and Rincón-Mora extracted the model parameters for both Li-ion and nickel-metal hydride (Ni-MH) battery cells under various discharge rates [81]. To model the performance of a larger battery system, Li, et al. extracted the model parameters for an Ultralife UBBL10 Li-ion module (consisting of several battery cells) under various discharge rates [85, 86]. To model the effect of temperature on performance, Bauer and Kelder fit the model

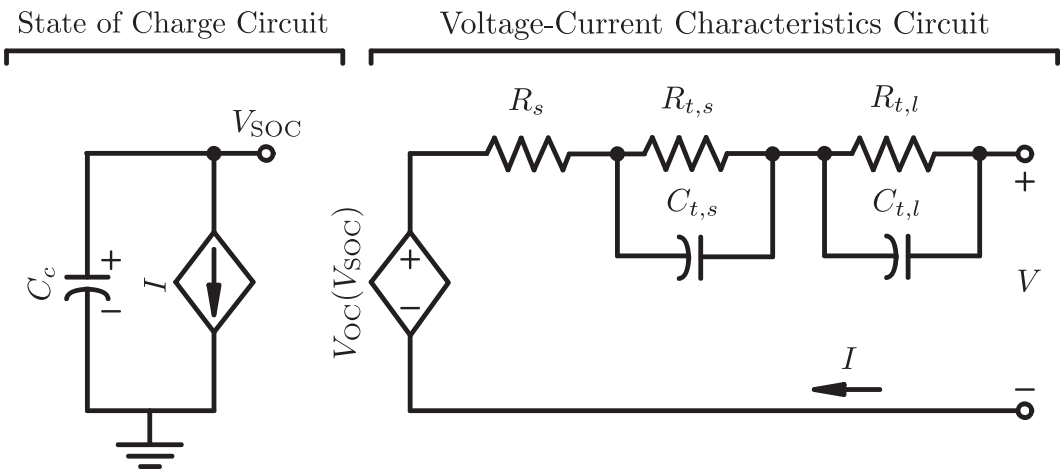

Figure 3.3: The battery lifetime circuit describes the dynamic nature of a battery's state of charge, and the voltage-current characteristics circuit describes how the terminal voltage of a battery is dynamically affected by state of charge and current load.

to a $LiFePO_4$ based Li-ion battery operating at 0 °C, 25 °C, and 40 °C [83]. Similarly, Kim, et al. fit the model to 100 Ah polymer Li-ion cells of various ages operating at 0 °C, 20 °C, and 40 °C [84].

To extract model parameters for the battery considered in this work, dynamic voltage data is collected at various current rates and operating temperatures. First, the initial value of the state-of-charge-circuit capacitance, C_c^i is calculated in Farads (F) from the battery's initial effective charge capacity in Ampere-hours (Ah), Cap_{Ah}, according to Equation 3.7.

$$C_c^i = 3,600 \ \mathrm{Cap}_{Ah} = 54,000 \ \mathrm{F} \tag{3.7}$$

The next step in extracting the model parameters is to develop a function to describe the battery open-circuit voltage, V_{OC}, as a function of the state of charge, V_{SOC}, approximated by the left-hand circuit in Figure 3.3. V_{OC} is determined by

the equilibrium electrochemical potential of the battery's charge-transfer reactions when no current is applied [56]. In a Li-ion battery, V_{OC} typically varies between approximately 2.75 V (fully discharged) and 4.2 V (fully charged), and decreases exponentially as the battery approaches 0% state of charge. To determine the relationship between state of charge and open-circuit voltage, a pulse discharging current is applied to the battery pack, with a cell current alternating between a discharge rate of 1 C (a one-hour discharge rate of 15 A/cell) and 0 A in five-minute intervals. Then, a similar alternating pulsed charge current is applied to the battery pack until it is fully charged. Figure 3.4a shows the applied pulse discharging current and simulated dynamic cell voltage returned from the electrochemical model. Similarly, Figure 3.4b shows the applied pulse charging current and observed voltage response. The results shown were simulated under a condition of strong forced convection at 5°C. Similar tests simulated at 25°C and 45°C showed no strong variation in open circuit voltage with temperature.

The voltage observed during each of the five-minute rest periods is used to approximate the open-circuit voltage at various levels of state of charge. An exponential and polynomial function given in Equation 3.8 is fit to these data using a least-squares fitting procedure implemented in Matlab. Figure 3.5 shows the same data presented in Figures 3.4a and 3.4b in the form of cell voltage versus state of charge, and the empirical function for V_{OC} given in Equation 3.8. A battery operator or manufacturer could use methods similar to those presented here to experimentally characterize the open-circuit voltage of their battery system.

$$V_{OC} = -0.99\exp\left(-53.6V_{\mathrm{SOC}}\right) + 3.39 + 0.858V_{\mathrm{SOC}} - 0.787V_{\mathrm{SOC}}^2 + 0.744V_{\mathrm{SOC}}^3 \quad (3.8)$$

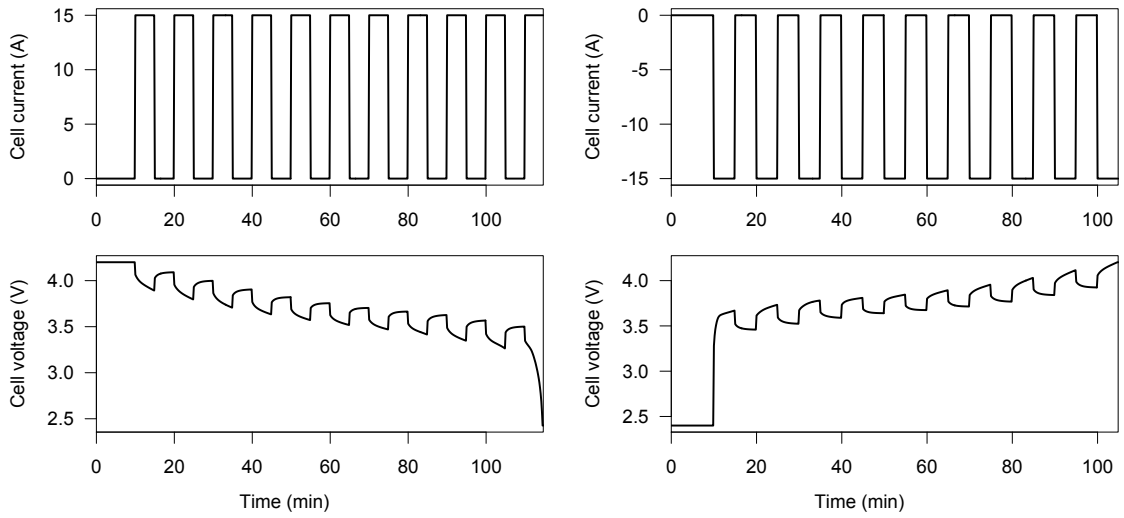

(a) Discharge test (b) Charge test

Figure 3.4: To approximate the open-circuit voltage of the battery at various levels of state of charge, a discharging and charging current alternating between 1C (15 A) and 0 A is applied at five-minute intervals. Results shown here are from an electrochemical model of the battery at an operating temperature of 5°C.

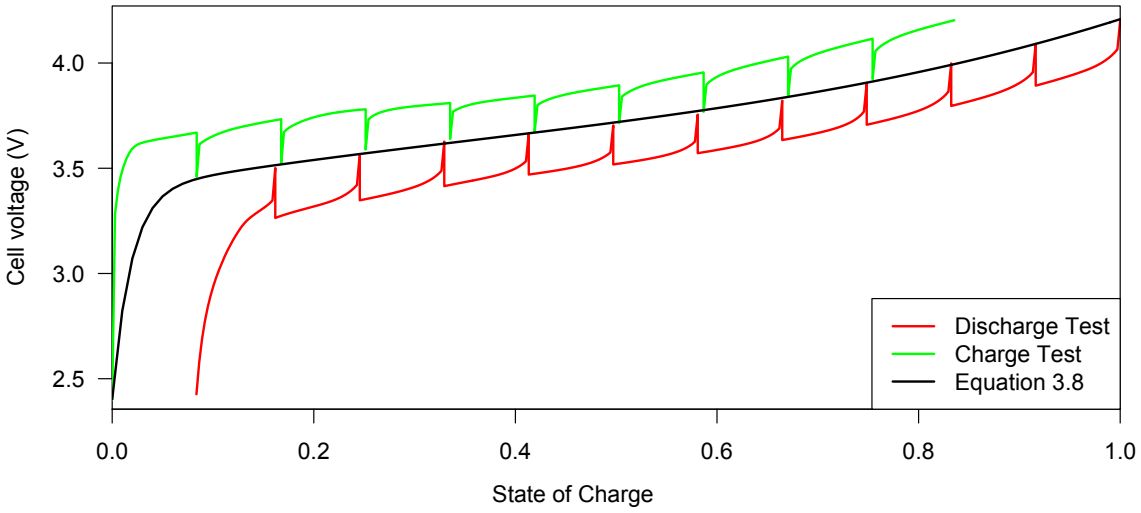

Figure 3.5: The empirical model given in Equation 3.8 is fit to values of voltage observed during the five-minute, zero-current rest periods of the charging and discharging tests illustrated in Figures 3.4a and 3.4b.

With a function developed to describe the nonlinear relationship between state of charge (V_{SOC}) and open-circuit voltage (V_{OC}) the next step is to extract the parameters for the remaining circuit components illustrated in Figure 3.3. The electrochemical model is used to simulate the dynamic voltage response to an alternately pulsed charging and discharging current, so that the voltage behavior at various levels of applied current and state of charge can be characterized. The applied current and resulting voltage behavior for a battery at 5 °C are shown in Figure 3.6.

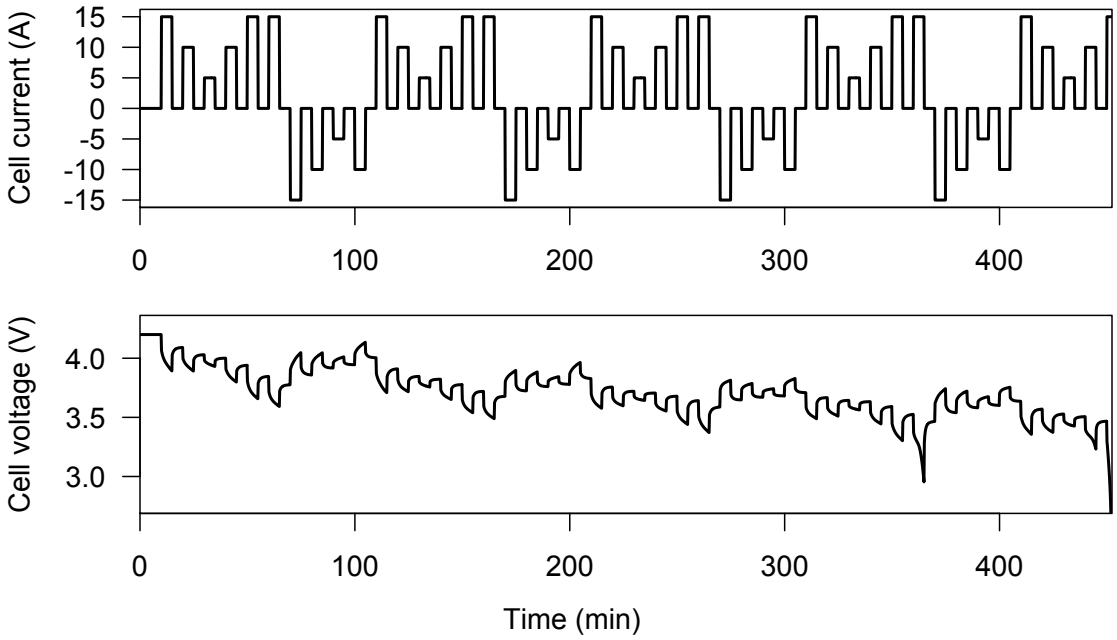

Figure 3.6: Application of an alternately pulsed charging and discharging current is simulated to characterize the dynamic behavior of the battery's voltage at various levels of applied current and state of charge. Results shown here are for a battery operating at 5 °C. The downward spikes observed at the end of the characterization test are caused by the exponentially decreasing voltage behavior that occurs as state of charge approaches 0%.

To extract the value of parameters for the "voltage-current characteristics circuit" illustrated in Figure 3.3 from performance data like those illustrated in Fig-

ure 3.6, Kirchoff's circuit laws are used to extract the mathematical equations that describe the dynamic state of the behavioral circuit model components, resulting in Equations 3.9–3.12.

$$\dot{V}_{SOC} = -\frac{I}{C_c} \tag{3.9}$$

$$\dot{V}_{t,s} = \frac{I}{C_{t,s}} - \frac{V_{t,s}}{R_{t,s}C_{t,s}} \tag{3.10}$$

$$\dot{V}_{t,\ell} = \frac{I}{C_{t,\ell}} - \frac{V_{t,\ell}}{R_{t,\ell}C_{t,\ell}} \tag{3.11}$$

$$V = V_{OC} - IR_s - V_{t,s} - V_{t,\ell} \tag{3.12}$$

To reduce the complexity of the model, it is assumed the parameters R_s, $R_{t,s}$, $C_{t,s}$, $R_{t,\ell}$, and $C_{t,\ell}$ are not a strong function of current rate or state of charge, as was found previously [85, 86]. To extract the value of these parameters, a nonlinear least-squares fitting procedure is carried out to minimize the difference between the cell voltage, V, predicted by Equations 3.9–3.12 and simulated cell voltage data from the electrochemical model. Data like those of Figure 3.6 are simulated for a battery operating at temperatures ranging from 5 °C to 45 °C, an then a constrained nonlinear optimization program is used to calculate point estimates for each of the model parameters at various levels of temperature. Within the optimization program, each value of resistance and capacitance is constrained so that it is strictly greater than zero. Furthermore, the time constants of the resistor-capacitor couples illustrated in Figure 3.3 are constrained to equal constant levels $\tau_s = R_{t,s}C_{t,s} = 10$ seconds, and $\tau_l = R_{t,\ell}C_{t,\ell} = 60$ seconds, which are selected based on the temporal characteristics

of grid operation and the quality of fit to the observed data. The resulting variation of the model parameters with temperature is illustrated in Figure 3.7. Note that confidence intervals for the parameters are not shown because the time constant of the resistor-capacitor couples is constrained within the nonlinear optimization program used to extract the model parameters, so it does not return a covariance matrix or corresponding confidence limits.

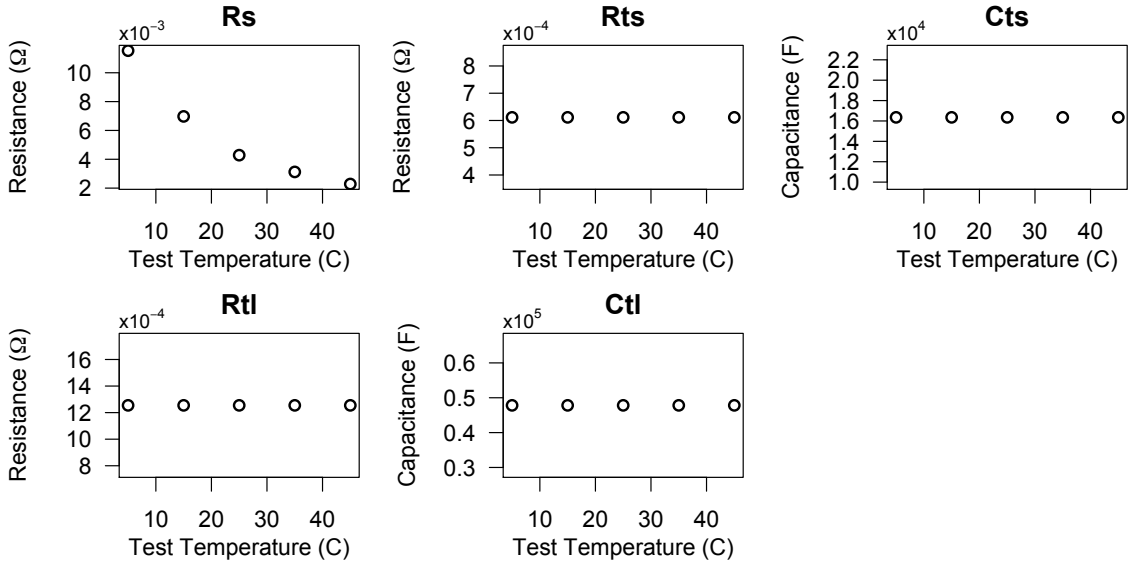

Figure 3.7: The characterization test current illustrated in Figure 3.6 is simulated at temperatures ranging from 5 °C to 45 °C to show the variation of the model parameters R_s, $R_{t,s}$, $C_{t,s}$, $R_{t,\ell}$, and $C_{t,\ell}$ with temperature.

Based on the results of Figure 3.7, only series resistance (R_s) demonstrates strong variation with temperature. To describe this behavior, the Arrhenius exponential function given in Equation 3.13 is fit to the parameter value at various temperatures, because Arrhenius functions have been found to predict the temperature-dependent behavior of Li-ion batteries in previous studies [101–103]. The resulting fit is illustrated in Figure 3.8.

$$R_s = 1.19 \times 10^{-8} \exp(3,830/T) \tag{3.13}$$

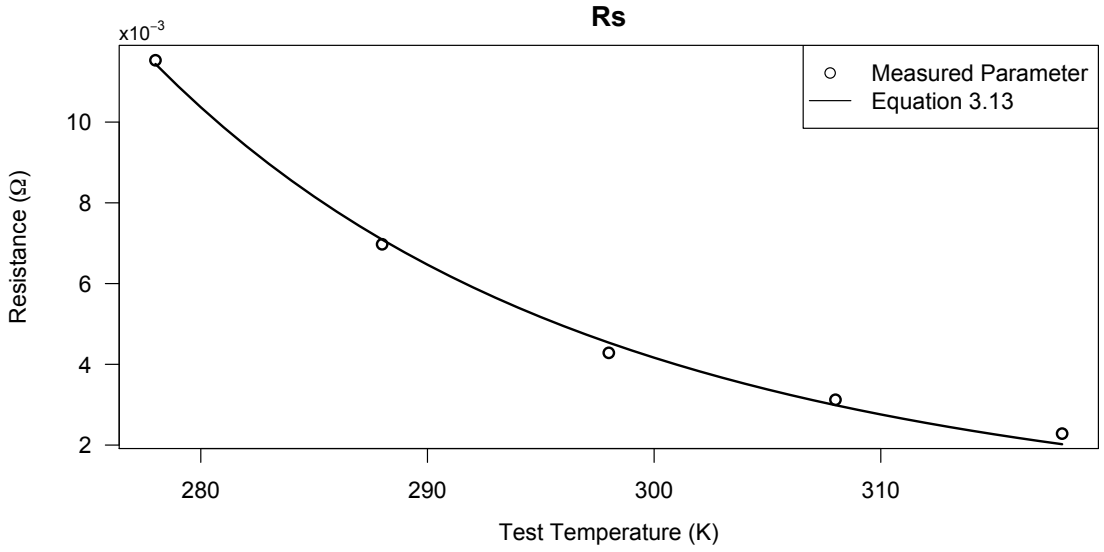

Figure 3.8: An empirical function is fit to the data of Figure 3.7 to describe the variation of series resistance (R_s) with temperature.

Table 3.4 summarizes the values and functions extracted for each of the model components illustrated in Figure 3.3. Using these model parameters, the voltage response to the current load illustrated in Figure 3.6 is simulated and compared to the data from the electrochemical model. The resulting fit is shown in Figure 3.9. The empirical voltage model accurately models the terminal voltage predicted by the electrochemical simulation, with the exception of the exponential behavior that occurs at very low values of state of charge ($< 10\%$). This deviation from the electrochemical model is acceptable because the battery would not typically operate in this region.

Table 3.4: The characterization procedure described in this section yields point estimates for each of the voltage model components identified in Figure 3.3.

Model parameter	Value	Units
C_c^i	54,000	F
V_{OC}	$-0.99\exp\left(-53.6V_{\text{SOC}}\right)+3.39+0.858V_{\text{SOC}}-0.787V_{\text{SOC}}^2+0.744V_{\text{SOC}}^3$	V
R_s	$1.19\times10^{-8}\ \exp(3,830/T)$	Ω
$R_{t,s}$	6.11×10^{-4}	Ω
$C_{t,s}$	1.64×10^{4}	F
$R_{t,\ell}$	1.25×10^{-3}	Ω
$C_{t,\ell}$	4.78×10^{4}	F

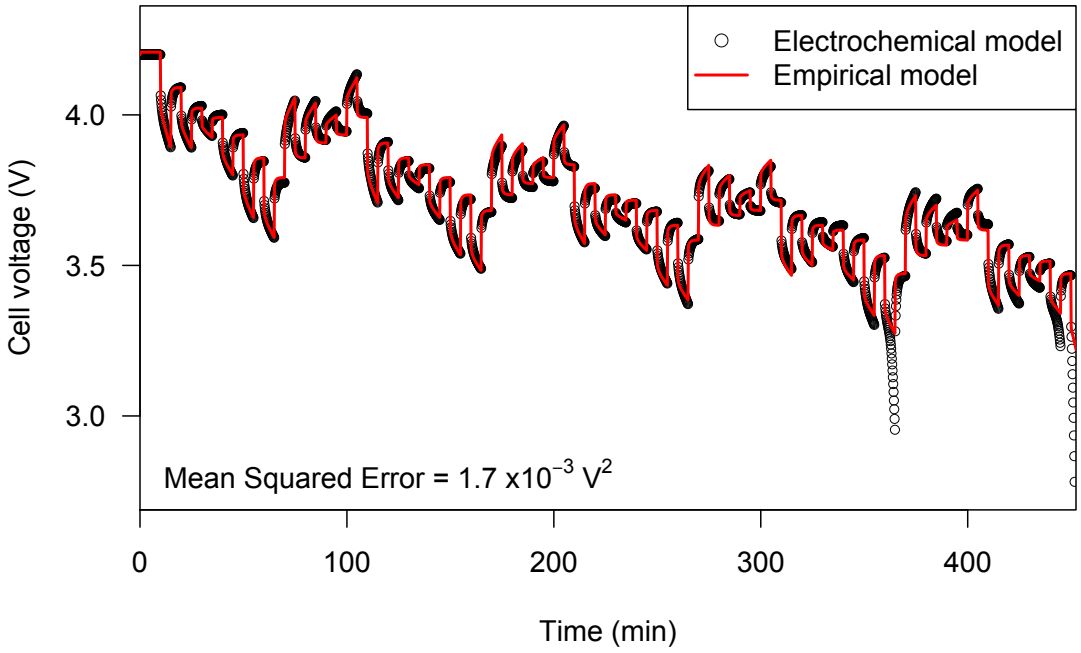

Figure 3.9: The empirical voltage model developed in this section can accurately describe the dynamic voltage behavior of the battery simulated with the computationally-intensive electrochemical model. The greatest model error occurs when the voltage exponentially decreases at very low values of state of charge ($< 10\%$). This deviation from the electrochemical model is acceptable because the battery would not typically operate in this region.

3.1.3 Thermal Model

With a model for the battery voltage behavior with temperature, current, and state of charge established, the next step is to model the temperature gain of the battery as a function of the applied current and thermal conditions. It is important to model temperature because: 1) temperature affects internal resistance, as demonstrated in the previous section, 2) temperature has a strong effect on Li-ion battery degradation [102, 104–106], and 3) it is important to constrain the internal cell temperature within certain limits during operation to prevent thermal runaway and other safety risks.

The thermal properties are considered at the level of the battery pack. The battery pack encapsulates the battery modules and facilitates the flow of coolant between the modules, as shown in Figure 3.2. To model the thermal behavior of a Li-ion battery pack, the temperature of the battery pack, its modules, and cells is considered uniform. Furthermore, it is assumed the battery pack is well insulated with the exception of heat rejection to the battery coolant. The variable temperature of the battery pack T is written as a function of its mass m, specific heat c_p, rate of heat generation $\dot{Q}_{\text{gen}}$, and rate of heat rejection to the coolant $\dot{Q}_c$, as given in Equation 3.18.

$$mc_p\dot{T} = \dot{Q}_{\text{gen}} - \dot{Q}_c \tag{3.14}$$

As discussed in Section 3.1.1, a hypothetical 30 kWh Li-ion battery pack is considered. The thermal specifications for the battery pack are approximated based on parameters provided by the U.S. Department of Energy [94, 96], and are given in Table 3.5.

Table 3.5: Thermal parameters for the Li-ion battery pack are approximated using data from a U.S. Department of Energy battery performance and cost model [94, 96].

Parameter	Value
Mass (m)	230 kg
Specific heat capacity (c_p)	850 J/kg-K
Total number of battery cells (N_{cells})	576
Cooling method	Forced liquid coolant
Coolant type	50% ethylene glycol, 50% water
Coolant-modules convection coefficient (h)	230 W/m^2-K
Coolant-modules effective area (A)	1.6 m^2
Average electric power for compressor and pump	260 W

The heat generation within the battery pack is approximated using the voltage model established in the previous section to predict Ohmic heating. The instantaneous internal resistance of a battery cell can be written as a function of the cell current I and the difference between the cell terminal voltage V and the open circuit voltage V_{OC}, or the overpotential [107, 108], as given in Equation 3.15.

$$R_{\text{eff}} = \frac{V_{OC} - V}{I} \tag{3.15}$$

Using the equation for Ohmic heating, the heat generation inside a battery pack containing a number of cells N_{cells} can be approximated as given in Equation 3.16. Note that $\dot{Q}_{\text{gen}}$ is strictly positive because for positive values of current (discharging) $V_{OC} > V$ and for negative values of current (charging) $V_{OC} < V$.

$$\dot{Q}_{\text{gen}} = N_{\text{cells}} I^2 R_{\text{eff}} = N_{\text{cells}} I (V_{OC} - V) \tag{3.16}$$

The rate of heat rejection to the coolant is calculated according to Newton's law of cooling, which relates the rate of heat transfer between two objects to the tem-

perature difference between them, the heat transfer coefficient h, and the contact area A. Q_c is written as a function of the battery temperature (T), the coolant temperature (T_c), and the thermal parameters given in Table 3.5, as given in Equation 3.17.

$$\dot{Q}_c = hA(T - T_c) \tag{3.17}$$

Substituting Equations 3.16 and 3.17 into Equation 3.18 results in the following differential equation to predict the temperature gain in the battery as a function of the current load applied to its cells I and the cell voltage V.

$$mc_p\dot{T} = N_{\text{cells}}I(V_{OC} - V) - hA(T - T_c) \tag{3.18}$$

Figure 3.10 compares the heat generation ($\dot{Q}_{\text{gen}}$), heat rejection ($\dot{Q}_c$), and temperature predicted by Equations 3.16–3.18 to the values returned by the electrochemical model for the pulsed current load illustrated in Figure 3.6. The model predicts the dynamic temperature behavior of the battery pack with reasonable accuracy across a range of operating currents and voltages. Any deviation from the electrochemical model stems from the fact that the model developed here does not consider second-order battery thermal effects such as entropic heating [107]. While this simplification reduces the accuracy of the model, it has the benefit of equating temperature gain as a smooth, continuous function of the other battery state variables.

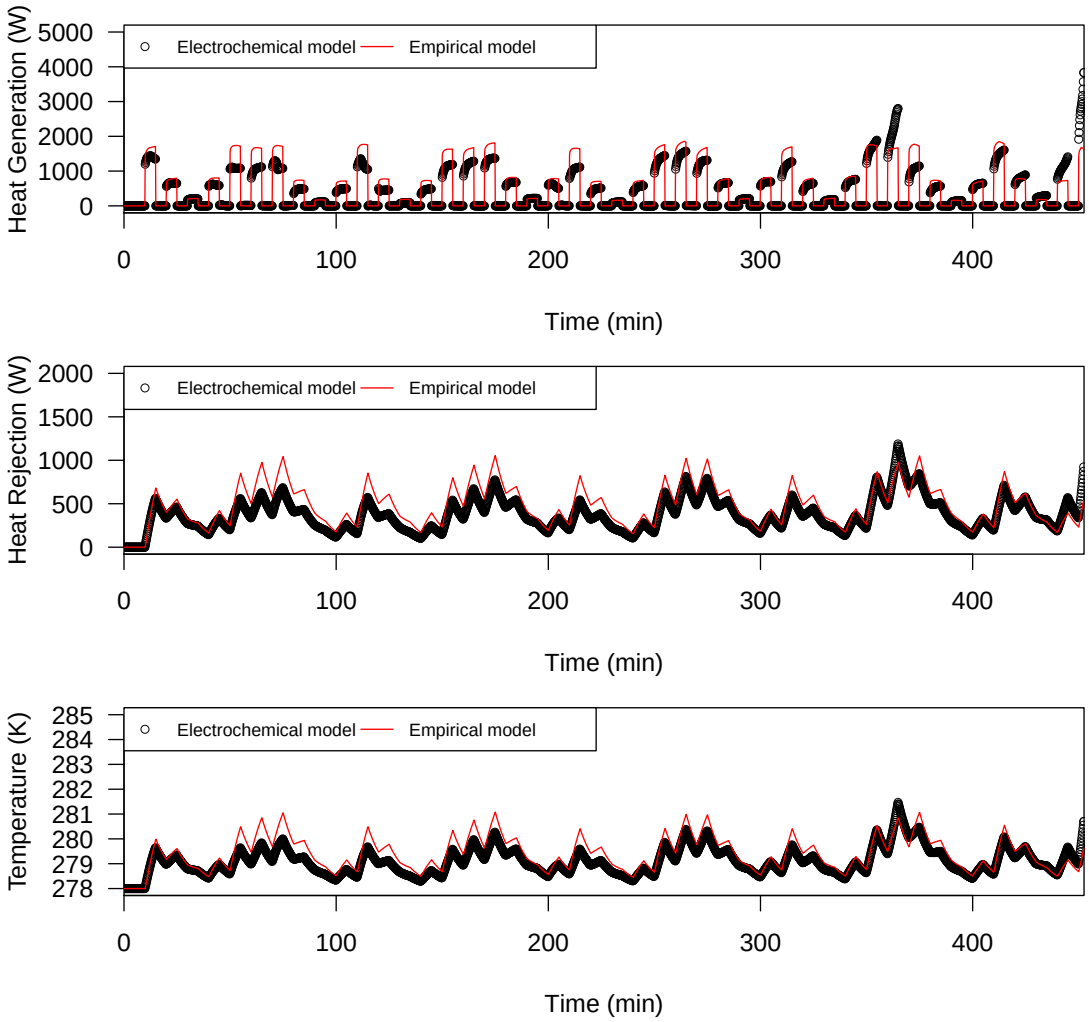

Figure 3.10: The empirical thermal model developed in this section is compared to thermal conditions returned from the electrochemical model for the pulsed current load illustrated in Figure 3.6. The model describes the dynamic temperature of the battery pack in response to the pulsed current load with reasonable accuracy across a wide range of operating currents and voltages. Any deviation from the electrochemical model stems from the fact that the model developed here does not consider second-order battery thermal effects such as entropic heating [107].

3.1.4 Capacity Degradation Model

The final battery characteristic modeled is the relationship between the Li-ion battery's operating state and its rate of capacity degradation. Li-ion batteries undergo both passive and active processes that cause the capacity of the battery to fade over time and with repeated cycling. One of the major sources of Li-ion capacity degradation is the growth of the solid electrolyte interphase (SEI) layer at the interface between the electrolyte and the graphite anode [65, 102, 104–106]. The SEI layer is formed the first time the battery is charged to protect the graphite anode from corrosion and the electrolyte from reduction [65]. Over time, the layer grows and consumes some of the battery's active lithium, reducing its effective energy capacity. SEI layer growth depends on the battery voltage and temperature, and occurs during both storage and utilization [65,102,104–106]. Another common source of capacity degradation is growth of an oxide layer between the cathode and the electrolyte, similar to the SEI layer [65]. Furthermore, additional active material can be isolated and lost during cycling due to volume changes and cracking that occur in the electrodes during cycling [64, 65]. The AutoLion-ST software uses rate equations to approximate the capacity loss due to each of these mechanisms [64].

Capacity degradation typically proceeds until the electrode potential at the anode falls below 0 V versus lithium during charging. After this point, the onset of lithium plating in the anode causes a dramatic reduction in cell capacity, and the battery cells are typically retired [90, 102]. The level of degraded capacity at which lithium plating begins and a Li-ion cell is retired is not well established. For the purposes of this work, an end-of-life capacity equal to 65% of the battery's initial capacity is assumed based on information in the literature and communication with industry [102, 109]. Chapter 4 tests the effect of this assumption by considering end

capacities ranging from 55%–75%.

In general, Li-ion capacity degradation can be divided into calendar aging, the passive loss of capacity over time, and cycle aging, the active loss of capacity due to cycling [102–106, 110]. To characterize the battery's rate of degradation under various conditions, electrochemical simulations are carried out to approximate both calendar aging and cycle aging.

Based on the results of previous studies [102, 103, 110] calendar aging is influenced by storage temperature and storage voltage. To measure the effect that voltage and temperature have on the battery's rate of degradation, simulations are carried out for battery packs stored at constant levels of voltage and temperature corresponding to the test matrix presented in Table 3.6.

Table 3.6: A large test matrix is used to characterize calendar aging capacity degradation at various temperatures and voltages. An X indicates that a characterization simulation is carried out at the corresponding values of voltage and temperature.

	Cell Voltage (V)								
	2.75	3.4	3.6	3.7	3.8	3.9	4.0	4.1	4.2
Cell Temperature (°C)									
5	X	X	X	X	X	X	X	X	X
25	X	X	X	X	X	X	X	X	X
45	X	X	X	X	X	X	X	X	X

Operation of the Li-ion battery pack at the constant temperatures and voltages specified in Table 3.6 is simulated using the AutoLion software. Within each simulation, a characterization procedure is carried out every 30 simulation days to measure the amount of available capacity remaining in the battery. The results of the simulations approximate the capacity degradation that would occur over time due to

calendar aging. Figures 3.11–3.13 show the simulated degradation behavior observed at 5 °C, 25 °C, and 45 °C, respectively.

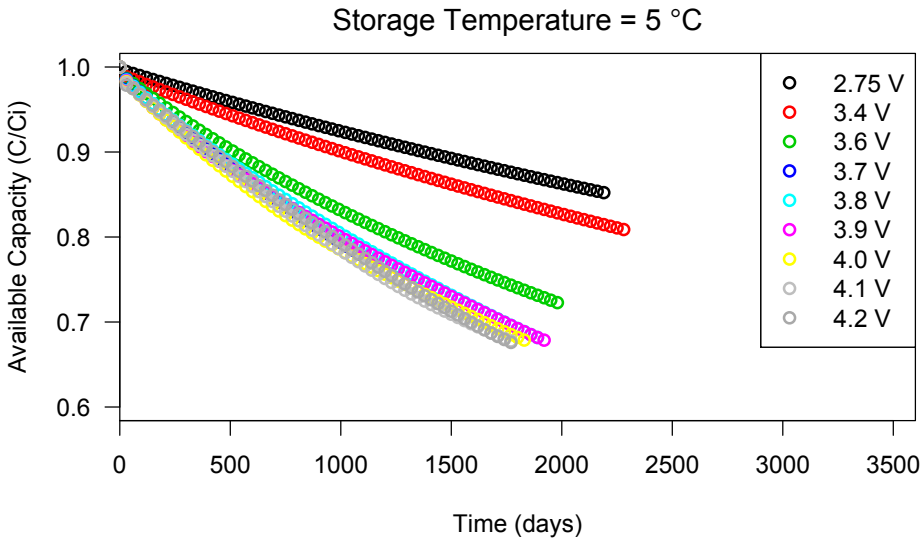

Figure 3.11: The electrochemical model is used to simulate the effect of calendar aging at a storage temperature 5 °C. The battery lasts longer if it is stored at a discharged state.

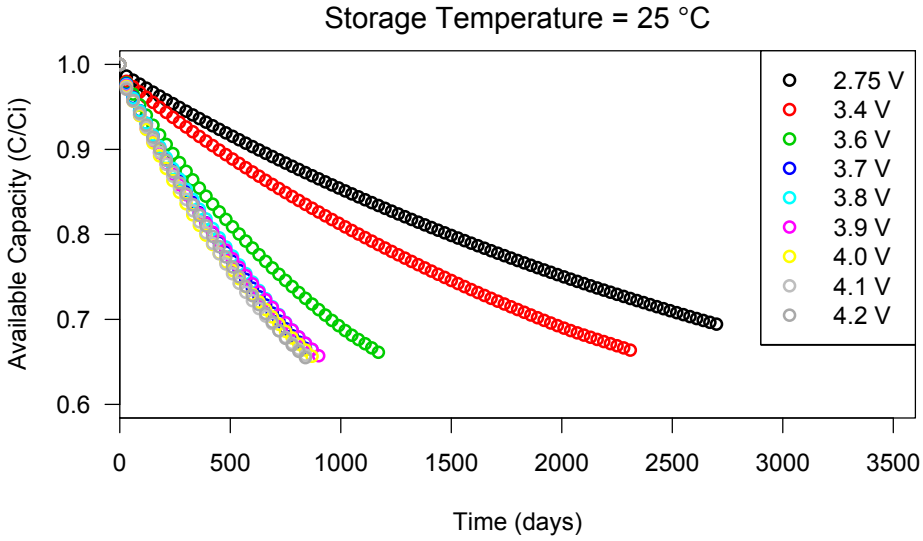

Figure 3.12: The electrochemical model is used to simulate the effect of calendar aging at a storage temperature of 25 °C. The battery lasts longer if it is stored at a discharged state.

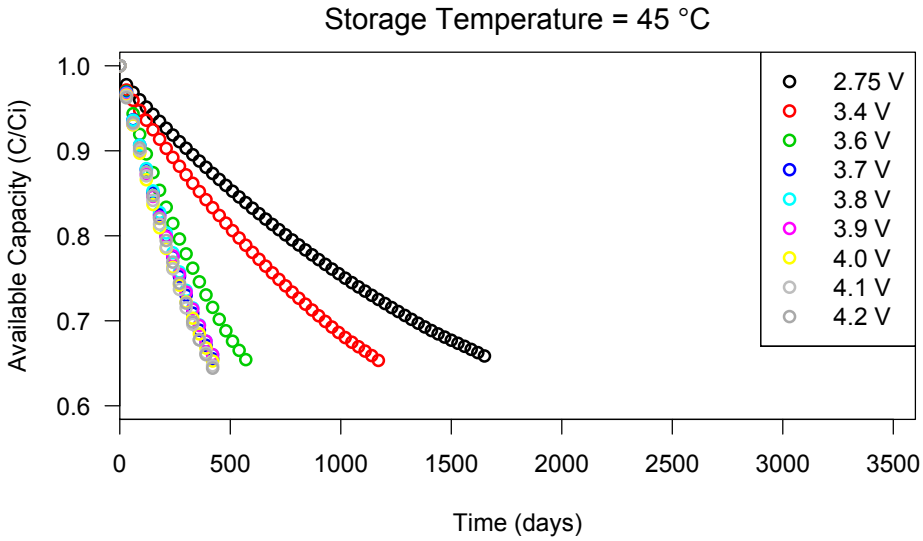

Figure 3.13: The electrochemical model is used to simulate the effect of calendar aging at a storage temperature of 45 °C. The battery lasts longer if it is stored at a discharged state.

Two trends emerge from the characterization data illustrated in Figures 3.11–3.13. First, the battery ages more quickly with increasing storage temperature, regardless of its voltage. Second, the battery ages more quickly at voltages greater than 3.4 V. To parameterize this behavior, calendar aging is modeled as proportional to $t^{3/4}$ (where t is time in days), similar to models developed previously [103–105]. The formula for the ratio between the degraded battery capacity C_c^d and the initial battery capacity C_c^i is defined as a function of calendar aging as presented in Equation 3.19, where $a(T, V)$ is a function of temperature and voltage.

$$(C_c^d / C_c^i)_{\text{cal}} = 1 - a(T, V)\, t^{3/4} \tag{3.19}$$

To extract the value of the parameter $a(T, V)$ from the simulated data shown in Figures 3.11–3.13, a least-squares linear fitting procedure is used to find the proportionality between $(C_c^d / C_c^i)_{\text{cal}}$ and $t^{3/4}$ at different levels of temperature and voltage.

Equation 3.20 is developed to describe the variation of $a(T, V)$ with temperature and voltage based on the voltage relationship illustrated in Figure 3.14 and 3.15. The hyperbolic tangent function describes the step-function-like behavior shown in Figure 3.14, and the exponential function describes the Arrhenius behavior illustrated in Figure 3.15. Figures 3.14 and 3.15 show the values of $a(T, V)$ measured from the data presented in Figures 3.11–3.13 and the modeled value predicted by Equation 3.20.

$$a(T, V) = (8.3 + 3.6 \tanh(7.5V - 26.8)) \exp(-2,561/T) \tag{3.20}$$

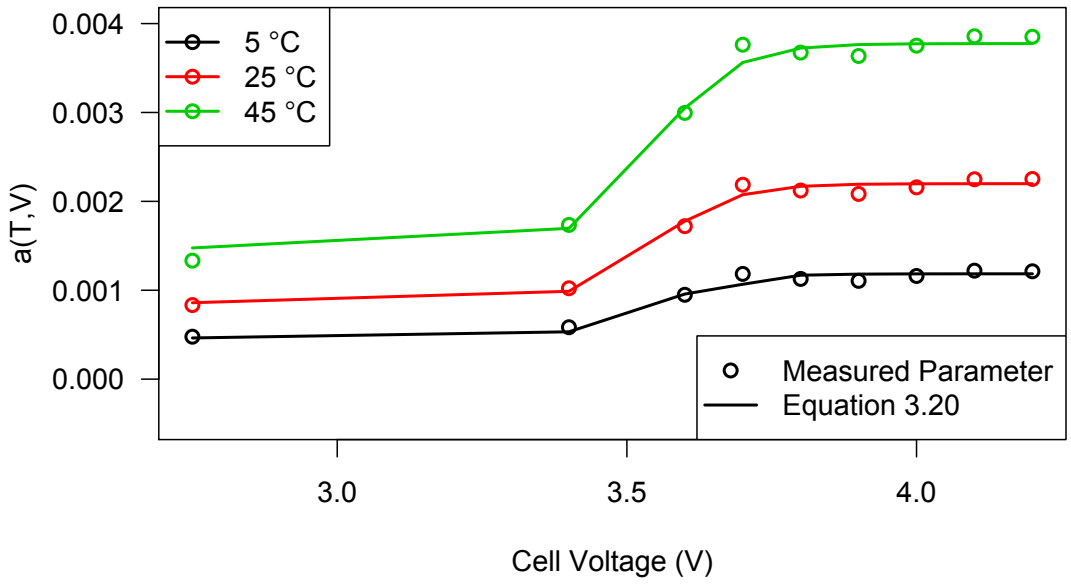

Figure 3.14: The rate of calendar aging $a(T, V)$ increases rapidly for voltages greater than 3.4 V.

To compare the rate of calendar aging predicted by the empirical model of Equation 3.19 to the simulated data from the electrochemical model, Figure 3.16 shows the modeled and simulated results for a battery stored at 25 °C. While the calendar aging behavior shown is similar to behavior found previously for NMC Li-ion cells [103, 104], it is important to note that the data of Figure 3.16 cannot be

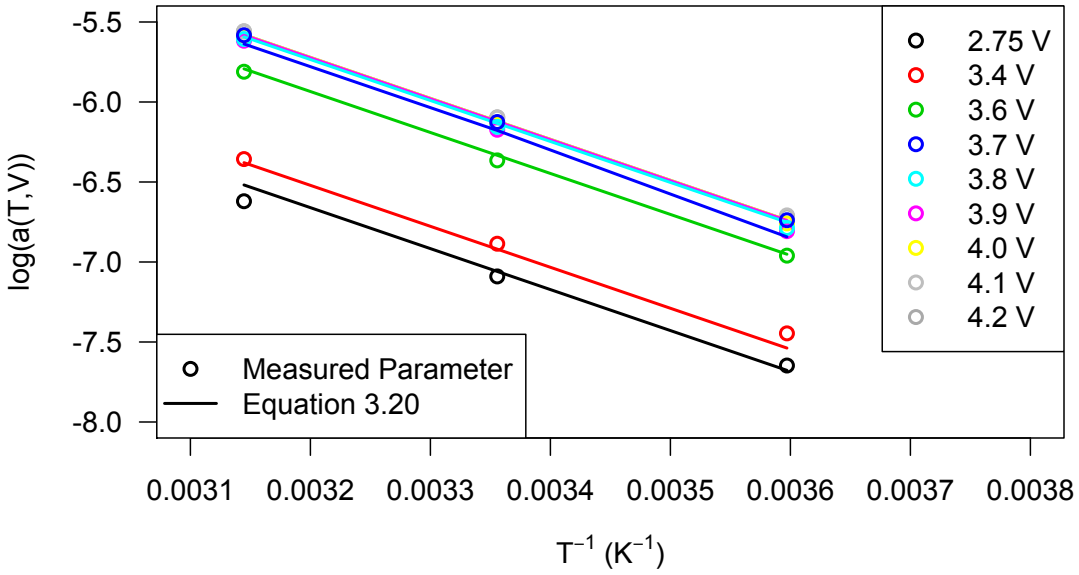

Figure 3.15: An Arrenhius relationship is found between rate of calendar aging $a(T, V)$ and temperature, as was found previously [103, 104].

generalized to all Li-ion batteries or even all NMC-based Li-ion batteries. Rather, the behavior shown is particular to the battery system considered, and developed for the express purpose of operating the system considered in a way that minimizes its degradation during grid operation. Battery energy storage operators seeking to operate their system using the methods developed in this chapter could carry out a similar characterization procedure to develop information about their own system.

With the calendar aging behavior of the system characterized, the next step is to characterize any incremental aging caused by the active charging and discharging of the battery system. To do so, a characteristic cycling power equal to 25 kW is applied at various levels of temperature and depth of discharge, both of which have been shown to influence the rate of cycle aging [103]. Table 3.7 illustrates the test matrix used to characterize cycle aging under various levels of depth of discharge and operating temperature. Each test occurs around an average state of charge equal to

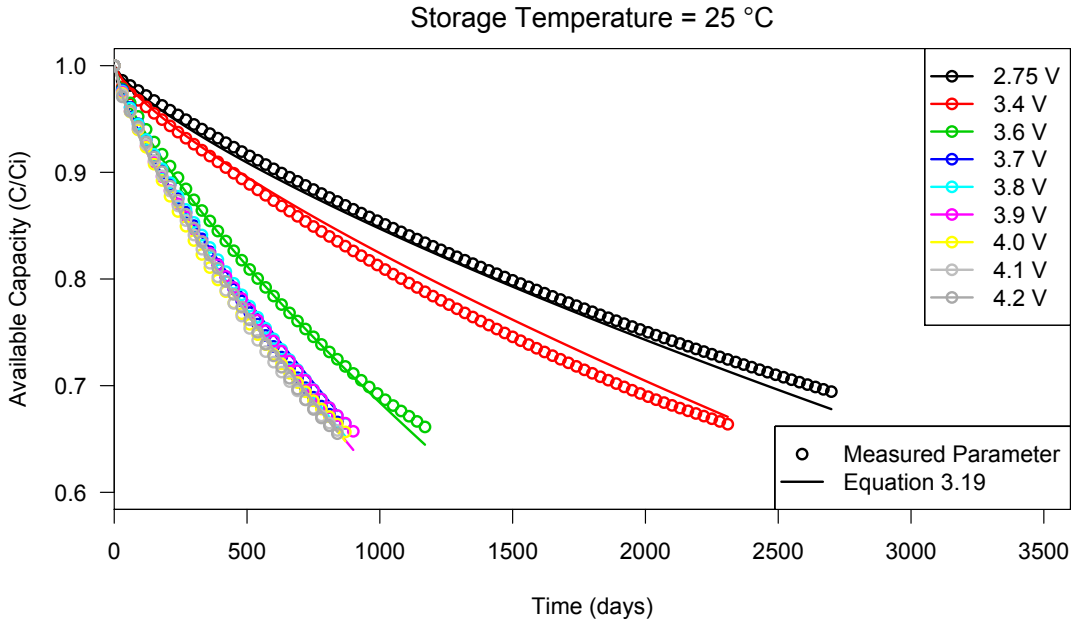

Figure 3.16: The empirical function to describe calendar aging given in Equation 3.19 is compared to simulated calendar aging data from the electrochemical model.

50%, which corresponds to an open-circuit cell voltage approximately equal to 3.71 V. For each test, the battery is charged to the corresponding level of state of charge at constant power, held at a constant voltage for one hour, discharged at constant power, and then held at a constant voltage for one hour. The cycle regime is repeated until the battery's capacity reaches the end-of-life criterion of 65% available capacity. Results from the cycling characterization electrochemical simulations are illustrated in Figure 3.17.

To isolate the aging effects that are caused purely by cycling the battery, Equation 3.19 is transformed so that it can be used to approximate calendar aging in a battery held at various levels of voltage during its lifetime, rather than a constant voltage. The goal is to discretize Equation 3.19 so that it can be applied to a battery held at a various levels of voltage $V_1, \cdots, V_n$ and temperatures $T_1, \cdots, T_n$ during time steps $\Delta t_1, \cdots, \Delta t_n$. Equation 3.21 is selected because it is exactly equal

Table 3.7: A test matrix is used to characterize cycle aging capacity degradation at various temperatures and levels of depth of discharge. All cycle tests occur around a mean state of charge equal to 50%. An X indicates that a characterization simulation is carried out at the corresponding values of depth of discharge and temperature.

	Depth of Discharge (%)				
	20	40	60	80	100
Cell Temperature (°C)					
5	X	X	X	X	X
25	X	X	X	X	X
45	X	X	X	X	X

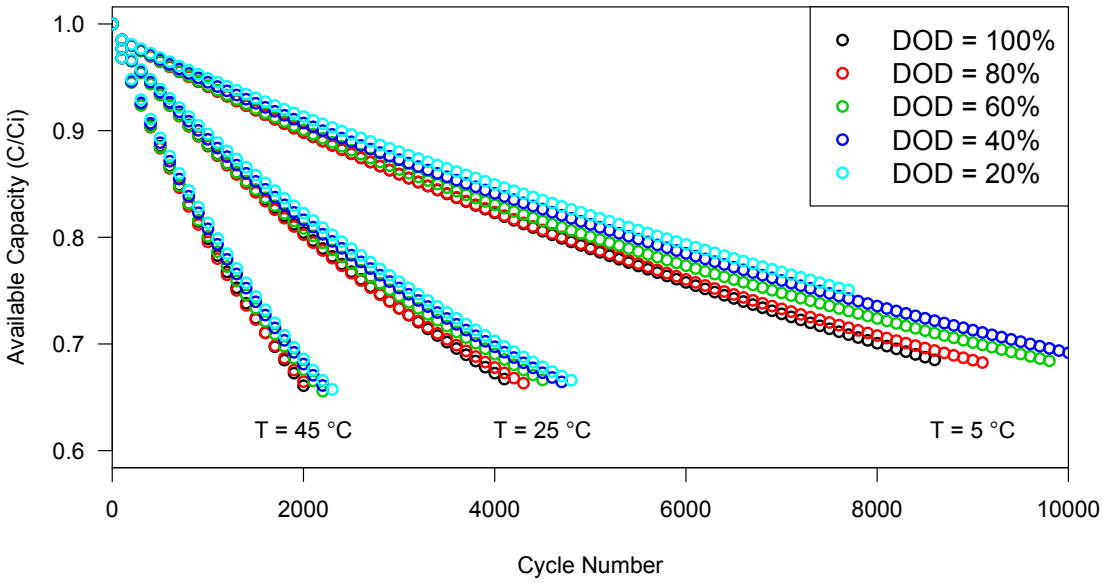

Figure 3.17: Conditions corresponding to those given in Figure 3.7 result in the given simulated cycle aging behavior. The battery can perform more cycles at lower values of temperature and depth of discharge.

to Equation 3.19 for the case where voltage and temperature are constant for the duration of the battery's life.

$$
\begin{aligned}
(C_c^d/C_c^i)_{\text{cal}} &= 1 - (a(T_1,V_1)^{4/3}\Delta t_1 + \cdots + a(T_n,V_n)^{4/3}\Delta t_n)^{3/4} \\
&\quad \text{if } V_1 = V_2, \cdots, V_n = V;\ T_1 = T_2, \cdots, T_n = T;\ \Delta t_1 = \Delta t_2, \cdots, \Delta t_n = \Delta t \\
&= 1 - (n\ a(T,V)^{4/3}\Delta t)^{3/4} = 1 - a(T,V)(n\Delta t)^{3/4} = 1 - a(T,V)t^{3/4}
\end{aligned}
\tag{3.21}
$$

Equation 3.21 is applied to the simulated cycling data illustrated in Figure 3.17 to isolate the effects of calendar aging from the effects of cycling. Figure 3.18 compares the observed cycle aging versus the modeled isolated calendar aging for cycle tests carried out at 100% depth of discharge and various temperatures. In all cases, including those not shown in Figure 3.18, cycling causes additional aging versus the pure calendar aging predicted by Equation 3.21.

Equation 3.22 is used to describe the incremental effect that cycling the battery has on aging versus pure calendar aging, similar to models developed previously to describe NMC Li-ion battery aging [103,105]. Pure cycling capacity loss is calculated by subtracting the modeled pure calendar aging $(C_c^d/C_c^i)_{\text{cal}}$ from the observed total aging C_c^d/C_c^i. The pure cycle aging is found to be proportional to q_{Ah}, which is the total charge throughput of the battery during its lifetime measured in Ampere-hours (Ah), as defined in Equation 3.23.

$$
(C_c^d/C_c^i)_{\text{cyc}} = C_c^d/C_c^i - (C_c^d/C_c^i)_{\text{cal}} = b(T, DOD)q_{Ah} \tag{3.22}
$$

$$
q_{Ah}(t) = \frac{1}{2}\int_{t=0}^{t} |I(t)|dt \tag{3.23}
$$

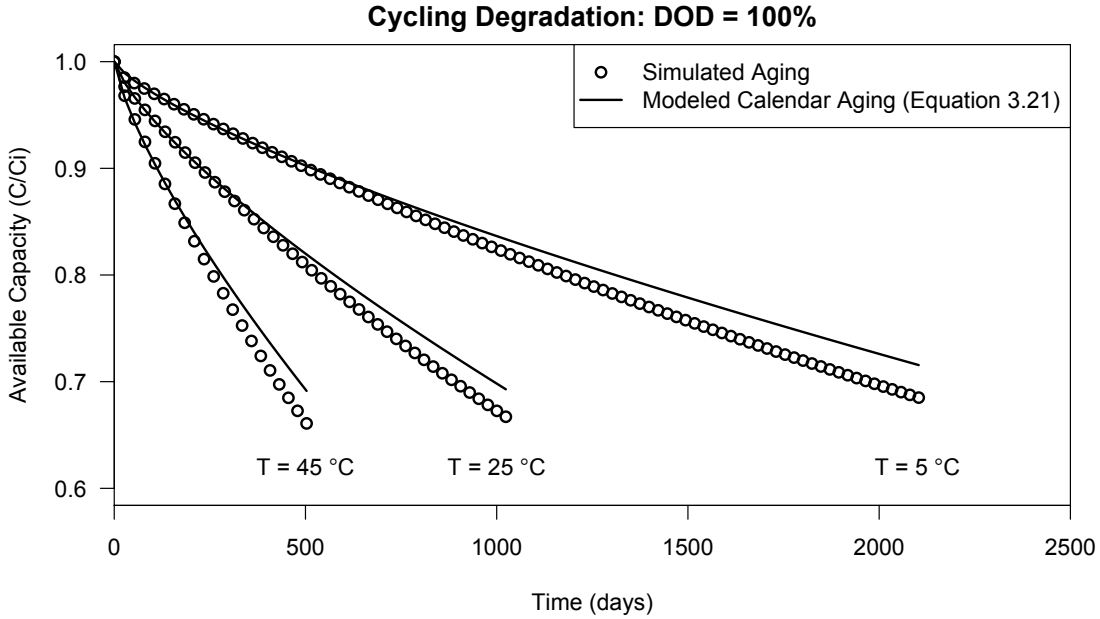

Figure 3.18: The cycle aging observed from the electrochemical model is compared to the pure calendar aging predicted using Equation 3.21.

A fitting procedure is carried out to find the proportionality between q_{Ah} and $(C_c^d/C_c^i)_{\text{cyc}}$ described by the parameter $b(T, DOD)$. $(C_c^d/C_c^i)_{\text{cyc}}$ is calculated for all of the test data illustrated in Figure 3.17, and then the value of $b(T, DOD)$ that minimizes the sum of the differences squared between the observed values and Equation 3.22 is calculated. The parameter b is found to be a strong function of temperature only, because the effect of depth of discharge influences both the voltage effects of Equation 3.21 and the magnitude of q_{Ah}. An Arrhenius relationship is found between temperature and the rate of cycle aging, b, as was found for other temperature-dependent parameters discussed previously in this section. Equation 3.24 gives the resulting function for b.

$$b(T) = 1.96 \times 10^{-7} + 64.8 \exp(-5,556/T) \tag{3.24}$$

$$C_c^d/C_c^i = 1 - \left(\sum_{i=1}^{n} a(T_i, V_i)^{4/3} \Delta t_i\right)^{3/4} - \sum_{i=1}^{n} b(T_i) q_{\mathrm{Ah},i} \tag{3.25}$$

Combining Equations 3.21–3.24 results in a model to describe capacity degradation under diverse storage and cycling conditions, as given in Equation 3.25. Figure 3.19 compares the total aging predicted by Equation 3.25 with the simulated data and pure calendar aging predicted for a battery cycling at 100% depth of discharge and various temperatures.

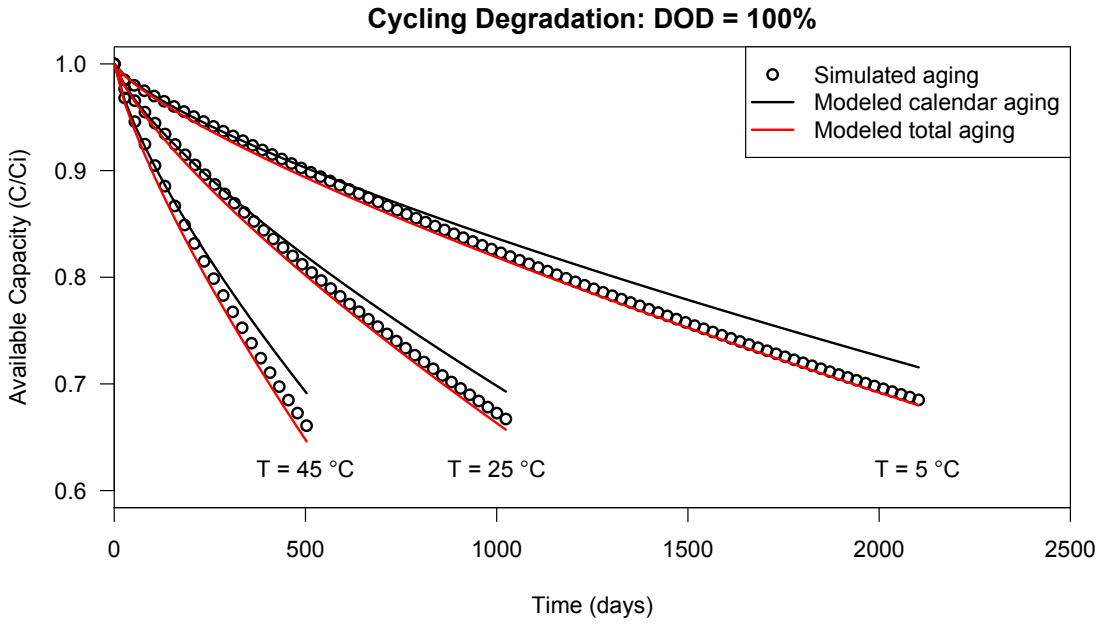

Figure 3.19: The cycle aging observed from the electrochemical model is compared to the pure calendar aging predicted by Equation 3.21 and the total aging predicted by Equation 3.25. The model accurately predicts the rate of capacity degradation for various operating temperatures and cycling/storage conditions.

3.1.5 Section Summary

The previous section has developed a framework to describe the dynamic voltage, temperature, and rate of degradation of a Li-ion battery system using empirical

equations. To demonstrate the use of this framework, model parameters were approximated for an NMC-based distributed Li-ion battery system. In practice, a Li-ion battery manufacturer or operator could carry out a similar procedure to characterize the dynamic performance and degradation of their battery system, so that its operation in an electricity market can be managed in a way that considers both instantaneous voltage-temperature behavior and long-term capacity degradation. The following section illustrates how the information about battery performance and degradation behavior developed in this section is input to an optimization program to not only maximize electricity-market operating revenue, but also minimize capacity degradation during operation.

3.2 An Optimization Program to Schedule Lithium-Ion Storage in Electricity Markets

A battery energy storage system can provide a number of different grid applications [21, 25, 40]. Typically, the decision variable for grid operation is the instantaneous level of charging or discharging power flowing between the electric grid and the battery device. The charging or discharging power applied to the battery affects its dependent state variables: current, voltage, temperature, and state of charge, all of which must be controlled within acceptable limits during battery operation. Moreover, the power applied to a battery affects it rate of capacity degradation.

The operation of Li-ion storage is planned by maximizing the value of an objective function, which is a quantity of interest expressed as a function of the optimization decision variables. Typically, the objective function for optimal operation of grid energy storage is calculated in terms of only the battery power and the prevailing electricity market prices during an operating day. Long-term capacity degradation effects are not considered explicitly in the decision of when the battery should charge

and discharge. Rather, capacity degradation is often controlled by artificially constraining the battery's voltage within predetermined limits. This approach is limited because it reduces the battery's effective energy capacity for the life of the system, which might cause the battery to miss opportunities to sell energy when electricity prices peak. Furthermore, the conventional method does not consider capacity loss that might occur from individual charge-discharge actions during a given operating day, so incremental capacity degradation cannot be controlled and reduced.

This work proposes a new objective function, which considers the effect of capacity degradation in battery operational management. In its most general form, the objective function can be written as in Equation 3.26, expressed as a function of the battery power, P, during each optimization time step, k, and the capacity loss, C^d_{loss}, incurred over the operating day in question.

$$\text{Objective} = f(P(k_1), \cdots, P(k_n), C^d_{\text{loss}}) \tag{3.26}$$

The functional relationship between the decision variables, P, and the dependent state variables I, V, V_{SOC}, T, C^d_{loss}, etc. is described using the empirical models developed in the previous section. To implement the dynamic equations for battery voltage (Equations 3.9–3.12) and temperature (Equation 3.18) in an optimization model, the equations are discretized using a forward-difference approximation. Equations 3.27–3.31 approximate each of the dynamic state variables at time step k of duration Δt. C^d_c is used to represent the degraded battery capacity at the beginning of the operating day.

$$V_{SOC}(k+1) = \left(-\frac{I(k)}{C^d_c}\right)\Delta t + V_{SOC}(k) \tag{3.27}$$

$$V_{t,s}(k+1) = \left(\frac{I(k)}{C_{t,s}} - \frac{V_{t,s}(k)}{R_{t,s}C_{t,s}}\right)\Delta t + V_{t,s}(k) \tag{3.28}$$

$$V_{t,\ell}(k+1) = \left(\frac{I(k)}{C_{t,\ell}} - \frac{V_{t,\ell}(k)}{R_{t,\ell}C_{t,\ell}}\right)\Delta t + V_{t,\ell}(k) \tag{3.29}$$

$$V(k) = V_{OC}(k) - I(k)R_s(k) - V_{t,s}(k) - V_{t,\ell}(k) \tag{3.30}$$

$$T(k+1) = (N_{\text{cells}}I(k)(V_{OC}(k) - V(k)) - hA(T(k) - T_c))\frac{\Delta t}{mc_p} + T(k) \tag{3.31}$$

Equality constraints are used to relate the dynamic state of the battery to its charge-discharge power schedule within the optimization program. Equation 3.32 relates the system power P at time step k to the cell current I, cell voltage V, number of cells per pack N_{cells}, and the total number of packs N_{packs} in the system. The remaining equality constraints of Equations 3.33–3.37 bind the dependent state variables to the decision variables P.

$$\forall k \;\; P(k) = (I(k)V(k))N_{\text{cells}}N_{\text{packs}} \tag{3.32}$$

$$\forall k \;\; V_{SOC}(k+1) = \begin{cases} V_{SOC,i} & \text{if } k = 0 \\ -\frac{I(k)}{C_c^d}\Delta t + V_{SOC}(k) & \text{if } k > 0 \end{cases} \tag{3.33}$$

$$\forall k \;\; V_{t,s}(k+1) = \begin{cases} V_{t,s,i} & \text{if } k = 0 \\ \left(\frac{I(k)}{C_{t,s}} - \frac{V_{t,s}(k)}{R_{t,s}C_{t,s}}\right)\Delta t + V_{t,s}(k) & \text{if } k > 0 \end{cases} \tag{3.34}$$

$$\forall k \;\; V_{t,\ell}(k+1) = \begin{cases} V_{t,\ell,i} & \text{if } k = 0 \\ \left(\frac{I(k)}{C_{t,\ell}} - \frac{V_{t,\ell}(k)}{R_{t,\ell}C_{t,\ell}}\right)\Delta t + V_{t,\ell}(k) & \text{if } k > 0 \end{cases} \tag{3.35}$$

$$\forall k \;\; V(k) = V_{OC}(k) - I(k)R_s(k) - V_{t,s}(k) - V_{t,\ell}(k) \tag{3.36}$$

$$\forall k \;\; T(k+1) = \begin{cases} T_i & \text{if } k = 0 \\ (N_{\text{cells}} I(k)(V_{OC}(k) - V(k)) - hA(T(k) - T_c))\frac{\Delta t}{mc_p} + T(k) & \text{if } k > 0 \end{cases} \tag{3.37}$$

In addition to equality constraints describing the dynamics of the battery, equality constraints are used to define the variables open-circuit voltage V_{OC} and series resistance R_s, as given in Equations 3.38 and 3.39. The voltage model parameters $R_{t,s}$, $C_{t,s}$, $R_{t,\ell}$, and $C_{t,\ell}$ are scalars as defined in Table 3.4. Similarly, the thermal model parameters h, A, m, and c_p are scalars as defined in Table 3.5. The degraded battery capacity at the beginning of the operating day C_c^d is calculated using Equation 3.25.

$$\begin{aligned} \forall k \;\; V_{OC}(k) = -0.99\exp(-53.6V_{\text{SOC}}(k)) + 3.39 + 0.858V_{\text{SOC}}(k) \\ - 0.787V_{\text{SOC}}(k)^2 + 0.744V_{\text{SOC}}(k)^3 \end{aligned} \tag{3.38}$$

$$\forall k \;\; R_s(k) = 1.19 \times 10^{-8} \;\; \exp(3,830/T(k)) \tag{3.39}$$

The capacity loss incurred over the operating day C_{loss}^d is calculated as the difference between the initial capacity ratio at the beginning of the day $(C_c^d/C_c^i)^i$ and the capacity ratio at the end of the operating day in question $(C_c^d/C_c^i)^e$. These ratios are defined according to Equations 3.40 and 3.41 based on the formula given in Equation 3.25. The index i is used for the battery state variables during the battery's lifetime prior to the operating day, and the index k is used for the battery state variables during the operating day in question.

$$(C_c^d/C_c^i)^i = 1 - \left(\sum_i^{\text{lifetime}} a(T(i), V(i))^{4/3} \Delta t \right)^{3/4} - \sum_i^{\text{lifetime}} b(T(i)) q_{Ah}(i) \tag{3.40}$$

$$\begin{aligned}(C_c^d/C_c^i)^e = 1 - &\left(\sum_i^{\text{lifetime}} a(T(i), V(i))^{4/3} \Delta t + \sum_k^{\text{day}} a(T(k), V(k))^{4/3} \Delta t \right)^{3/4} \\ &- \sum_i^{\text{lifetime}} b(T(i)) q_{Ah}(i) - \sum_k^{\text{day}} b(T(k)) q_{Ah}(k)\end{aligned} \tag{3.41}$$

$$C_{\text{loss}}^d = (C_c^d/C_c^i)^e - (C_c^d/C_c^i)^i \tag{3.42}$$

The charge throughput of the battery q_{Ah} is equal to the total charge passed through the battery during cycling. The charge throughput at time step k is approximated by equally allocating cycling degradation between charging and discharging, according to Equation 3.43. Because the absolute value function used in Equation 3.43 has a discontinuity in its derivative at zero, Equation 3.44 is used to approximate $q_{Ah}(k)$ within the optimization program, which requires smooth functions to describe each of its variables. The hyperbolic tangent function $\tanh(x)$ quickly approaches -1 for negative values of x and 1 for positive values of x.

$$q_{Ah}(k) = |I(k)| \Delta t/2 \tag{3.43}$$

$$q_{Ah}(k) \approx I(k) \tanh(20 I(k))/2 \tag{3.44}$$

Finally, the inequality constraints of Equations 3.45–3.48 are used to bound the relevant state variables within limits established by the battery system operator

or battery cell manufacturer, so that an optimal charge-discharge schedule can be found that does not violate the battery's limits.

$$\forall k \;\; I_{\text{charge,max}} \leq I(k) \leq I_{\text{discharge,max}} \tag{3.45}$$

$$\forall k \;\; V_{\min} \leq V(k) \leq V_{max} \tag{3.46}$$

$$\forall k \;\; SOC_{\min} \leq V_{SOC}(k) \leq SOC_{\max} \tag{3.47}$$

$$\forall k \;\; T_{\min} \leq T(k) \leq T_{\max} \tag{3.48}$$

Table 3.8: Values for the operating parameters that define the inequality constraints of Equations 3.45–3.48 are developed based the specifications for the system considered and practical operational limits on state of charge.

Operating Parameter	Value
$I_{\text{charge,max}}$	15 A
$I_{\text{discharge,max}}$	15 A
$V_{\min}$	2.75 V
$V_{\max}$	4.2 V
$SOC_{\min}$	10%
$SOC_{\max}$	100%
$T_{\min}$	278 K
$T_{\max}$	318 K

Based on the specifications for the battery cell considered and other operational limitations, the variables are bound as given in Table 3.8. State of charge is constrained to be greater than 10% as a factor of safety, so that the battery can

deliver the energy it commits to the electricity market even in the case of model error or another contingency.

The following chapter will implement the optimization program described here to demonstrate how it could be used to schedule the battery system in a particular electricity market context. Results from this analysis will be used to gauge the robustness of the model and approximate the revenue potential of Li-ion storage under various scenarios.

3.3 Chapter Conclusion

This chapter has developed methods to extract information about the dynamic performance and degradation of a Li-ion battery system, and then incorporate this information into an optimization program for operational management of the battery in an electricity market. Section 3.1 introduced empirical models to describe voltage, temperature, and capacity degradation, and then demonstrated how to extract the model parameters for a particular battery system. Then, Section 3.2 discretized the model equations, and integrated them within a nonlinear optimization program to schedule the operation of the battery during a given operating day. The optimization program developed can schedule the operation of the battery in any grid application where the instantaneous level of battery power is the quantity of interest. Moreover, the objective function of the optimization program includes the incremental capacity loss caused by operation of the battery, so that capacity degradation can be penalized within the optimization framework, and therefore minimized.

It is important to note that the optimization program developed here could be used to manage the operation of any Li-ion battery system, provided it can be characterized using the methods and models introduced in Section 3.1. To demonstrate

use of the optimization program and test its robustness, the following chapter applies it to the case of Li-ion energy storage operating in Texas's electricity market.

Chapter 4

Operational Management of Lithium-Ion Energy Storage in Texas's ERCOT Electricity Market and Assessment of Its Revenue Potential[1]

The previous chapter introduced a framework to characterize and model the voltage, temperature, and capacity degradation behavior of a lithium-ion (Li-ion) battery system, and then incorporate this information into an optimization program to schedule the battery's participation in an electricity market. To demonstrate how the framework developed in the previous chapter is applied to a particular system and market context, this chapter applies the framework to the case of Li-ion energy storage operating in Texas's restructured electricity market, which is administered by the Electric Reliability Council of Texas (ERCOT). First, an optimization objective function and decision variables are developed for a battery system that provides energy and ancillary services to ERCOT. Second, historic ERCOT price data from 2002–2014 are used to test how the optimization program responds to different price scenarios and assess its robustness. Results from the optimization are used to assess the battery's revenue potential, and gauge the value of considering capacity degradation in grid battery operational management. Scenarios are considered to show the effect of uncertain or variable parameters, including end-of-life capacity, operating temperature, and price foresight.

[1]Portions of this chapter were previously published in: Fares, R. L., and Webber, M. E. (2014). A flexible model for economic operational management of grid battery energy storage. *Energy*, 78, 768-776. Michael E. Webber contributed to the work as the research supervisor.

The remainder of this chapter is organized as follows: Section 4.1 introduces the ERCOT market and develops an optimization objective function and decision variables to schedule the battery for energy and ancillary services. Section 4.2 applies the optimization program to historic ERCOT price data to simulate operation of the battery for wholesale energy arbitrage only (Section 4.2.1) and a combination of energy and ancillary services (Section 4.2.2), and assess its revenue and lifetime under various operating scenarios. Finally, Section 4.3 summarizes this chapter's key findings.

4.1 Objective Function for Energy and Ancillary Services in ERCOT

To reliably and economically distribute electric energy around Texas, ERCOT organizes markets for both energy and ancillary services. The energy market facilitates transactions for bulk electric energy sold to end users. The ancillary services market is a smaller market set up by ERCOT to procure capacity required to maintain reliable operation of the power system, including in the case of a contingency. Table 4.1 provides a description for each of the ancillary services in the ERCOT market.

ERCOT calculates the price of energy and ancillary services through an auction process, which begins 24 hours before the operating day. ERCOT market operations can be divided into three phases: the day-ahead period, the adjustment period, and the operating period.

During the day-ahead period, ERCOT first publishes the conditions of the grid system, its forecast for system-wide load, and the amount of ancillary services capacity it will procure for reliability purposes [16]. Then, electricity resources submit hourly

Table 4.1: ERCOT procures the given ancillary services from electric generation, load resources, and energy storage to maintain adequate control of grid frequency at all times [16].

Ancillary Service	Description
	Regulation Services
Regulation Up (RU)	The capability to increase power output within five seconds to correct downward deviations in grid frequency
Regulation Down (RD)	The capability to decrease power output within five seconds to correct upward deviations in grid frequency
Fast Responding Regulation Up (FRRU)	The capability to increase power output within 60 cycles (one second) to correct downward deviations in grid frequency
Fast Responding Regulation Down (FRRD)	The capability to decrease power output within 60 cycles (one second) to correct upward deviations in grid frequency
	Reserve Services
Responsive Reserve (RRS)	The capability to increase power output within a few seconds to arrest system frequency decay during a contingency event
Non-Spinning Reserve (NSRS)	The capability to increase power output within 30 minutes to arrest system frequency decay during a contingency event

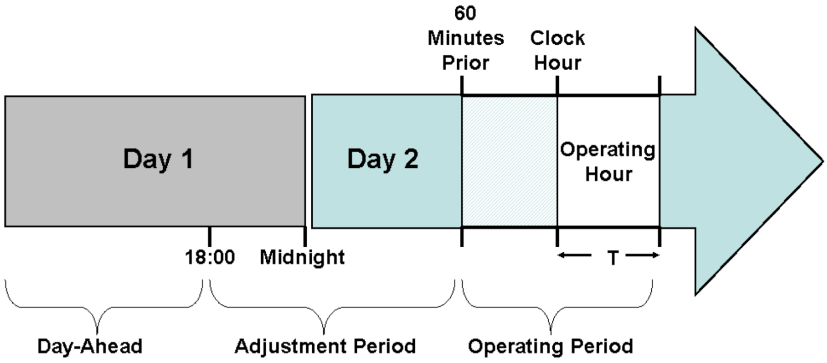

Figure 4.1: The Electric Reliability Council of Texas (ERCOT) market timeline consists of a day-ahead period, an adjustment period, and an operating period [16].

ancillary service and energy offers. An ancillary service offer specifies the amount of capacity offered (in MW) and the resource operator's willingness to sell that capacity (in $/MW per hour). An energy offer consists of a monotonically increasing offer curve indicating both price (in $/MWh) and quantity (in MW) from an electric generating resource [16]. At 10:00 am of the day-ahead period, ERCOT uses a mixed-integer linear program to decide which resources should be online to minimize the overall cost of electricity while consistently meeting electric demand, thereby clearing the market and establishing an hourly day-ahead price for energy and ancillary services [16].

The adjustment period begins at 6:00 pm on the day preceding the operating day, after the day-ahead market has cleared, and continues until 60 minutes in advance of the operating hour [16]. During the adjustment period, electricity resources can update their energy offer curves, or register a self-assigned output schedule with ERCOT [16]. An output schedule specifies a resource's output (in MW) during each 5-minute interval remaining in the operating day for which an energy offer curve has not been submitted [16].

The operating period immediately follows the adjustment period, and consists of the operating hour and the hour immediately preceding it [16]. During the operating period, ERCOT uses information provided by electricity resources during the adjustment period and commitments made in the day-ahead market to compute the power output required from each online resource to minimize the overall cost of electricity while maintaining electric reliability [16]. This security-constrained economic dispatch (SCED) process clears the market, and establishes a real-time price for energy for each 15-minute interval of the day [16].

The market price of energy varies both temporally and spatially due to diurnal variations in electric demand and the effect of electricity transmission con-

straints. ERCOT establishes a time-varying locational-marginal price (LMP) at over 8,000 nodes located throughout the transmission grid [16]. For practical purposes, ERCOT calculates the load-weighted average price for the state's four major load regions, designated North, Houston, South, and West, as identified in Figure 4.2. Unlike the energy price, market prices for ancillary services vary only temporally and not spatially, because the grid's electrical frequency is synchronized throughout the transmission system.

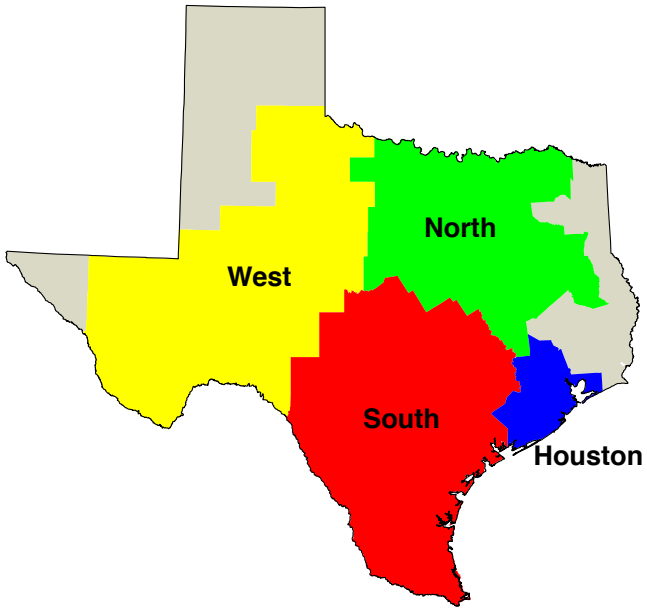

Figure 4.2: ERCOT calculates prices for four regional hubs, designated North, Houston, South, and West. The hub price represents a load-weighted average of the nodal LMPs within a given region [16].

Battery energy storage can provide electric energy to ERCOT by performing wholesale energy arbitrage: buying low-cost electricity for later sale during on-peak hours, when the price for electricity is higher. A battery can also provide ancillary services by committing to either discharge or charge on demand in order to increase or decrease its net power output. Notably, batteries can respond more quickly to grid

operator signals than conventional forms of electricity generation, so they can offer "fast" ancillary services such as FRRU and FRRD identified in Table 4.1. ERCOT accepts interconnection requests from electricity generators and storage devices with a rated power capacity of 10 MW or greater [111]. Even if a storage device is smaller than 10 MW, it could be aggregated with other small storage devices by a qualified scheduling entity (QSE) to facilitate its interaction with the ERCOT market. Storage resources that have been accepted for interconnection to ERCOT can purchase charging electricity from and sell stored electricity to the ERCOT electricity market at the corresponding real-time energy price [111].

Operation of a single battery pack is considered for the purposes of demonstrating the proposed optimization program and assessing the revenue potential of the battery under different scenarios. Li-ion systems of various sizes could be constructed by interconnecting battery packs in series and parallel. Thus, the results for a single battery pack can be scaled to approximate the revenue potential of Li-ion battery systems of various sizes.

The battery could provide a combination of energy and ancillary services to the market. Ancillary services FRRU and FRRD are selected from the list given in Table 4.1, because they are designed for fast-responding resources like a battery system, and the price for regulation service is typically higher than the price for reserves. Capacity committed for FRRU and FRRD is deployed based on how much frequency has deviated from 60 Hz, using a methodology specified by ERCOT [112].

The optimization program discussed in the previous section is implemented to manage the operation of the battery system for wholesale energy arbitrage and Fast Responding Regulation Service (FRRS) in ERCOT. To develop an objective function to maximize revenue and minimize degradation during a given operating day, equa-

tions are developed to represent daily revenue from energy arbitrage, daily revenue from FRRS, and the marginal "cost" of battery capacity loss. The equations are written in terms of the battery's DC power P to simplify the optimization program, based on the assumption that any energy losses in the power conditioning system (PCS) that connects the battery to the grid do not significantly affect the decision of when to offer power to the market. These losses and energy used for the thermal controls will included in the estimate of annual revenue potential presented later in this chapter.

Because ERCOT establishes a real-time price for electricity every 15 minutes [16], the revenue from wholesale energy arbitrage is written in terms of the battery power provided for energy P_E during every quarter-hour interval, q, of the day. Equation 4.1 defines the daily revenue from the energy market R_E^d, where negative values of $P_E(q)$ denote charging power, positive values of $P_E(q)$ denote discharging power, and $\pi_E(q)$ denotes the price for electricity during price settlement interval q of duration $\Delta t_q = 15$ minutes. In practical operation, a predicted or published value would be used for the energy price π_E in the objective function. The following section shows the results of the optimization with historic prices assuming perfect foresight, and then tests the value of perfect foresight versus day-ahead foresight only.

$$R_E^d = \sum_q P_E(q) \Delta t_q \pi_E(q) \tag{4.1}$$

ERCOT establishes a price for frequency regulation service on an hourly basis. Capacity procured for FRRU, $C_{FRRU}(h)$, during a given hour h is paid the corresponding market price for regulation up $\pi_{RU}(h)$. Likewise, capacity procured for FRRD, $C_{FRRD}(h)$, during a given hour h is paid the corresponding market price for regulation down $\pi_{RD}(h)$. The actual power output of a battery committed for

FRRS is determined from the dispatch order assigned by ERCOT within each operating hour. The dispatch of the battery for FRRS is modeled at time steps k of duration $\Delta t = 12$ seconds. Equation 4.2 defines the battery power dispatched for FRRS, P_{FRRS}, as a function of the dispatch orders for up regulation, D_{FRRU}, and down regulation, D_{FRRD}, at each time step k. Both D_{FRRU} and D_{FRRD} range from 0 to 1 and represent the fraction of committed capacity dispatched at time step k.

$$\forall h, \forall k \in h, \;\; P_{FRRS}(k) = C_{FRRU}(h) D_{FRRU}(k) - C_{FRRD}(h) D_{FRRD}(k) \tag{4.2}$$

To approximate the dispatch orders D_{FRRU} and D_{FRRD} that would be assigned to a battery, data provided by ERCOT from an FRRS pilot project are used. The data provide the dispatch orders assigned to battery committed for FRRS during the month of April, 2013 [112]. Before the optimization program is executed, dispatch orders are generated by sampling a random day from the month of data provided by ERCOT [112], and then these data are used by the optimization program. Figure 4.3 shows sample FRRS dispatch data collected on April 10, 2013. The battery is dispatched at various levels of power depending on the level of grid frequency using a methodology established by ERCOT. Dispatch orders do not last longer than 60 seconds [112].

Any power dispatched for FRRS is credited at the prevailing energy price $\pi_E(q)$. The daily revenue from FRRS, R^d_{FRRS}, is equal to revenue from any capacity procured plus the net revenue or cost of dispatched power, as given in Equation 4.3. In practical operation, the regulation prices π_{RU}, π_{RD}, and dispatch orders D_{FRRU} and D_{FRRD} would be approximated using heuristic or predicted values. To apply the optimization program, the following section assumes perfect foresight using historic data, and then shows results for the case of day-ahead foresight only.

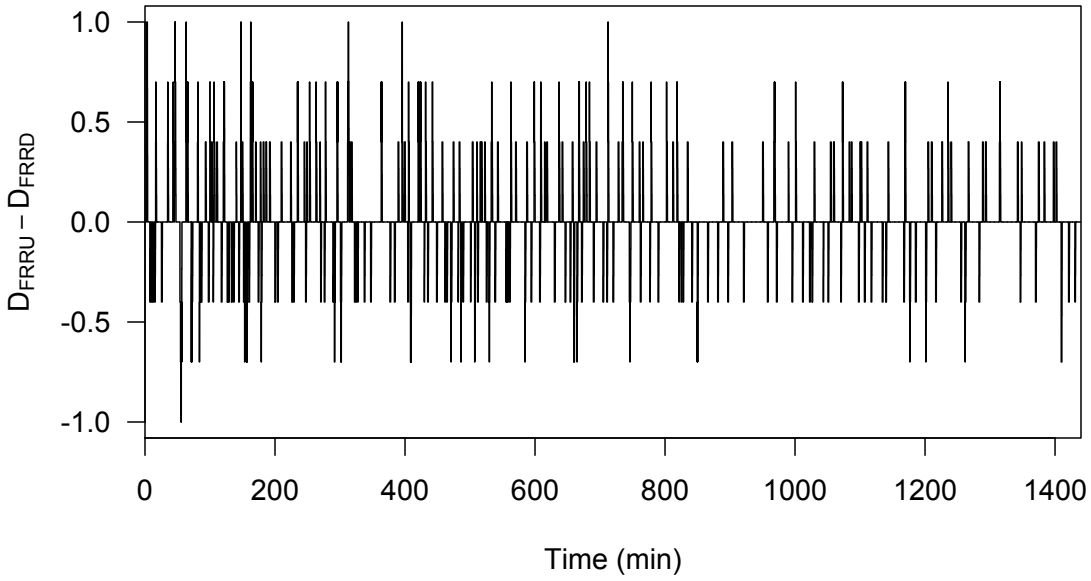

Figure 4.3: The FRRS dispatch orders D_{FRRU} and D_{FRRD} are approximated using data provided by ERCOT. Data shown here were collected on April 10, 2013.

$$R^d_{FRRS} = \sum_h (C_{FRRU}(h)\pi_{RU}(h) + C_{FRRD}(h)\pi_{RD}(h)) + \sum_q \sum_{k \in q} P_{FRRS}(k)\pi_E(q)\Delta t \tag{4.3}$$

To consider the impact of capacity degradation within the optimization objective function, the "cost" of capacity degradation over the day $\Gamma^d_{\text{degradation}}$ is calculated as a function of the end-of-life capacity of the battery C_{end}, the price of the battery modules π_{modules}, and the capacity loss over the operating day, C^d_{loss}, as given in Equation 4.4. This formulation corresponds to $\Gamma^d_{\text{degradation}} = \pi_{\text{modules}}$ for the limiting case where the capacity loss over one day causes the battery to reach its end-of-life capacity ($C^d_{\text{loss}} = 1 - C_{\text{end}}$).

$$\Gamma^d_{\text{degradation}} = \pi_{\text{modules}} \frac{C^d_{\text{loss}}}{1 - C_{\text{end}}} \tag{4.4}$$

The cost of the battery modules is approximated using the Battery Performance and Cost Model (BatPaC) developed by Argonne National Laboratory. Chapter 6 discusses cost modeling of the battery in detail. Table 4.2 provides values for π_{modules} and C_{end}. The normalized cost of the modules in \$/kWh is also provided for reference. A base-case value $C_{\text{end}} = 0.65$ is assumed based on the discussion of Section 3.1.4.

Table 4.2: Values for the cost of the battery modules and the end-of-life capacity are approximated to account for the cost of battery degradation in the objective function.

Parameter	Value
Total battery modules cost (π_{modules})	\$7,870
Normalized battery modules cost	\$262/kWh
End-of-life capacity (C_{end})	0.65

The general objective function to be maximized is written by combining Equations 4.1–4.4, as given in Equation 4.5. The following sections will consider various forms of this objective function to show the revenue potential of a battery used for energy only versus energy and ancillary services, and the lifetime of a battery operated when capacity loss is penalized with $\Gamma^d_{\text{degradation}}$ versus when capacity loss is neglected ($\Gamma^d_{\text{degradation}} = 0$).

$$Obj = R^d_E + R^d_{FRRS} - \Gamma^d_{\text{degradation}} \tag{4.5}$$

To constrain the battery within its operational limits, bounds are developed for the optimization decision variables. The amount of power capacity the battery can

offer for FRRS is constrained within a value $P_{\max} = 40$ kW, which is greater than the battery's design power but less than its maximum technical power capability. This value is selected because the battery would rarely be dispatched at the full power it has committed for FRRS [112]. The constraint of Equation 3.45 is still imposed at every time step k to ensure the instantaneous current rate does not exceed the rate specified in Table 3.8 (1 C = 15 A per cell). The same bound $P_{\max}$ is imposed on the variable P_E to reduce the domain, though this constraint is superseded by the constraint of Equation 3.45 within the optimization program. Furthermore, the constraints of Equations 4.9 and 4.10 are applied to ensure the battery does not offer more combined power capacity than $P_{\max}$ for energy and FRRS.

$$\forall q, \;\; P_{\max} \leq P_E(q) \leq P_{\max} \tag{4.6}$$

$$\forall h, \;\; P_{\max} \leq C_{FRRU}(h) \leq P_{\max} \tag{4.7}$$

$$\forall h, \;\; P_{\max} \leq C_{FRRD}(h) \leq P_{\max} \tag{4.8}$$

$$\forall h, \forall q \in h, \;\; P_E(q) + C_{FRRU}(h) \leq P_{\max} \tag{4.9}$$

$$\forall h, \forall q \in h, \;\; P_E(q) - C_{FRRD}(h) \geq -P_{\max} \tag{4.10}$$

To relate the objective function to the equations that define the battery's dynamic state and capacity loss over the day, Equation 4.11 relates the battery power P to power dispatched for energy arbitrage P_E and the power dispatched for FRRS

P_{FRRS}. The remaining equality and inequality constraints that describe the dynamic state of the battery and its operating limits are defined as given in Section 3.2, with a dynamic time step $\Delta t = 12$ seconds and a domain of one operating day or 24 hours.

$$\forall q, \forall k \in q, \quad P(k) = P_E(q) + P_{FRRS}(k) \tag{4.11}$$

The following section demonstrates the use of this optimization framework using historic ERCOT data from 2002–2014 to simulate the operation of the battery over several years.

4.2 Simulation of Market Operation Using Historic Price Data

The objective of this section is to apply the optimization framework to the specified Li-ion battery pack operating in the ERCOT market. Results from this analysis will be used to show how the optimization program responds to electricity prices under various scenarios, approximate the revenue potential of the battery system, and assess its lifetime.

For the purposes of this analysis, perfect foresight of electricity prices is assumed, so that the maximum potential revenue of the battery under historic price scenarios can be evaluated. Price data are collected from ERCOT, which releases historic prices for energy and ancillary services to the public [113]. To show geographic variations in battery revenue potential, prices from ERCOT zones/hubs North, Houston, South, and West are used. Before December 2010, ERCOT operated a "zonal" market, where generation was balanced between four pricing zones [114]. The energy price was called the market clearing price for energy (MCPE) and was set based on the load-generation balance within each zone and the flow of balancing energy between

zones [114]. Beginning December 2010, ERCOT transitioned to a "nodal" market, with LMPs established at over 8,000 nodes across the state. ERCOT provides the load-weighted average of LMPs at hubs corresponding to the four pricing zones that existed before December 2010 [114]. To consider operation of a battery over many years, the zonal MCPE is used for 2002–November 2010, and the nodal real-time hub energy price is used for December 2010–2014 as the energy price π_E used by the optimization program. Similarly, the hourly market clearing price for capacity (MCPC) from 2002–2014 is used as an input to the optimization program for ancillary service prices π_{RU} and π_{RD}.

A constant coolant temperature of $T_c = 5$ °C is assumed, because operating at a lower temperature significantly decreases the rate of degradation, and it is assumed 5 °C is the minimum temperature at which full battery power could be reliably produced [94]. To show the effect that higher coolant temperatures have on the lifetime of the battery system, the simulation is repeated with a coolant temperature of 15 °C and 25 °C.

To reduce computation time so that operation from 2002–2014 can be simulated, the capacity loss over the day C^d_{loss} defined in Equations 3.40–3.42 is approximated according to Equations 4.12–4.13. Before the optimization program is executed, the capacity ratio at the beginning of the day is calculated according to Equation 3.40. Then, within the optimization program the capacity ratio at the end of day is approximated by sampling the battery's state at every 20 time steps (every 4 minutes), as given in Equation 4.12. This approximation is used because the voltage and temperature do not vary significantly over small time scales, and they have the strongest effect on battery degradation. The capacity loss over the day C^d_{loss} is approximated according to Equation 4.13. The approximation is found to significantly

reduce optimization computation time without strongly affecting the solution.

$$(C_c^d/C_c^i)^e \approx 1 - \left(\sum_{i=1,2,\cdots}^{\text{lifetime}} a(T(i),V(i))^{4/3}\Delta t + \sum_{k=20,40,\cdots}^{\text{day}} a(T(k),V(k))^{4/3}\ 20\Delta t \right)^{3/4} - \sum_{i=1,2,\cdots}^{\text{lifetime}} b(T(i))q_{Ah}(i) - \sum_{k=20,40,\cdots}^{\text{day}} b(T(k))\ 20q_{Ah}(k) \tag{4.12}$$

$$C_{\text{loss}}^d \approx (C_c^d/C_c^i)^e - (C_c^d/C_c^i)^i \tag{4.13}$$

Two different operational scenarios are considered: 1) a battery used for wholesale energy arbitrage only that does not offer capacity for FRRS, and 2) a battery that provides both energy and FRRS. For each scenario, the effect that penalizing capacity loss in the objective function has on lifetime is tested. Section 4.2.1 presents results for the case of a battery used for wholesale energy arbitrage only, and then Section 4.2.2 presents results for a battery used for wholesale energy arbitrage and FRRS.

4.2.1 Operation for Wholesale Energy Arbitrage

To schedule the battery for energy arbitrage only, the equality constraints of Equations 4.14 and 4.15 are used to constrain the power offered for FRRS so that it is strictly equal to 0.

$$\forall h,\ \ C_{FRRU}(h) = 0 \tag{4.14}$$

$$\forall h,\ \ C_{FRRD}(h) = 0 \tag{4.15}$$

To demonstrate the effect of considering the capacity loss in the objective function, two different objectives are considered: Equations 4.16 and 4.17. Equation 4.16 considers the cost of capacity degradation $\Gamma^d_{\text{degradation}}$, while Equation 4.17 neglects capacity degradation. The remainder of the optimization program is defined as discussed previously. Table 4.3 summarizes the variables and equations that define the optimization problem.

$$Obj_{CD,E} = R^d_E - \Gamma^d_{\text{degradation}} \tag{4.16}$$

$$Obj_{ND,E} = R^d_E \tag{4.17}$$

Table 4.3: The optimization program for wholesale energy arbitrage considers the following decision and dependent variables with the given equality and inequality constraints.

Variable	Domain	Time Step	Equality Constraints	Inequality Constraints
		Decision Variables		
P_E	q	15 min.	Eq. 4.11	Eq. 4.6, 4.9, 4.10
		Dependent Variables		
P	k	12 sec.	Eq. 3.32, 4.11	Inherited
I	k	12 sec.	Eq. 3.32, 3.44	Eq. 3.45
V_{SOC}	k	12 sec.	Eq. 3.33, 3.38	Eq. 3.47
V_{OC}	k	12 sec.	Eq. 3.36–3.38	Inherited
$V_{t,s}$	k	12 sec.	Eq. 3.34, 3.36	Inherited
$V_{t,l}$	k	12 sec.	Eq. 3.35, 3.36	Inherited
R_s	k	12 sec.	Eq. 3.36, 3.39	Inherited
V	k	12 sec.	Eq. 3.32, 3.36, 3.37, 4.13	Eq. 3.46
T	k	12 sec.	Eq. 3.37, 4.13	Eq. 3.48
q_{Ah}	k	12 sec.	Eq. 3.44, 4.13	Inherited
C^d_{loss}	N/A	N/A	Eq. 4.13	Inherited
R^d_E	N/A	N/A	Eq. 4.1	Inherited
$\Gamma^d_{\text{degradation}}$	N/A	N/A	Eq. 4.4	Inherited

The optimization program is implemented using the General Algebraic Modeling System (GAMS) [115]. An operating period of 24 hours is considered, corresponding to the day-ahead operating timeline of the ERCOT market [16]. Thus, the optimization program considers 96 decision variables (the charging or discharging power $P_E(q)$ during each 15-minute price interval, q) and 7,200 dependent variables (one for each 12-second discretized time step, k) for each of the dependent variables identified in Table 4.3. The nonlinear, interior-point optimization algorithm is used to find optimum values for the decision variables based on the electricity prices entered into the program. The software package R is used to prepare ERCOT price data, enter the data to GAMS, and then store the results of the optimization routine [116].

Figure 4.4 illustrates how the optimization program responds to energy prices from four different operating days in ERCOT South. These days are selected because of they represent different price fluctuations that can occur over the day in ERCOT. Figure 4.4a corresponds to a scenario where the price is between \$0 and \$35/MWh for the duration of the operating day; Figure 4.4b illustrates a moderate price peak (≈\$150/MWh) occurring in the afternoon; Figure 4.4c shows a sudden, high price peak (≈\$500/MWh) occurring in the afternoon; and Figure 4.4d illustrates a moderate price peak occurring in the morning. In each case, results are shown for the objective function that considers the effect of degradation (Equation 4.16), and the objective function that neglects degradation (Equation 4.17). The fact that the charge-discharge schedule returned by the algorithm corresponds to charging when the electricity price is low and discharging when the price is high shows that it responds appropriately to price fluctuations. When the effect of capacity degradation is neglected, the battery cycles frequently to exploit any difference that exists in the energy price. When capacity degradation is controlled, the battery only cycles when the price difference is sufficient to compensate for the capacity loss incurred.

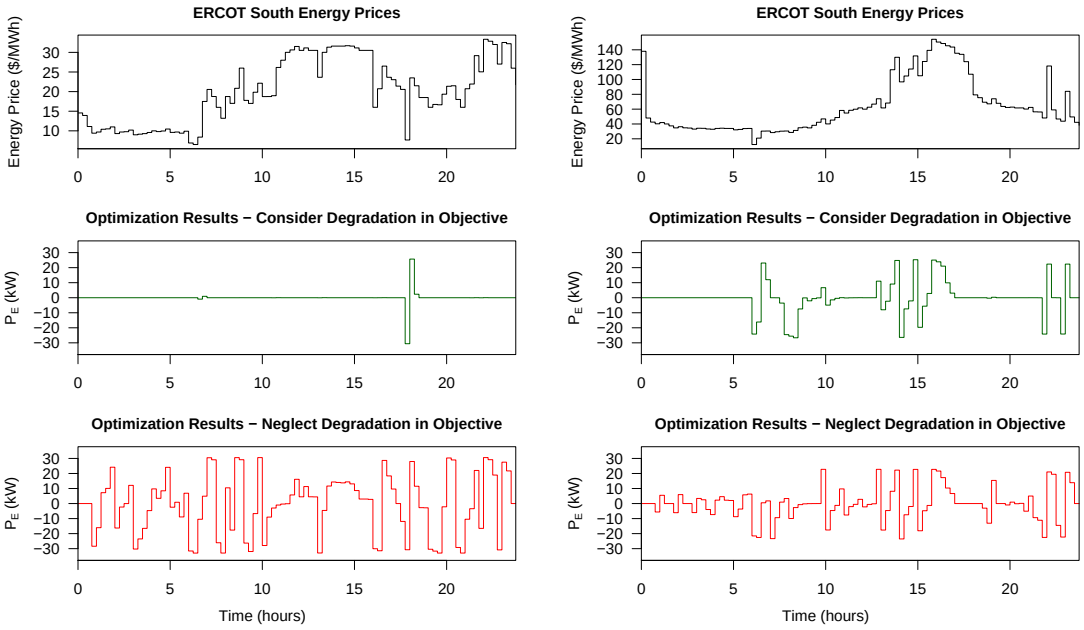

(a) April 10, 2002

(b) July 19, 2006

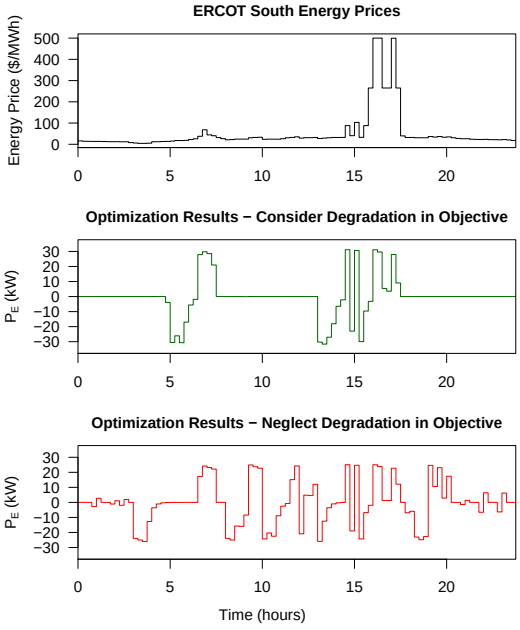

(c) October 27, 2010

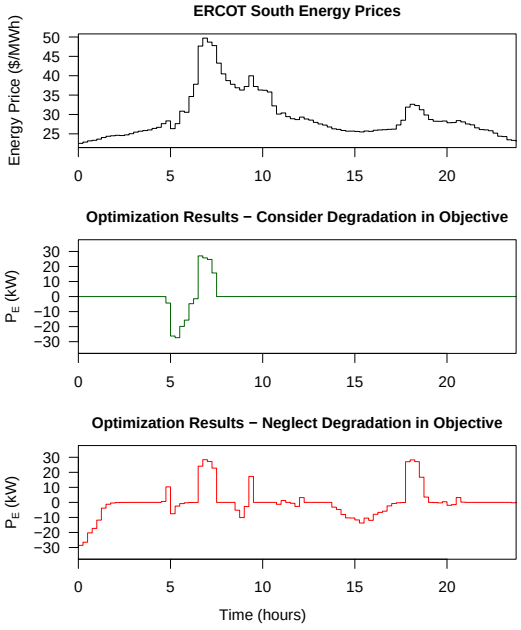

(d) January 15, 2014

Figure 4.4: To illustrate how the optimization program responds to electricity prices, results are shown for four different operating days. The battery preferentially charges when the electricity price is low and discharges when the price is high. When the effect of capacity loss is considered, the battery only performs a charge-discharge cycle when there is a large electricity price difference.

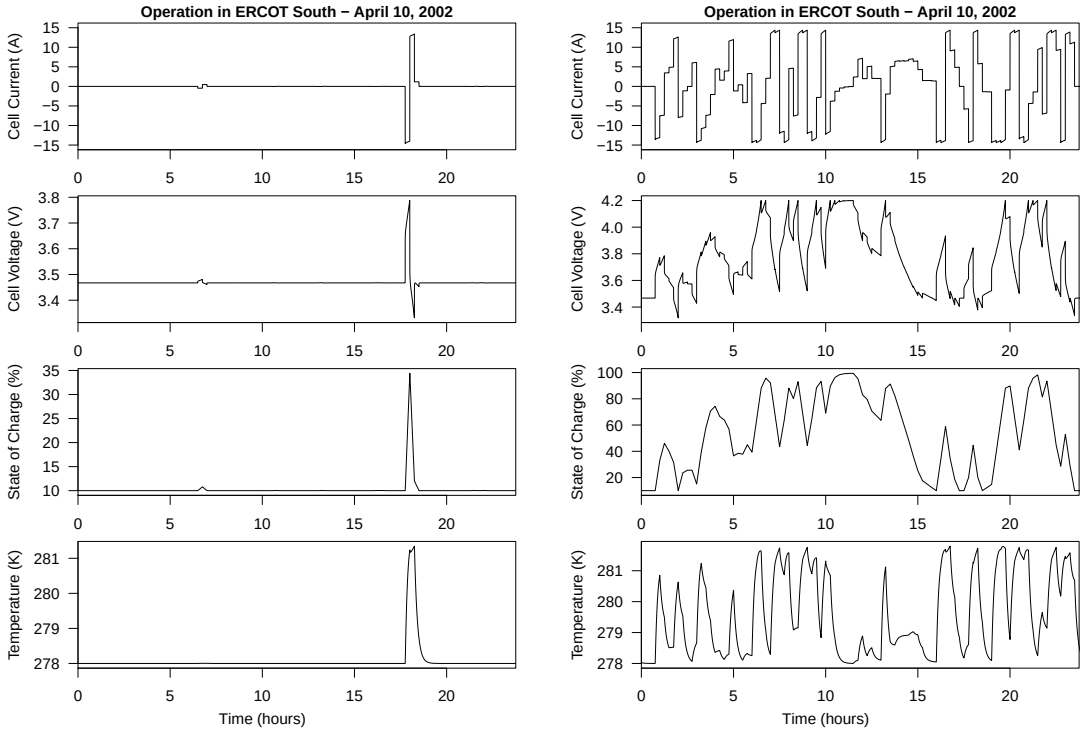

(a) Consider degradation effects (b) Neglect degradation effects

Figure 4.5: The optimization program models the dynamic state of the battery to constrain current, voltage, state of charge, and temperature. When the effect of capacity degradation is penalized in the optimization, higher levels of temperature and voltage are avoided to prolong the battery's life.

Figure 4.5 shows the value of dynamic state variables I, V, V_{SOC}, and T approximated by the battery model encapsulated within the optimization program for the case illustrated in Figure 4.4a. When the effect of capacity degradation is considered in the objective function, the optimization program seeks to minimize temperature gain in the battery and maintain a minimum state of charge and voltage whenever possible, because increasing temperature or voltage increases the rate of capacity loss. On the other hand, when the effect of capacity degradation is not penalized in the objective function, the battery charges and discharges to maximize its operating revenue regardless of its temperature or voltage gain.

To calculate the revenue potential of a battery from its optimal charge-discharge schedule, the actual AC power flowing between the battery and the grid P_{grid} is calculated by accounting for losses in the PCS and power required for the thermal controls. A PCS efficiency $\eta_{\text{AC-DC}} = \eta_{\text{DC-AC}} = 95\%$ is assumed based on information in the literature [21, 117, 118]. The electric power required for cooling P_c is assumed constant and equal to the value specified in Table 3.5, $P_c = 260$ W. The AC power flowing between the battery system and grid is calculated as given in Equation 4.18. Then, the total potential revenue over the day R^d is calculated according to Equation 4.19. The revenue observed over each day is normalized by the battery pack's rated energy capacity $E_{\text{rated}} = 30$ kWh, as given in Equation 4.20.

$$P_{\text{grid}} = \begin{cases} P/\eta_{\text{DC-AC}} - P_c & \text{if charging } (P < 0) \\ \eta_{\text{DC-AC}} P - P_c & \text{if discharging } (P > 0) \\ -P_c & \text{if idle } (P = 0) \end{cases} \tag{4.18}$$

$$R^d = \sum_{q=1}^{96} P_{E,\text{grid}}(q) \Delta t_q \pi_E(q) \tag{4.19}$$

$$R^d_{\text{kWh}} = \frac{R^d}{E_{\text{rated}}} \tag{4.20}$$

To understand how the revenue potential of a Li-ion battery system operating for wholesale energy arbitrage in Texas varies from day to day, the optimization problem is solved for each day of 2002–2014 using electricity prices from each of ERCOT's four hubs. Figure 4.6 illustrates R^d_{kWh} for the case where capacity degradation is considered in the objective function. Likewise, Figure 4.7 illustrates R^d_{kWh} for the case where the effect of capacity degradation is not considered. In each of ERCOT's four trading hubs, the potential revenue from energy arbitrage varies significantly from day to day.

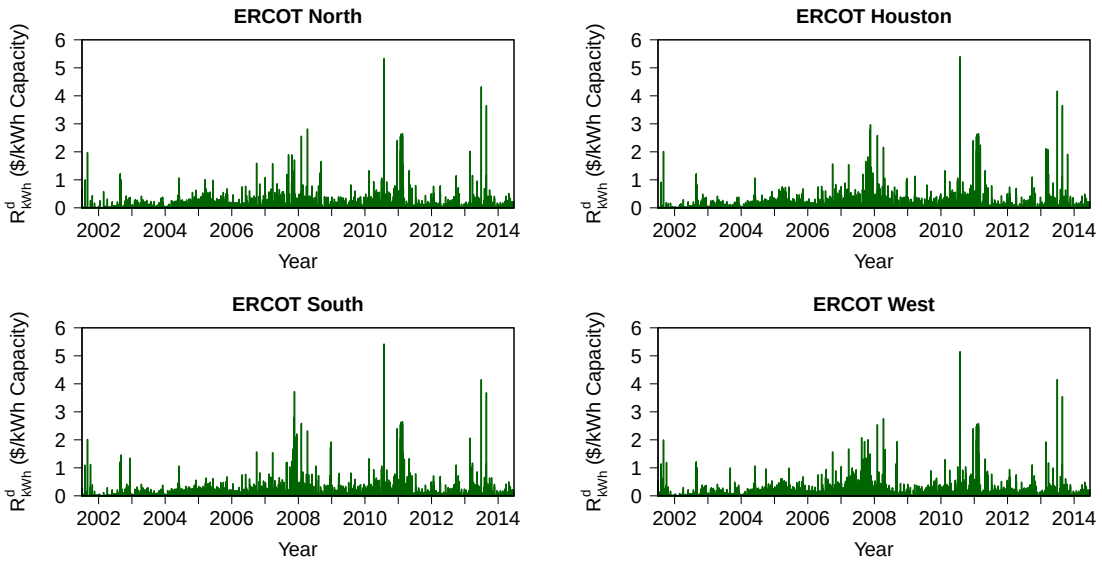

Figure 4.6: The optimization problem is solved using price data from 2002–2014 for each of ERCOT's four trading hubs. Results shown here are for the case where capacity loss is controlled in the objective function, as defined in Equation 4.16.

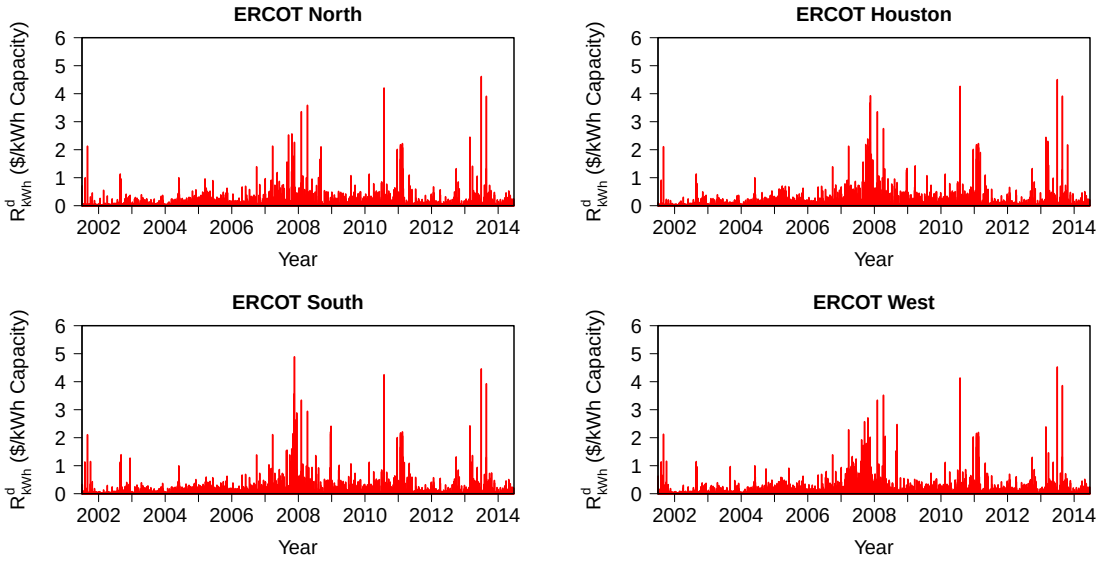

Figure 4.7: The optimization problem is solved using price data from 2002–2014 for each of ERCOT's four trading hubs. Results shown here are for the case where capacity loss is not considered in the objective function, as defined in Equation 4.17.

To approximate the revenue from the sale of stored energy on an annual basis, the total annual revenue per kWh of battery energy capacity is calculated according to Equation 4.21. The top portion of Figure 4.8 shows the annual revenue per kWh of battery capacity R^{y}_{kWh} during each operating year considered. The height of each bar indicates the average revenue across all ERCOT regions, and the ranges illustrated indicate the range of revenues observed across all regions during a given year.

$$R^{y}_{\text{kWh}} = \sum_{d}^{\text{year}} R^{d}_{\text{kWh}} \tag{4.21}$$

To estimate the lifetime of the battery under the operating regimes considered, the capacity ratio at the beginning of each operating day is calculated according to Equation 3.40. The bottom portion of Figure 4.8 shows the value of the capacity ratio over time for each of the cases considered. Note that the corresponding value of degraded capacity is used by the optimization program for each operating day considered, so the results illustrated in the top portion of Figure 4.8 reflect the actual battery capacity available during operation.

When the effect of capacity loss is considered in the objective function, the battery captures less revenue during most of the operating years considered. However, the lifetime of the battery is extended significantly. When the battery responds to price signals in an economic way without considering degradation effects, it operates for approximately 5.6 years before its modeled capacity ratio reaches the end-of-life value of 0.65, and the battery modules are replaced. When capacity loss is considered and controlled in the objective function, the battery can operate for approximately 8.3 years before its modules must be replaced. Thus, considering degradation effects in the optimization objective function extends the battery modules' lifetime by approximately 50%.

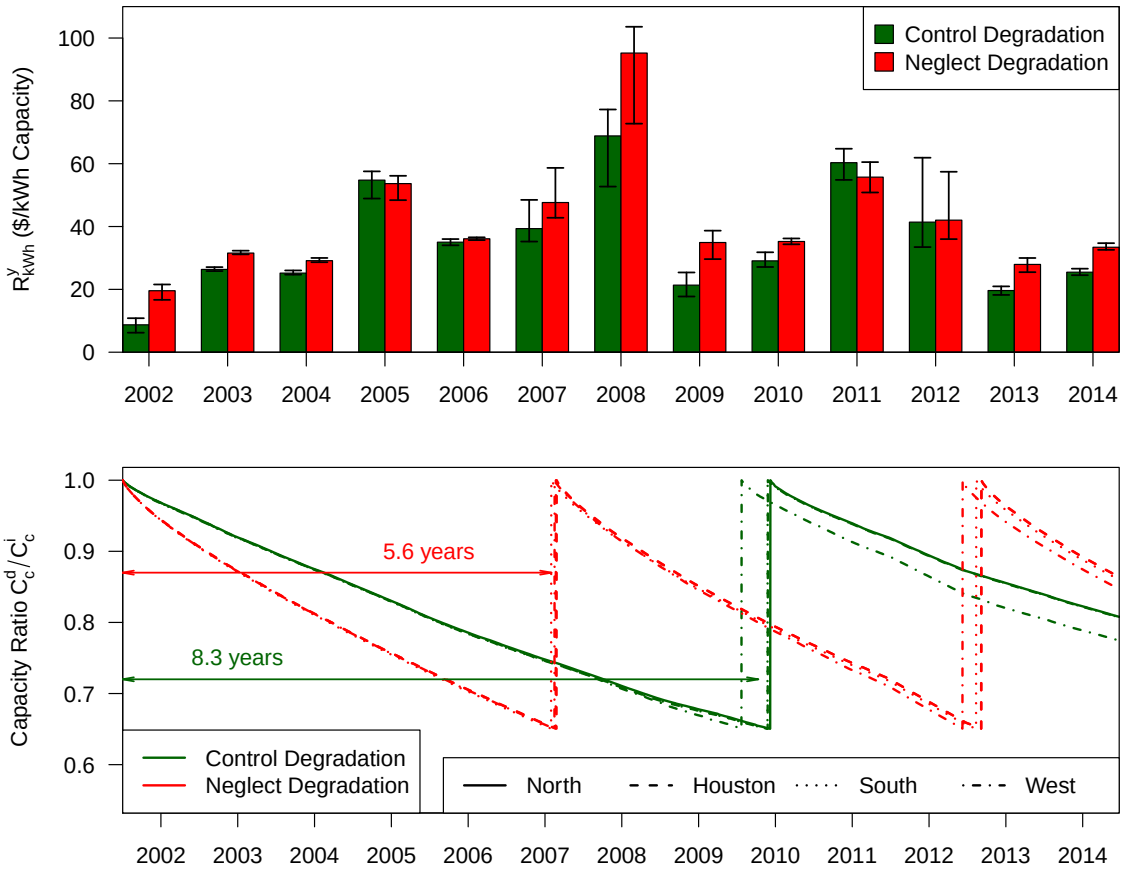

Figure 4.8: The annual revenue potential of the battery system considered is calculated for each of the operating years, ERCOT regions, and objective functions considered. The average annual revenue potential across all ERCOT regions is indicated by the height of each bar, and the observed regional variation in revenue is indicated by the ranges illustrated for each bar. The corresponding modeled capacity loss is illustrated in the bottom portion of the figure. The point at which the battery modules are replaced is indicated by a sudden increase in the capacity ratio. The modules are replaced approximately every 5.6 years when capacity loss is neglected versus 8.3 years when capacity loss is controlled. However, the annual revenue potential is greater when capacity loss is neglected versus when it is controlled.

To gauge the impact that variable and uncertain parameters have on the annual revenue potential and lifetime of the battery used for wholesale energy arbitrage, the following sections test the impact of different values of end-of-life capacity and

operating temperature. Then, the value of perfect price foresight is approximated by calculating the revenue potential of a battery with only day-ahead price foresight.

4.2.1.1 Sensitivity Analysis: End-Of-Life Capacity Ratio

In practical operation, the effective end-of-life capacity ratio of the battery might differ from the value assumed ($C_{\text{end}} = 0.65$), because variation in material properties and manufacturing processes can affect the point at which a Li-ion battery must be retired [102, 109, 119]. Thus, a range of end-of-life capacity ratios from 0.55–0.75 is considered to show the effect this parameter has on the ultimate lifetime and revenue potential of the battery.

The optimization program is implemented as discussed above, with the variables and constraints defined in Table 4.3, and a range of end-of-life capacity ratios $C_{\text{end}} = [0.55, 0.65, 0.75]$. Two different objective functions are considered: Equation 4.16 that penalizes the effect of capacity loss and Equation 4.17 that neglects the effect of capacity loss.

The optimization routine is applied to ERCOT price data from 2002–2014. Because there is not strong regional variation in the annual revenue potential or capacity loss illustrated in Figure 4.8, the optimization routine is only carried out for prices from ERCOT South. This region is selected for the sensitivity analysis because the results obtained for ERCOT South in the previous section are closest to average of the results achieved for all regions. Limiting the analysis to ERCOT South significantly reduces the required computation time, and provides sufficient insight about how temperature affects battery lifetime and revenue.

Results from the optimization routine are used to approximate the revenue potential and lifetime of the Li-ion battery system operating with the range of end-

of-life capacity ratios considered. The annual revenue potential from wholesale energy arbitrage is calculated according to Equations 4.18–4.21, and the degraded capacity ratio of the battery at the beginning of each operating day considered is calculated according to Equation 3.40.

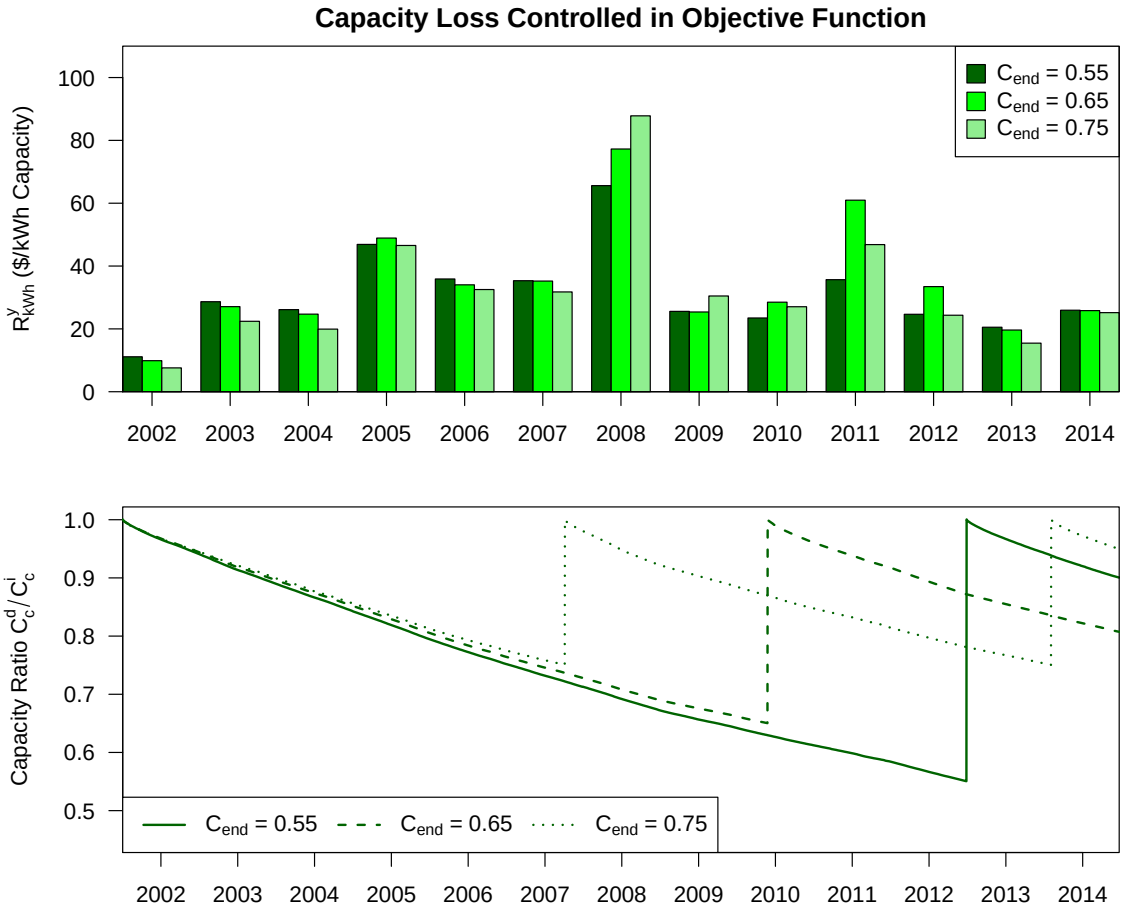

Figure 4.9: The annual revenue potential of the battery system considered is calculated for each of the operating years and end-of-life capacity ratios considered. The corresponding modeled capacity loss is illustrated in the bottom portion of the figure. The end-of-life capacity range considered corresponds to a difference in observed operating lifetime approximately equal to ± 2.5 years.

Figure 4.9 shows the resulting annual revenue potential and capacity degradation behavior for the case where capacity loss is penalized in the objective function

(Equation 4.16). No strong difference in annual revenue potential is observed across the end-of-life capacity ratios considered, with the exception of operating years where the different capacity degradation behavior across the cases considered caused a large difference in the effective energy capacity available for wholesale energy arbitrage (e.g. 2008, 2011).

The end-of-life capacity ratio is found to have a strong effect on the battery's lifetime in years. For the base case value $C_{\text{end}} = 0.65$, the battery lasts approximately 8.4 years before the battery modules are replaced. Decreasing the end-of-life capacity ratio to $C_{\text{end}} = 0.55$ increases the module lifetime to approximately 11 years. Increasing the end-of-life capacity ratio to $C_{\text{end}} = 0.75$ decreases the module lifetime to approximately 6.1 years, prompting 2 required battery module replacements during the 13-year period studied. Notably, the optimization algorithm recognizes the greater "cost" of capacity loss for increasing values of C_{end}, as defined in Equation 4.4, so it seeks to reduce the rate of capacity loss as C_{end} increases. By operating year 2007, the capacity ratio of the battery is noticeably greater for greater values C_{end}.

Figure 4.10 shows similar results for the case where capacity loss is not considered in the objective function, and the battery simply responds to any difference that exists in the real-time electricity market price. Any variation observed in the annual revenue potential is caused by the different battery module replacement intervals required for the three cases, and the corresponding level of energy capacity that is available during a given operating year.

As was found previously, the battery module lifetime is consistently shorter when capacity loss is not penalized in the optimization objective function. For the base case end-of-life capacity value $C_{\text{end}} = 0.65$, the battery modules last approximately 5.6 years before they are replaced, versus 8.4 years for the case where capacity

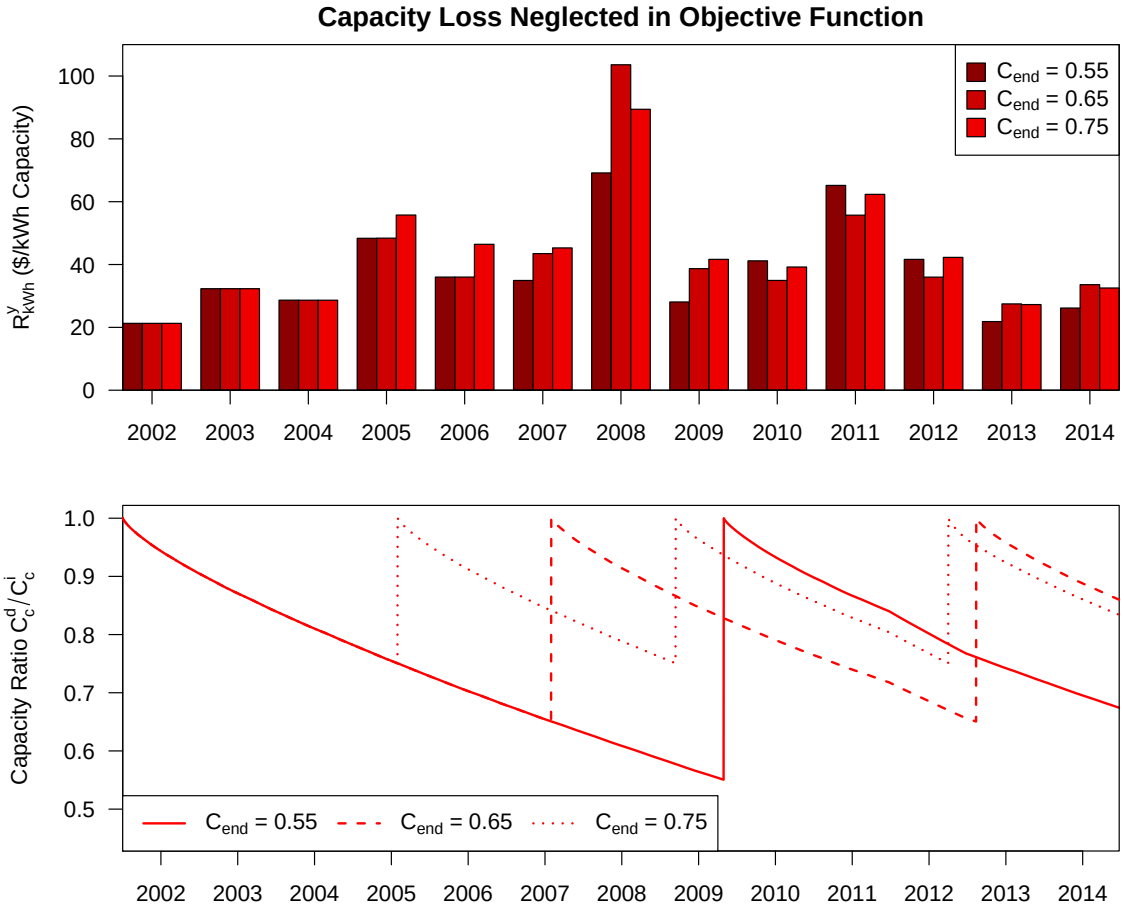

Figure 4.10: The annual revenue potential of the battery system considered is calculated for each of the operating years and coolant temperatures considered. The corresponding modeled capacity loss is illustrated in the bottom portion of the figure. The battery module lifetime is consistently shorter versus the case where capacity degradation is controlled in the objective function (Figure 4.9).

loss is penalized and controlled. When the end-of-life capacity ratio is decreased to $C_{\text{end}} = 0.55$, the lifetime of the battery modules in the uncontrolled case is extended to approximately 7.8 years. Likewise, when the end-of-life capacity ratio is increased to $C_{\text{end}} = 0.75$, the battery module lifetime is shortened to approximately 3.6 years.

In all of the cases considered, penalizing capacity loss in the objective function extends the battery module lifetime by approximately 40–50%. Thus, controlling the

effect of capacity degradation in Li-ion battery operational management as proposed in this work can extend the lifetime of a battery regardless of its end-of-life capacity ratio. However, controlling capacity degradation slightly decreases the annual revenue potential. Thus, there is a tradeoff between reduced revenue and a longer battery module lifetime and better utilization of capital equipment.

4.2.1.2 Sensitivity Analysis: Operating Temperature

To show the effect that operating at an average temperature greater than the 5 °C assumed has on the lifetime and revenue potential of the Li-ion battery system considered, the optimization routine is repeated with coolant temperatures ranging from 5–25 °C ($T_c = [5, 15, 25]$ °C). Because the rate of heat transfer between the coolant and the battery pack is high, the battery typically operates at or near the temperature of the coolant that is pumped between its modules. Thus, considering higher values of T_c shows the effect that higher operating temperatures caused by insufficient thermal management or poor insulation from the environment might have on the lifetime and revenue of the Li-ion battery pack considered.

The optimization program is implemented as discussed above, with the variables and constraints defined in Table 4.3, and a coolant temperature range $T_c = [5, 15, 25]$ °C. Two different objective functions are considered: Equation 4.16 that penalizes the effect of capacity loss and Equation 4.17 that neglects the effect of capacity loss.

The optimization routine is applied to ERCOT price data from 2002–2014. Because there is not strong regional variation in the annual revenue potential or capacity loss illustrated in Figure 4.8 the optimization routine is only carried out for prices from ERCOT South. Limiting the analysis to ERCOT South significantly reduces the required computation time, and provides sufficient insight about how

temperature affects battery lifetime and revenue.

Results from the optimization routine are used to approximate the revenue potential and lifetime of the Li-ion battery system operating at the range of temperatures considered. The annual revenue potential from wholesale energy arbitrage is calculated according to Equations 4.18–4.21, and the degraded capacity ratio of the battery at the beginning of each operating day considered is calculated according to Equation 3.40.

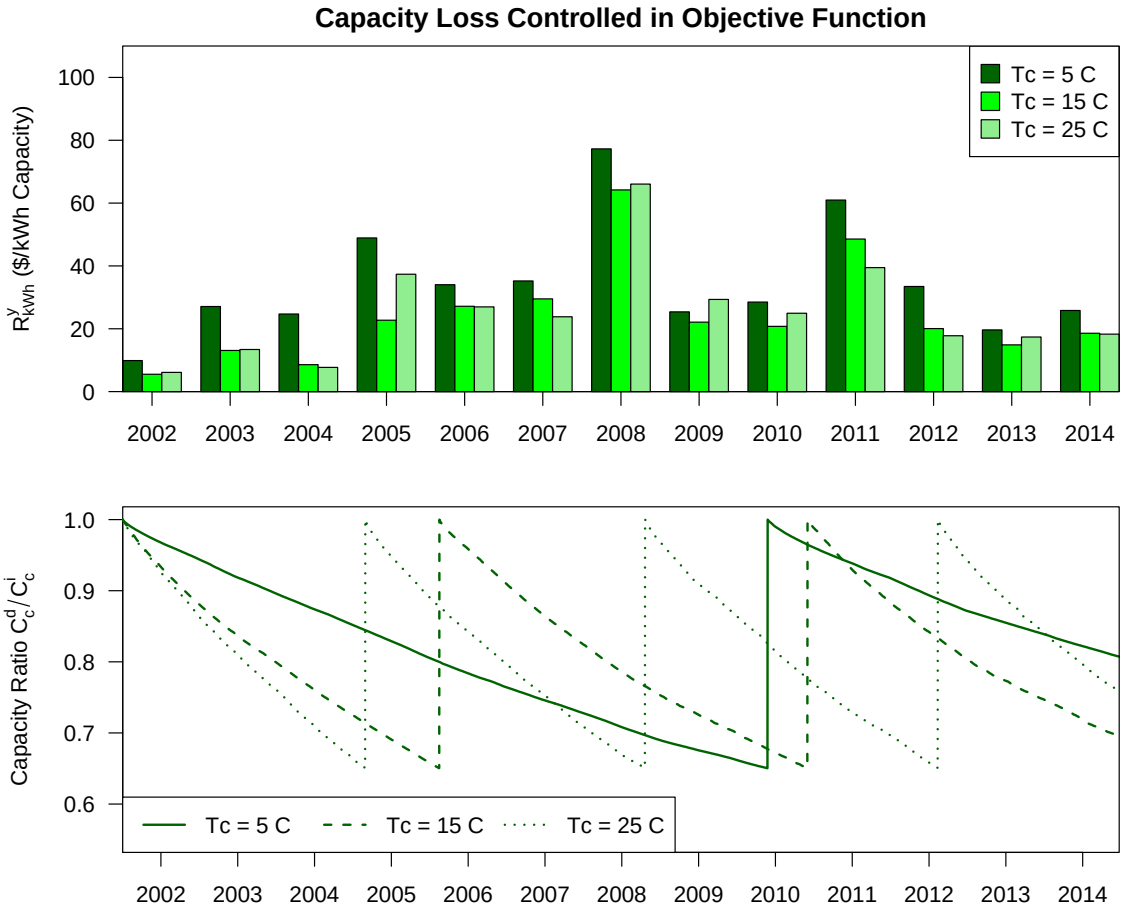

Figure 4.11: The annual revenue potential of the battery system considered is calculated for each of the operating years and coolant temperatures considered. The corresponding modeled capacity loss is illustrated in the bottom portion of the figure. The battery lasts longer and produces more revenue when it is cooled to 5 °C.

Figure 4.11 shows the resulting annual revenue potential and capacity degradation behavior for the case where capacity loss is penalized in the objective function (Equation 4.16). For most of the operating years analyzed, the battery cooled to 5 °C has a greater revenue potential than batteries cooled to 15 °C or 25 °C. This behavior results from the fact that the optimization program seeks to not only maximize energy market revenue, but also control battery degradation. When the battery operates at a higher temperature, the algorithm is less likely to perform a charge-discharge cycle and more likely to maintain a low voltage to extend the battery's lifetime as long as possible.

The operating temperature is found to have a strong effect on the battery's lifetime, as was found from the battery characterization tests carried out in Section 3.1.4. The battery cooled to 5 °C lasts approximately 8.4 years before its capacity ratio falls below 0.65, and the battery modules are replaced. During the 13-year period studied, the modules are replaced only once. When the battery is cooled to 15 °C, it lasts approximately 4.5 years before its modules are replaced, resulting in 2 required replacements during the 13-year period studied. If the battery coolant temperature is increased to 25 °C, the battery modules last approximately 3.5 years before they are replaced, resulting in 3 required replacements during the 13-year period studied. The nonlinear difference in battery lifetime observed is caused by the exponential, Arrhenius relationship that exists between temperature and the rate of capacity loss, as given in Equations 3.20 and 3.24.

Figure 4.12 shows similar results for the case where capacity loss is not considered in the objective function, and the battery simply responds to any difference that exists in the real-time electricity market price. For all of the cases illustrated in Figure 4.12, the annual revenue potential is greater than the revenue illustrated

in Figure 4.11. This behavior is caused by the fact that the battery performs more charge-discharge cycles and collects more revenue when the effect of capacity loss is not considered in the objective function.

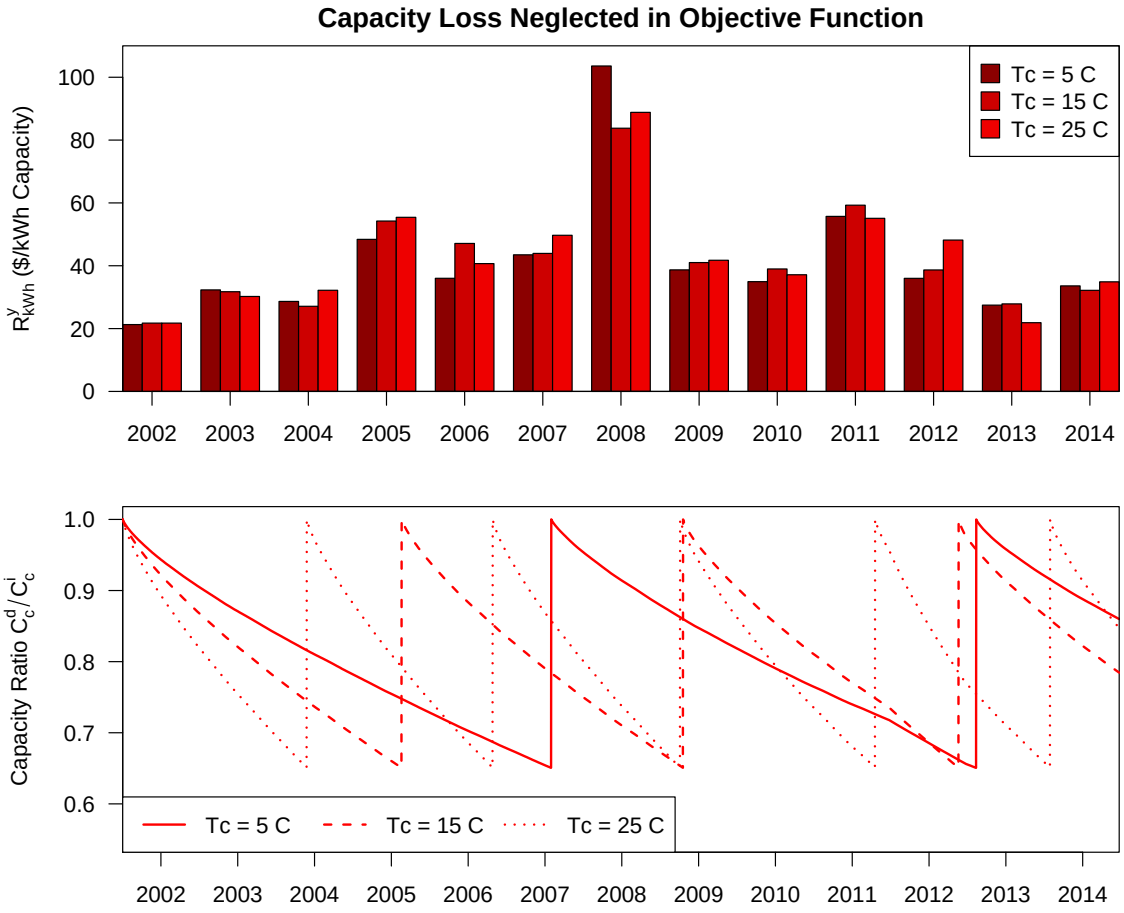

Figure 4.12: The annual revenue potential of the battery system considered is calculated for each of the operating years and coolant temperatures considered. The corresponding modeled capacity loss is illustrated in the bottom portion of the figure. The battery lasts significantly longer when it is cooled to 5 °C.

While the annual revenue potential is greater, the battery lifetime is consistently shorter when the effect of capacity degradation is not penalized in the objective function. The battery cooled to 5 °C lasts approximately 5.6 years before its capacity ratio falls below 0.65, and its modules are replaced. Increasing the coolant tempera-

ture to 15 or 25 °C decreases the module lifetime to 3.6 years or 2.4 years, respectively.

In all of the temperature cases considered, penalizing capacity loss in the objective function extends the battery module lifetime by approximately 25–50%. Thus, controlling the effect of capacity degradation in Li-ion battery operational management as proposed in this work can extend the lifetime of a battery regardless of its operating temperature.

4.2.1.3 The Value of Perfect Price Foresight for Wholesale Energy Arbitrage

The previous sections assumed perfect foresight of ERCOT electricity prices to show the revenue potential of the Li-ion battery system considered, and how penalizing the effect of capacity loss in operational management affects the battery's lifetime and revenue potential. Because volatility in electricity market prices can be caused by factors that are difficult to predict, such as load-forecasting errors, unexpected generator outages, or unexpected shortfalls or surpluses of renewable generation, it might be difficult for Li-ion storage to realize the revenue potential calculated in previous sections using perfect foresight of the real-time electricity price.

To assess the value of perfect electricity price foresight, this section considers the case of a battery that operates with only knowledge of day-ahead energy market prices. These prices are available from ERCOT by 6:00 pm on the day before a given operating day, and available to the public [16]. Unlike the real-time electricity prices, the day-ahead prices do not reflect sudden price volatility that might be caused by unexpected real-time operating phenomena. Rather, they only reflect routine electricity price volatility that is caused by the varying marginal costs of different electricity generators that commit energy to the day-ahead market. To show the revenue potential of a battery system without foresight of the real-time prices, day-

ahead market prices are entered into the optimization program to plan the operation of the battery. While the day-ahead price is used for operational planning, the battery is credited at the real-time market price. Any discrepancies between the day-ahead and real-time prices are reflected in the revenue potential calculated for the battery.

The optimization program for wholesale energy arbitrage in ERCOT is implemented with the variables and constraints defined in Table 4.3, a constant coolant temperature $T_c = 5$ °C, and an end-of-life capacity $C_{\text{end}} = 0.65$. Two different objective functions are considered: Equation 4.16 that penalizes the effect of capacity loss and Equation 4.17 that neglects the effect of capacity loss.

The optimization routine is applied only to ERCOT price data from years 2011–2014, after the ERCOT nodal market transition was completed [114]. Before 2011, there was no explicit day-ahead energy market organized by ERCOT, and no publicly-available day-ahead information about the price of energy. Because a battery operating in today's ERCOT market would have day-ahead price information available, only operation from 2011–2014 is considered to show the impact that foresight has on the battery's revenue potential.

Results from the optimization routine are used to approximate the revenue potential and lifetime of the Li-ion battery system when it responds to the day-ahead price versus when it responds to the real-time market price with perfect foresight. In both cases, energy flowing between the battery and the grid is credited at the real-time market price, because the battery does not submit an output schedule to ERCOT until after the day-ahead market is settled.

To demonstrate how the optimization program plans the charge-discharge schedule of the battery system for the case of day-ahead versus perfect foresight, Figure 4.13 shows the prices that are used by the optimization program for operat-

ing day January 15, 2014 and the resulting charge-discharge schedule for the case of day-ahead foresight versus perfect foresight. Figure 4.13a shows results for the case where capacity loss is penalized in the objective function, while Figure 4.13b shows the results when capacity loss is not penalized and the battery simply responds to electricity market price signals.

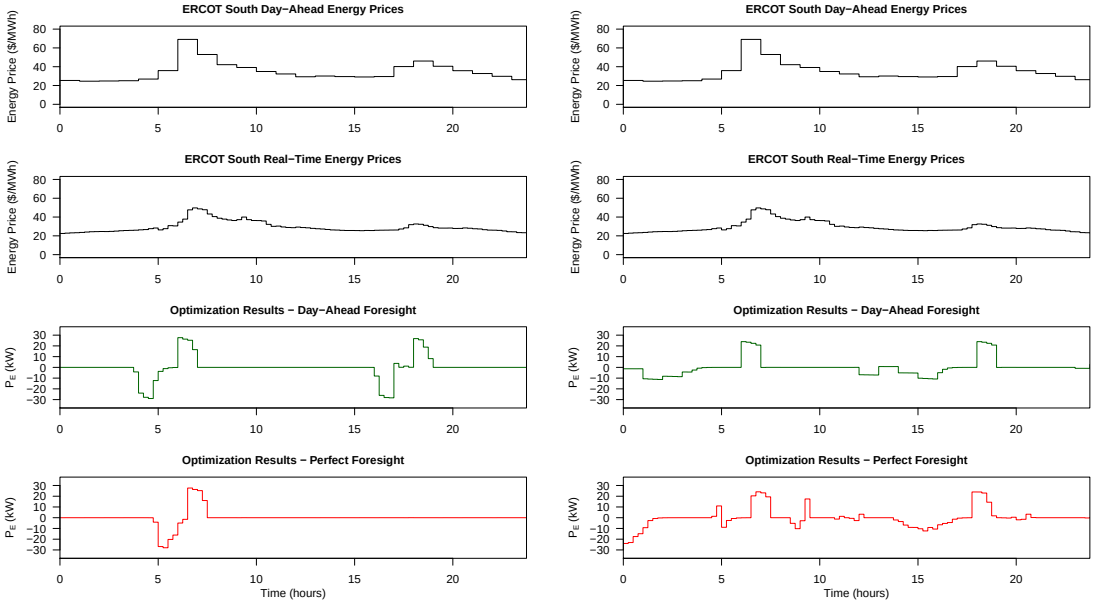

(a) Capacity loss penalized

(b) Capacity loss neglected

Figure 4.13: To illustrate the case of day-ahead foresight versus perfect foresight, the electricity prices input to the optimization program and the resulting charge-discharge schedules are shown for operating day January 15, 2014 in ERCOT South. With day-ahead foresight, the optimization program responds to the day-ahead market price. With perfect foresight, the optimization program responds to the real-time market price.

The day-ahead market prices illustrated in Figure 4.13 roughly correspond to the real-time market prices. The peaks observed in the electricity price occur at roughly the same times of day. However, the day-ahead prices peak at higher values than the real-time prices. Because the price peaks occur at roughly the same times

of day, the charge-discharge schedule returned from the optimization program is not significantly different for the case of day-ahead foresight versus perfect foresight for the day shown. However, for the case where capacity loss is penalized in the objective function, the greater price difference observed in the day-ahead price between 15:00 and 20:00 versus the real-time price causes the battery to perform a charge-discharge cycle it would not perform with perfect information about the real-time energy price.

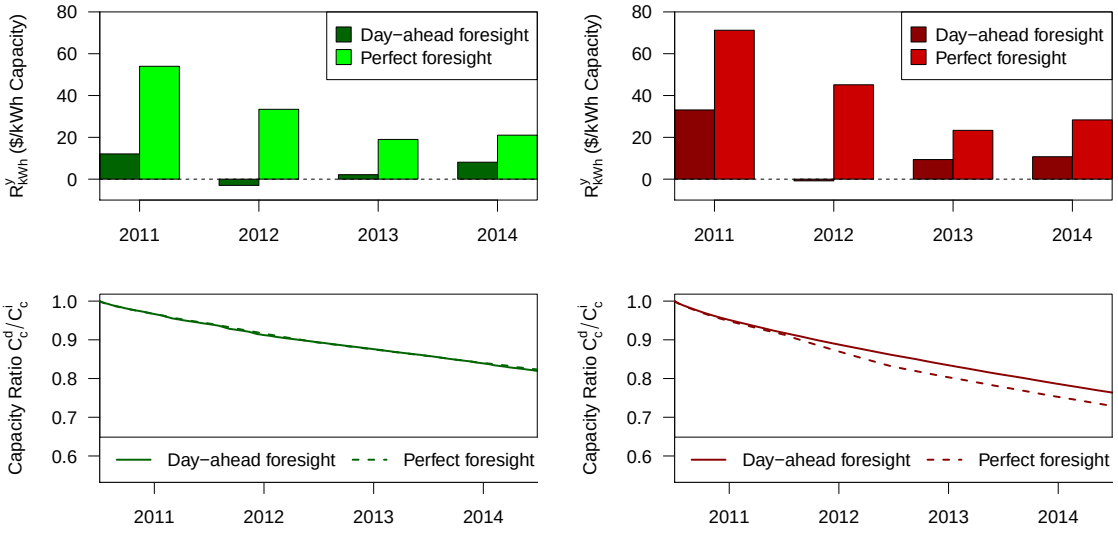

(a) Capacity loss penalized

(b) Capacity loss neglected

Figure 4.14: Perfect foresight significantly increases the revenue potential from wholesale energy arbitrage. However, the battery can typically produce positive revenue by simply responding to the day-ahead energy prices, which are publicly available in advance of an operating day.

To assess how price foresight affects the revenue potential from wholesale energy arbitrage over time, the annual revenue potential of the battery is calculated according to Equations 4.18–4.21, with the real-time price of energy used to calculate revenue for the case of both day-ahead foresight and perfect foresight. Figure 4.14a contrasts the annual revenue potential of the battery for day-ahead foresight versus perfect foresight for the case where the objective function penalizes capacity loss.

Figure 4.14b shows similar results for the case where capacity loss is not penalized in the objective. In both cases, the battery can produce significantly more revenue with perfect foresight of real-time electricity prices. This behavior occurs because the real-time electricity price is typically more volatile than the day-ahead electricity price due to forecasting errors, unlpanned generator or transmission outages, and other real-time operating phenomena [120–122]. This increased volatility in the real-time price allows the optimization program with perfect foresight to reveal more opportunities for energy arbitrage than the optimization program with day-ahead foresight.

While perfect foresight significantly increases the annual revenue potential from energy arbitrage, the battery can still achieve a positive revenue over the year with day-ahead foresight, because the day-ahead energy prices align sufficiently with real-time prices. The value of perfect information for the battery operating in the ERCOT energy market, $VOPI_E$, is calculated by taking the difference between the results illustrated in Figure 4.14 corresponding to perfect foresight and day-ahead foresight, as given in Equation 4.22. $VOPI_E$ is defined in terms of dollars per kWh of rated battery energy capacity per operating year. A battery manufacturer or operator could use the value estimated in Equation 4.22 to gauge the value of an energy-price forecasting service. Previous analysis of compressed-air energy storage (CAES) operating in ERCOT has shown that existing price-forecasting methods can capture approximately 95% of the operating revenue available with perfect price foresight [123].

$$VOPI_E = (R^y_{\text{kWh}})_{\text{Perfect Foresight}} - (R^y_{\text{kWh}})_{\text{Day-Ahead Foresight}} = \$13\text{–}46/\text{kWh per year} \tag{4.22}$$

As was found in previous sections, considering the effect of capacity degrada-

tion in the objective function of the optimization program reduces the capacity loss in the battery over time. When capacity loss is penalized in operational management, the capacity ratio of the battery at the end of the 4-year period studied is approximately 82%. When capacity loss is not controlled, the capacity ratio at the end of the 4-year period studied is approximately 74%.

4.2.1.4 Summary of Results for the Wholesale Energy Arbitrage Application

The previous sections implemented an optimization program to manage the operation of a Li-ion battery system used for wholesale energy arbitrage in Texas's ERCOT electricity market. The results of the analysis showed that the proposed optimization program has the ability to 1) model and constrain the battery's dynamic state variables, 2) reveal a charge-discharge schedule that maximizes revenue from energy market transactions, and 3) model and control the capacity loss incurred from cycling the battery.

Figure 4.15 summarizes the annual revenue potential from wholesale energy arbitrage calculated for each of the end-of-life capacity scenarios and coolant temperature scenarios considered in this section. The height of each bar corresponds to the average annual revenue potential observed across calendar years 2002–2014 for each case. The range illustrated for each bar corresponds to the range observed between the minimum and maximum annual revenues calculated across the same time period. For each case considered, the average annual revenue potential is higher when capacity degradation is not controlled in the optimization objective function. This finding stems from the fact that the battery charges and discharges more conservatively when the optimization program is trying to both reduce capacity loss and maximize energy-market revenue. However, the difference observed between the case where capacity

loss is controlled versus when capacity loss is neglected in the objective function is lesser in magnitude than the variation observed in revenue potential from year to year (indicated by the range illustrated for each bar).

Figure 4.16 summarizes the battery module lifetime calculated for each case. The height of each bar corresponds to the average battery module lifetime observed, and the range illustrated shows maximum and minimum lifetimes observed for cases where the battery modules are replaced more than once or operation in more than one ERCOT region is considered. Note that for the case where $C_{\text{end}} = 0.55$, the battery modules are replaced only once, so only a point estimate is shown. When capacity loss is controlled in the optimization objective function, the battery modules last 25–50% longer than when the optimization program simply responds to any difference that exists in the real-time electricity price. To reveal the associated tradeoff between revenue potential and battery module lifetime, Chapter 6 approximates the cost of battery system using the Li-ion pack considered to assess the net-present value (NPV) of the battery system under different scenarios, and the value of controlling capacity loss.

The results illustrated in Figures 4.15 and 4.16 were calculated assuming perfect foresight of real-time electricity prices to show the technical revenue potential of the battery system considered and measure the effect of controlling capacity degradation in the optimization objective function as proposed in this work. To assess the value of price foresight, the analysis was repeated for operating years 2011–2014 (after the ERCOT day-ahead energy market opened [114]) to test the revenue potential of the battery with perfect real-time electricity price foresight versus the case of day-ahead foresight, where the battery's operation is planned using only the publicly-available, day-ahead market electricity prices. Figure 4.17 summarizes the annual

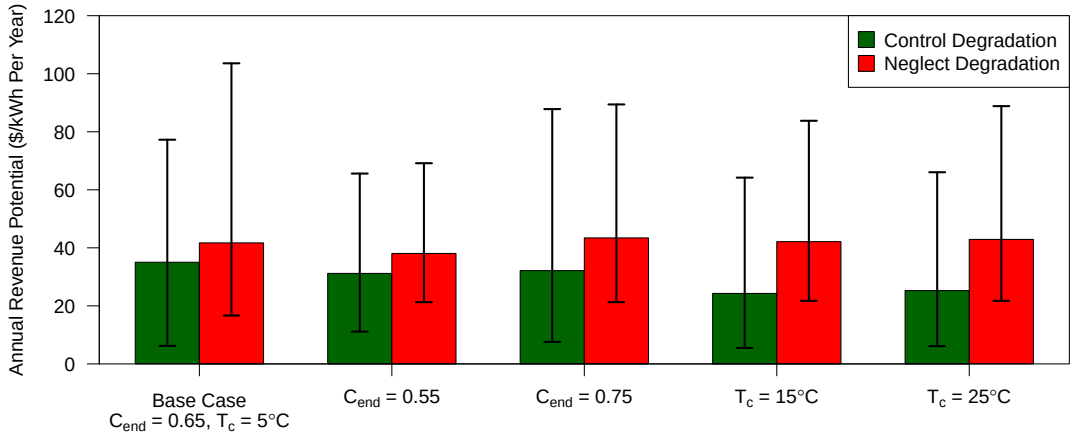

Figure 4.15: The annual revenue potential of a battery operating for wholesale energy arbitrage in ERCOT is summarized here. The height of each bar corresponds to the average value observed for each scenario, and the range illustrated corresponds to the extent between the maximum and minimum values across years 2002–2014. Controlling capacity degradation in the objective function has a small effect on revenue potential with respect to the variance observed from one operating year to the next.

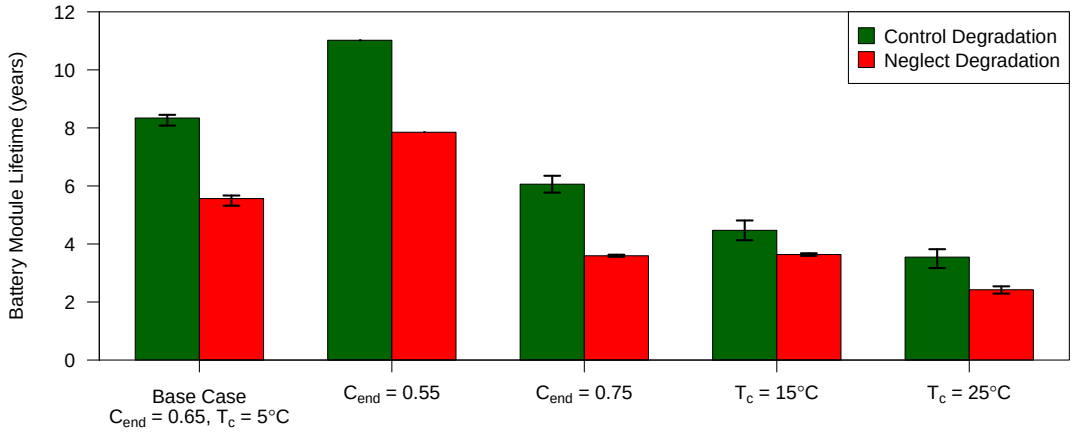

Figure 4.16: The module lifetime of a battery operating for wholesale energy arbitrage in ERCOT is summarized here. The height of each bar corresponds to the average value observed for each scenario, and the range illustrated corresponds to the extent between the maximum and minimum values observed across years 2002–2014. Controlling capacity degradation increases the battery module lifetime by 25–50%.

revenue potential of the battery for the case of perfect foresight versus day-ahead foresight, and shows the calculated value of perfect price information. Price foresight is worth approximately $13–46/kWh annually.

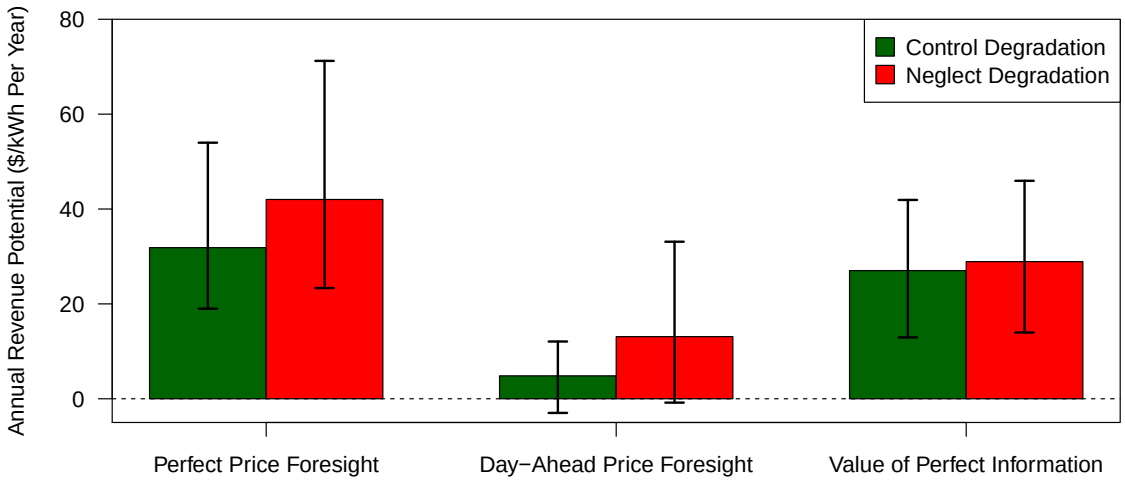

Figure 4.17: The annual revenue potential of a battery operating for wholesale energy arbitrage with perfect price foresight and day-ahead price foresight was simulated to assess the value of perfect information. Previous analysis of CAES operating in ERCOT has shown that existing price-forecasting methods can capture approximately 95% of the operating revenue available with perfect price foresight [123].

The following section performs similar analysis to that shown in this section to assess the revenue and lifetime of the Li-ion battery pack considered when it is used for energy and FRRS in the ERCOT market.

4.2.2 Operation for Wholesale Energy Arbitrage and FRRS

The optimization program for operational management of the battery for energy and ancillary services is formulated as discussed previously, with the equality constraints that constrain the battery to only perform transactions in the energy market (Equations 4.14 and 4.15) removed.

To demonstrate the effect of considering the capacity loss in the objective function, two different objectives are considered: Equations 4.23 and 4.24. Equation 4.23 considers capacity loss, while Equation 4.24 neglects capacity loss. The remainder of the optimization program is defined as discussed previously. Table 4.4 summarizes the variables and equations that define the optimization problem.

$$Obj_{CD,E,FRRS} = R^d_E + R^d_{FRRS} - \Gamma^d_{\text{degradation}} \tag{4.23}$$

$$Obj_{ND,E,FRRS} = R^d_E + R^d_{FRRS} \tag{4.24}$$

Table 4.4: This table summarizes the decision and dependent variables considered by the optimization program for wholesale energy arbitrage and FRRS.

Variable	Domain	Time Step	Equality Constraints	Inequality Constraints
		Decision Variables		
P_E	q	15 min.	Eq. 4.11	Eq. 4.6, 4.9, 4.10
C_{FRRU}	h	1 hour	Eq. 4.2, 4.14	Eq. 4.7, 4.9
C_{FRRD}	h	1 hour	Eq. 4.2, 4.15	Eq. 4.8, 4.10
		Dependent Variables		
P_{FRRS}	k	12 sec.	Eq. 4.2, 4.11	Inherited
P	k	12 sec.	Eq. 3.32, 4.11	Inherited
I	k	12 sec.	Eq. 3.32, 3.44	Eq. 3.45
V_{SOC}	k	12 sec.	Eq. 3.33, 3.38	Eq. 3.47
V_{OC}	k	12 sec.	Eq. 3.36–3.38	Inherited
$V_{t,s}$	k	12 sec.	Eq. 3.34, 3.36	Inherited
$V_{t,l}$	k	12 sec.	Eq. 3.35, 3.36	Inherited
R_s	k	12 sec.	Eq. 3.36, 3.39	Inherited
V	k	12 sec.	Eq. 3.32, 3.36, 3.37, 4.13	Eq. 3.46
T	k	12 sec.	Eq. 3.37, 4.13	Eq. 3.48
q_{Ah}	k	12 sec.	Eq. 3.44, 4.13	Inherited
C^d_{loss}	N/A	N/A	Eq. 4.13	Inherited
R^d_E	N/A	N/A	Eq. 4.1	Inherited
R^d_{FRRS}	N/A	N/A	Eq. 4.3	Inherited
$\Gamma^d_{\text{degradation}}$	N/A	N/A	Eq. 4.4	Inherited

The optimization program is implemented using GAMS [115]. An operating period of 24 hours is considered, corresponding to the day-ahead operating timeline of the ERCOT market [16]. The nonlinear, interior-point optimization algorithm is used to find optimum values for the decision variables based on the electricity prices entered into the program. The software package R is used to prepare ERCOT price data, enter the data to GAMS, and then store the results of the optimization routine [116].

The optimization program considers two categories of decision variables: power delivered for energy (P_E), and capacity delivered for FRRS (C_{FRRU}, C_{FRRD}). Figure 4.18 illustrates the values of P_E returned from four different operating days in ERCOT South. Results are shown for the objective function that considers the effect of degradation (Equation 4.23), and the objective function that neglects degradation (Equation 4.24). In general, the battery performs fewer energy market transactions when operation for both energy and ancillary services is considered versus the case of wholesale energy arbitrage only illustrated in Figure 4.4.

Figures 4.19–4.20 illustrate the values of C_{FRRU} and C_{FRRD} returned from the same operating days illustrated in Figure 4.18. In general, the battery preferentially offers capacity for FRRS service in lieu of offering power to the energy market, because more revenue can be gained from FRRS.

Figure 4.21 illustrates the value of dynamic state variables I, V, V_{SOC}, and T approximated by the battery model encapsulated within the optimization program for the case illustrated in Figures 4.18a and 4.19a. When the effect of capacity degradation is considered in the objective function, the optimization program seeks to minimize temperature gain in the battery and maintain a minimum state of charge and voltage whenever possible, because increasing temperature or voltage increases

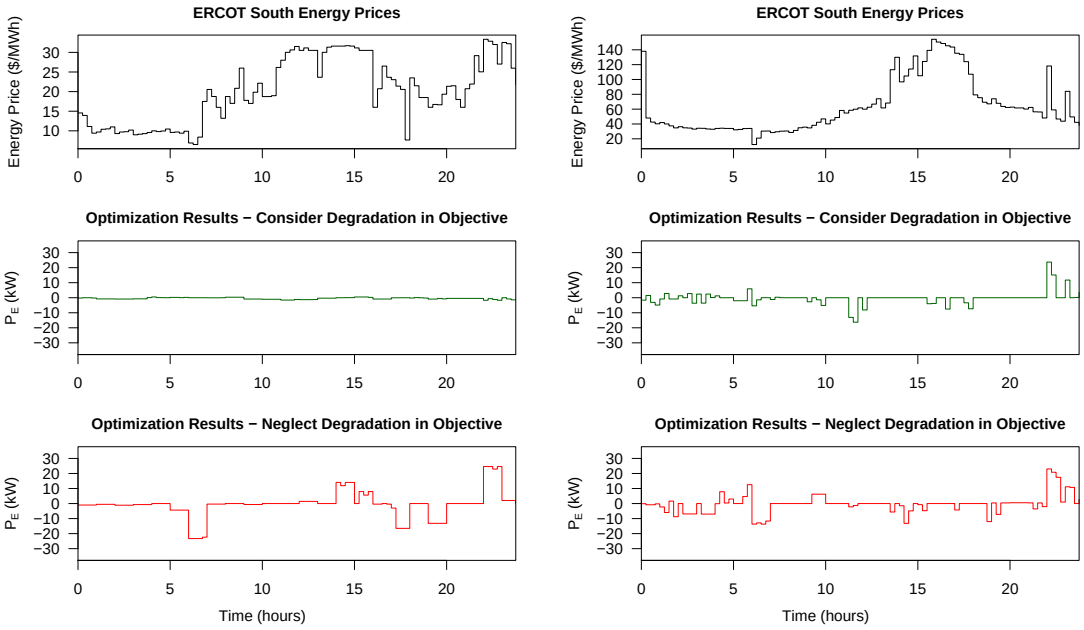

(a) April 10, 2002

(b) July 19, 2006

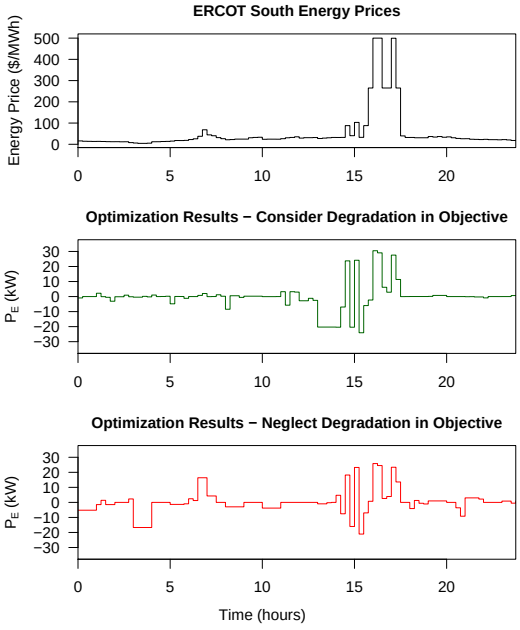

(c) October 27, 2010

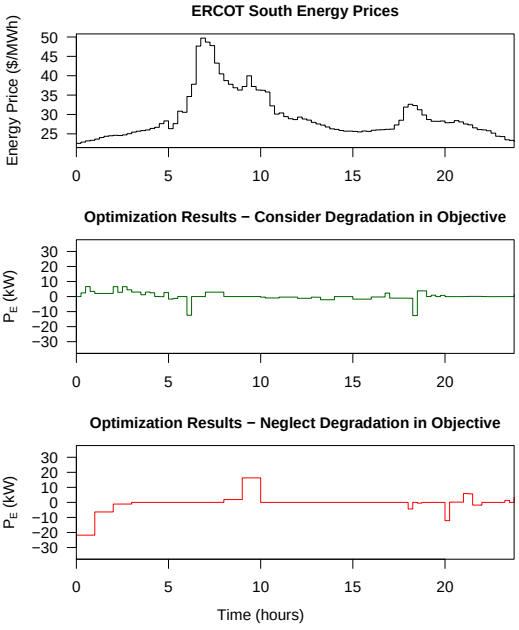

(d) January 15, 2014

Figure 4.18: To illustrate how the optimization program responds to energy prices, results are shown for four different operating days. In comparison to Figure 4.4, the battery performs fewer energy market transactions when operation for both energy and ancillary services is considered.

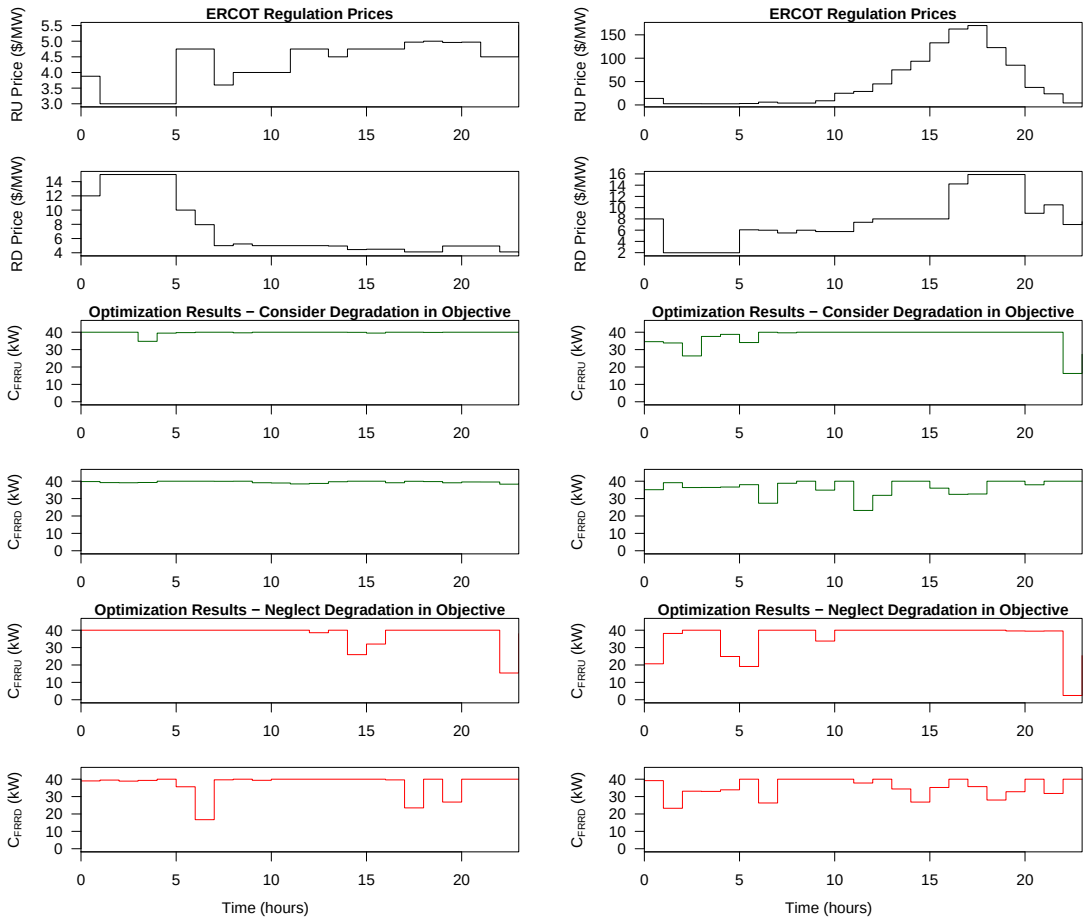

(a) April 10, 2002 (b) July 19, 2006

Figure 4.19: To illustrate how the optimization program responds to FRRS prices, results are shown for the different operating days illustrated in Figure 4.18.

the rate of capacity loss. Thus, less power is offered to the energy market, and the battery offers its capacity for FRRS while operating within a small voltage, state-of-charge, and temperature range. When the effect of capacity degradation is not penalized in the objective function, the battery performs energy market transactions that cause its voltage to increase for several hours over the day, exacerbating its rate of degradation.

To calculate the revenue potential of a battery from its optimal charge-discharge

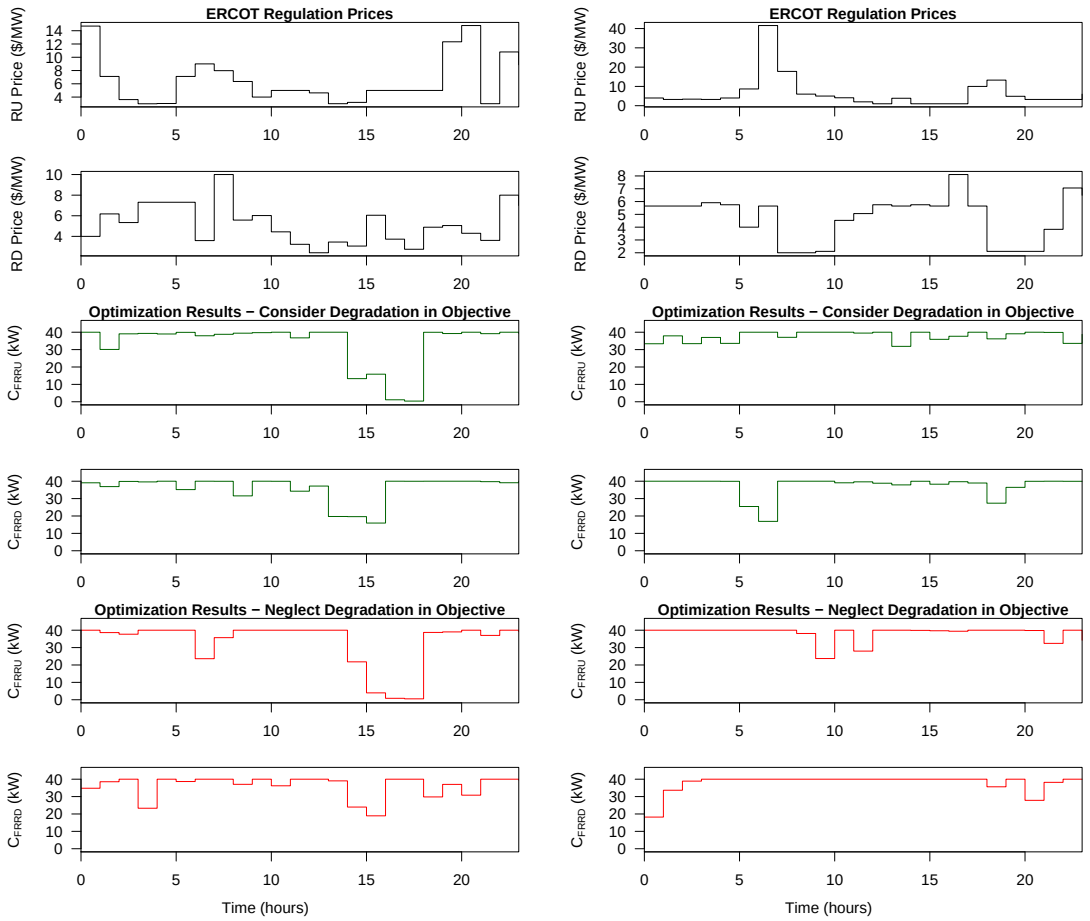

(a) October 27, 2010 (b) January 15, 2014

Figure 4.20: To illustrate how the optimization program responds to FRRS prices, results are shown for the different operating days illustrated in Figure 4.18.

schedule, P_{FRRS} is calculated according to Equation 4.2, and then the values for P_E, C_{FRRU}, C_{FRRD}, and P_{FRRS} are corrected for inverter/rectifier losses and power required for thermal controls, as given in Equation 4.18. Then, the total potential revenue over the day R^d is calculated according to Equation 4.25.

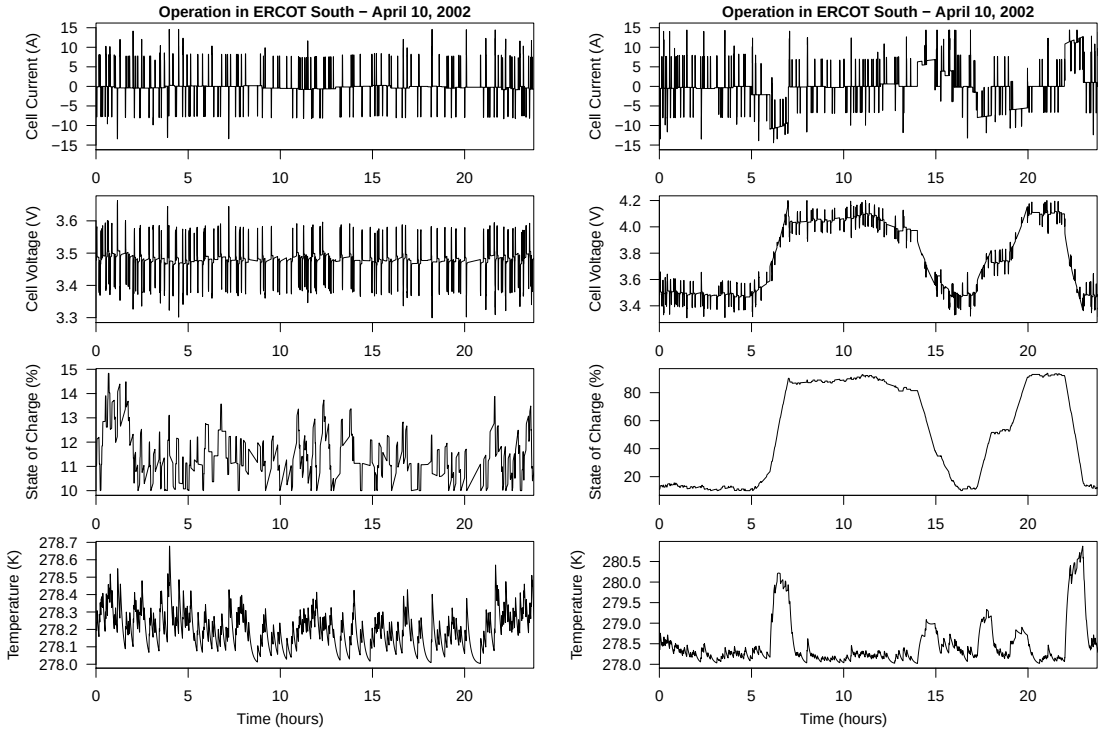

(a) Consider degradation effects (b) Neglect degradation effects

Figure 4.21: The optimization program models the dynamic state of the battery to constrain current, voltage, state of charge, and temperature. When the effect of capacity degradation is penalized in the optimization, less energy market transactions are carried out to avoid higher levels of temperature and voltage and prolong the battery's life.

$$R^d = \sum_{q=1}^{96} P_{E,\text{grid}}(q)\Delta t_q \pi(q) + \sum_{h=1}^{24} (C_{FRRU,\text{grid}}(h)\pi_{RU}(h) + C_{FRRD,\text{grid}}(h)\pi_{RD}(h)) + \sum_{q=1}^{96}\sum_{k\in q} P_{FRRS,\text{grid}}(k)\Delta t \pi_E(q) \tag{4.25}$$

To understand how the revenue potential varies from one day to the next, the optimization problem is solved for each day of 2002–2014 using electricity prices from each of ERCOT's four hubs. The total revenue over each day R_d is converted

to the revenue per kWh of battery energy capacity according to Equation 4.20, and then the results are plotted. Figure 4.22 illustrates R^d_{kWh} for the case where capacity degradation is considered in the objective function. Likewise, Figure 4.23 illustrates R^d_{kWh} for the case where the effect of capacity degradation is not considered. In each of ERCOT's four trading hubs, the revenue potential varies significantly from day to day.

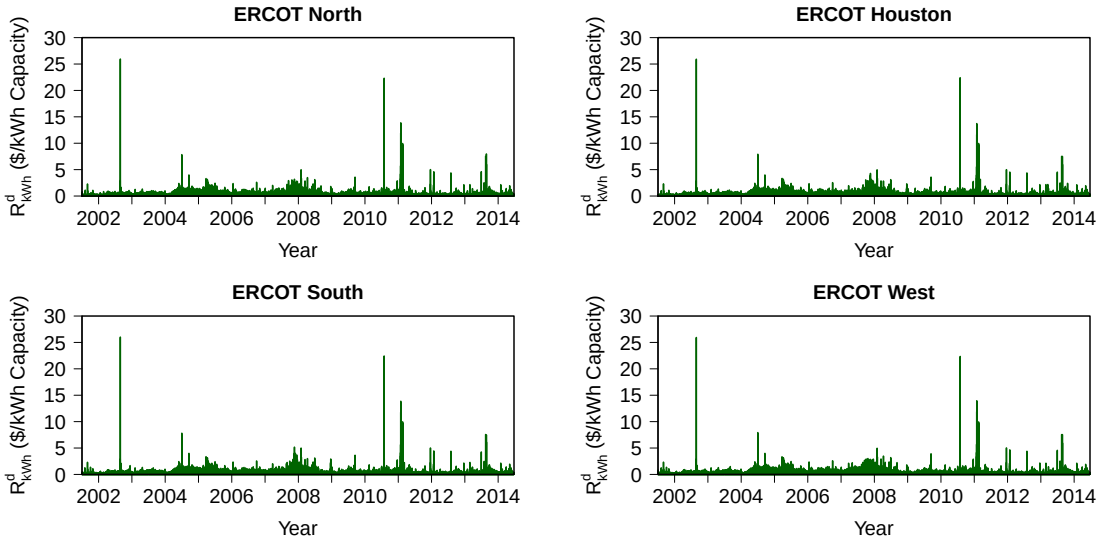

Figure 4.22: The optimization problem is solved using price data from 2002–2014 for each of ERCOT's four trading hubs. Results shown here are for the case where capacity loss is controlled in the objective function, as defined in Equation 4.23.

To approximate the revenue from operation for energy and FRRS on an annual basis, the total annual revenue per kWh of battery energy capacity is calculated according to Equation 4.21. The top portion of Figure 4.24 shows the annual revenue per kWh of battery capacity R^y_{kWh} during each operating year considered. The height of each bar indicates the average revenue across all ERCOT regions, and the ranges illustrated indicate the range of revenues observed across all regions during a given year. There is less geographic variation in revenue versus the results of Figure 4.8

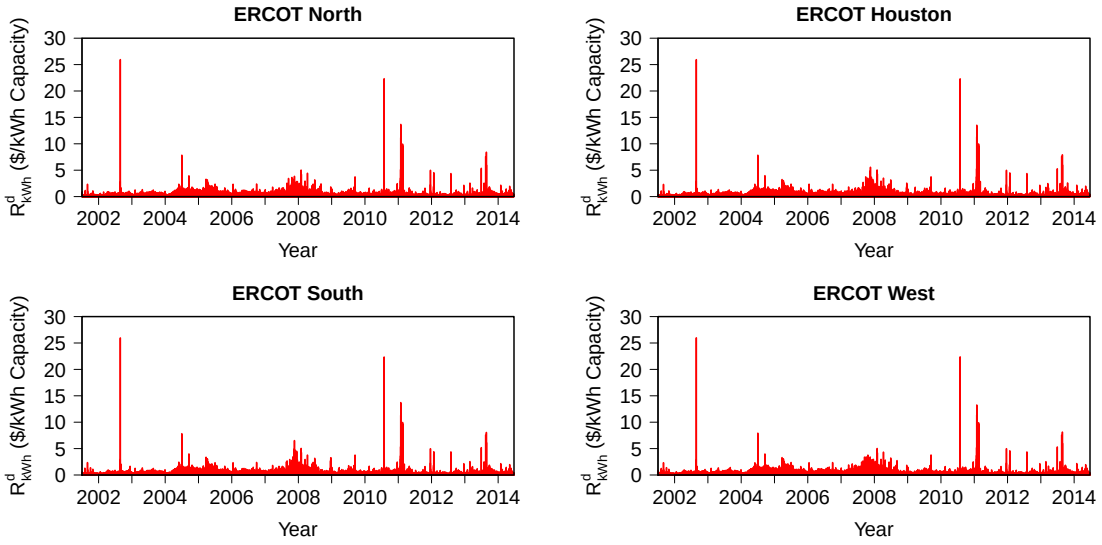

Figure 4.23: The optimization problem is solved using price data from 2002–2014 for each of ERCOT's four trading hubs. Results shown here are for the case where capacity loss is not considered in the objective function, as defined in Equation 4.24.

because ancillary service prices are not locational in nature.

To estimate the lifetime of the battery under the operating regimes considered, the capacity ratio at the beginning of each operating day is calculated according to Equation 3.40. The bottom portion of Figure 4.24 shows the value of the capacity ratio over time for each of the cases considered. Note that the corresponding value of degraded capacity is used by the optimization program for each operating day considered, so the results illustrated in the top portion of Figure 4.24 reflect the actual battery capacity available during operation.

Like the results for a battery that is used in the energy market only, the results of Figure 4.24 show that accounting for capacity loss in operational management of a grid-connected Li-ion battery can significantly increase its lifetime without significantly affecting its revenue potential. When the effect of capacity loss is not considered in the optimization program for energy and FRRS, the battery modules

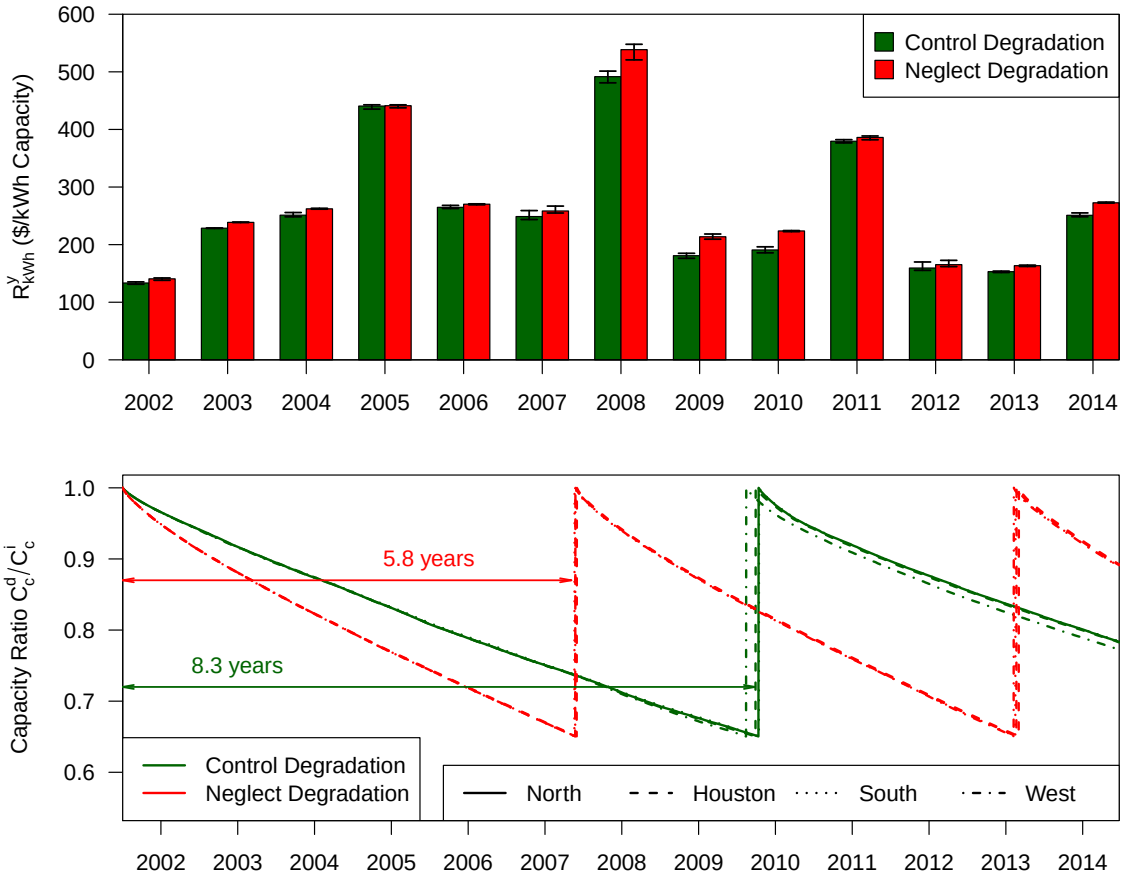

Figure 4.24: The annual revenue potential of the battery system considered is calculated for each of the operating years, ERCOT regions, and objective functions considered. The average annual revenue potential across all ERCOT regions is indicated by the height of each bar, and the observed regional variation in revenue is indicated by the ranges illustrated for each bar. The corresponding modeled capacity loss is illustrated in the bottom portion of the figure. The point at which the battery modules are replaced is indicated by a sudden increase in the capacity ratio. The modules are replaced approximately every 5.8 years when capacity loss is neglected versus 8.3 years when capacity loss is controlled. However, the annual revenue potential is greater when capacity loss is neglected versus when it is controlled.

operate for approximately 5.8 years before their end-of-life capacity is reached. When capacity loss is penalized in the optimization objective function, the battery module lifetime is extended to approximately 8.3 years, an increase of approximately 40%. This result suggests that controlling capacity loss as proposed in this work could increase the overall value of a Li-ion battery system by extending its lifetime without significantly affecting its revenue potential.

To test the effect of uncertain and variable parameters, the following sections perform a sensitivity analysis using different end-of-life capacity ratios and coolant temperatures, as was done for the case of a battery used for wholesale energy arbitrage only. Furthermore, the value of perfect price foresight is approximated by simulating operation of a battery with only information about the day-ahead energy price.

4.2.2.1 Sensitivity Analysis: End-Of-Life Capacity Ratio

The optimization program is implemented as discussed above, with the variables and constraints defined in Table 4.4, and a range of end-of-life capacity ratios $C_{\text{end}} = [0.55, 0.65, 0.75]$. Two different objective functions are considered: Equation 4.23 that penalizes the effect of capacity loss and Equation 4.24 that neglects the effect of capacity loss.

The optimization routine is applied to ERCOT price data from 2002–2014. As before, the optimization routine is only carried out for prices from ERCOT South. This region is selected for the sensitivity analysis because the results obtained for ERCOT South in the previous section are closest to average of the results achieved for all regions. Limiting the analysis to ERCOT South significantly reduces the required computation time, and provides sufficient insight about how temperature affects battery lifetime and revenue.

Results from the optimization routine are used to approximate the revenue potential and lifetime of the Li-ion battery system operating at the range of temperatures considered. The annual revenue potential from wholesale energy arbitrage and FRRS is calculated according to Equations 4.21 and 4.25, and the degraded capacity ratio of the battery at the beginning of each operating day considered is calculated according to Equation 3.40.

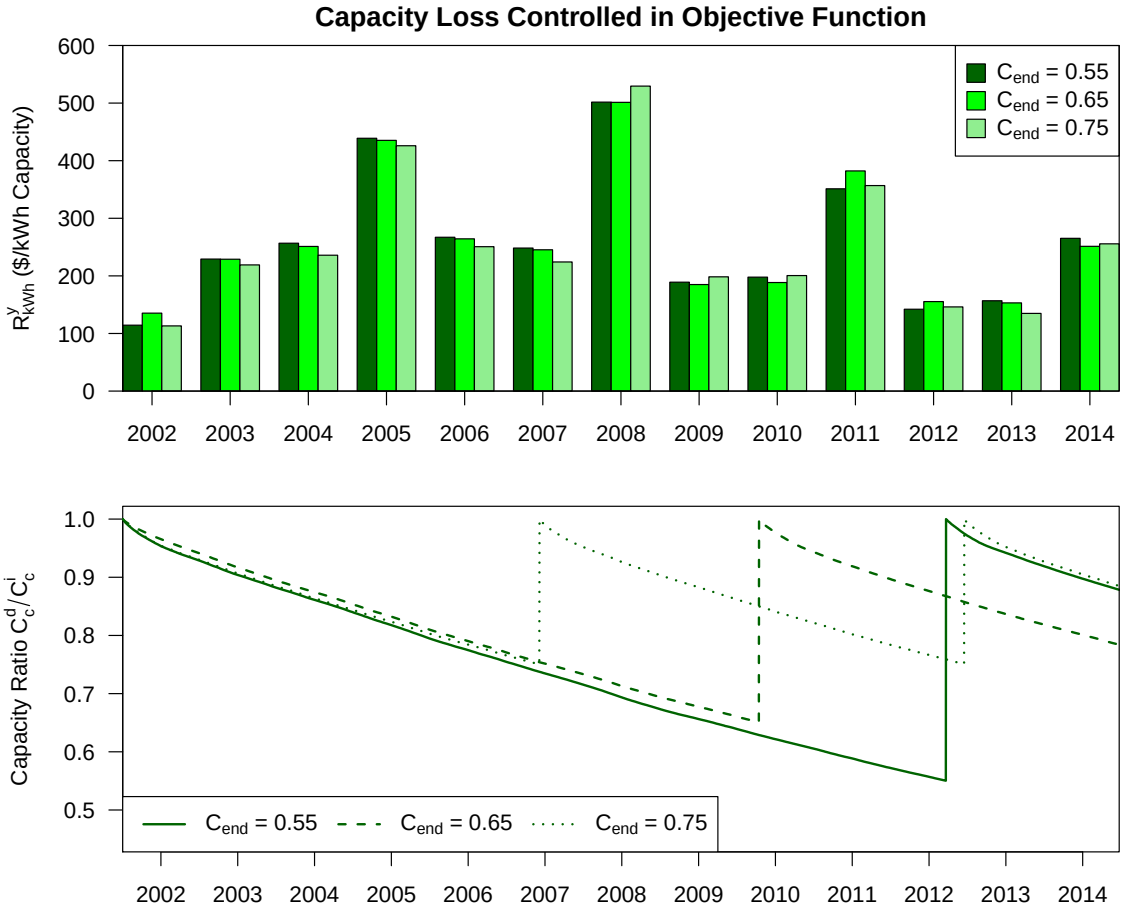

Figure 4.25: The annual revenue potential of the battery system considered is calculated for each of the operating years and end-of-life capacity ratios considered. The corresponding modeled capacity loss is illustrated in the bottom portion of the figure. The end-of-life capacity range considered corresponds to a difference in observed operating lifetime approximately equal to ± 2.7 years.

Figure 4.25 shows the resulting annual revenue potential and capacity degradation behavior for the case where capacity loss is penalized in the objective function (Equation 4.23). Little difference in annual revenue potential is observed across the end-of-life capacity ratios considered, because most of the battery's revenue comes from FRRS, which does not require a large energy capacity and is less sensitive to the amount of energy capacity available during a given operating year.

The end-of-life capacity ratio is found to have a strong effect on the battery's lifetime in years. For the base case value $C_{\text{end}} = 0.65$, the battery lasts approximately 8.3 years before the battery modules are replaced. Decreasing the end-of-life capacity ratio to $C_{\text{end}} = 0.55$ increases the module lifetime to approximately 10.7 years. Increasing the end-of-life capacity ratio to $C_{\text{end}} = 0.75$ decreases the module lifetime to approximately 5.4 years, prompting 2 required battery module replacements during the 13-year period studied. As was found for the case of a battery used for wholesale energy arbitrage only, the optimization algorithm recognizes the greater "cost" of capacity loss for increasing values of C_{end}, as defined in Equation 4.4, so it seeks to reduce the rate of capacity loss as C_{end} increases. By operating year 2007, the capacity ratio of the battery is noticeably greater for greater values C_{end}.

Figure 4.26 shows similar results for the case where capacity loss is not considered in the objective function. The annual revenue potential approximated is similar to the results when capacity loss is controlled in the objective function, because FRRS requires less deviation from the values of voltage and temperature than minimize capacity degradation. Furthermore, a large amount of energy capacity is not required to provide FRRS, so the annual revenue is not strongly affected by the amount of available energy capacity during a given operating year.

As was found previously, the battery module lifetime is consistently shorter

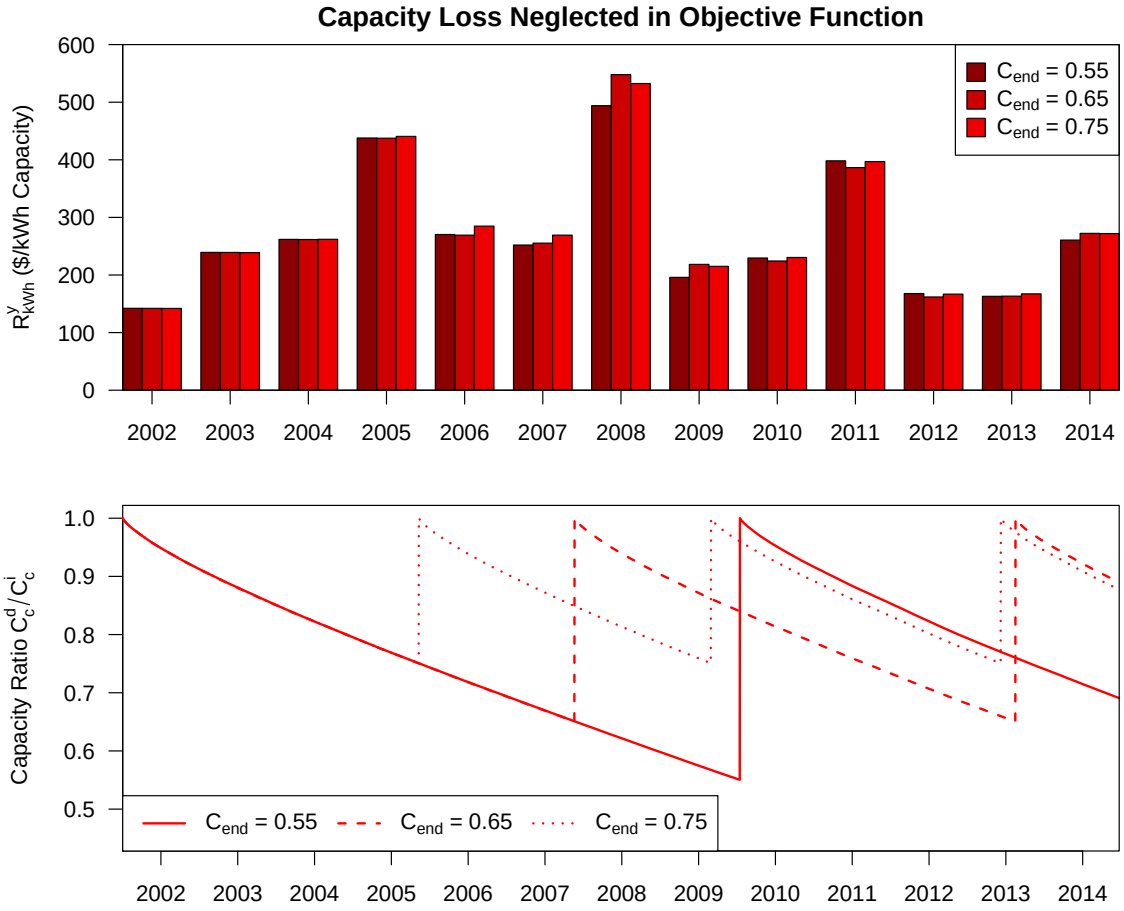

Figure 4.26: The annual revenue potential of the battery system considered is calculated for each of the operating years and end-of-life capacity ratios considered. The corresponding modeled capacity loss is illustrated in the bottom portion of the figure. The battery module lifetime is consistently shorter versus the case where capacity degradation is controlled in the objective function (Figure 4.25).

when capacity loss is not penalized in the optimization objective function. For the base case end-of-life capacity value $C_{\text{end}} = 0.65$, the battery modules last approximately 5.8 years before they are replaced, versus 8.3 years for the case where capacity loss is penalized and controlled. When the end-of-life capacity ratio is decreased to $C_{\text{end}} = 0.55$, the lifetime of the battery modules is extended to approximately 8.1 years. Likewise, when the end-of-life capacity ratio is increased to $C_{\text{end}} = 0.75$, the

battery module lifetime is shortened to approximately 3.8 years.

In all of the cases considered, penalizing capacity loss in the objective function extends the battery module lifetime by approximately 30–40%. Thus, controlling the effect of capacity degradation in Li-ion battery operational management as proposed in this work can extend the lifetime of the battery used for energy and ancillary services regardless of its end-of-life capacity ratio.

4.2.2.2 Sensitivity Analysis: Operating Temperature

To show the effect that operating at an average temperature greater than the 5 °C assumed has on the lifetime and revenue potential of the Li-ion battery system considered, the optimization routine is repeated with coolant temperatures ranging from 5–25 °C ($T_c = [5, 15, 25]$ °C). Because the rate of heat transfer between the coolant and the battery pack is high, the battery typically operates at or near the temperature of the coolant that is pumped between its modules. Thus, considering higher values of T_c shows the effect that higher operating temperatures caused by insufficient thermal management or poor insulation from the environment might have on the lifetime and revenue of the Li-ion battery pack considered.

The optimization program for energy and FRRS in ERCOT is implemented as discussed in Section 4.2.2, with the variables and constraints defined in Table 4.4, and a coolant temperature range $T_c = [5, 15, 25]$ °C. Two different objective functions are considered: Equation 4.23 that penalizes the effect of capacity loss and Equation 4.24 that neglects the effect of capacity loss.

The optimization routine is applied to ERCOT price data from 2002–2014. Because there is not strong regional variation in the annual revenue potential or capacity loss illustrated in Figure 4.24, the optimization routine is only carried out

for prices from ERCOT South.

Results from the optimization routine are used to approximate the revenue potential and lifetime of the Li-ion battery system operating at the range of temperatures considered. The annual revenue potential from wholesale energy arbitrage and FRRS is calculated according to Equations 4.21 and 4.25, and the degraded capacity ratio of the battery at the beginning of each operating day considered is calculated according to Equation 3.40.

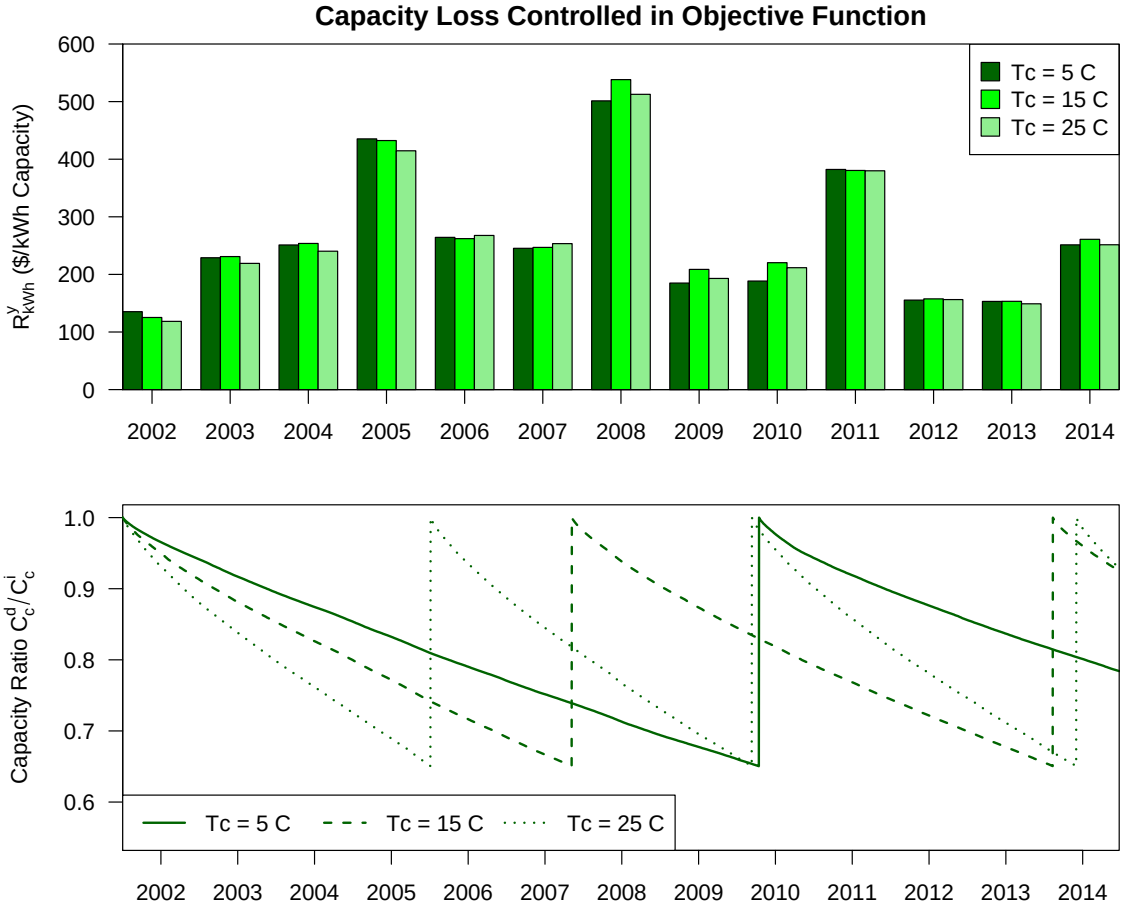

Figure 4.27: The annual revenue potential of the battery system considered is calculated for each of the operating years and coolant temperatures considered. The corresponding modeled capacity loss is illustrated in the bottom portion of the figure. The battery lasts significantly longer when it is cooled to 5 °C.

Figure 4.27 shows the resulting annual revenue potential and capacity degradation behavior for the case where capacity loss is penalized in the objective function. Adjusting the coolant temperature does not strongly affect the annual revenue potential observed from year to year, because most of the battery's revenue comes from FRRS, which is less dependent on the battery's energy capacity and internal resistance than the wholesale energy arbitrage application.

The operating temperature is found to have a strong effect on the battery's lifetime, as was found for the case of a battery used for wholesale energy arbitrage only. The battery cooled to 5 °C can operate for approximately 8.3 years before its capacity ratio falls below 0.65, and the battery modules are replaced. During the 13-year period studied, the modules are replaced only once. When the battery is cooled to 15 °C, it can provide energy and FRRS for approximately 6.0 years before its modules are replaced, resulting in 2 required replacements during the 13-year period studied. If the battery coolant temperature is increased to 25 °C, the battery modules last approximately 4.2 years before they are replaced, resulting in 3 required replacements during the 13-year period studied. The nonlinear difference in battery lifetime observed is caused by the exponential, Arrhenius relationship that exists between temperature and the rate of capacity loss, as given in Equations 3.20 and 3.24.

Figure 4.28 shows similar results for the case where capacity loss is not considered in the objective function, and the battery responds to electricity market price signals only. There is less difference between the revenue potential estimated in Figures 4.27 and 4.28 versus Figures 4.11 and 4.12, because the FRRS application requires less deviation from the values of voltage that minimize capacity degradation than the wholesale energy arbitrage application, and most of the potential revenue

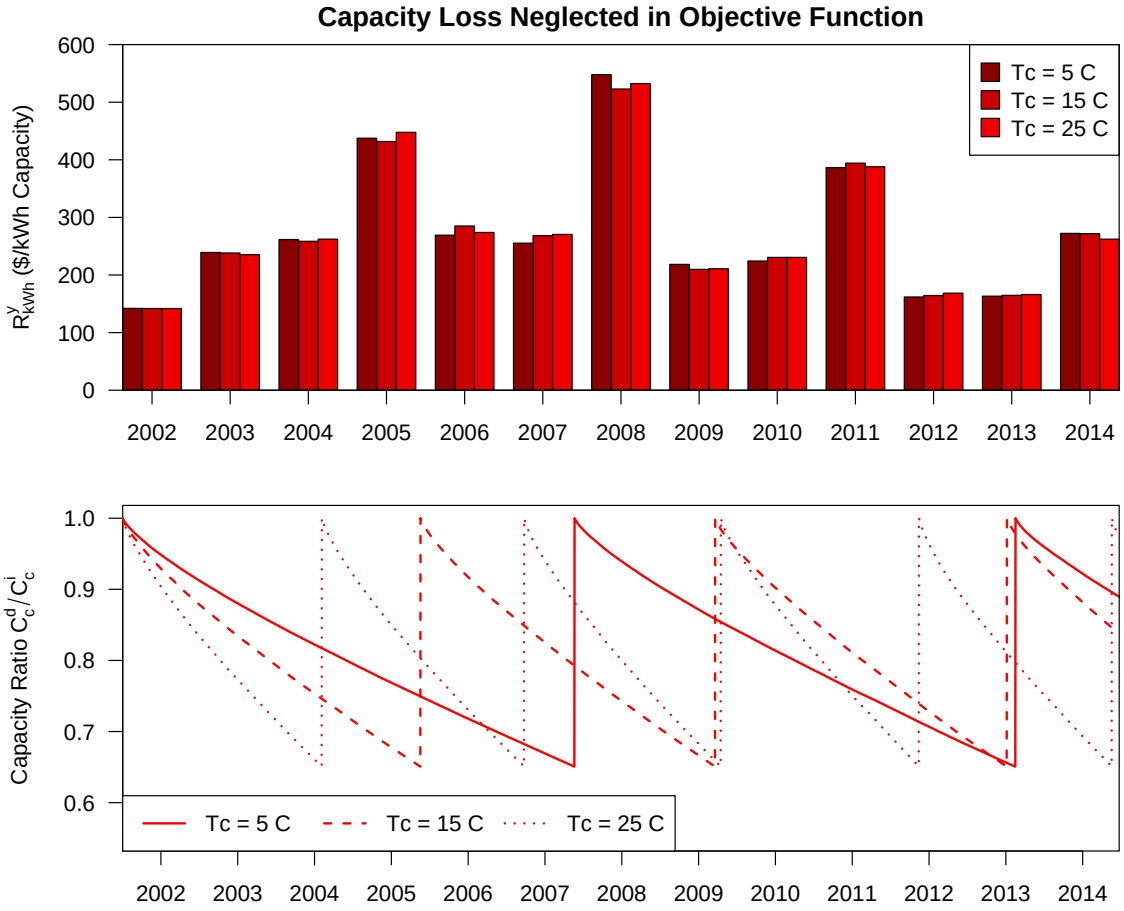

Figure 4.28: The annual revenue potential of the battery system considered is calculated for each of the operating years and coolant temperatures considered. The corresponding modeled capacity loss is illustrated in the bottom portion of the figure. The battery lasts significantly longer when it is cooled to 5 °C.

comes from FRRS. That is, penalizing capacity degradation has a stronger impact on revenue from energy arbitrage than revenue from FRRS.

As was found for the case of a battery providing wholesale energy arbitrage only, the lifetime of the battery modules is consistently shorter when capacity loss is not penalized in the objective function. The battery cooled to 5 °C lasts approximately 5.8 years before its capacity ratio falls below 0.65, and its modules are replaced.

Increasing the coolant temperature to 15 or 25 °C decreases the module lifetime to 3.8 years or 2.6 years, respectively. In all of the temperature cases considered, penalizing capacity loss in the objective function extends the battery module lifetime by approximately 40–60%. Thus, controlling the effect of capacity degradation in Li-ion battery operational management as proposed in this work can extend the lifetime of a battery regardless of its operating temperature.

4.2.2.3 The Value of Perfect Price Foresight for Energy and FRRS

The previous sections assumed perfect foresight of the real-time electricity price in order to show the technical revenue potential of the Li-ion battery pack when it is used for energy and FRRS in the ERCOT electricity market. To assess the value of perfect energy price foresight, this section assess the revenue potential of a battery used for energy and FRRS that plans its operation using only the day-ahead energy and ancillary service prices.

The optimization program for energy and FRRS in ERCOT is implemented as discussed in Section 4.2.2, with the variables and constraints defined in Table 4.4, and a constant coolant temperature $T_c = 5$ °C. Two different objective functions are considered: Equation 4.23 that penalizes the effect of capacity loss and Equation 4.24 that neglects the effect of capacity loss.

As was done for Section 4.2.1.3, the optimization routine is applied only to ERCOT price data from years 2011–2014, after the ERCOT nodal market transition was completed [114]. Before 2011, there was no explicit day-ahead energy market organized by ERCOT, and no publicly-available day-ahead information about the price of energy. Because a battery operating in today's ERCOT market would have day-ahead price information available, only operation from 2011–2014 is considered to show the impact that foresight has on the battery's revenue potential.

It is assumed the battery system can submit an offer for FRRS to ERCOT, and then update its FRRS offer schedule once the day-ahead electricity market has cleared and the day-ahead energy prices are available. This assumption allows the battery system to co-optimize its energy and FRRS offers in order to charge during appropriate times to maintain an acceptable voltage and state of charge during FRRS operation and discharge when the price of electric energy peaks.

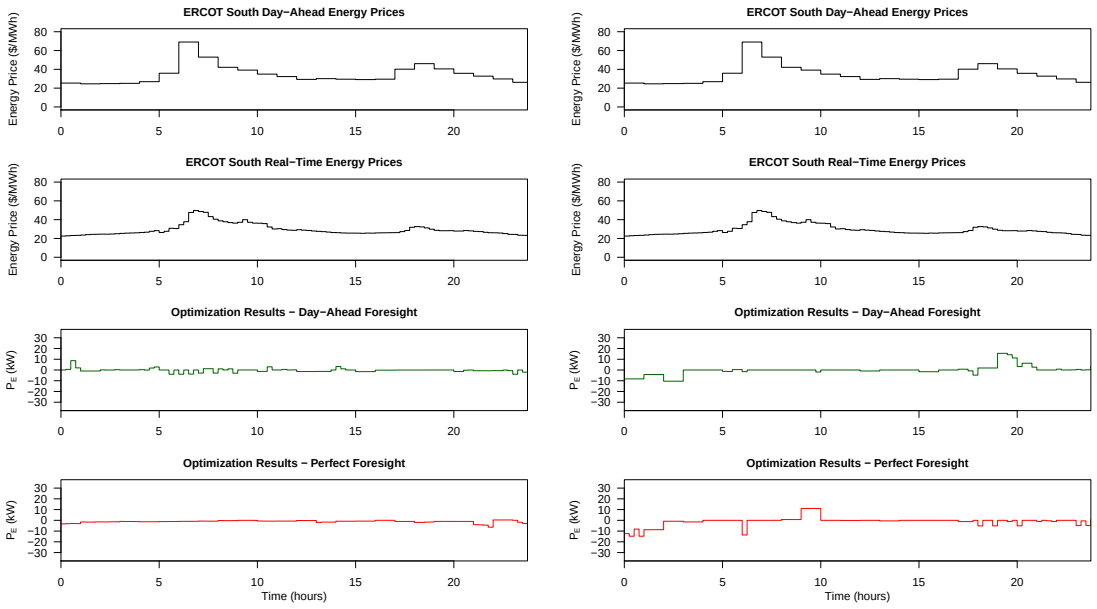

(a) Capacity loss penalized (b) Capacity loss neglected

Figure 4.29: To illustrate how foresight affects the energy market output schedule of a battery used for energy and FRRS, the input prices and the resulting energy market schedule are shown for the case of day-ahead foresight and perfect foresight for operating day January 15, 2014. In both cases, few energy market transactions are performed because the battery can gain more revenue from FRRS.

To demonstrate how the optimization program plans the energy market schedule of the battery system for the case of day-ahead foresight only versus perfect foresight, Figure 4.29 shows the energy prices that are used by the optimization program for operating day January 15, 2014 and the resulting charge-discharge schedule for

the case of day-ahead foresight versus perfect foresight. Figure 4.13a shows results for the case where capacity loss is penalized in the objective function, while Figure 4.13b shows the results when capacity loss is not penalized and the battery simply responds to electricity market price signals. In both cases, the battery performs few charge-discharge actions, because it can gain more revenue from FRRS than it can from wholesale energy arbitrage.

Figure 4.30 shows the resulting FRRS offer schedule resulting from the optimization program for the same operating day illustrated in Figure 4.29. In all cases, the optimization program uses the day-ahead regulation prices to plan its operation for FRRS. Regardless of energy-price foresight, the optimization program seeks to maximize capacity offered for FRRS, because the battery can receive more revenue from FRRS than it can from energy transactions.

To assess how price foresight affects the revenue potential from energy and FRRS over time, the annual revenue potential of the battery is calculated according to Equations 4.21 and 4.25, with the real-time price of energy used to calculate energy-market revenue and costs for the case of both day-ahead foresight and perfect foresight. Figure 4.31a contrasts the annual revenue potential of the battery for day-ahead foresight versus perfect foresight for the case where the objective function penalizes capacity loss. Figure 4.31b shows similar results for the case where capacity loss is not penalized in the objective function. In both cases, foresight does not strongly affect the annual revenue potential, because the battery can receive payment for both charging and discharging FRRS actions, unlike the case of a battery used in the energy market only. Any difference that exists between the annual revenue approximated for the case of day-ahead foresight versus perfect foresight stems from the fact that the real-time electricity price is typically more volatile than the day-

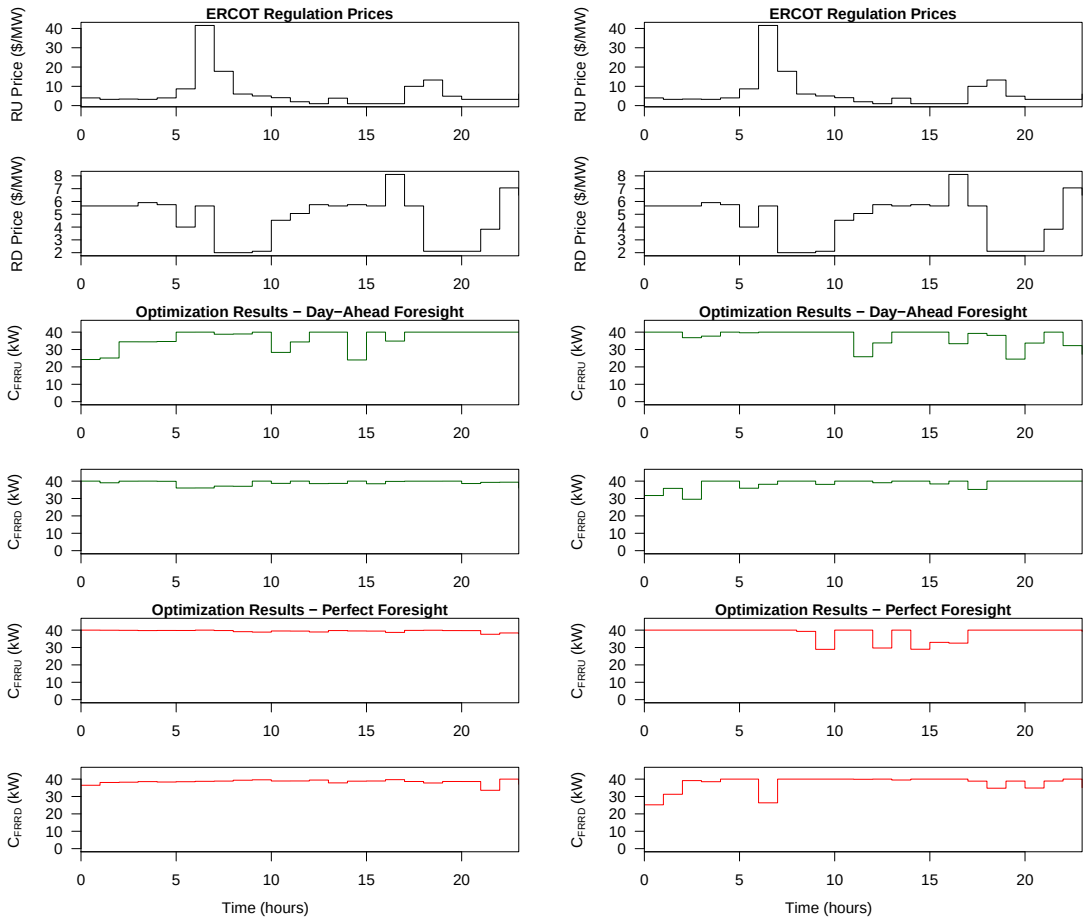

(a) Capacity loss penalized

(b) Capacity loss neglected

Figure 4.30: To illustrate how foresight affects the FRRS schedule returned from the optimization program, the resulting FRRS schedules are shown for the case day-ahead foresight and perfect foresight. In both cases, the optimization program seeks to maximize the capacity it offers for FRRS because it can gain more revenue from FRRS than it can from energy.

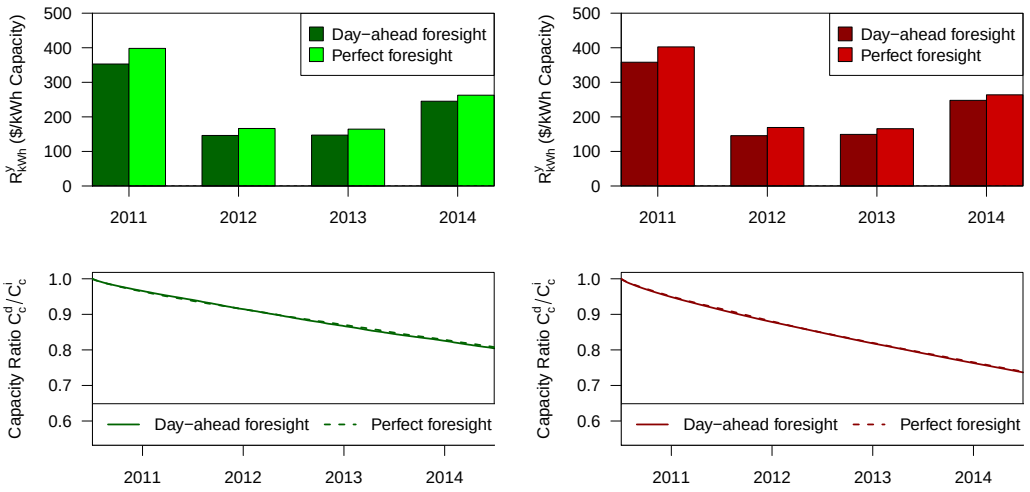

(a) Capacity loss penalized (b) Capacity loss neglected

Figure 4.31: Perfect foresight has less impact on revenue potential for energy and FRRS than was found for wholesale energy arbitrage only (Figure 4.14), because the battery receives payment for FRRS charging and discharging capacity.

ahead electricity price due to forecasting errors, forced outages, and other real-time operating phenomena [120–122]. This increased volatility in the real-time price allows the optimization program with perfect foresight to reveal more opportunities for revenue-positive energy-market transactions than the optimization program with only day-ahead foresight. However, because the battery gains most of its revenue from FRRS, perfect foresight has less effect on annual revenue potential than the case of a battery used for energy arbitrage only as illustrated in Figure 4.14.

The value of perfect information for the battery operating in ERCOT for energy and FRRS, $VOPI_{E,FRRS}$, is calculated by taking the difference between the results illustrated in Figure 4.31 corresponding to perfect foresight and day-ahead foresight, as given in Equation 4.26. $VOPI_{E,FRRS}$ is defined in terms of dollars per kWh of rated battery energy capacity per operating year. A battery manufacturer or operator could use the value estimated in Equation 4.26 to gauge the value of an

energy-price forecasting service. The value estimated for $VOPI_{E,FRRS}$ is similar to the value calculated in the previous section for $VOPI_E$, because perfect energy-price information provides similar opportunities for energy-market actions in response to the more-volatile, but less-predictable real-time energy prices. However, because the battery used for energy and FRRS gains most of its revenue from the ancillary services market, foresight has less overall impact on the annual revenue potential observed over the period studied.

$$VOPI_{E,FRRS} = (R^{y}_{\text{kWh}})_{\text{Perfect Foresight}} - (R^{y}_{\text{kWh}})_{\text{Day-Ahead Foresight}} = \$16\text{–}45/\text{kWh per year} \tag{4.26}$$

As was found in previous sections, considering the effect of capacity degradation in the objective function of the optimization program reduces the capacity loss in the battery over time. When capacity loss is penalized in operational management, the capacity ratio of the battery at the end of the 4-year period studied is approximately 81%. When capacity loss is not controlled, the capacity ratio at the end of the 4-year period studied is approximately 74%.

4.2.2.4 Summary of Results for the Energy and FRRS Application

The previous sections implemented an optimization program to manage the operation of a Li-ion battery system used for energy and FRRS in Texas's ERCOT electricity market. The results of the analysis showed that the proposed optimization program has the ability to 1) model and constrain the battery's dynamic state variables, 2) reveal an operating schedule that maximizes revenue from energy and ancillary services market transactions, and 3) model and control the capacity loss incurred from cycling the battery.

Figure 4.32 summarizes the annual revenue potential from energy and FRRS calculated for each of the end-of-life capacity scenarios and coolant temperature scenarios considered in this section. The height of each bar corresponds to the average annual revenue potential observed across calendar years 2002–2014 for each case. The range illustrated for each bar corresponds to the range observed between the minimum and maximum annual revenues calculated across the same time period. For each case considered, the average annual revenue potential is slightly higher when capacity degradation is not controlled in the optimization objective function. This finding stems from the fact that the battery charges and discharges more conservatively when the optimization program is trying to both reduce capacity loss and maximize energy-market revenue. However, the difference observed between the case where capacity loss is controlled versus when capacity loss is neglected in the objective function is smaller in magnitude than the variation observed in revenue potential from year to year (indicated by the range illustrated for each bar). Furthermore, the difference between the estimated annual revenue potential when capacity loss is controlled versus when it is neglected is smaller than the difference observed for a battery used for wholesale energy arbitrage only (Figure 4.15), because the battery can provide FRRS while maintaining its voltage and temperature within a range that minimizes capacity loss.

Figure 4.33 summarizes the battery module lifetime calculated for each case. The height of each bar corresponds to the average battery module lifetime observed, and the range illustrated shows maximum and minimum lifetimes observed for cases where the battery modules are replaced more than once or operation in more than one ERCOT region is considered. Note that for the case where $C_{\text{end}} = 0.55$, the battery modules are replaced only once, so only a point estimate is shown. When capacity loss is controlled in the optimization objective function, the battery modules

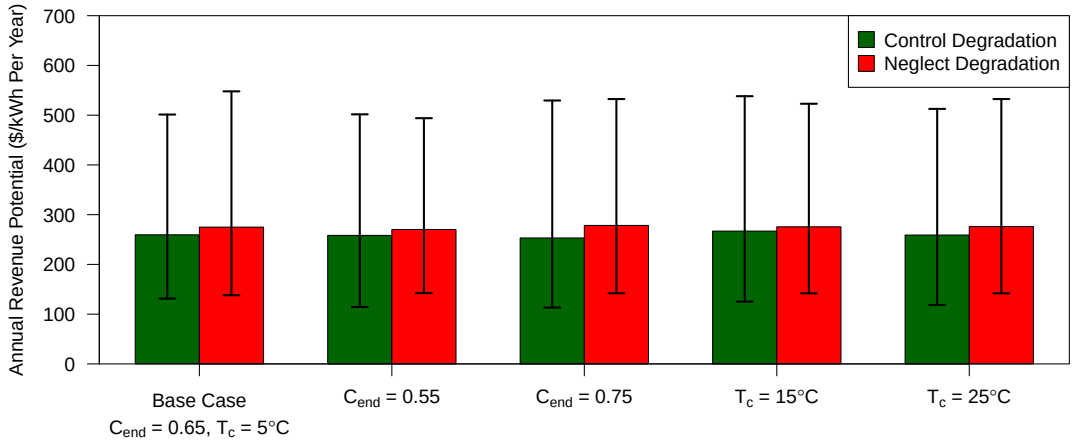

Figure 4.32: The annual revenue potential of a battery operating for energy and FRRS is summarized here. The height of each bar corresponds to the average value observed for each scenario, and the range illustrated corresponds to the extent observed across years 2002–2014. Controlling the effect of capacity degradation in the objective function has a small effect on revenue potential with respect to the variance observed from one operating year to the next.

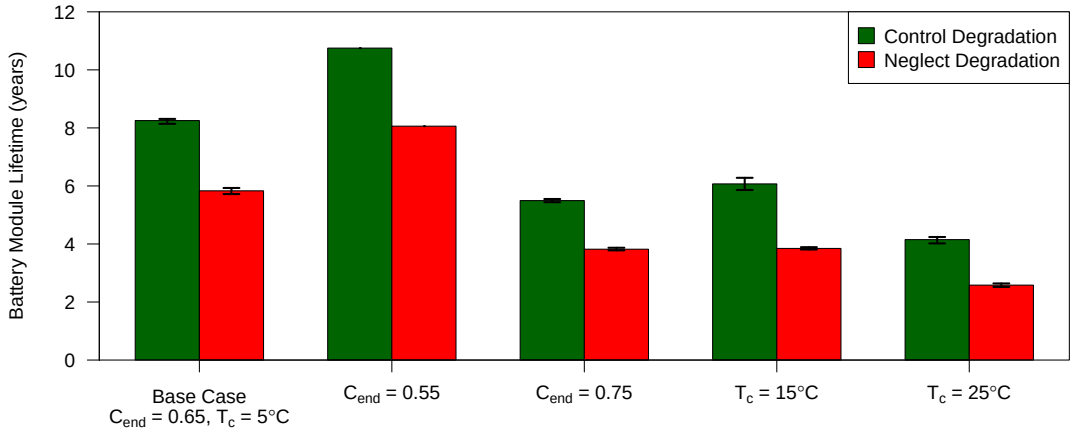

Figure 4.33: The module lifetime of a battery operating for energy and FRRS is summarized here. The height of each bar corresponds to the average value observed for each scenario, and the range illustrated corresponds to the extent observed across years 2002–2014. Controlling capacity degradation increases the battery module lifetime by 30–60%.

last 30–60% longer than when the optimization program simply responds electricity market price signals with no regard for capacity loss. To reveal the associated tradeoff between revenue potential and battery module lifetime, Chapter 6 approximates the cost of battery system using the Li-ion pack considered to assess the NPV of the battery system under different scenarios, and the value of controlling capacity loss as proposed in this work.

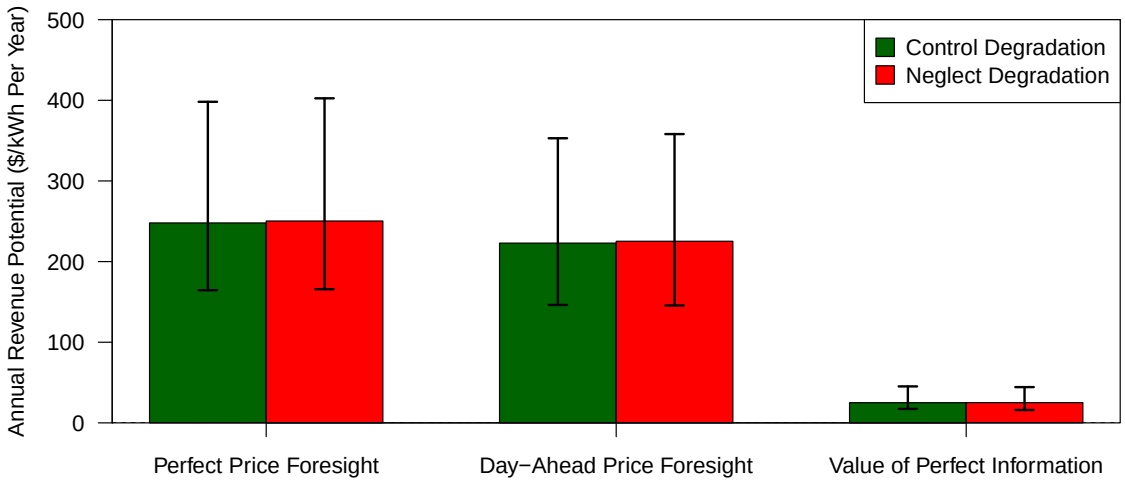

Figure 4.34: The annual revenue potential of a battery operating for energy and FRRS with perfect price foresight and day-ahead price foresight was simulated to assess the value of perfect information.

The results illustrated in Figures 4.32 and 4.33 were calculated assuming perfect foresight of real-time electricity prices to show the technical revenue potential of the battery system considered and measure the effect of controlling capacity degradation in the optimization objective function as proposed in this work. To assess the value of price foresight, the analysis was repeated for operating years 2011–2014 (after the ERCOT day-ahead energy market opened [114]) to test the revenue potential of the battery with perfect real-time electricity price foresight versus the case

where the battery's operation is planned using only the publicly-available, day-ahead market electricity prices. Figure 4.34 summarizes the annual revenue potential of the battery for the case of perfect foresight versus day-ahead foresight, and shows the calculated value of perfect price information. Price foresight is worth approximately \$16–45/kWh annually.

4.3 Chapter Conclusion

This chapter applied the optimization framework developed in Chapter 3 to the case of Li-ion battery storage operating in Texas's ERCOT electricity market. Historic price data from 2002–2014 were used to simulate 13 years of operation in the electricity market, so that the revenue potential and lifetime of the battery could be assessed under different scenarios.

Results from the analysis revealed that the optimization program developed in Chapter 3 has the capability to 1) model the dynamic state of a Li-ion battery during market operation, 2) reveal a charge-discharge schedule that maximizes electricity market revenue, and 3) model and control capacity loss in a dynamic fashion that considers capacity loss from both calendar and cycle aging.

The electricity market operation schedules returned by the optimization program were used to assess the revenue potential of the Li-ion battery pack when it is used for wholesale energy arbitrage or a combination of energy and FRRS in the ERCOT electricity market. The annual revenue potential from wholesale energy arbitrage varies widely from approximately \$6–\$104/kWh of battery energy capacity per year, depending on the volatility of market electricity prices during the year. The revenue potential calculated for wholesale energy arbitrage under different scenarios is summarized in Figure 4.15. The annual revenue potential for energy and FRRS

is significantly higher than the revenue potential for wholesale energy arbitrage only, and also varies widely from $113–$548/kWh of battery energy capacity per year, depending on the magnitude of the frequency regulation service prices during a given year. Figure 4.32 summarizes the revenue potential calculated for the battery under different scenarios.

To show the value of perfect foresight of real-time energy prices, Sections 4.2.1.3 and 4.2.2.3 simulated operation of the battery system with only knowledge of day-ahead energy prices, which are available to the public in advance of an operating day. It was found that a significant portion of the revenue potential for wholesale energy arbitrage comes from periods of volatility in the real-time market price that don't perfectly align with periods of volatility in the day-ahead market price. Thus, the value of perfect price foresight in the wholesale energy arbitrage application was found to be significant compared to the annual market revenue potential. However, price foresight was found to be less significant in the energy and FRRS application, because the battery gains most of its revenue from FRRS service, which pays the battery system to charge or discharge in response to a signal from the grid operator and does not require the battery operator to identify temporal differences in the real-time electricity price to obtain revenue.

The capacity degradation behavior modeled during market operation was used to approximate the lifetime of the battery modules under different operating scenarios, and the effect of controlling capacity loss in the optimization objective function as proposed in this work. It was found that controlling capacity degradation reduces the annual revenue potential for both wholesale energy arbitrage and FRRS, because the battery charges and discharges more conservatively to extend its lifetime. However, the reduction in annual revenue potential from controlling capacity loss is lesser in

magnitude than the variance observed from one year to the next caused by differing electricity prices. While controlling capacity loss in the objective function has a relatively small impact on annual revenue potential, it was found to have a significant impact on the battery module lifetime, extending the operating lifetime by 30–60%. Thus, considering the effect of capacity loss in Li-ion battery operational management as proposed in this work could have a positive impact on the overall value of a battery system. Chapter 6 approximates the cost of the battery pack considered and other grid battery system components to assess the NPV of the battery system under different scenarios.

With the electricity market revenue potential and operating lifetime of the battery system considered established, the following chapter assesses the reliability benefit that the battery could provide by isolating downstream electricity customers during an electric outage.

Chapter 5

Analysis of the Potential for Distributed Lithium-Ion Storage to Isolate Residential Electricity Customers During an Electric Outage[1]

The previous chapters introduced a framework to operate lithium-ion (Li-ion) energy storage that is used in an electricity market. Chapter 3 introduced methods to characterize and model the voltage, temperature, and capacity degradation behavior of a Li-ion battery pack, and then integrated these models within an optimization framework to schedule the battery's electricity market operation. Then, Chapter 4 applied the optimization framework to the case of Li-ion energy storage operating in Texas's electricity market. The results of the optimization program were used to approximate the market revenue potential and operating lifetime of the Li-ion battery pack under various scenarios.

With the market revenue potential of the battery system approximated in Chapter 4, the objective of this chapter is to assess the service that distributed Li-ion storage can provide for electric reliability. One feature of energy storage located at the grid's distribution level is that it can isolate a node of the distribution system during an electric outage to provide backup power and integrate any local sources of distributed electricity generation available [21, 92, 124]. The goal of this chapter

[1]Portions of this chapter were previously published in: Fares, R. L., and Webber, M. E. (2015). Combining a dynamic battery model with high-resolution smart grid data to assess microgrid islanding lifetime. *Applied Energy*, 137, 482-489. Michael E. Webber contributed to the work as the research supervisor.

is to model the state of a distributed battery system used to isolate downstream electric loads, so that the potential backup power duration after an outage can be approximated. It is difficult to gauge how long a battery could isolate downstream loads because electric demand often varies widely with ambient temperature, time of day, and other factors. Furthermore, the power load placed on a battery affects its available capacity [66, 67]. To approximate how long a battery could power downstream loads, information must be known about the power load on the battery and the battery's dynamic performance characteristics.

For the purposes of this analysis, the models developed in Section 3.1 are used to predict the dynamic voltage and temperature of the battery as a function of the power load that is applied to it during an electric outage. Results from the models are used to approximate how long the battery could isolate downstream electric loads before it reaches its minimum acceptable cell voltage and its energy is depleted.

To approximate the load that would be applied to the battery system during an electric outage, high-resolution electricity data collected from an Austin, Texas smart grid test bed are used. The data were collected by Pecan Street Inc. [125] as part of its ongoing smart grid demonstration study [126]. The study utilizes a test bed of 250 modern, green-built homes constructed after 2007, and 160 homes ranging from 10–92 years in age [127]. The homes are instrumented with electricity, gas, and water metering equipment. Of the 250 homes in the study, 185 are outfitted with rooftop solar photovoltaic (PV) panels [127], which are metered separately from electric demand. For the purposes of this work, electric demand and PV generation data with a one-minute time resolution collected from 21 homes over calendar year 2012 are used.

The remainder of this chapter is organized as follows: Section 5.1 discusses

how the dynamic battery model introduced in Section 3.1 is used to approximate the state of a battery system powering a downstream homes; Section 5.2 uses the battery model with empirical electricity data to calculate how long a battery system could power downstream loads under various scenarios; Section 5.3 shows the results of the analysis and quantifies the reliability benefit of islanding service; and Section 5.4 discusses the results and prospects for future work.

5.1 Battery System Specifications and Model

A system similar to a community energy storage (CES) system proposed by American Electric Power, a major U.S. electric utility, is considered [92]. The specifications for CES were developed by a consortium of large U.S. electric utilities and other relevant stakeholders under the organization of the Electric Power Research Institute (EPRI). A schematic for the proposed system is provided in Figure 5.1. The system connects to the low-voltage distribution grid at the distribution transformer, and uses electric-vehicle type Li-ion battery modules to store energy.

It is assumed the battery system uses Li-ion cells with specifications given in Table 3.1, and that these cells are interconnected to form battery packs with the configuration given in Table 3.2 and thermal conditions given in Table 3.5. Thus, the models to describe voltage and temperature developed in Section 3.1 can be used to describe the dynamic state of the Li-ion battery system. The battery system's DC power (P) is written as a function of the battery cell voltage (V), cell current (I), the number of cells per battery pack (N_{cells}), and the total number of battery packs in the system (N_{packs}), as given in Equation 5.1. Equations 5.2–5.8 relate the battery pack's DC power to its dynamic state. The model parameters are defined as given in Tables 3.4 and 3.5. A constant coolant temperature $T_c = 5$ °C is assumed.

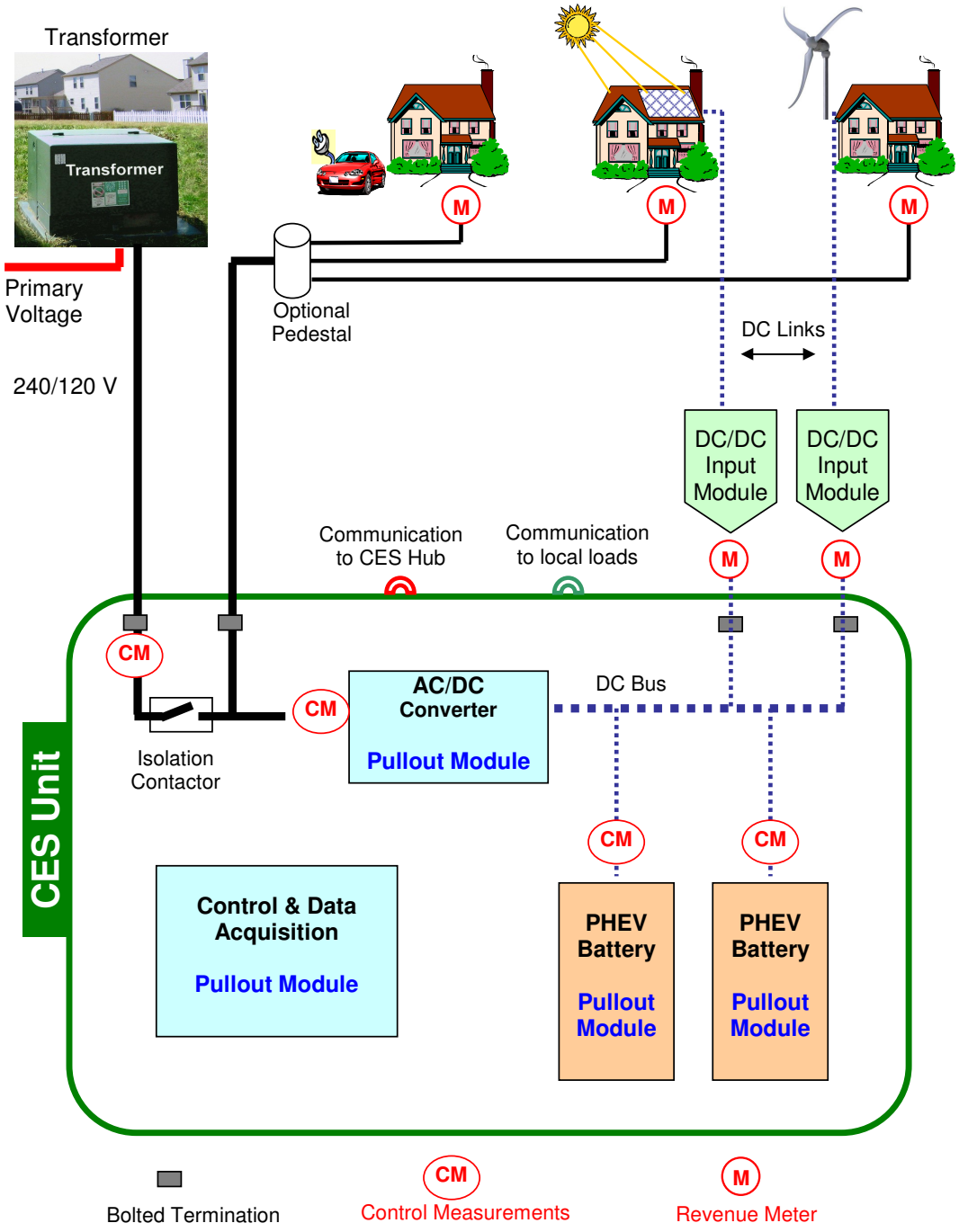

Figure 5.1: The system considered is a distributed Li-ion storage system that uses electric-vehicle type battery modules to store energy. This figure shows a schematic for a similar proposed CES system [92].

$$P = IVN_{\text{cells}}N_{\text{packs}} \tag{5.1}$$

$$\dot{V}_{SOC} = -\frac{I}{C_c} \tag{5.2}$$

$$\dot{V}_{t,s} = \frac{I}{C_{t,s}} - \frac{V_{t,s}}{R_{t,s}C_{t,s}} \tag{5.3}$$

$$\dot{V}_{t,l} = \frac{I}{C_{t,l}} - \frac{V_{t,l}}{R_{t,l}C_{t,l}} \tag{5.4}$$

$$V_{OC} = -0.99\exp\left(-53.6V_{\text{SOC}}\right) + 3.39 + 0.858V_{\text{SOC}} - 0.787V_{\text{SOC}}^2 + 0.744V_{\text{SOC}}^3 \tag{5.5}$$

$$R_s = 1.19 \times 10^{-8}\ \exp(3,830/T) \tag{5.6}$$

$$V = V_{OC} - IR_s - V_{t,s} - V_{t,l} \tag{5.7}$$

$$mc_p\dot{T} = N_{\text{cells}}I(V_{OC} - V) - hA(T - T_c) \tag{5.8}$$

Assuming that battery packs can be ideally lumped, the model for an individual pack can be scaled up to describe battery units of various sizes. Battery systems with an energy capacity of 30 kWh, 60 kWh, and 90 kWh are considered based on the energy capacity requirements developed for CES [92]. Table 5.1 shows the number of battery packs connected in series required to match the specified energy capacities, and the corresponding number of battery cells per system.

Table 5.1: Distributed Li-ion battery systems ranging from 30–90 kWh are considered. Each system connects to the grid at the distribution system transformer, and is constructed from Li-ion battery packs specified in Table 3.2.

Energy Capacity (kWh)	Number of Battery Packs (N_{packs})	Total Number of Battery Cells ($N_{\text{cells}}N_{\text{packs}}$)
30	1	576
60	2	1,152
90	3	1,728

The input to the battery model is the AC power required by downstream electric loads during an outage, P_{AC}. To model the state of the battery, the AC power demand placed on the battery system is converted to the level of DC power placed on the battery packs by accounting for AC-DC inverter/rectifier losses and energy required for the battery pack thermal controls. A one-way AC-DC and DC-AC energy efficiency of $\eta_{\text{AC-DC}} = \eta_{\text{DC-AC}} = 95\%$ is assumed for the inverter/rectifier bridge connecting the battery pack to the grid, consistent with values reported in the literature [117, 118]. A constant cooling demand $P_c = 260$ W per pack is assumed based on the battery pack specifications given in Table 3.5. Equation 5.9 defines the DC power applied to the battery system P as a function of its AC power load P_{AC}, the number of battery packs in the system N_{packs}, and the power consumed by the inverter/rectifier and thermal controls. Note that positive values of power indicate discharging while negative values indicate charging.

$$P = \begin{cases} \eta_{\text{DC-AC}}(P_{\text{AC}} + N_{\text{packs}}P_c) & \text{if charging } (P_{\text{AC}} < 0) \\ (P_{\text{AC}} + N_{\text{packs}}P_c)/\eta_{\text{DC-AC}} & \text{if discharging } (P_{\text{AC}} > 0) \\ N_{\text{packs}}P_c/\eta_{\text{DC-AC}} & \text{if idle } (P_{\text{AC}} = 0) \end{cases} \tag{5.9}$$

Figure 5.2 illustrates how the voltage model for a single battery cell discussed in Section 3.1.2 is used to to describe the dynamic voltage of the battery system as a

function of its instantaneous power load. In the following section, real-life smart grid data are used as the model input P_{AC} to assess the potential for the system to isolate downstream homes after an outage.

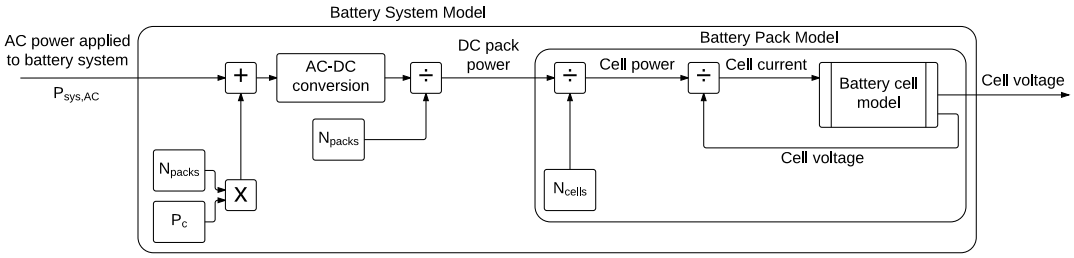

Figure 5.2: The models developed in Section 3.1 are used to describe the the dynamic voltage behavior of the battery system considered. The AC power required for the battery thermal controls is added to the power required by downstream loads, and then the net AC power flow is converted in a rectifier/inverter bridge and input to the battery unit's packs. The flow of DC power is equally divided amongst each of the battery cells, so that a single-cell battery model can be used to describe the dynamic voltage of an integrated battery system.

5.2 Electricity Data and Islanding Simulations

The Li-ion system considered in this work and other grid-connected battery systems have the rapid power-delivery capability required to provide frequency control for a small power system consisting of a handful of energy sources and energy sinks. This ability permits distributed energy storage to provide reliable power to an isolated portion of the grid during an electric outage. If distributed energy sources are available (e.g. rooftop PV panels), local battery storage can balance electricity production with demand, maintaining power quality and reliability even in the presence of intermittent energy production and consumption [128, 129].

Electric load and PV energy production data collected from 21 homes in

Austin, Texas are used to model the state of the battery system when it is used to power an islanded section of the distribution system during an outage. Each of the homes has south-facing and/or west-facing rooftop PV panels installed. Table 5.2 contains information about each of the 21 homes' PV array size, electricity use, and PV energy production. The data were recorded with one-minute time resolution. This level of resolution allows the backup duration to be approximated to the nearest minute. Data from calendar year 2012 are used to show how seasonal and diurnal variability in electricity use and PV energy production affects how long the battery can power downstream homes before its energy is depleted.

A hypothetical portion of the grid composed of the 21 homes identified in Table 5.2 is considered, with the battery system considered installed at the distribution transformers. Because a residential transformer typically serves 5–8 homes, it is assumed the homes are served by 3 residential transformers and 3 battery units, with 7 homes allocated to each transformer and battery.

In normal operation, it is assumed that the battery units freely exchange energy with the wider electricity grid using an operating regime resembling the one discussed in Chapter 4. At the precise moment that power from the grid is interrupted, the battery systems isolate the area considered and provide backup power until they reach their minimum acceptable voltage (2.75 V per cell), and their energy is depleted. Three configurations are considered: (1) the battery is deployed in a residential neighborhood with no PV panels installed; (2) the battery is deployed in a residential neighborhood where approximately half of the homes have rooftop PV panels installed; and (3) the battery is deployed in a residential neighborhood where every home has rooftop PV panels installed. These three scenarios contrast the present, centralized power system with a system that has a large share of rooftop

Table 5.2: The electricity production and consumption data were collected from 21 Austin, Texas homes with south and/or west-facing rooftop PV panels. The PV array size, total energy use, and total energy production for each of the homes is shown here.

House ID	South-Facing PV Capacity (kW)	West-Facing PV Capacity (kW)	Total 2012 Energy Use (MWh)	Total 2012 Energy Production (MWh)
1	4	2.25	6.52	8.65
2	4	2.25	7.49	8.98
3	2.5	3.5	10.39	7.86
4	2.21	3.92	9.74	8.03
5	1.96	3.92	9.16	8.29
6	4.25	3.92	7.55	6.45
7	6.25	0	10.13	6.54
8	3.43	3.43	13.37	10.08
9	4	0	7.76	6.01
10	5.15	0	6.85	7.84
11	0	4.8	14.7	6.05
12	4.66	0	12.68	7.09
13	0	4.5	10.71	5.72
14	0	5.25	13.85	6.96
15	4	0	5.94	5.02
16	No Data	No Data	12.71	8.89
17	6.25	0	12.41	9.12
18	5.92	0	9.52	6.47
19	2.04	4.07	21.77	9.01
20	4.25	0	10.43	5.79
21	2.04	4.07	12.67	8.35
Aggregate	66.89	45.88	226.35	157.19

PV. Considering these three scenarios also illustrates the relative benefit of deploying energy storage in a neighborhood with a high penetration of PV panels versus a neighborhood with little or no PV penetration.

In the first scenario, the three battery units equally provide all of the electric power required by the 21 homes comprising the microgrid, essentially acting as an uninterruptible power supply (UPS) until the batteries are depleted or grid power is restored.

In the second and third scenarios, the three battery units equally match electricity production from local PV systems with the electric demand of the 21 homes comprising the microgrid. During periods of high solar PV power production, the batteries might be unable to capture solar electricity because they are fully charged. In this case, solar energy that would overload the batteries is curtailed and lost. At all other times, the battery captures solar PV electricity and powers the community until its energy is depleted or grid power is restored. It should be noted that it is assumed the distributed energy resource (DER) interconnection standards of IEEE 1547 [130] do not apply to the system considered here. Presently, IEEE 1547 mandates that grid-tied solar power DC-AC inverters automatically disconnect from the grid during an outage [130]. This work assumes that PV inverters in the hypothetical system considered remain connected during an outage, so that PV electricity can be used in islanded mode.

For each scenario, initial values of state of charge ranging from 10–100% are considered to show how the initial state of the battery affects its potential to island downstream loads during and outage. In each case, 8,784 independent outages are simulated corresponding to hypothetical electricity service interruptions occurring at the beginning of each hour of 2012 (a leap year). The results observed from these

simulations are used to show the expected backup power duration at different times of the day during different seasons of the year.

5.3 Potential Islanding Duration and Assessment of Reliability Benefits

The model discussed in Section 5.1 is used to describe the state of the battery system in response to a stepwise-constant power load consistent with data collected from a smart grid test bed. Operation of the battery system in island mode is modeled during hypothetical outages beginning each hour of 2012, and the observed islanding duration before the battery's energy is depleted is recorded for each outage.

To contextualize the potential islanding durations observed, the average U.S. outage duration is calculated using data reported by U.S. electric utilities [131]. U.S. electric utilities typically quantify their electric reliability using two indices, the system average interruption frequency index (SAIFI) and the system average interruption duration index (SAIDI) [131, 132]. SAIFI indicates how often the average electricity customer experiences a sustained power interruption and is defined mathematically as in Equation 5.10 [132]. SAIDI indicates the total duration of interruption for the average electricity customer and is defined mathematically as in Equation 5.11 [132]. The customer average interruption duration index (CAIDI) can be computed from the common reliability indices SAIFI and SAIDI and is mathematically defined as in Equation 5.12 [132]. CAIDI represents the average time required to restore electrical service after an outage [132]. SAIDIs and SAIFIs reported by 123 U.S. electric utilities [131] are used to calculate the average U.S. CAIDI. The average U.S. SAIDI, SAIFI, and CAIDI are given in Table 5.3.

$$\text{SAIFI} = \frac{\sum \text{Total Number of Customers Interrupted}}{\text{Total Number of Customers Served}} \tag{5.10}$$

$$\text{SAIDI} = \frac{\sum \text{Customer Interruption Durations}}{\text{Total Number of Customers Served}} \tag{5.11}$$

$$\text{CAIDI} = \frac{\sum \text{Customer Interruption Durations}}{\sum \text{Total Number of Customers Interrupted}} = \frac{\text{SAIDI}}{\text{SAIFI}} \tag{5.12}$$

Table 5.3: The average values of reliability indices reported by 123 different U.S. electric utilities representing 58% of total electricity sales are used to contextualize the islanding durations observed from the simulations [131].

Reliability Metric	U.S. Average Reported Value
SAIDI	244 minutes
SAIFI	1.49
CAIDI = SAIDI/SAIFI	164 minutes

Figures 5.3–5.5 show the observed islanding duration of the three battery system sizes considered (30, 60, and 90 kWh) for initial values of state of charge equal to 10, 50, and 100%. For each scenario considered, the islanding durations observed for outages beginning each hour of the day are shown using boxplots, which summarize the data by showing upper and lower quartiles, the median, and outliers [116]. Whiskers extend up to 1.5 times the interquartile range of the upper and lower quartiles. Any points beyond the whiskers are considered outliers, and appear as points.

Figure 5.3 illustrates the distribution of islanding durations observed across various scenarios for the case of a 30 kWh battery system. The system can island the community for 0.1–23 hours, depending on the amount of solar generation available

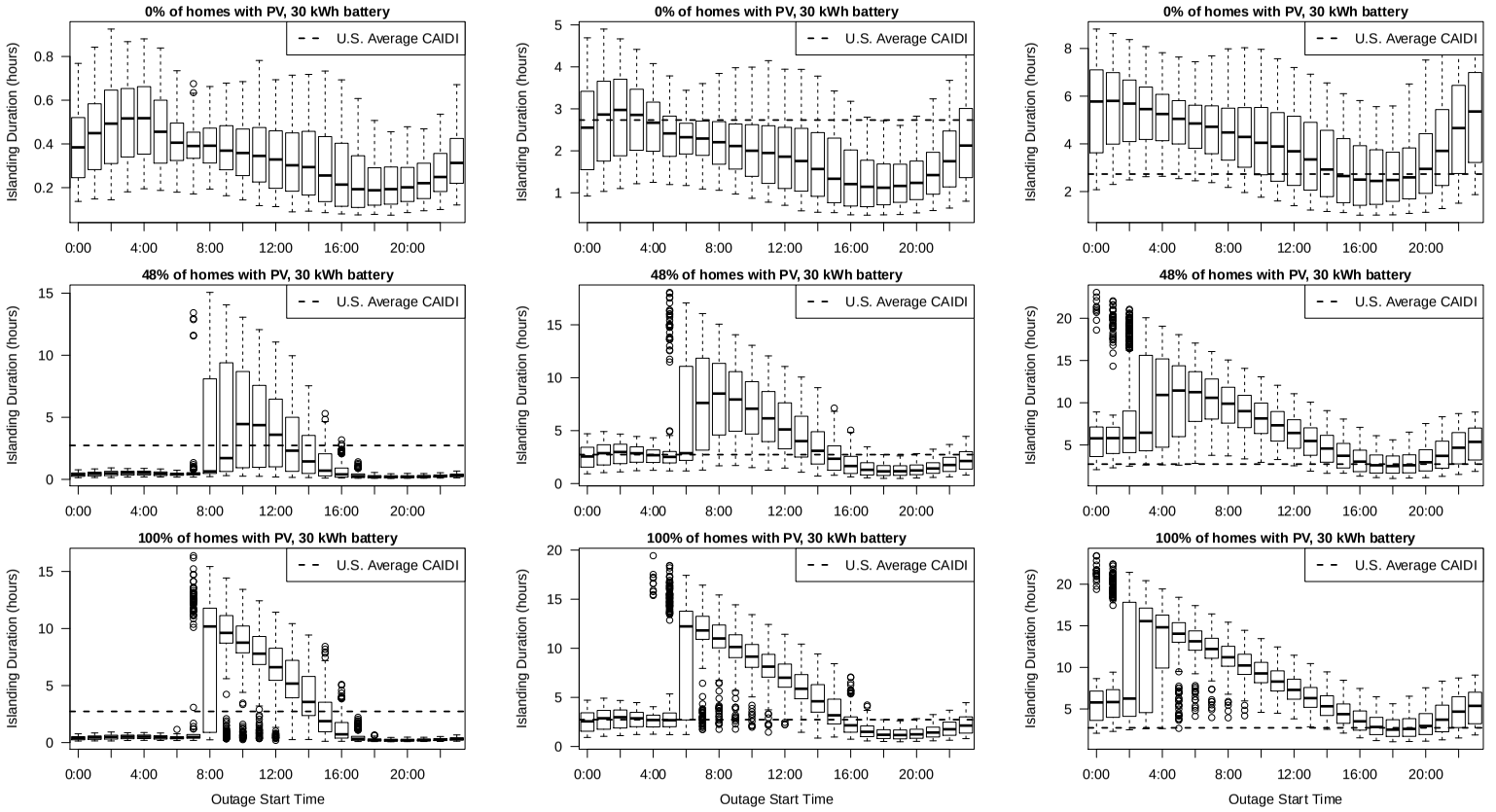

(a) Initial State of Charge = 10% (b) Initial State of Charge = 50% (c) Initial State of Charge = 100%

Figure 5.3: To gauge the reliability benefit of utilizing 30 kWh transformer-level battery storage, the distribution of islanding lifetimes observed from simulated outages occurring at the beginning of each hour of 2012 are shown. Data are shown for values of initial state of charge ranging from 10–100% and values of solar penetration ranging from 0–100%. The resulting islanding durations are contrasted with the average of CAIDIs reported by U.S. electric utilities.

and the battery's initial state of charge. Without solar panels installed, the battery can isolate the community for up to approximately 9 hours, depending on when an outage occurs during the day. The longest potential islanding durations correspond to outages occuring after 22:00 and before 5:00. The minimum islanding duration corresponds to outages occurring in the late afternoon, when electricity demand typically peaks. If the battery is fully charged in advance of an outage, it can withstand an average duration U.S. outage at least 50% of the time with the exception of outages occurring between 15:00 and 20:00. Adding solar panels to the community significantly increases the islanding duration after early-morning outages, because the battery can recharge as solar generation increases over the day. With solar panels installed on at least 48% of homes, the 30 kWh battery system can typically isolate the community for 5–15 hours after outages beginning in the early morning, depending on when an outage occurs, the level of solar generation available, and the battery's initial state of charge. However, adding solar panels does not significantly affect the islanding duration for outages occuring after 15:00, because solar energy production begins to decline after this point. On average, the measured PV electricity production peaked at approximately 13:00. By 17:00, the aggregate level of PV generation typically falls below one third of it's peak value, and by 19:00, PV electricity production stopped completely. Crucially, this cut-off point occurs during peak-demand hours, when the minimum observed islanding duration typically occurs.

The distribution of islanding durations observed for the 60 and 90 kWh battery system are shown in Figures 5.4 and 5.5, respectively. Increasing the energy capacity of the battery to 60 or 90 kWh extends the potential islanding duration across all of the cases considered. The variation observed in islanding duration over the day is similar to the behavior observed for the 30 kWh battery. In general, increasing the energy capacity of the battery gives it a greater opportunity to store solar energy,

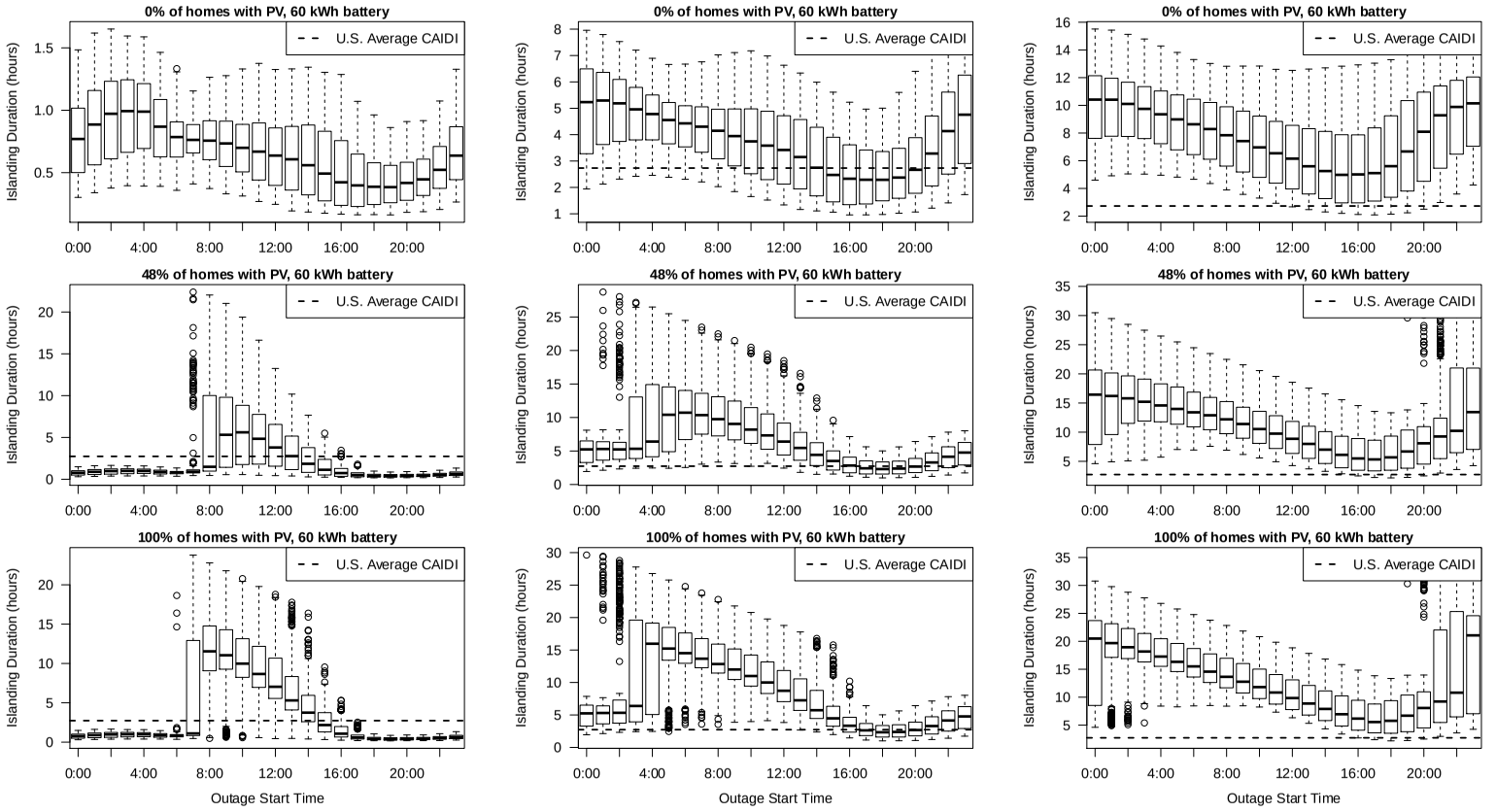

(a) Initial State of Charge = 10% (b) Initial State of Charge = 50% (c) Initial State of Charge = 100%

Figure 5.4: To gauge the reliability benefit of utilizing 60 kWh transformer-level battery storage, the distribution of islanding lifetimes observed from simulated outages occurring at the beginning of each hour of 2012 are shown. Data are shown for values of initial state of charge ranging from 10–100% and values of solar penetration ranging from 0–100%. The resulting islanding durations are contrasted with the average of CAIDIs reported by U.S. electric utilities.

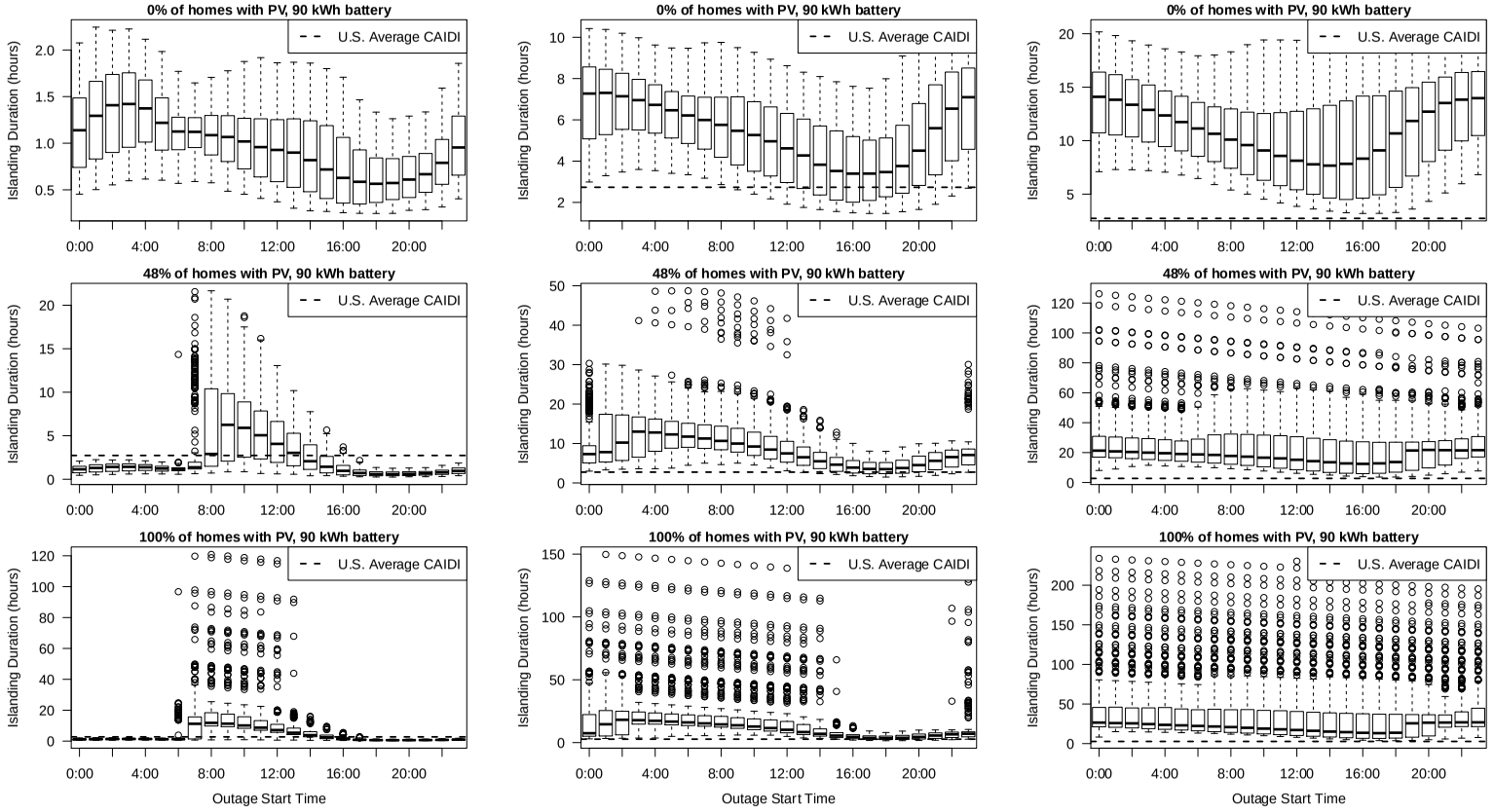

(a) Initial State of Charge = 10% (b) Initial State of Charge = 50% (c) Initial State of Charge = 100%

Figure 5.5: To gauge the reliability benefit of utilizing 90 kWh transformer-level battery storage, the distribution of islanding lifetimes observed from simulated outages occurring at the beginning of each hour of 2012 are shown. Data are shown for values of initial state of charge ranging from 10–100% and values of solar penetration ranging from 0–100%. The resulting islanding durations are contrasted with the average of CAIDIs reported by U.S. electric utilities.

allowing it to power the community for greater than 24 hours during some instances where solar generation is plentiful. The greatest islanding duration observed across all of the data was 239 hours for the 90 kWh battery system operating in a community with 100% solar penetration.

How often the battery system could withstand an average duration outage is indicated by the number of observations greater than the average of CAIDIs reported by U.S. electric utilities. Figure 5.6 summarizes the distribution of potential islanding durations observed over the year for all of the scenarios considered, and contrasts these data with the average U.S. CAIDI. Table 5.4 uses these data to show the probability that the battery system can withstand an average duration U.S. outage under each scenario considered, where $p_{\text{withstand}}$ is equal to the ratio between the number of islanding durations observed greater than the average U.S. CAIDI divided by the total number of simulated islanding events.

Table 5.4: The probability that the battery system could withstand an average duration U.S. outage, $p_{\text{withstand}}$, is calculated using the results illustrated in Figure 5.6. The resulting value of $p_{\text{withstand}}$ for each scenario considered is given here.

Energy Capacity (kWh)	Solar Penetration (%)	$p_{\text{withstand}}$ $\text{SOC}_i = 10\%$	$\text{SOC}_i = 50\%$	$\text{SOC}_i = 100\%$
30	0	0	0.22	0.74
30	48	0.14	0.47	0.83
30	100	0.27	0.55	0.86
60	0	0	0.70	0.96
60	48	0.17	0.80	0.99
60	100	0.29	0.83	0.99
90	0	0	0.86	1.00
90	48	0.19	0.92	1.00
90	100	0.31	0.94	1.00

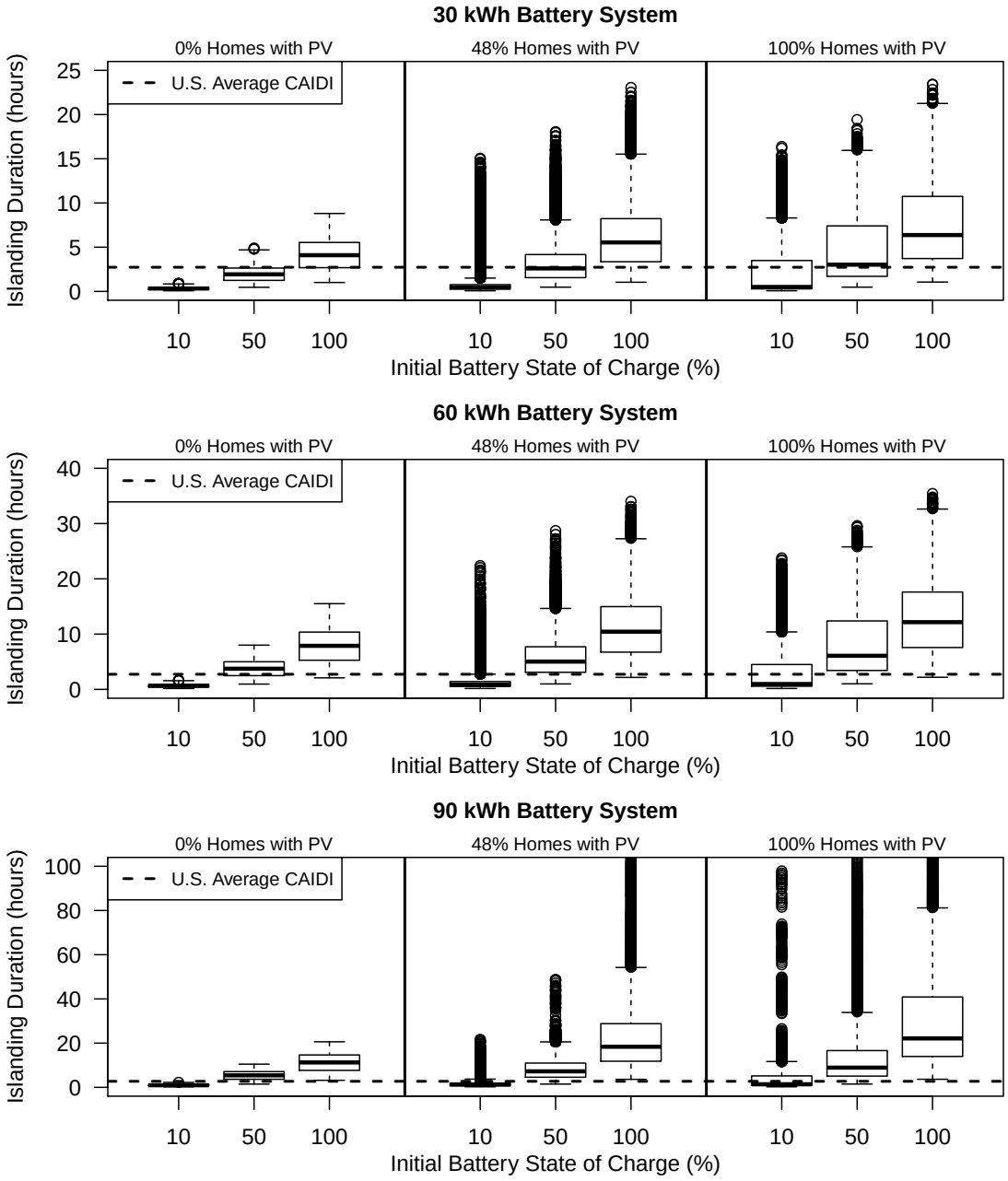

Figure 5.6: The results of Figures 5.3–5.5 are combined and contrasted with the average U.S. CAIDI to assess how often the battery system could withstand an average duration outage under various scenarios. Note the difference in the y-axis scale between the three battery sizes considered. Outliers are trimmed from the 90 kWh case for clarity.

The values given in Table 5.4 indicate how varying the battery system capacity and the fraction of homes with PV panels affects how often the community considered could withstand a typical U.S. outage. Adding solar PV to the community has the greatest effect on the ability to withstand an outage for the case where the battery's initial state of charge is low before an outage begins. In this case, none of the battery systems considered can withstand an average duration outage without solar panels available. Increasing solar penetration to 100% allows all three battery sizes considered to withstand an average duration outage outage approximately 30% of the time. However, adding solar panels to the system has diminishing returns for greater initial values of state of charge and larger battery sizes, because often the minimum potential islanding duration occurs in the late afternoon, when electricity demand peaks, and solar energy will not be available for another 10–14 hours. For a fully-charged, 30 kWh battery system, increasing solar penetration from 0% to 100% only increases $p_{\text{withstand}}$ from 0.74 to 0.86.

To approximate the monetary value of using the battery system considered for islanding service, and how this value compares with the market revenue potential estimated in Chapter 4, the cost of an outage event experienced by a residential electricity customer is approximated using estimates from the U.S. Department of Energy [133]. These estimates were calculated using data from electric utility surveys, which asked residential customers to express their willingness to pay to avoid a given outage event [133]. The resulting costs for outage events experienced by a residential customer are given in Table 5.5.

Without battery storage available, it is assumed a residential customer experiences an average of 1.49 outage events per year, corresponding to the average of SAIFIs reported by U.S. electric utilities given in Table 5.3. With the addition of the

Table 5.5: The cost of an outage event experienced by a residential electricity customer is approximated using estimates calculated by the U.S. Department of Energy [133].

Event Duration	Residential Customer Cost Per Outage Event (C_{outage})
Momentary	\$2.70
30 minutes	\$3.30
1 hour	\$3.90
4 hours	\$7.80
8 hours	\$10.70

battery system at the distribution transformer, it is assumed that the average outage frequency is reduced according to the probabilities $p_{\text{withstand}}$ given in Table 5.4. The annual reliability benefit per customer R^y_{customer} from the addition of transformer-level battery storage is calculated according to Equation 5.13 as a function of the avoided outage costs. The annual reliability benefit per customer is used to calculate the annual reliability benefit per unit of battery energy capacity R^y_{kWh} in terms of the battery's energy capacity E_{rated} and the number of residential customers per battery system $N_{\text{customers}} = 7$. Table 5.6 gives the ranges considered for each parameter and the resulting range estimated for R^y_{kWh}. In each case, the low end of the given range represents the minimum values of $p_{\text{withstand}}$ and C_{outage} given in Tables 5.4–5.5 and the high end represents the maximum values of $p_{\text{withstand}}$ and C_{outage} given in Tables 5.4–5.5.

$$R^y_{\text{customer}} = C_{\text{outage}}\text{SAIFI} - (1 - p_{\text{withstand}})C_{\text{outage}}\text{SAIFI} \tag{5.13}$$

$$R^y_{\text{kWh}} = R^y_{\text{customer}} N_{\text{customers}} / E_{\text{rated}} \tag{5.14}$$

Table 5.6: The expected range of avoided residential outage costs is calculated using the data of Tables 5.4–5.5 according to Equations 5.13–5.14.

Energy Capacity (kWh)	Solar Penetration (%)	$p_{\text{withstand}}$	R^{y}_{kWh} ($/kWh capacity per year)
30	0	0–0.74	$0–2.80
30	48	0.14–0.83	$0.13–3.10
30	100	0.27–0.86	$0.25–3.20
60	0	0–0.96	$0–1.80
60	48	0.17–0.99	$0.08–1.80
60	100	0.29–0.99	$0.14–1.80
90	0	0–1.00	$0–1.20
90	48	0.19–1.00	$0.06–1.20
90	100	0.31-1.00	$0.10–1.20

Based on the data given in Table 5.6, addition of Li-ion storage to the residential transformer could have an annual reliability benefit of $0–3 per kWh of battery energy capacity, depending on the battery energy capacity, level of solar generation available, and battery state of charge in advance of an outage. This reliability benefit comes from avoided outages, and the cost of an outage perceived by a residential electricity customer. The wide range observed stems from the fact that each of the battery systems considered could either provide less than 1 hour or greater than 24 hours of islanding service, depending on when an outage occurs, the level of solar generation available, and the initial state of the battery before an outage begins. Because no data are available about when outages typically occur and the likely state of charge in advance of an outage is uncertain, it is difficult to say precisely what reliability benefit the battery could provide. Furthermore, customers might value the reliability service provided by solar panels and batteries very differently under different scenarios. Nevertheless, the data of Table 5.6 provide a useful range for the

reliability benefit of transformer-level storage installed in a residential community.

5.4 Chapter Conclusion

This chapter implemented a dynamic, system-level battery model to describe the state-dependent performance of a lithium-ion battery energy storage system installed at the distribution transformer in a residential community. The model was used with one-minute electricity consumption and production data collected from an Austin, Texas smart grid test bed to simulate a operation in islanded mode. Then, 8,784 independent islanding events occurring at the beginning of each hour of 2012 were simulated, and the observed islanding durations were recorded to show the distribution of islanding durations expected under different scenarios.

The results of the analysis showed how the amount of battery storage installed, the level of solar penetration, and the initial state of the battery system affects how often it could withstand an average duration U.S. outage, and the distribution of islanding durations observed at various times of day. Based on the results, increasing the amount of PV installed alongside transformer-level Li-ion storage does not significantly increase how often it could withstand an average outage, because peak electric demand occurs in the evening when PV production is low. On the other hand, increasing the amount of PV in the system significantly increases the median islanding duration observed after morning outages, especially when the initial state of charge of the battery system is low.

The distribution of observed islanding durations under various operational scenarios was used to assess how often the battery system could withstand an average duration U.S. outage. The resulting probability of withstanding an outage was used with a measure of the cost of an outage event perceived by a residential customer

to assess the reliability benefit of adding Li-ion storage at the distribution transformer. The battery systems considered could provide an annual reliability benefit of approximately $0–3/kWh, depending on the state of the battery before an outage, when the outage occurs, and the level of solar penetration. The monetary value of islanding service approximated in this chapter serves as a useful comparison between the reliability benefit of distributed Li-ion storage and the market revenue potential approximated in Chapter 4. The following chapter will compare the annual market revenue potential and reliability benefit from islanding service to the approximated cost of the Li-ion battery system considered to assess its net-present value (NPV).

While this chapter approximates the monetary benefit of islanding service to compare it to the benefits from operating in the electricity market, it is important to note that there is significant uncertainty and variability associated with the perceived benefit of avoided residential outages, and the ability to withstand extended outage events. In areas where utility customers perceive a greater risk of outages due to extreme weather events or other causes, there might be a greater willingness to pay for the security offered by distributed Li-ion storage than the value approximated here. At the same time, customers in areas less prone to outages might place little or no value on the security offered by the addition of battery storage to the distribution grid. Future work could investigate niche cases and regions where distributed Li-ion storage might provide a greater reliability than the values reported here for a typical case.

Future work could also explore the tradeoffs that exist for the decision to curtail electric load during an outage event in order to extend the islanding duration of the battery system. During an extended outage scenario, such as after a hurricane, it might be desirable to interrupt individual electric loads to extend the lifetime of an

isolated portion of the distribution grid. Quantifying the value of extending islanding duration versus the cost of curtailed load is a difficult exercise requiring knowledge about the preferences of electric customers within the system. It would be valuable to explore these tradeoffs to reveal best practices for distribution system control during an extended outage event.

Chapter 6

Assessment of Lithium-Ion Energy Storage System Cost and Net-Present Value

The previous chapters developed methods to characterize and model the performance of a lithium-ion (Li-ion) battery system that is used on the electric grid. Chapter 3 introduced methods to characterize and model the voltage, temperature, and capacity degradation behavior of a Li-ion battery system using experimental or simulated performance data, and then introduced an optimization framework to schedule the battery system's participation in an electricity market while dynamically controlling its voltage, temperature, and capacity loss during operation. To demonstrate use of the proposed optimization framework, Chapter 4 applied the framework to the case of Li-ion storage operating in Texas's electricity market. Results from the optimization program were used to assess the revenue potential of the battery system considered under various scenarios, and show how modeling and controlling capacity loss as proposed in this work can extend the lifetime of Li-ion batteries in grid applications. Then, Chapter 5 assessed the potential for Li-ion storage installed at the residential distribution transformer to isolate downstream homes during an electric outage and integrate any electricity generation available from rooftop photovoltaic (PV) panels. Results from this analysis were used to quantify the reliability benefit from avoided outage costs that distributed Li-ion storage could provide over the year.

Put together, the results presented in Chapters 4–5 show the annual market revenue and reliability benefit that a Li-ion battery system using the battery packs

considered could provide, and the operating lifetime of the battery modules. To assess the tradeoff between revenue potential, battery module lifetime, and battery system cost, this chapter approximates the costs associated with an integrated Li-ion energy storage system. These measures of cost are then used with the results of Chapters 4–5 to perform a cash flow analysis for the Li-ion storage system considered and assess its net-present value (NPV) under different scenarios.

The remainder of this chapter is organized as follows: Section 6.1 approximates the cost of major Li-ion energy storage system components and the routine costs associated with operation and maintenance; Section 6.2 performs a cash flow analysis and approximates NPV under various conditions; and Section 6.3 concludes and summarizes this chapter's key findings.

6.1 Estimated Cost for Lithium-Ion Energy Storage System Components

A Li-ion battery system consists primarily of three categories of components: 1) the Li-ion battery packs, which contain the electrochemical cells that are used to store energy; 2) the power conditioning system (PCS), which uses power electronics to control the battery system and convert the battery's DC power to AC power with a voltage and frequency acceptable for the electric grid; and 3) balance of plant components including housing for the battery packs, utility-interconnection equipment, construction costs, etc. Figure 6.1 illustrates the various components of an integrated energy storage system and how they are connected. The storage device is made up of one or many interconnected battery packs. The monitors and controls device regulates the temperature within the battery pack(s) and balances the voltage and state of charge of the battery cells. The PCS converts the battery's DC power into AC electricity appropriate for the grid and vice versa. Note that the monitors and con-

trols for the battery section could also be incorporated into the PCS [21]. The AC transformer adjusts the voltage at the output of the PCS to a level appropriate for where the battery system is installed on the electric grid.

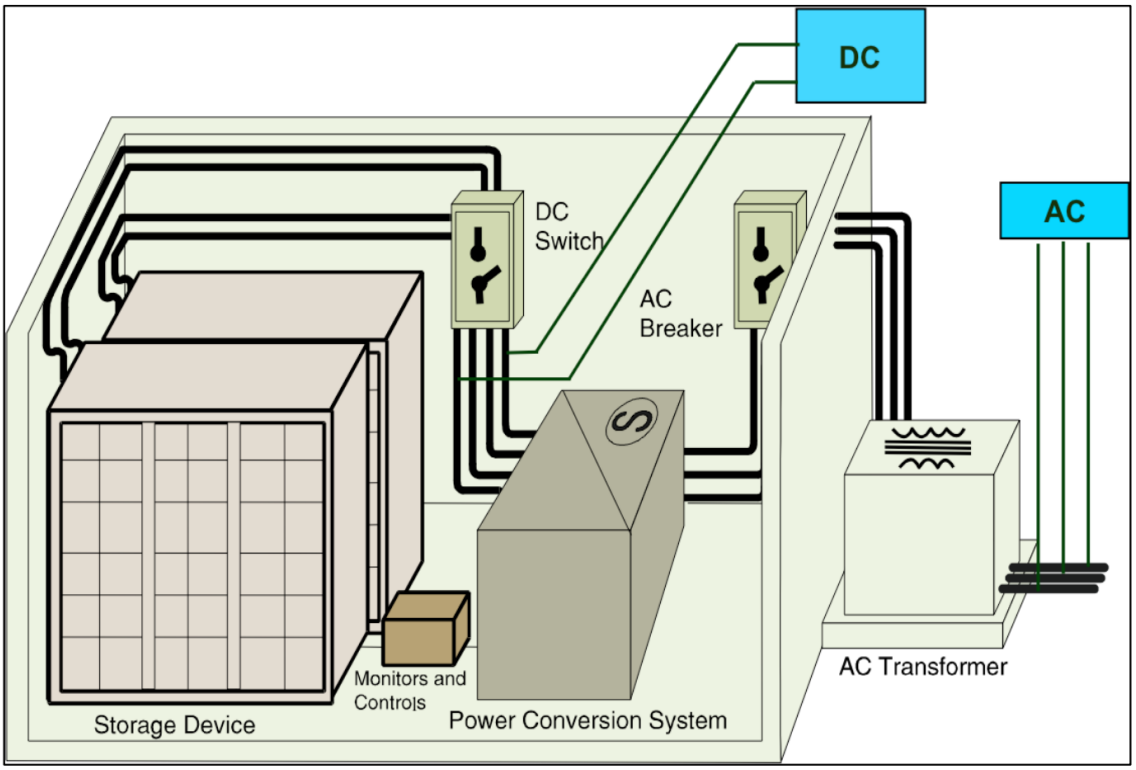

Figure 6.1: An energy storage system consists of one or more battery packs to store energy, monitors and controls for the battery section, a PCS to convert between DC and AC power, and a transformer to adjust the system voltage to a level appropriate for where the battery system is installed on the electric grid. Figure from [21].

The following sections present estimates for the cost of the battery portion, the PCS, the balance of plant components, and routine operation and maintenance.

6.1.1 Lithium-Ion Battery Pack

Specifications for the battery cells and the integrated battery pack considered in this work are identified in Section 3.1.1. They are also given here for reference.

Table 6.1 gives the specifications for the Li-ion battery cells that were modeled and evaluated in prior portions of this work. Figure 3.2 illustrates how Li-ion cells are configured to form modules and the battery pack. Table 6.2 gives the specifications for the 30 kWh Li-ion battery pack considered in this work.

To approximate the cost of the battery pack specified in Tables 6.1–6.2, the Battery Performance and Cost Model (BatPaC) model developed by the U.S. Department of Energy is used [96]. BatPaC is the product of long-term research at Argonne National Laboratory on the design, performance modeling, and cost modeling of Li-ion battery packs for electric vehicles [94,95,134–139]. The model iteratively designs the detailed aspects of Li-ion battery cells, modules, and packs based on the input cell chemistry, pack energy requirements, and design constraints (e.g. electrode coating thickness) [94]. Then, BatPaC utilizes an inventory of specific costs for Li-ion electrode materials, electrolytes, separators, current-collecting foils, cell terminals, cell casing, module casing, and other battery components to approximate the cost of materials required for the Li-ion battery pack [94–96]. Furthermore, the model inventories the unit processes required to prepare battery materials, assemble battery cells, and produce an integrated battery pack, and then approximates the associated cost of labor, capital equipment, and plant floorspace associated with each unit process [94–96]. The result is an approximation of the original equipment manufacturer (OEM) price for the Li-ion battery pack. The BatPaC software and a manual providing a detailed explanation of the methodology and assumptions used in the software are available from Argonne National Laboratory [94, 96].

Because BatPaC is intended to predict the future cost of manufacturing batteries, its results reflect the expected cost of Li-ion battery packs in the year 2020 [94,95]. It assumes that Li-ion batteries are manufactured in a large-scale, purpose-built fa-

Table 6.1: Section 3.1.1 introduced specifications for the hypothetical generic electric vehicle Li-ion battery cell considered in this work. The specifications are given here for reference.

Parameter	Value
Cell Specifications	
Cell format	Stacked electrode prismatic pouch
Cell width	79 mm
Cell height	260 mm
Cell thickness	6.5 mm
Cell weight	268 g
Cell capacity	15 Ah
Positive Electrode Specifications	
Current collector material	Aluminum
Current collector thickness	20 μm
Active material	$LiNi_{1/3}Mn_{1/3}Co_{1/3}O_2$ (NMC)
Conductive agent	Carbon
Binder	polyvinylidene difluoride (PVdF)
Electrode loading	3.8 mAh/cm^2
Electrode thickness	208 μm
Electrode porosity	0.32
Number of electrode layers	12
Negative Electrode Specifications	
Current collector material	Copper
Current collector thickness	12 μm
Active material	Graphite
Binder	PVdF
Electrode loading	5.1 mAh/cm^2
Electrode thickness	212 μm
Electrode porosity	0.34
Number of electrode layers	13
Electrolyte and Seaparator Specifications	
Separator type	Celgard microporous membrane
Separator thickness	20 μm
Electrolyte salt	Lithium hexafluorophosphate ($LiPF_6$)
Electrolyte solvent	EC-EMC-DMC
Electrolyte concentration	1.2 mol/L

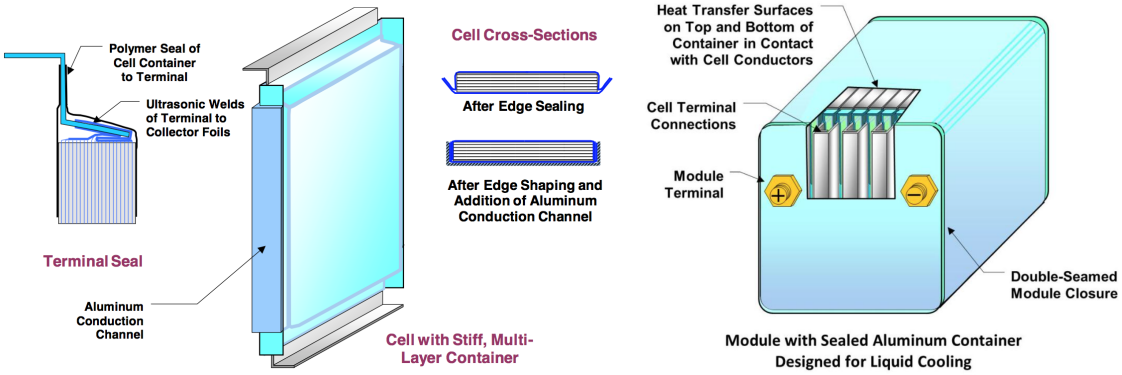

(a) Prismatic Li-ion Cell

(b) Module Consisting of Several Cells

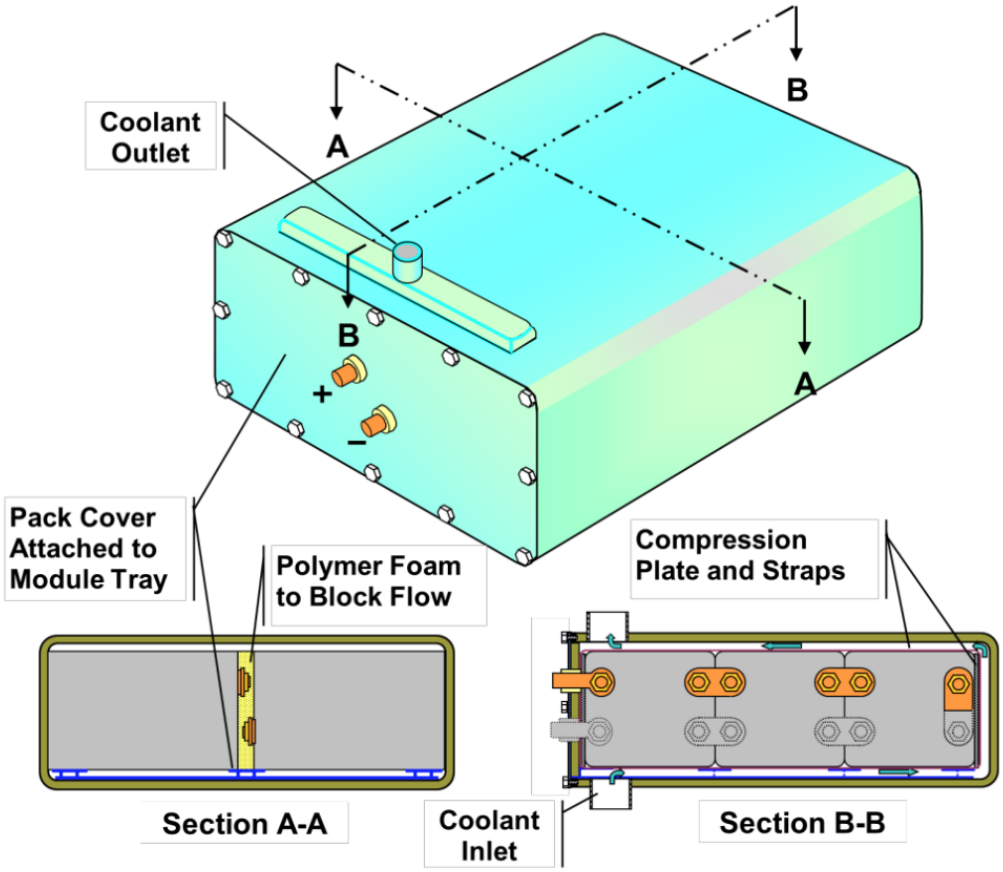

(c) Pack Consisting of Several Modules and Coolant Channels

Figure 6.2: The Li-ion battery pack considered consists of a number of interconnected battery modules, which themselves contain a number of interconnected battery cells. Coolant flows across the surface of the battery modules to regulate the battery's internal temperature. Figures from [94].

Table 6.2: Section 3.1.1 introduced specifications for the battery pack considered in this work. The specifications are given here for reference.

Parameter	Value
Battery Pack Parameters	
Rated energy capacity	30 kWh
Maximum power capability (10-second pulse)	110 kW
Design power	25 kW
Mass	230 kg
Number of modules in series	8
Battery Module Parameters	
Number of cells per parallel group	3
Number of parallel groups in series	24
Total number of cells per module	72

cility, and that manufacturing processes have matured [94, 95]. Thus, cost estimates produced from BatPaC should be considered optimistic. Nevertheless, BatPaC is one of the best tools currently available to approximate the cost of Li-ion batteries because: 1) it uses a bottom-up cost approximation that accounts for the specific active material and format of the battery considered; 2) it allows for sensitivity analysis on individual component costs and production scale; 3) it uses transparent assumptions that have been reviewed by major battery manufacturers; and 4) it is freely available to the public [94–96].

The cell- and pack-level specifications given in Tables 6.1–6.2 are entered into the BatPaC software, and then the software's database is used to approximate the various costs associated with the battery pack considered. A baseline manufacturing rate of 100,000 battery packs per year is assumed. Figure 6.3 illustrates the cost breakdown for the complete battery pack and only the Li-ion battery modules, which house the battery cells as illustrated in Figure 3.2. The costs for the complete pack

and only the modules are identified separately because it is assumed only the battery modules are replaced due to the effect of capacity loss with repeated cycling. That is, the purchased items that integrate the battery modules to form the battery pack and the battery management system (BMS) are replaced less frequently than the battery modules, because they do not degrade as quickly.

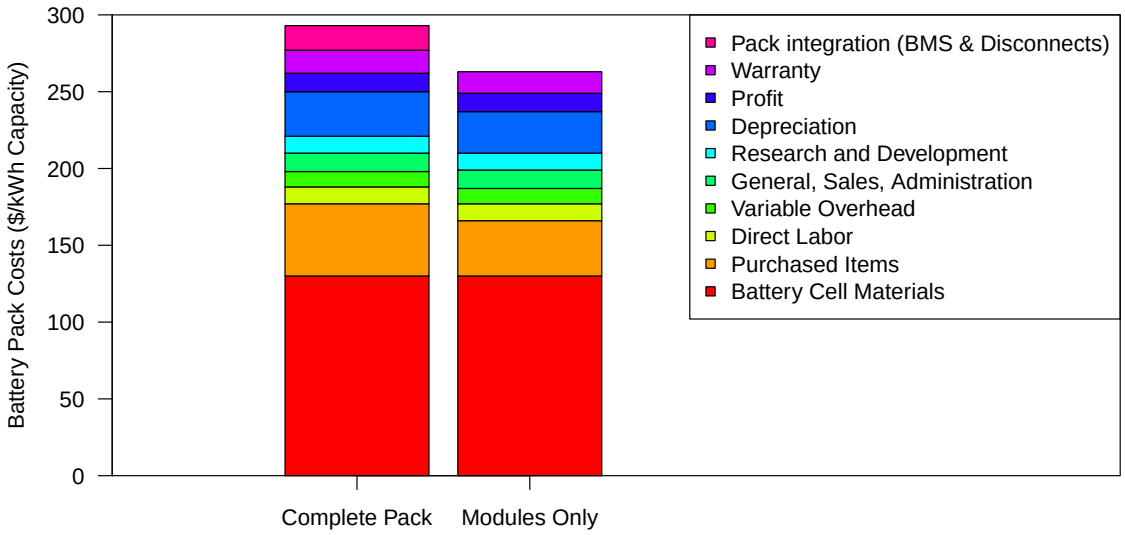

Figure 6.3: Cost breakdowns for the complete battery pack and the battery modules are estimated using the BatPaC software [96]. The difference between the pack and modules cost is primarily driven by the cost of additional purchased items and the BMS and disconnects that integrate the modules into the pack.

To assess how production scale, the unit costs of materials, and capital equipment costs affect the overall cost of the battery pack and modules, a sensitivity analysis is performed. Table 6.3 gives the parameters that are considered in the sensitivity analysis. These parameters are considered because they are the largest contributors to the overall battery price [94]. The ranges considered for each parameter are based on those given in the BatPaC manual [94].

Figure 6.4 shows the results of the sensitivity analysis on battery pack cost.

Table 6.3: Ranges are considered for the largest contributors to the overall battery cost in order to show how each factor affects the price of the battery pack and modules. The range considered for each parameter is based on values given in the BatPaC manual [94].

Cost Input	Low	Medium	High	Units
Manufacturing Rate	20,000	100,000	500,000	packs/year
Separator	0.75	2	4	$/m^2
Copper Foil Current Collector	1	1.8	2.6	$/m^2
Electrolyte	18	21.6	25.2	$/L
Graphite Anode Active Material Coating	12	19	25	$/kg
NMC Cathode Active Material Coating	22	31	34	$/kg
SOC Regulator and Safety Monitors	1.5	2.5	3.5	$/cell
Electrode Coating Captial Equipment	5	8	12	$ (millions)
Formation Cycling Capital Equipment	20	30	50	$ (millions)

The center of each bar corresponds to the cost of the battery when the Medium value for each parameter identified in Table 6.3 is entered into the BatPaC software. The extent of each bar indicates the range observed when the corresponding parameter is adjusted to its Low value and High value while other parameters remain held at their Medium values. The topmost bar labeled Low-High illustrates the cost range observed when all of the parameters in Table 6.3 are set to their low and high values. Results are shown for the complete battery pack. For all of the cases illustrated in Figure 6.4 the cost of the battery modules only is approximately $30/kWh less than the cost shown for the battery pack, because the cost of purchased items and the BMS is not sensitive to the parameters of Table 6.3.

Manufacturing rate has the greatest impact on the cost of the battery pack by far. This result makes sense, as electric vehicle market leader Tesla recently announced plans to invest $4-5 billion in a battery factory with a production scale of 500,000 battery packs per year to reduce the cost of its Li-ion battery packs and

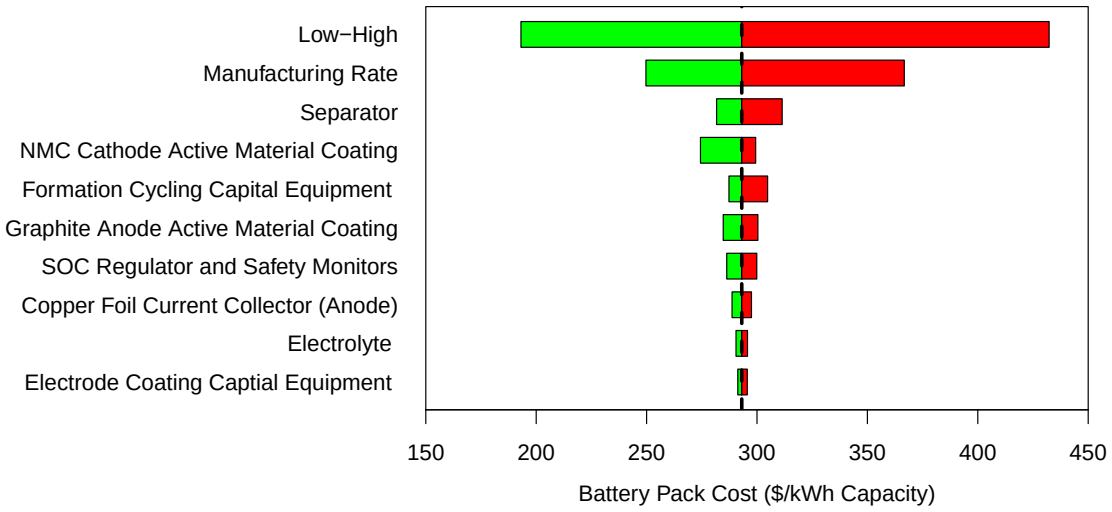

Figure 6.4: A sensitivity analysis is performed on battery pack cost to show how the parameters identified in Table 6.3 affect the cost of the battery. Manufacturing rate has the strongest effect on the battery cost, followed by the cost of the separator and the positive electrode active material.

vehicles [140]. After production scale, the costs of the microporous separator that divides the cathode from the anode and the cathode active material have the greatest impact of the overall cost of the battery, though their impact is relatively small ($\pm$ <\$20/kWh).

To validate the battery pack costs approximated using the BatPaC software, the results are compared to results from a recent review of Li-ion battery cost studies, which developed confidence intervals for the price of electric vehicle Li-ion battery packs for market leaders (Tesla, Nissan) and for the whole industry based on cost data reported by manufacturers, expert statements, journal publications, technical reports, and other sources [39]. Figure 6.5 compares the range illustrated in Figure 6.4 with the confidence intervals and point estimates for market leaders and the whole electric vehicle industry [39]. The range approximated from the BatPaC model is within

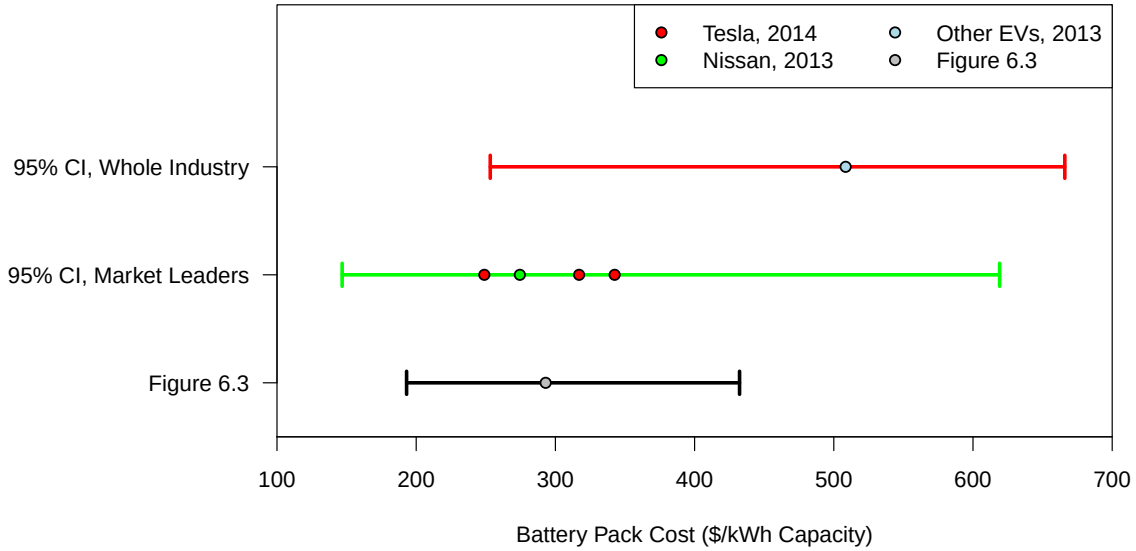

Figure 6.5: The cost range illustrated in Figure 6.4 is compared to confidence intervals (CIs) developed for the price of Li-ion battery packs based on cost data reported by manufacturers, expert statements, journal publications, technical reports, and other sources [39]. The cost approximated by the BatPaC model corresponds to current battery costs for electric vehicle market leaders [39].

the confidence interval for market leaders and the whole industry, and aligns with the most recent battery pack costs reported by electric vehicle market leaders [39]. While the BatPaC approximation is less than the price paid by other electric vehicle manufacturers in 2013, it is expected that the cost gap between market leaders and the wider industry will narrow in the coming years, and that the cost for Li-ion battery packs will converge to around $230/kWh by 2017–2018 [39]. Thus, the range of costs returned from the BatPaC model are used to approximate the cost of the battery pack considered in this work.

Table 6.4 summarizes the range of costs considered for the battery pack and the battery modules. Note that battery systems of various sizes could be constructed by placing more than one battery pack in series or parallel, so the costs given can be

used to approximate the cost of a larger battery system.

Table 6.4: Ranges are established for the costs of the complete battery pack and the battery modules only using the BatPaC software.

Component	Cost Range ($/kWh)		
	Low	Medium	High
Battery Modules	164	262	399
Battery Pack (Modules + BMS)	193	293	432

6.1.2 Power Conditioning System

With a range of costs approximated for the battery pack itself, the next step is to approximate the cost of the PCS, which facilitates the flow of power between the battery pack and the grid using an inverter/rectifier and appropriate controls.

The cost of the PCS is approximated using data from the literature and technical reports by the U.S. Department of Energy and The Electric Power Research Institute (EPRI) [21, 25, 117, 141–146]. Figure 6.6 illustrates the range of costs reported for battery energy storage system PCS equipment and installation in each of these references. Costs are reported in $/kW of rated PCS power capability. The point estimate for each reference is indicated by the height of each bar. For those references that provide a range of PCS costs, the minimum and maximum values reported are indicated by the range illustrated for each bar.

The references roughly agree on the range of costs for the PCS with the exception of the 2013 U.S. Department of Energy/EPRI Energy Storage Handbook by Akhil et al. [21]. The higher PCS costs estimated by this reference correspond to small-scale battery systems between 50 kW and 100 kW. Table 6.5 gives the range of PCS costs estimated by Akhil et al. for PCS ranging from 50–100,000 kW in rated

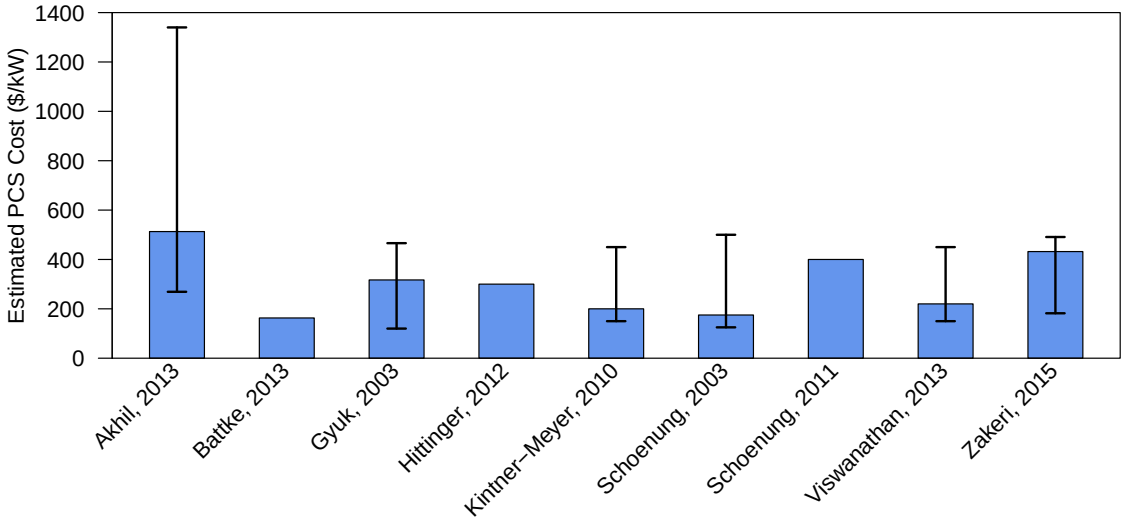

Figure 6.6: Literature references report a wide range of costs for the PCS [21, 25, 117, 141–146]. The higher costs reported by Akhil et al. correspond to battery systems of 50–100 kW. Costs reported in Gyuk et al. correspond to a power rating of 1–10 MW. Other literature references did not provide the PCS power ratings over which the given costs are applicable.

power capacity. Note that the point estimate given for this reference in Figure 6.6 corresponds to the average of the values given in Table 6.5. For larger battery systems, the PCS cost converges to approximately $300/kW [21].

Other references identified in Figure 6.6 did not specify the power capacity of the PCS considered for their cost estimates, with the exception of the 2003 U.S. Department of Energy/EPRI Energy Storage Handbook by Gyuk et al., which specified applicability for systems with a power capacity of 1–10 MW [25]. Thus, it is unclear whether the PCS costs given are representative of kW-scale battery systems or only larger MW-scale systems. Regardless, the cost of the PCS is expected to vary based on the particular battery system. A 2014 survey of battery system providers found that all manufacturers currently design PCS equipment in house and source

Table 6.5: Akhil et al. report a wider range of PCS costs than other literature references. The higher PCS costs correspond to small-scale battery systems with a rated power of 50–100 kW. The reported PCS cost converges to approximately $300/kW for power capacities greater than 1,000 kW. Only a point estimate was presented for each level of power capacity [21].

PCS Power Capacity (kW)	PCS Cost ($/kW)
50	1,340
100	1,185
250	658
500	584
1,000	459
2,000	327
2,500	321
3,000	312
5,000	304
10,000	342
25,000	288
50,000	281
100,000	269

manufacturing to other power electronics component manufacturers [147]. Thus, PCS systems designed for the same applications and power capability might vary in cost per kW due to different design decisions made by the battery system provider.

To estimate the cost of an integrated battery energy storage system using the Li-ion battery packs considered in this work, the range of PCS costs identified in Table 6.6 is considered. The rationale for each cost scenario is given. While the PCS costs considered vary by an order of magnitude, this variation is not caused exclusively by uncertainty in the PCS price. Rather, variation is caused by differing levels of production scale, standardization, and installed PCS capacity.

Table 6.6: A low, medium, and high cost for the PCS is developed based on the cost estimates illustrated in Figure 6.6 and the relationship between rated power cost identified in Table 6.5.

PCS Cost ($/kW)	Classification	Comments
120	Low	Represents a scenario with standardization and large-scale production of the PCS equipment and cost parity between kW-scale and MW-scale systems
300	Medium	Represents current prices for MW-scale systems and a cost target for kW-scale systems
1,300	High	Represents current prices for a 50 kW pilot system

6.1.3 Balance of Plant

With a range of costs established for the battery pack and the required PCS equipment, the final major component of the integrated energy storage system is the "balance of plant," which consists of a building or enclosure for the battery packs and PCS, utility interconnection equipment such as conductors and transformers, construction costs, and other miscellaneous costs [25, 141]. These costs can vary from one battery system to another, depending on where the battery system is installed on the grid, and the amount of new infrastructure required to interconnect and site the battery system.

Literature references are used to approximate the upfront balance of plant costs. Figure 6.7 summarizes the range of balance of plant costs approximated in the literature [21, 25, 117, 141, 144]. Costs are expressed in $/kW of installed power capacity. The typical cost reported is approximately $100/kW. Few literature references consider balance of plant costs in detail. Rather, many references ignore balance of

plant costs or assume they are insignificant [142, 143, 145, 146]. The range given by Viswanathan et al. was developed from a review of the literature. The wider range given by Akhil et al. was developed by considering various utility interconnection scenarios, and the associated upfront infrastructure cost in each scenario [21]. The high cost reported by Akhil et al. of \$500/kW corresponds to a 250 kW system that requires a new remote switch and step-up transformer [21]. The low cost of \$10/kW corresponds to a 100 kW system that is installed at an existing distribution transformer [21]. The average reported cost of \$150/kW is approximately equal to other balance of plant costs given in the literature [21, 25, 117, 141, 144].

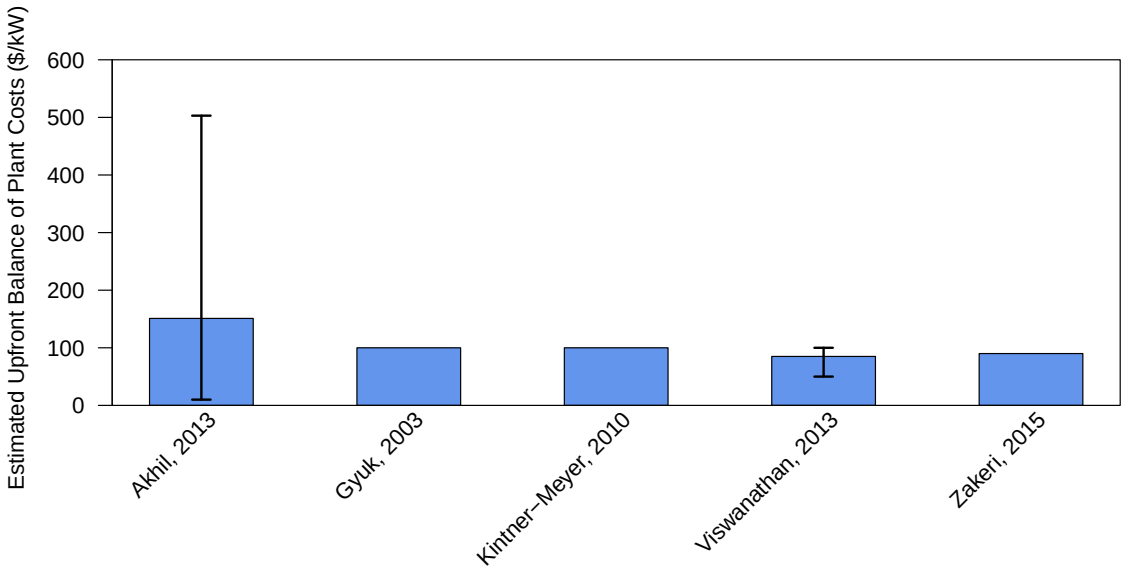

Figure 6.7: Literature references that quantify upfront balance of plant costs report a cost of approximately \$100/kW of installed power capacity [21, 25, 117, 141, 144]. The wider range reported in Akhil et al. stems from the fact that it considers a range of required new utility interconnection equipment, from only smart metering equipment to a new feeder, substation, and transformers [21]. Other studies do not discuss the specific components of balance of plant costs [25, 117, 141, 144].

Based on the upfront balance of plant cost range illustrated in Figure 6.7, this work considers a range of upfront balance of plant costs from \$10–\$500/kW

and a point estimate equal to $100/kW. The low cost considered corresponds to a scenario where the energy storage system can be added to a section of the grid without significant new infrastructure required (i.e. only civil engineering costs), while the high cost corresponds to a scenario where new utility infrastructure is required to interconnect the system with the grid [21].

6.1.4 Operation and Maintenance

Like a conventional power plant, a Li-ion energy storage plant has costs associated with operation and maintenance (O&M). For a grid battery system, fixed operation and maintenance costs are the annual costs associated with a regular maintenance program [25]. Variable O&M costs are incremental costs associated with power conversion efficiencies, energy for thermal management, and other parasitic energy losses associated with operating the battery system [25]. Because the analysis of Chapter 4 included the costs associated with energy losses in the battery pack, PCS, and thermal management system to calculate the Li-ion battery system's annual revenue potential, only fixed O&M costs are considered for this analysis.

Fixed O&M costs are approximated from values reported in the literature. Figure 6.8 compares fixed O&M costs approximated for Li-ion battery energy storage in the literature. Costs are approximated in $/kW of rated system power capacity on an annual bases. Estimates from various literature sources roughly agree on the expected O&M costs for a Li-ion energy storage system, and place the annual cost at approximately $2–$40/kW per year.

Based on the literature data illustrated in Figure 6.8, this work assumes a point estimate for fixed O&M costs equal to $13/kW per year and a possible range of O&M costs from $2–$40/kW per year.

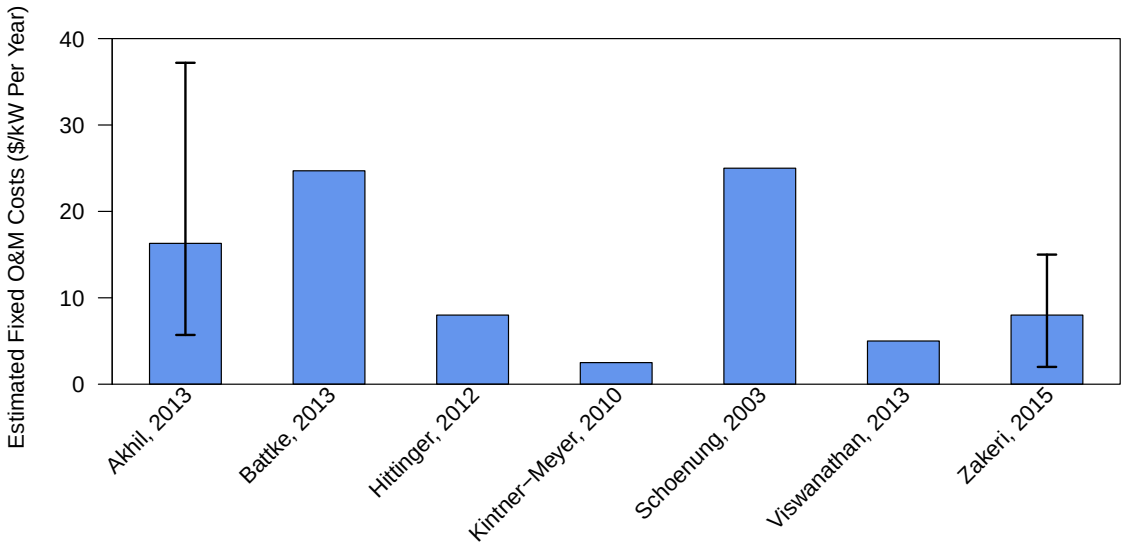

Figure 6.8: Literature references are used to approximate the annual O&M costs associated with a Li-ion energy storage system [21, 117, 141–144, 146].

6.2 Cash Flow Analysis and Approximation of Net-Present Value

The cost ranges developed for various Li-ion energy storage system components in the previous section are used to perform a cash flow analysis, which calculates the NPV of an energy storage system as a function of the positive and negative cash flows that occur during its lifetime. Section 6.2.1 introduces general calculations to approximate the NPV of a Li-ion battery system using the battery pack considered, and then Sections 6.2.2 and 6.2.3 apply the methodology to show the NPV of a battery used in particular applications.

6.2.1 Cash Flow Analysis and Financial Assumptions

To calculate the NPV of a battery system, information must be known about 1) the battery system's lifetime and the duration of the investment, 2) the recurring

revenue or benefits from the battery system, 3) the upfront and recurring costs of the battery system, and 4) the rate of inflation and the discount rate [21, 25, 40, 148].

To show the value of a system using the battery pack considered in a general way, the NPV is calculated by normalizing costs and benefits into units of $/kWh of energy storage capacity. This normalization method is used because energy capacity is the cost-determining factor for the battery pack considered [94,95]. Battery systems of various sizes could be constructed by connecting a number of battery packs in series or parallel.

The lifetime of the battery system and the total duration of capital investment are estimated at 15 years [21, 25, 40, 145]. A range of 10–20 years is considered to show the effect of this parameter on NPV [21, 25, 40, 145]. The lifetime of the battery modules is less than the lifetime of the battery system, and approximated from the results of Chapter 4, which modeled the lifetime of the battery modules under different operational scenarios. The modules are replaced when their end-of-life capacity is reached, and then retired when the remainder of the battery system reaches the end of its useful life.

To model the replacement of the battery modules with sufficient temporal resolution, the cash flow of the battery system is modeled on a monthly basis. The NPV of a battery system that operates for N years with monthly normalized cash flows R^m_{kWh} is calculated according to Equation 6.1. The variable d_m is the effective monthly nominal discount rate, which adjusts the value of future cash flows based on the cost of capital for the owner of the energy storage system. The monthly discount rate is calculated from the annual nominal discount rate d according to Equation 6.2. Similarly, i_m is the effective monthly inflation rate calculated from the annual inflation rate i according to Equation 6.3. The annual nominal discount rate is

estimated at 7.5% per year, corresponding to the weighted average cost of capital for an investor-owned utility [21]. To show the effect that discount rate has on the overall NPV, a range of discount rates from 5–10% is considered, where 5% corresponds to a municipal utility and 10% corresponds to an independent investor [21]. Likewise, the annual inflation rate is estimated at 3% per year and a range of 1–5% is considered to show the impact of the assumed inflation rate on the overall NPV.

$$NPV = \sum_{m=0}^{12N} \frac{R_{kWh}^{m}(1+i_m)^m}{(1+d_m)^m} \tag{6.1}$$

$$d_m = (1+d)^{(1/12)} - 1 \tag{6.2}$$

$$i_m = (1+i)^{(1/12)} - 1 \tag{6.3}$$

The upfront cost for the battery packs, PCS, and balance of plant are modeled as a negative cash flow at month $m = 0$. Equation 6.4 calculates the upfront cost of the battery system per unit of energy storage capacity as a function of the battery pack cost (C_{kWh}^{Pack}), PCS cost (C_{kW}^{PCS}), and balance of plant cost (C_{kW}^{BOP}). As given in the previous section, the battery pack cost is expressed per kWh of energy capacity while the PCS and balance of plant costs are expressed per kW of rated power. To express these costs per kWh of energy storage capacity, the power to energy ratio P/E of the battery pack is used, as defined in Equation 6.5. The values for P_{max} and E_{rated} are defined as given in Chapter 4.

$$C_{kWh}^{\text{Upfront}} = -C_{kWh}^{\text{Pack}} - C_{kW}^{PCS}(P/E) - C_{kW}^{\text{BOP}}(P/E) \tag{6.4}$$

$$P/E = P_{\max}/E_{\text{rated}} = 40\text{kW}/30\text{kWh} = 4/3\ \text{h}^{-1} \tag{6.5}$$

The cost associated with replacing the battery modules is modeled as a negative cash flow that occurs at months $m = m_1^r, \cdots, m_n^r$, where m_n^r indicates the month during which the nth module replacement occurs. The corresponding module replacement cost C_{kWh}^{Modules} is the cost for the modules only calculated in Section 6.1.1. The number of module replacements required is calculated using the results of Chapter 4, which modeled the lifetime of the battery modules under different operational scenarios. The following sections calculate NPV for module replacement intervals corresponding to different operational scenarios.

Because the battery modules might be replaced a number of times during the lifetime of the energy storage system, the modules could have a remaining useful life after the energy storage system is decommissioned. To account for any value retained by the battery modules at the end of the investment, it is assumed the modules can be sold at a depreciated price during the final investment month $m = 12N$. The depreciated module price $C_{kWh}^{\text{Modules,d}}$ is defined in Equation 6.6 in terms of the remaining module lifetime in years ($y_{\text{remaining}}^{\text{Modules}}$) and the expected module lifetime in years ($y_{\text{lifetime}}^{\text{Modules}}$).

$$C_{kWh}^{\text{Modules,d}} = \frac{y_{\text{remaining}}^{\text{Modules}}}{y_{\text{lifetime}}^{\text{Modules}}} C_{kWh}^{\text{Modules}} \tag{6.6}$$

The upfront cost of the battery system and the cost of replacing the battery modules are the greatest magnitude cash flows that occur over the lifetime of the investment. Remaining cash flows from electricity market revenue, the avoided cost of electric outages, and routine O&M costs are modeled as uniform monthly costs or benefits that occur throughout the life of the system. The recurring monthly benefit

from market revenue and avoided electric outages (B^m_{kWh}) is calculated in terms of the annual market revenue potential ($R^{\text{Market},y}_{kWh}$) and annual reliability benefit ($R^{\text{Reliability},y}_{kWh}$) approximated in Chapters 4 and 5, respectively, according to Equation 6.7. Likewise, the recurring monthly O&M costs per kWh of energy storage capacity $C^{OM,m}_{kWh}$ are calculated from the annual O&M costs per kW ($C^{OM,y}_{kW}$) approximated in Section 6.1.4, as defined in Equation 6.8.

$$B^m_{kWh} = \frac{R^{\text{Market},y}_{kWh} + R^{\text{Reliability},y}_{kWh}}{12} \tag{6.7}$$

$$C^{OM,m}_{kWh} = \frac{C^{OM,y}_{kW}(P/E)}{12} \tag{6.8}$$

The value of the monthly cash flow R^m_{kWh} is summarized in Equation 6.9. Month $m = 0$ is the upfront period before the battery system commences operation. Months $m = m^r_1, \cdots, m^r_n$ are the months when the battery modules are replaced. Month $m = 12N$ is the final month of operation, during which the modules are sold are at their depreciated value defined in Equation 6.6. During all other operating months the cash flow is equal to the difference between the benefit defined in Equation 6.7 and the O&M costs defined in Equation 6.8.

$$R^m_{kWh} = \begin{cases} -C^{\text{Upfront}}_{kWh} & \text{if } m = 0 \\ -C^{\text{Modules}}_{kWh} & \text{if } m = m^r_1, \cdots, m^r_n \\ C^{\text{Modules,d}}_{kWh} & \text{if } m = 12N \\ B^m_{kWh} - C^{OM,m}_{kWh} & \text{otherwise} \end{cases} \tag{6.9}$$

Table 6.7 summarizes the ranges considered for costs and financial parameters that affect that NPV of the battery system. The following sections use these parameters and the methodology developed in this section to calculate the NPV of battery system used for wholesale energy arbitrage and a combination of energy and Fast

Responding Regulation Service (FRRS) in the Electric Reliability Council of Texas (ERCOT) electricity market.

Table 6.7: Literature data and a U.S. Department of Energy Battery Performance and Cost Model (BatPaC) model were used to approximate the cost and financial parameters for a Li-ion energy storage system. The ranges considered for each parameter are summarized here.

			Value		Units
Parameter	Variable	Low	Medium	High	
Battery Modules Cost	C_{kWh}^{Modules}	164	262	399	$/kWh
Battery Pack Cost	C_{kWh}^{Pack}	193	293	432	$/kWh
PCS Cost	C_{kW}^{PCS}	120	300	1,300	$/kW
Balance of Plant Cost	C_{kW}^{BOP}	10	100	500	$/kW
O&M Cost	C_{kW}^{OM}	2	13	40	$/kW Per Year
Discount Rate	d	5	7.5	10	%/year
Inflation Rate	i	1	3	5	%/year
System Lifetime	N	10	15	20	years

6.2.2 Calculation of NPV for Wholesale Energy Arbitrage

The positive cash flows accumulated during the investment period are approximated from the results of Chapters 4 and 5, which calculated the annual market revenue potential and reliability benefit, respectively. The annual market revenue potential $R_{kWh}^{\text{Market},y}$ is approximated from the results of Figure 4.15, which summarizes the market revenue potential calculated for the wholesale energy arbitrage application in the ERCOT market. Table 6.8 summarizes the ranges considered for market revenue potential when capacity degradation is controlled in the optimization objective function and when capacity degradation is neglected and the battery simply responds to electricity market price signals. Likewise, Table 6.9 presents the range considered for the potential annual reliability benefit $R_{kWh}^{\text{Reliability},y}$ from avoided residential electric

outages.

Table 6.8: Ranges are developed for the annual market revenue potential $R_{kWh}^{\text{Market},y}$ for wholesale energy arbitrage based on the results illustrated in Figure 4.15.

Market Application	Control Degradation	Annual Revenue Potential ($/kWh Per Year) Low	Medium	High
Energy arbitrage	Yes	6	35	88
Energy arbitrage	No	17	42	104

Table 6.9: A range is developed for the potential annual reliability $R_{kWh}^{\text{Reliability},y}$ from avoided electric outages based on the results of Table 5.6.

Reliability Application	Annual Reliability Benefit ($/kWh Per Year) Low	Medium	High
Residential islanding service	0	1.5	3

The lifetime of the battery modules depends on whether capacity degradation is considered in the optimization objective function for wholesale energy arbitrage, the battery's operating temperature, and the modules' end-of-life capacity ratio. The modeled lifetime of the battery modules in the wholesale energy arbitrage application is summarized in Figure 4.16. Table 6.10 presents the range of battery module lifetimes $y_{\text{lifetime}}^{\text{Modules}}$ considered to calculate the battery system NPV in the wholesale energy arbitrage application.

The values for the parameters that affect NPV developed in this section are used with the parameters given in Table 6.7 to calculate the monthly cash flow per kWh of rated energy capacity R_{kWh}^{m} defined in Equation 6.9, and then NPV is calculated according to Equation 6.1. The resulting NPV range observed is illustrated in Figure 6.9. Figure 6.9a shows the NPV range when capacity degradation is controlled

Table 6.10: Ranges are developed for the lifetime of the battery modules used in the wholesale energy arbitrage application based on the results illustrated in Figure 4.16.

Market Application	Control Degradation	Estimated Module Lifetime (years) Low	Medium	High
Energy arbitrage	Yes	3.2	8.3	11.0
Energy arbitrage	No	2.3	5.6	7.9

in the optimization objective function that is used to schedule the battery system in the electricity market. Figure 6.9b shows the NPV range when capacity degradation is neglected in the optimization objective function. The dashed vertical line indicates the point estimate for NPV calculated when each parameter is set to its given Medium value. The green bar indicates the NPV calculated when the corresponding parameter is set to its Low value, and the red bar indicates the value calculated when the corresponding parameter is set to its High value.

Regardless of whether capacity degradation is considered in the optimization objective function, the NPV of the battery system is negative for the wholesale energy arbitrage application. The NPV ranges from approximately $-\$2,190$/kWh to $-\$180$/kWh across the range of values considered for the parameters that affect NPV. This result aligns with previous studies that have found there is insufficient revenue from wholesale energy arbitrage alone to cover the present cost of a battery system [45, 149, 150].

However, considering capacity degradation is shown to increase NPV by an average of \$100/kWh across the range of parameters considered. Thus, for the case of a battery used for wholesale energy arbitrage, the overall value of the battery system is increased when capacity degradation is considered in battery operational management as proposed in this work. Any revenue lost from operating in a more conservative

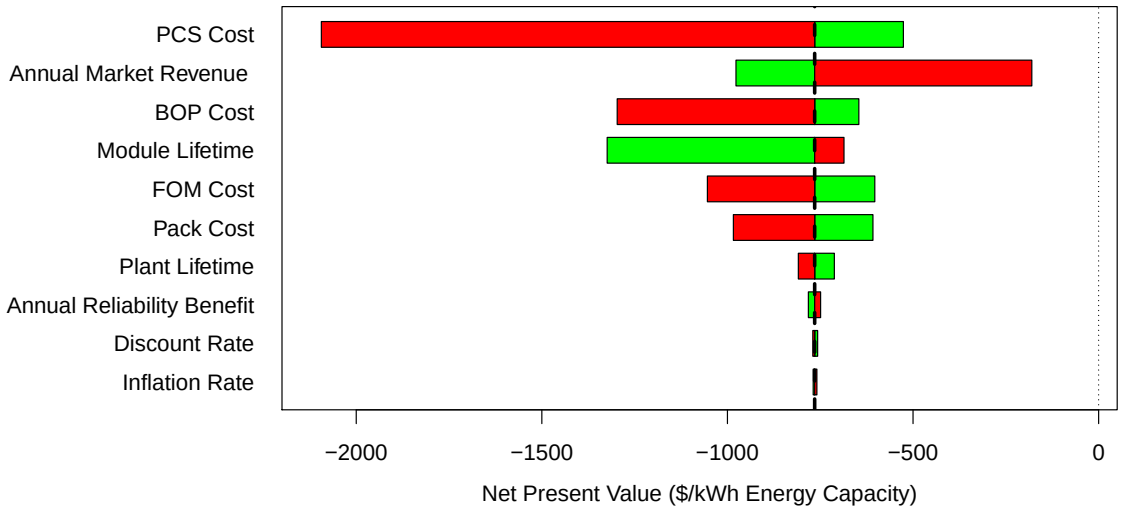

(a) Control Degradation in Optimization Objective Function

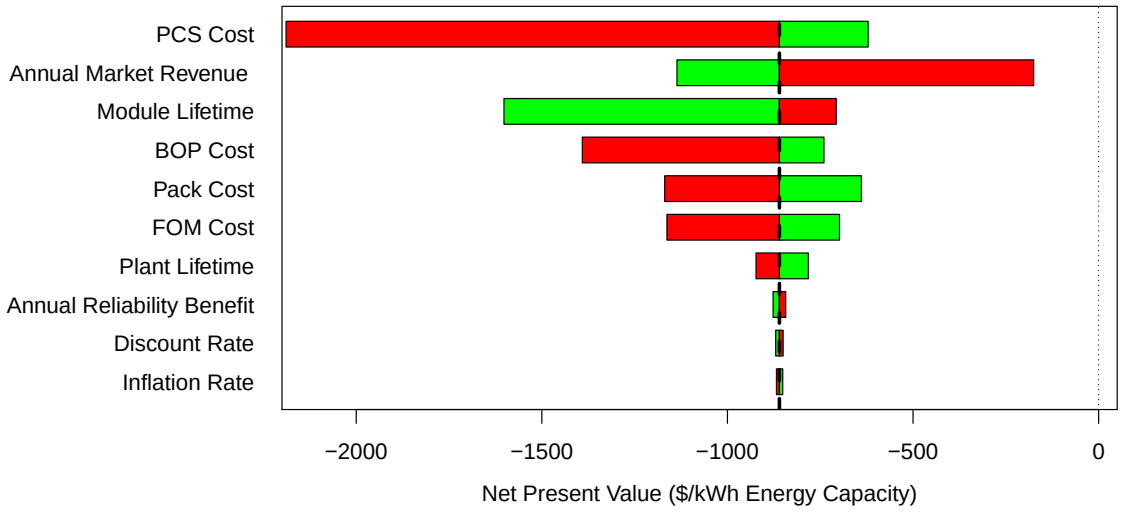

(b) Neglect Degradation in Optimization Objective Function

Figure 6.9: The NPV of the battery system in the wholesale energy arbitrage application is shown for the range of values considered for each parameter. The bold dashed vertical line indicates the NPV calculated when each parameter is set equal to its Medium value. The green bar indicates the NPV calculated when the corresponding parameter is set to its Low value, and the red bar indicates the value calculated when the corresponding parameter is set to its High value. Considering capacity degradation in the objective function increases the NPV by approximately \$100/kWh. However, the NPV is negative for all of the scenarios considered.

fashion is made up for by the greater module lifetime attained when capacity loss is controlled in the optimization objective function. The observed increase in value is similar in magnitude to the increase resulting from reducing O&M costs, balance of plant costs, or the cost of the battery pack.

While considering capacity degradation in the optimization objective function increases the NPV for energy arbitrage, doing so has a smaller effect on NPV than other uncertain and variable parameters considered. Based on the results of Figure 6.9, the PCS cost has the greatest impact on the NPV of the battery system. This result was obtained because a wide range was considered for the PCS cost based on a lack of agreement between different literature references. While PCS cost significantly affects the battery system NPV, the cost of the PCS could most likely be controlled and reduced by standardizing the PCS design, increasing production scale, or increasing the rated power of the battery system, as discussed in Section 6.1.2. However, the literature typically treats the cost of the PCS with little detail compared to the cost of the battery pack itself, so the PCS cost might be different than the range assumed in this work. Future work should treat the cost of the PCS in more detail, because it has a strong effect on the NPV of the battery system.

Notably, the second most important parameter identified in Figure 6.9 is the annual revenue from energy arbitrage. In other words, the volatility present in electricity market prices has a significant impact on the value of the battery system. This finding agrees with previous findings for the case of energy storage operating in New York State [46]. Unlike the PCS cost, a battery system investor would have little or no control over the electricity market prices. Rather, these prices would be subject to external factors like the price of natural gas, the amount of renewable energy installed, and local congestion in the transmission network [120–122].

Another parameter that has a significant effect on the NPV of the battery system used in the wholesale energy arbitrage application is the lifetime of the battery modules. If the module lifetime is less than expected (the Low values given in Table 6.10), the NPV of the battery system is reduced by approximately \$560–\$740/kWh. However, extending the module lifetime has a smaller effect on NPV, increasing value by only \$80–\$150/kWh for the High values of module lifetime considered. This finding stems from the fact that extending the module lifetime provides diminishing returns as the lifetime of the battery modules approaches the lifetime of the battery system and the total duration of capital investment. This fact also causes the module lifetime to be less significant for the case where capacity degradation is controlled versus the case where capacity degradation is neglected.

Balance of plant costs also have the potential to significantly reduce the NPV of the battery system. Unlike some of the other parameters considered, balance of plant costs could be controlled and reduced by 1) installing energy storage in areas of the grid where it will not require significant new infrastructure, or 2) maximizing the amount of energy storage capacity installed per dollar of required investment in supporting infrastructure. Balance of plant costs are often not treated with sufficient detail or ignored in the literature. Because these costs have been shown to be significant, future work could seek to provide a more detailed accounting of balance of plant costs.

With the value of a battery used for wholesale energy arbitrage approximated, the following section carries out a NPV analysis for a battery that is used for a combination of energy and FRRS in the ERCOT market.

6.2.3 Calculation of NPV for Energy and FRRS

As was done for the battery used for wholesale energy arbitrage, the positive cash flows accumulated during the investment period are approximated from the results of Chapters 4 and 5, which calculated the annual market revenue potential and reliability benefit, respectively. The annual market revenue potential $R_{kWh}^{\text{Market},y}$ is approximated from the results of Figure 4.32, which summarizes the market revenue potential of the battery system providing energy and FRRS in the ERCOT market. Table 6.11 summarizes the ranges considered for market revenue potential when capacity degradation is controlled in the optimization objective function and when capacity degradation is neglected and the battery simply responds to electricity market price signals. Likewise, Table 6.12 presents the range considered for the potential annual reliability benefit $R_{kWh}^{\text{Reliability},y}$ from avoided residential electric outages.

Table 6.11: Ranges are developed for the annual market revenue potential $R_{kWh}^{\text{Market},y}$ for energy and FRRS based on the results illustrated in Figure 4.32.

Market Application	Control Degradation	Annual Revenue Potential ($/kWh Per Year) Low	Medium	High
Energy and FRRS	Yes	113	259	538
Energy and FRRS	No	138	275	548

Table 6.12: A range is developed for the potential annual reliability $R_{kWh}^{\text{Reliability},y}$ from avoided electric outages based on the results of Table 5.6.

Reliability Application	Annual Reliability Benefit ($/kWh Per Year) Low	Medium	High
Residential islanding service	0	1.5	3

The lifetime of the battery modules depends on whether capacity degradation

is considered in the optimization objective function used to schedule the battery for energy and FRRS, the battery's operating temperature, and the modules' end-of-life capacity ratio. The modeled lifetime of the battery modules in the energy and FRRS application is summarized in Figure 4.33. Table 6.13 presents the range of battery module lifetimes $y_{\text{lifetime}}^{\text{Modules}}$ considered to calculate the battery system NPV.

Table 6.13: Ranges are developed for the lifetime of the battery modules used in the energy and FRRS application based on the results illustrated in Figure 4.33.

Market Application	Control Degradation	Estimated Module Lifetime (years) Low	Medium	High
Energy and FRRS	Yes	4.0	8.3	10.8
Energy and FRRS	No	2.5	5.8	8.1

The values for the parameters that affect NPV developed in this section are used with the parameters given in Table 6.7 to calculate the monthly cash flow per kWh of rated energy capacity R_{kWh}^{m} defined in Equation 6.9, and then NPV is calculated according to Equation 6.1. The resulting NPV range observed is illustrated in Figure 6.10. Figure 6.10a shows the NPV range when capacity degradation is controlled in the optimization objective function that is used to schedule the battery system in the electricity market. Figure 6.10b shows the NPV range when capacity degradation is neglected in the optimization objective function. The dashed vertical line indicates the point estimate for NPV calculated when each parameter is set to its given Medium value. The green bar indicates the NPV calculated when the corresponding parameter is set to its Low value, and the red bar indicates the value calculated when the corresponding parameter is set to its High value.

The NPV of the battery used for a combination of energy and FRRS is positive across all of the parameters considered. Regardless of whether capacity degradation

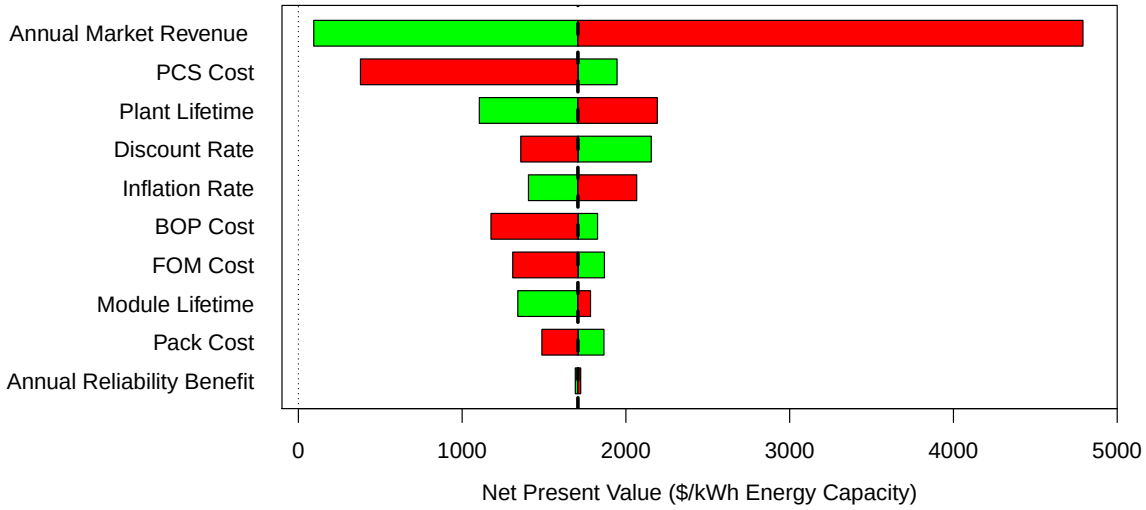

(a) Control Degradation in Optimization Objective Function

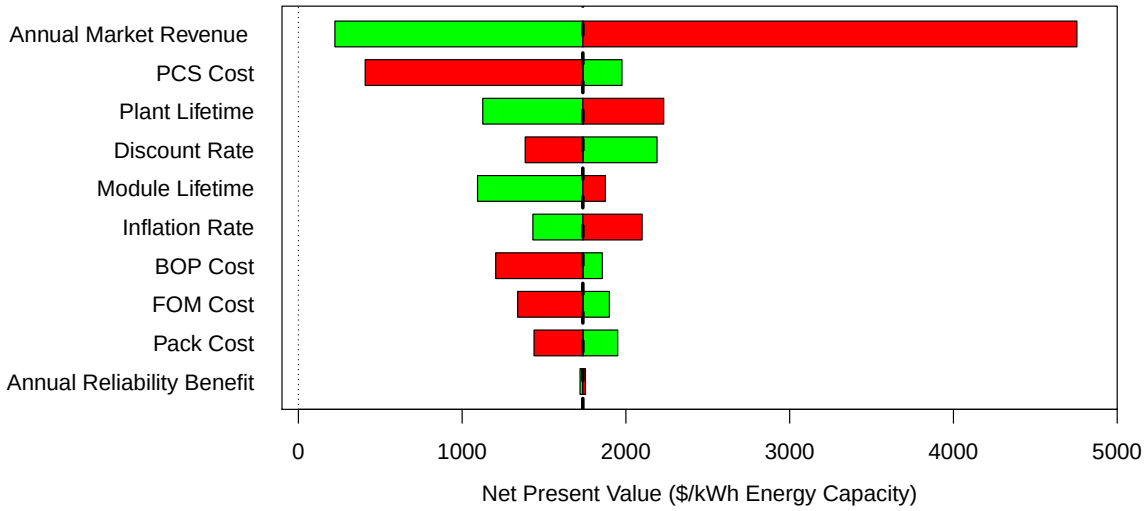

(b) Neglect Degradation in Optimization Objective Function

Figure 6.10: The NPV of the battery system in the energy and FRRS application is shown for the range of values considered for each parameter. The dashed vertical line indicates the NPV calculated when each parameter is set equal to its Medium value. The green bar indicates the NPV calculated when the corresponding parameter is set to its Low value, and the red bar indicates the value calculated when the corresponding parameter is set to its High value. The NPV is positive for all of the values of the parameters considered.

is considered or neglected in the optimization objective function, the point estimate for NPV corresponding to the Medium value of all parameters considered is approximately \$1,700/kWh, corresponding to an internal rate of return approximately equal to 38%. This finding aligns with previous studies that have found frequency regulation service to be a significantly more valuable application for grid energy storage than wholesale energy arbitrage [40, 41, 45, 46, 151, 152]. The maximum NPV calculated across the range of parameters considered is approximately \$4,800/kWh, and the minimum is approximately \$94/kWh.

Unlike the battery used for wholesale energy arbitrage only, there is little difference between the results obtained when capacity loss is controlled in the objective function versus when capacity loss is neglected and the optimization program simply responds to market price signals. The point estimate for NPV is \$1,707/kWh when capacity loss is considered and \$1,737/kWh when capacity loss is neglected. This finding occurs because the annual revenue potential is significantly higher in the energy and FRRS application, so the cost and lifetime of the battery modules have less overall impact on NPV.

While controlling capacity loss has a small impact on NPV for most of the cost and benefit parameters considered, doing so causes NPV to be less sensitive to the variation in the lifetime of the battery modules caused by varying temperature conditions or uncertainty in the end-of-life capacity ratio. The module lifetime is the eighth most significant parameter when capacity loss is controlled, and the fifth most important parameter when capacity loss is neglected. Furthermore, if the module lifetime is less than expected (the Low value identified in Table 6.13), the NPV is nearly \$300/kWh greater when capacity loss is controlled. Thus, controlling capacity loss in the battery operational management as proposed in this work might be a useful

strategy to reduce the risks associated with unexpected, accelerated capacity fade in the battery cells.

Notably, the calculated NPV is relatively insensitive to the lifetime of the battery system, balance of plant costs, the lifetime of the battery modules, the discount rate, O&M costs, the cost of the battery pack, and the benefit from avoided electric outages. A broad range was considered for each of these parameters based on values that have been published in the literature and analysis carried out in this work, yet adjusting these parameters does not cause the NPV to fall below approximately $1,090/kWh.

The parameter with the strongest effect on NPV by far is the annual market revenue potential from energy and FRRS. The market revenue potential is driven by the prevailing prices for up- and down-regulation service. These prices are typically correlated with the real-time price of electricity, which itself is correlated with the external price of natural gas [121]. During years when the natural gas price was high (e.g. 2008), the revenue potential from energy and FRRS was significantly higher. However, even If the annual revenue from energy and FRRS is equal to the Low values given in Table 6.11 for the duration of the investment, the battery system can still achieve a positive NPV. Thus, a Li-ion battery system could provide FRRS to ERCOT at a profit even if the prices for regulation service are lower than is typical.

In addition to the external electricity market prices, the cost of the PCS also has a significant impact on the NPV of the battery system, as was found for the case of a battery used for wholesale energy arbitrage only. This finding stems from the wide range of costs that was considered for the PCS due to disagreement between literature references on the cost of the PCS equipment. Typically, studies focus on the cost of the battery modules and the revenue of the battery system, but treat the

cost of the PCS without sufficient detail. Because the PCS cost significantly affects NPV, future work should seek to more accurately identify the cost the of the PCS under various scenarios.

6.3 Chapter Conclusion

This chapter approximated the cost of components that make up a Li-ion energy storage system to approximate the NPV of a Li-ion battery system used for wholesale energy arbitrage or a combination of energy and FRRS in Texas's ERCOT electricity market.

First, the BatPaC model developed by the U.S. Department of Energy was used to approximate the expected range of costs for the Li-ion battery pack that was characterized, modeled, and evaluated in previous portions of this work. Then, the costs for the PCS, balance of plant, and routine O&M were approximated using literature data. Put together, the costs estimated show the range of upfront and recurring costs expected for a Li-ion energy storage system installed on the electric grid.

The cost approximated for the Li-ion energy storage system was combined with the annual market revenue potential and reliability benefit from avoided electric outages approximated in Chapters 4 and 5, respectively, to estimate the NPV of the battery system under different operational scenarios.

The NPV range approximated for the wholesale energy arbitrage application showed that a positive NPV cannot be achieved at today's Li-ion battery system costs and level of electricity price volatility. The cost of the PCS and the level of electricity market price volatility were found to have the greatest impact on the NPV of the battery system considered. The cost of the PCS could most likely be

reduced by standardizing the PCS design, increasing production scale, or increasing the rated power of the battery system, as discussed in Section 6.1.2. However, there is disagreement in the literature about the cost of the PCS. Future work should seek to clarify the expected price of PCS equipment for battery energy storage systems. Unlike the PCS cost, the level of electricity price volatility could not be controlled by a battery system investor or operator. Rather, the level of price volatility depends on factors that can be difficult to predict, such as the level of electric demand, the price of natural gas, transmission system congestion, and the level of electric generation from any intermittent renewable energy resources.

While the NPV of the battery system in the wholesale energy arbitrage application was found to be negative, the NPV analysis revealed that controlling capacity degradation in Li-ion battery operational management as proposed in this work could increase the NPV of the battery system by approximately \$100/kWh of energy storage capacity by extending the operating lifetime of the battery modules. Any revenue lost from operating in a more conservative fashion is made up for by the greater module lifetime attained when capacity loss is controlled in the optimization objective function. Controlling capacity loss in the objective function was found to have similar potential to increase NPV as reducing O&M costs, balance of plant costs, or the cost of the battery pack. Future work should explore the value of modeling and controlling capacity loss using the optimization framework proposed in this work for different battery chemistries to test the effect of controlling capacity loss for systems with different capacity degradation mechanisms that those of the Li-ion battery pack considered.

Unlike the results for the wholesale energy arbitrage application, the NPV approximated for the energy and FRRS application was found to be positive across

all of the parameters considered and insensitive to most cost parameters. Thus, Li-ion battery energy storage could most likely provide a combination of energy and FRRS service to the ERCOT electricity market with sufficient operating profits to cover the cost of the battery system and provide a suitable return on investment. The prices for frequency regulation service were found to have the greatest impact on the value of the battery system. However, even for the lowest annual revenue potential calculated using price data from years 2002–2014, the battery system could still achieve a NPV that is positive. Thus, the battery system could likely still produce sufficient operating profits even when the prices for frequency regulation are low.

Controlling capacity degradation in the optimization objective function was found to have less impact on the value for energy and FRRS than was for the case of a battery used for wholesale energy arbitrage only. By operating more conservatively, the battery system extends the lifetime of its battery modules but foregoes some operating revenue from energy and FRRS. The resulting tradeoff between module lifetime and annual revenue causes the NPV when capacity loss is controlled to be approximately equal to the NPV when capacity loss is neglected. However, controlling capacity loss in operational management of the battery system caused the NPV to become less sensitive to uncertainty about the lifetime of the battery modules. Thus, controlling capacity loss as proposed in this work could be used as a strategy to reduce the risks associated with accelerated battery module capacity loss.

Chapter 7

Conclusion

This work introduced methods to characterize lithium-ion (Li-ion) battery energy storage, optimally schedule its participation in electricity markets, assess its market revenue potential and reliability benefit from avoided electric outages, and approximate its net-present value (NPV).

Chapter 3 developed methods to characterize a Li-ion battery system using performance data collected from experiments or electrochemical simulations. Data collected from an electrochemical model of a Li-ion battery pack were used to characterize its dynamic voltage behavior, dynamic temperature gain, and capacity degradation behavior using empirical models. The models developed were found to accurately predict the Li-ion battery pack's dynamic performance and degradation under diverse operating conditions, despite the fact that they require significantly less computational power than a first-principles electrochemical model. To schedule a Li-ion battery system in an electricity market while controlling its voltage, temperature, and rate of capacity degradation, the empirical models developed to describe the battery system were discretized and integrated with a nonlinear optimization program. The model-based optimization framework developed could be used to manage the operation of any Li-ion battery system. To implement the framework, a Li-ion battery manufacturer or operator would characterize their system using experiments or electrochemical simulation software. Then, the models developed to describe voltage, temperature, and capacity loss would be fit to the extracted performance data.

Finally, the model parameters would be entered into the optimization program developed in Section 3.2, so that the battery's participation in an electricity market could be optimally scheduled while its voltage, temperature, and capacity loss are controlled.

To demonstrate the use of the proposed optimization framework, Chapter 4 applied it to the case of Li-ion energy storage operating in Texas's electricity market. It was found that the proposed optimization framework can 1) robustly find a charge-discharge schedule that maximizes electricity market revenues, 2) model and constrain the dynamic voltage, current, temperature, and state of charge of the Li-ion battery system considered, and 3) model and control capacity loss that results from using the Li-ion battery system in the electricity market. To assess the value of a Li-ion battery system operating over many years, the optimization program was applied to historic Electric Reliability Council of Texas (ERCOT) electricity prices from 2002–2014. Results from the analysis revealed the revenue potential of a Li-ion battery system used for wholesale energy arbitrage only and a combination of energy and Fast Responding Regulation Service (FRRS). The annual revenue potential was found to vary significantly based on the energy price volatility and frequency regulation price magnitude during the operating year. The calculated revenue potential for energy arbitrage ranged from \$6–\$104/kWh of energy capacity per year, while the annual revenue potential for energy and FRRS combined ranged from \$114–\$548/kWh. It was found that controlling capacity degradation in the optimization objective function used to schedule the battery system's participation in the electricity market increases its lifetime by 30–60% without significantly reducing its market revenue potential.

To investigate the market-external reliability benefits of adding Li-ion energy storage to the grid, Chapter 5 simulated Li-ion energy storage installed at the residen-

tial distribution transformer that is used to isolate downstream electricity customers during an electric outage. Electricity use and production data collected from 21 Austin, Texas homes were used to approximate the electric load that would be placed on the battery system during an electric outage. It was found that a 30 kWh battery system installed at the distribution transformer could withstand an average duration outage up to 74% of the time, even if no solar panels are installed in the community. Occasions when the battery system cannot withstand an average duration outage were found to typically occur between the hours of 15:00 and 20:00, when electricity demand peaks in Texas. Because solar energy production peaks before this period, adding solar panels to the community was not found to significantly increase the ability to withstand an average duration outage. Increasing solar penetration from 0% to 100% only increased the probability of the 30 kWh battery system withstanding an outage from 74% to 86%. However, adding solar panels to the community was found to significantly increase the potential islanding duration after morning outages, allowing the 30 kWh battery system to power downstream homes for up to approximately 15 hours, even when its initial state of charge is only 10%. The results of the analysis were used to approximate the annual reliability benefit from avoided residential electric outages. The annual reliability benefit was found to range from \$0–\$3/kWh of energy storage capacity, depending on when an outage occurs, the amount of solar generation available, the battery system's initial state of charge before an outage, and its rated energy capacity.

With the market revenue potential and reliability benefit from avoided residential electric outages estimated, Chapter 6 approximated the cost of an integrated Li-ion energy storage system in order to calculate its NPV under different operational scenarios. The cost of the Li-ion battery pack was estimated using a bottom-up Battery Performance and Cost Model (BatPaC) developed by the U.S. Department of

Energy, and a sensitivity analysis was performed to show the impact that various parameters have on the overall cost of the battery pack. The cost of the battery pack was found to range from \$190–\$430/kWh of rated energy capacity, depending on the unit cost of materials and the level of production scale. The costs for remaining Li-ion energy storage system components including the power conditioning system (PCS), balance of plant, and routine operation and maintenance (O&M) were estimated using literature data. Then, a cash flow analysis was performed to assess the NPV of the battery system when it is used for wholesale energy arbitrage and a combination of energy and FRRS in the ERCOT electricity market.

It was found that the NPV of a battery system used for wholesale energy arbitrage only is consistently negative across the range of cost and revenue parameters considered. However, controlling capacity loss in the optimization objective function as proposed in this work was found to increase the system's NPV by approximately \$100/kWh of rated energy storage capacity, similar in magnitude to the benefit achieved by reducing O&M costs, balance of plant costs, or the cost of the battery pack. Any revenue lost from operating in a more conservative fashion was made up for by the greater module lifetime attained when capacity loss was controlled in the optimization objective function. Thus, controlling capacity degradation in Li-ion energy storage operational management as proposed in this work could be a useful strategy to increase the NPV of Li-ion energy storage used for wholesale energy arbitrage in electricity markets.

The NPV of Li-ion energy storage used for a combination of energy and FRRS in ERCOT was found to be positive across all of the cost and benefit parameters considered in the NPV calculations. Thus, Li-ion battery energy storage could most likely provide a combination of energy and FRRS service to the ERCOT electricity

market with sufficient operating profits to cover the cost of the battery system and provide a suitable return on investment. The prices for frequency regulation service were found to have the greatest impact on the value of the battery system. Because these prices are influenced by the price of electric energy, the level of electric demand, the price of natural gas, and other factors, it might be difficult for a battery system investor to predict the expected future prices for frequency regulation service. Nevertheless, even for the lowest annual revenue potential calculated using price data from years 2002–2014, the battery system could still achieve a positive NPV. Thus, the battery system could likely still produce sufficient operating profits even when the prices for frequency regulation are low.

Unlike the results for the wholesale energy arbitrage application, controlling capacity degradation in the optimization objective function for energy and FRRS was not found to strongly impact the NPV of the battery system. By operating more conservatively, the battery system extends the lifetime of its battery modules but foregoes some operating revenue from energy and FRRS. The resulting tradeoff between module lifetime and annual revenue caused the NPV when capacity loss is controlled to be approximately equal to the NPV when capacity loss is neglected. However, controlling capacity loss in the optimization objective function made the NPV of the battery system less sensitive to unexpected deviations in the lifetime of the battery modules caused by temperature variation or uncertainty associated with electrochemical degradation processes. Thus, controlling capacity degradation as proposed in this work could be a useful strategy to reduce the risks associated with premature battery cell failure due to capacity loss.

To build on the methods and analysis introduced in this work, future work could explore the potential to model and control capacity degradation in other battery

chemistries that might be used on the electric grid in the future. Depending on the battery chemistry, the mechanisms that control capacity loss might be different than those for the $LiNi_{1/3}Mn_{1/3}Co_{1/3}O_2$ (NMC) Li-ion battery system modeled in this work. By characterizing and modeling capacity degradation behavior in different battery chemistries, future researchers could identify a chemistry for which controlling capacity loss using methods similar to those introduced in this work significantly increases the overall NPV of the battery system.

Furthermore, if sufficient tests are carried out for a particular battery cell configuration, information about its capacity degradation under different conditions could be disseminated in a standard form that allows engineers using the battery cell in various applications to model and control its capacity degradation, potentially reducing the cost burden associated with the relatively short lifetime of some battery cells compared to other capital equipment.

Future work could also expand on the methods developed in this work to explore the potential for using partially-degraded automotive Li-ion batteries in stationary grid applications. The partially-degraded state of a used automotive Li-ion battery could be used as the initial state in the optimization program developed in this work so that the secondary market revenue potential of an automotive Li-ion battery pack can be approximated.

To improve the framework to model and optimize the operation of Li-ion storage introduced in this work, future work could explore the potential to reduce the complexity of the models used to describe dynamic battery performance and integrate them into a model-predictive control (MPC) framework. By reducing the number of resistor-capacitor couples used to describe the diffusion of ions within the Li-ion battery, approximating the voltage behavior as linear over a predefined state

of charge window, or other methods, future researchers could simplify the proposed optimization framework and implement it within an MPC framework to show the potential to make electricity market decisions within a real-time control context with imperfect foresight.

To improve the economic performance of grid-connected battery energy storage, future work could investigate the costs associated with PCS equipment and other balance of plant costs required to site and interconnect a battery energy storage system. The literature and technical reports typically focus on the cost of the battery packs themselves, and treat PCS and balance of plant costs with less detail. However, this work found that these costs can have a strong impact on the value of a Li-ion energy storage system. To understand and reduce these costs in the future, researchers could seek to disseminate more information about the specific costs associated with PCS equipment and other ancillary costs required to integrate an energy storage system with the electric grid.

This work modeled Li-ion energy storage that responds to historic electricity prices to investigate the value of first-entry Li-ion energy storage and show the impact of modeling and controlling capacity loss in battery operational management. If sufficient energy storage capacity is installed on the electric grid, it would influence the prices for both energy and ancillary services. Future work could investigate the influence that increasing levels of energy storage capacity would have on electricity prices. Furthermore, future work could investigate electricity market designs that can be used to schedule energy storage as part of the independent system operator (ISO) security-constrained economic dispatch (SCED) program that is used to schedule conventional power generation. Today, battery energy storage is not fully integrated with SCED scheduling programs, because they do not model the remaining energy

capacity of grid connected batteries or other energy storage devices.

As the cost of grid energy storage technologies declines, they will see increasing use on the electric grid, and there will be a growing need for effective operational frameworks and electricity market designs to coordinate energy storage with other electricity generating technologies, including both dispatchable and intermittent forms of generation. If operational methods can be developed at a pace that matches the development of energy storage technologies, there is an opportunity for energy storage to fundamentally transform the electric grid, and overcome limitations that have persisted since its inception.

Bibliography

[1] U.S. Energy Information Administration. (2014) Electricity. [Online]. Available: ww.eia.gov/electricity

[2] Electric Advisory Committee and U.S. Department of Energy, "Energy Storage Activities in the United States Electric Grid," U.S. Department of Energy, Tech. Rep., 2011.

[3] C.-J. Yang and R. B. Jackson, "Opportunities and barriers to pumped-hydro energy storage in the united states," *Renewable and Sustainable Energy Reviews*, vol. 15, no. 1, pp. 839 – 844, 2011.

[4] R. A. Walling and GE Energy, "Analysis of wind generation impact on ERCOT ancillary services requirements," General Electric Energy, Tech. Rep., 2008.

[5] M. Hand, S. Baldwin, E. DeMeo, J. Reilly, T. Mai, D. Arent, G. Porro, M. Meshek, and D. Sandor, "Renewable Electricity Futures Study: Executive Summary," Tech. Rep., 2012.

[6] U.S. Department of Energy, "DOE Global Energy Storage Database." [Online]. Available: http://www.energystorageexchange.org/

[7] A. Dehamna and S. Jaffe, "Executive Summary: Energy Storage for the Grid and Ancillary Services," Navigant Research, Tech. Rep., 2014. [Online]. Available: https://www.navigantresearch.com/research/energy-storage-for-the-grid-and-ancillary-services

[8] Frost & Sullivan, "Innovation Across Key Industries to Quadruple Revenues for Lithium-Ion Batteries," Tech. Rep., 2014. [Online]. Available: http://ww2.frost.com/news/press-releases/innovation-across-key-industries-quadruple-revenues-lithium-ion-batteries/

[9] Public Utilities Commission of the State of California, "Decision Adopting Energy Storage Procuremant Framework and Design Program," 2013. [Online]. Available: http://docs.cpuc.ca.gov/PublishedDocs/Published/G000/M079/K533/79533378.PDF

[10] ConEdison, "Demand management incentives." [Online]. Available: http://www.coned.com/energyefficiency/demand_management_incentives.asp

[11] N. Y. State, "Reforming the energy vision (rev)." [Online]. Available: http://www3.dps.ny.gov/W/PSCWeb.nsf/All/26BE8A93967E604785257CC40066B91A?OpenDocument

[12] J. Chang, I. Karkatsouli, J. Pfeifenberger, L. Regan, K. Spees, J. Mashal, and M. Davis, "The Value of Distributed Electricity Storage in Texas," The Brattle Group, Tech. Rep. November, 2014. [Online]. Available: http://www.brattle.com/system/news/pdfs/000/000/749/original/The_Value_of_Distributed_Electricity_Storage_in_Texas.pdf

[13] W. M. Warwick, "A Primer on Electric Utilities, Deregulation, and Restructuring of U.S. Electricity Markets," Pacific Northwest National Laboratory, Tech. Rep., 2002. [Online]. Available: http://www.pnl.gov/main/publications/external/technical_reports/PNNL-13906.pdf

[14] The Electric Energy Market Competition Task Force, "Report to congress on competition in wholesale and retail markets for electric energy," Federal

Energy Regulatory Commission, Tech. Rep., 2005. [Online]. Available: http://www.ferc.gov/legal/fed-sta/ene-pol-act/epact-final-rpt.pdf

[15] Federal Energy Regulatory Commission, "Energy Primer: A Handbook of Energy Market Basics," Federal Energy Regulatory Commission, Tech. Rep., 2012. [Online]. Available: http://www.ferc.gov/market-oversight/guide/energy-primer.pdf

[16] ERCOT, "ERCOT Nodal Protocols," 2014.

[17] R. Baldick. Restructured electricity markets: Locational marginal pricing. [Online]. Available: http://users.ece.utexas.edu/~baldick/classes/394V/EE394V.html

[18] S. Stoft, *Power System Economics: Designing Markets for Electricity.* Wiley-IEEE Press, 2002.

[19] D. S. Kirschen and G. Strbac, *Fundamentals of Power System Economics.* Wiley, 2004.

[20] Federal Energy Regulatory Commission. North American Regional Transmission Organizations. [Online]. Available: http://www.ferc.gov/market-oversight/mkt-electric/overview/elec-ovr-rto-map.pdf

[21] A. A. Akhil, G. Huff, A. B. Currier, B. C. Kaun, D. M. Rastler, S. B. Chen, A. L. Cotter, D. T. Bradshaw, and W. D. Gauntlett, "DOE/EPRI 2013 Electricity Storage Handbook in Collaboration with NRECA," Sandia National Laboratories, Tech. Rep. July, 2013.

[22] D. Connolly, "A Review of Energy Storage Technologies For the integration of fluctuating renewable energy," University of Limerick, Tech. Rep.

August, 2009. [Online]. Available: http://vbn.aau.dk/files/100570335/Energy_Storage_Techniques_v4.1.pdf

[23] H. Ibrahim, A. Ilinca, and J. Perron, "Energy storage systemsCharacteristics and comparisons," *Renewable and Sustainable Energy Reviews*, vol. 12, no. 5, pp. 1221–1250, Jun. 2008. [Online]. Available: http://linkinghub.elsevier.com/retrieve/pii/S1364032107000238

[24] S. Vazquez, S. M. Lukic, E. Galvan, L. G. Franquelo, and J. M. Carrasco, "Energy Storage Systems for Transport and Grid Applications," *IEEE Transactions on Industrial Electronics*, vol. 57, no. 12, pp. 3881–3895, 2010. [Online]. Available: http://ieeexplore.ieee.org/lpdocs/epic03/wrapper.htm?arnumber=5582228

[25] I. Gyuk, S. Eckroad, U.S. Department of Energy, and The Electric Power Research Institute, "EPRI-DOE Handbook of Energy Storage for Transmission & Distribution Applications," EPRI-DOE, Tech. Rep. December, 2003.

[26] H. Chen, T. N. Cong, W. Yang, C. Tan, Y. Li, and Y. Ding, "Progress in electrical energy storage system: A critical review," *Progress in Natural Science*, vol. 19, no. 3, pp. 291–312, Mar. 2009.

[27] B. Dunn, H. Kamath, and J. M. Tarascon, "Electrical Energy Storage for the Grid: A Battery of Choices," *Science*, vol. 334, no. 6058, pp. 928–935, Nov. 2011.

[28] A. A. Akhil, J. D. Boyes, P. C. Butler, and D. H. Doughty, "Batteries for Electrical Energy Storage Applications," in *Linden's Handbook of Batteries*, 4th ed. McGraw Hill, 2011, ch. 30, pp. 30.1–30.45.

[29] Z. Yang, J. Zhang, M. C. W. Kintner-Meyer, X. Lu, D. Choi, J. P. Lemmon, and J. Liu, "Electrochemical energy storage for green grid." *Chemical reviews*, vol. 111, no. 5, pp. 3577–613, May 2011. [Online]. Available: http://www.ncbi.nlm.nih.gov/pubmed/21375330

[30] A. Z. Weber, M. M. Mench, J. P. Meyers, P. N. Ross, J. T. Gostick, and Q. Liu, "Redox flow batteries: a review," *Journal of Applied Electrochemistry*, vol. 41, no. 10, pp. 1137–1164, Sep. 2011. [Online]. Available: http://www.springerlink.com/index/10.1007/s10800-011-0348-2

[31] I. Hadjipaschalis, A. Poullikkas, and V. Efthimiou, "Overview of current and future energy storage technologies for electric power applications," *Renewable and Sustainable Energy Reviews*, vol. 13, no. 6-7, pp. 1513–1522, 2009.

[32] H. L. Ferreira, R. Garde, G. Fulli, W. Kling, and J. P. Lopes, "Characterisation of electrical energy storage technologies," *Energy*, vol. 53, pp. 288–298, 2013. [Online]. Available: http://dx.doi.org/10.1016/j.energy.2013.02.037

[33] A. Evans, V. Strezov, and T. J. Evans, "Assessment of utility energy storage options for increased renewable energy penetration," *Renewable and Sustainable Energy Reviews*, vol. 16, no. 6, pp. 4141–4147, 2012. [Online]. Available: http://dx.doi.org/10.1016/j.rser.2012.03.048

[34] "A ten-mile storage battery," *Popular Science*, July 1930. [Online]. Available: https://books.google.com/books?id=sigDAAAAMBAJ

[35] C.-J. Yang and R. B. Jackson, "Opportunities and barriers to pumped-hydro energy storage in the United States," *Renewable and Sustainable Energy Reviews*, vol. 15, no. 1, pp. 839–844, Jan. 2011.

[36] B. Roberts and J. Harrison, "Energy Storage Activities in the United States Electricity Grid," Electricity Advisory Committee, Tech. Rep., 2011.

[37] B. Diouf and R. Pode, "Potential of lithium-ion batteries in renewable energy," *Renewable Energy*, vol. 76, pp. 375–380, 2015. [Online]. Available: http://dx.doi.org/10.1016/j.renene.2014.11.058

[38] P. Kurzweil, *Lithium Battery Energy Storage : State of the Art Including Lithium e Air and Lithium e Sulfur Systems*. Elsevier B.V., 2015. [Online]. Available: http://dx.doi.org/10.1016/B978-0-444-62616-5.00016-4

[39] B. Nykvist and M. n. Nilsson, "Rapidly falling costs of battery packs for electric vehicles," *Nature Climate Change*, vol. 5, no. April, pp. 100–103, 2015. [Online]. Available: http://www.nature.com/doifinder/10.1038/nclimate2564

[40] J. Eyer and G. Corey, "Energy Storage for the Electricity Grid: Benefits and Market Potential Assessment Guide A Study for the DOE Energy Storage Systems Program," Sandia National Laboratories, Tech. Rep. February, 2010.

[41] J. Eyer and B. Norris, "Guide to Estimating Benefits and Market Potential for Electricity Storage in New York," Tech. Rep., 2007.

[42] S. M. Schoenung, J. M. Eyer, J. J. Iannucci, and S. A. Horgan, "Energy Storage for a Competitive Power Market," *Annual Review of Energy and the Environment*, vol. 21, no. 1, pp. 347–370, Nov. 1996. [Online]. Available: http://arjournals.annualreviews.org/doi/abs/10.1146/annurev.energy.21.1.347

[43] I. Gyuk, P. Kulkarni, J. Sayer, J. Boyes, G. Corey, and G. Peek, "The united states of storage," *IEEE Power and Energy Magazine*, vol. 3, no. 2, pp. 31 – 39, march-april 2005.

[44] P. C. Butler, J. Iannucci, and J. Eyer, "Innovative Business Cases For Energy Storage In a Restructured Electricity Marketplace," Sandia National Laboratories, Tech. Rep. February, 2003.

[45] A. Zucker, T. Hinchliffe, and A. Spisto, "Assessing Storage Value in Electricity Markets: A literature review," European Commission Joint Research Centre, Tech. Rep., 2013.

[46] R. Walawalkar, J. Apt, and R. Mancini, "Economics of electric energy storage for energy arbitrage and regulation in New York," *Energy Policy*, vol. 35, no. 4, pp. 2558–2568, Apr. 2007.

[47] S. J. Kazempour, M. P. Moghaddam, M. R. Haghifam, and G. R. Yousefi, "Electric energy storage systems in a market-based economy: Comparison of emerging and traditional technologies," *Renewable Energy*, vol. 34, no. 12, pp. 2630–2639, Dec. 2009. [Online]. Available: http://linkinghub.elsevier.com/retrieve/pii/S0960148109001906

[48] C. K. Ekman and S. r. H. j. Jensen, "Prospects for large scale electricity storage in Denmark," *Energy Conversion and Management*, vol. 51, no. 6, pp. 1140–1147, Jun. 2010. [Online]. Available: http://linkinghub.elsevier.com/retrieve/pii/S0196890409005299

[49] R. Sioshansi, P. Denholm, T. Jenkin, and J. Weiss, "Estimating the value of electricity storage in PJM: Arbitrage and some welfare effects," *Energy Economics*, vol. 31, no. 2, pp. 269–277, Mar. 2009.

[50] X. He, E. Delarue, W. D'haeseleer, and J.-M. Glachant, "A novel business model for aggregating the values of electricity storage," *Energy Policy*,

vol. 39, no. 3, pp. 1575–1585, Mar. 2011. [Online]. Available: http://linkinghub.elsevier.com/retrieve/pii/S030142151000933X

[51] X. He, R. Lecomte, A. Nekrassov, E. Delarue, and E. Mercier, "Compressed air energy storage multi-stream value assessment on the french energy market," in *2011 IEEE Trondheim PowerTech*. IEEE, Jun. 2011, pp. 1–6. [Online]. Available: http://ieeexplore.ieee.org/lpdocs/epic03/wrapper.htm?arnumber=6019395

[52] E. Drury, P. Denholm, and R. Sioshansi, "The value of compressed air energy storage in energy and reserve markets," *Energy*, vol. 36, no. 8, pp. 4959–4973, Aug. 2011. [Online]. Available: http://linkinghub.elsevier.com/retrieve/pii/S0360544211003665

[53] P. Balducci, W. Colella, M. Elizondo, C. Jin, T. Nguyen, V. Viswanathan, and Y. Zhang, "National Assessment of Energy Storage for Grid Balancing and Arbitrage: Phase 1, WECC," Pacific Northwest National Laboratory, Tech. Rep. June, 2012. [Online]. Available: http://energyenvironment.pnnl.gov/pdf/PNNL-21388_National_Assessment_Storage_Phase_1_final.pdf

[54] D. Keles, R. Hartel, D. Most, and W. Fichtner, "Compressed-air energy storage power plant investments under uncertain electricity prices: an evaluation of compressed-air energy storage plants in liberalized energy markets," *The Journal of Energy Markets*, vol. 5, no. 1, 2012.

[55] H. Lund, G. Salgi, B. Elmegaard, and a. Andersen, "Optimal operation strategies of compressed air energy storage (CAES) on electricity spot markets with fluctuating prices," *Applied Thermal Engineering*, vol. 29,

no. 5-6, pp. 799–806, Apr. 2009. [Online]. Available: http://linkinghub.elsevier.com/retrieve/pii/S1359431108002469

[56] J. Newman, *Electrochemical Systems*. Prentice-Hall, 1972.

[57] M. Doyle, J. Newman, A. S. Gozdz, C. N. Schmutz, and J.-M. Tarascon, "Comparison of Modeling Predictions with Experimental Data from Plastic Lithium Ion Cells," *Journal of The Electrochemical Society*, vol. 143, no. 6, p. 1890, 1996. [Online]. Available: http://jes.ecsdl.org/cgi/doi/10.1149/1.1836921

[58] J. Newman, K. E. Thomas, H. Hafezi, and D. R. Wheeler, "Modeling of lithium-ion batteries," *Journal of Power Sources*, vol. 119-121, pp. 838–843, Jun. 2003.

[59] K. a. Smith, C. D. Rahn, and C.-Y. Wang, "Control oriented 1D electrochemical model of lithium ion battery," *Energy Conversion and Management*, vol. 48, no. 9, pp. 2565–2578, Sep. 2007. [Online]. Available: http://linkinghub.elsevier.com/retrieve/pii/S0196890407000908

[60] D. W. Dees, V. S. Battaglia, and A. Bélanger, "Electrochemical modeling of lithium polymer batteries," *Journal of Power Sources*, vol. 110, no. 2, pp. 310–320, Aug. 2002. [Online]. Available: http://linkinghub.elsevier.com/retrieve/pii/S0378775302001933

[61] C. Wang and V. Srinivasan, "Computational battery dynamics (CBD)electrochemical/thermal coupled modeling and multi-scale modeling," *Journal of Power Sources*, vol. 110, no. 2, pp. 364–376, Aug. 2002. [Online]. Available: http://linkinghub.elsevier.com/retrieve/pii/S0378775302001994

[62] J. Kalupson, G. Luo, and C. E. Shaffer, "AutoLion: A Thermally Coupled Simulation Tool for Automotive Li-Ion Batteries," Tech. Rep., Apr. 2013. [Online]. Available: http://www.sae.org/technical/papers/2013-01-1522

[63] T. Yoshida, M. Takahashi, S. Morikawa, C. Ihara, H. Katsukawa, T. Shiratsuchi, and J.-i. Yamaki, "Degradation Mechanism and Life Prediction of Lithium-Ion Batteries," *Journal of The Electrochemical Society*, vol. 153, no. 3, p. A576, 2006.

[64] EC Power, "Predictive Physics-based Degradation Modeling," Tech. Rep., 2013.

[65] A. Barré, B. Deguilhem, S. Grolleau, M. Gérard, F. Suard, and D. Riu, "A review on lithium-ion battery ageing mechanisms and estimations for automotive applications," *Journal of Power Sources*, vol. 241, pp. 680–689, Nov. 2013. [Online]. Available: http://linkinghub.elsevier.com/retrieve/pii/S0378775313008185

[66] W. Peukert, "Über die abhängigkeit der kapazität von der entladestromstärke bei bleiakkumulatoren," *Elektrotechnische Zeitschrift*, vol. 20, pp. 20–21, 1897.

[67] D. Doerffel and S. A. Sharkh, "A critical review of using the Peukert equation for determining the remaining capacity of lead-acid and lithium-ion batteries," *Journal of Power Sources*, vol. 155, no. 2, pp. 395–400, Apr. 2006.

[68] D. Rakhmatov, S. Vrudhula, and D. Wallach, "A model for battery lifetime analysis for organizing applications on a pocket computer," *IEEE Transactions on Very Large Scale Integration (VLSI) Systems*, vol. 11, no. 6, pp. 1019–1030, Dec. 2003.

[69] J. F. Manwell and J. G. McGowan, "Lead acid battery storage model for hybrid energy systems," *Solar Energy*, vol. 50, no. 5, pp. 399–405, May 1993.

[70] P. Rong, S. Member, and M. Pedram, "An Analytical Model for Predicting the Remaining Battery Capacity of Lithium-Ion Batteries," *IEEE Transactions on Very Large Scale Integration (VLSI) Systems*, vol. 14, no. 5, pp. 441–451, 2006.

[71] P. Pascoe and A. Anbuky, "VRLA Battery Discharge Reserve Time Estimation," *IEEE Transactions on Power Electronics*, vol. 19, no. 6, pp. 1515–1522, Nov. 2004.

[72] V. Agarwal and K. Uthaichana, "Development and Validation of a Battery Model Useful for Discharging and Charging Power Control and Lifetime Estimation," *IEEE Transactions on Energy Conversion*, vol. 25, no. 3, pp. 821–835, 2010.

[73] Z. Salameh, M. Casacca, and W. Lynch, "A mathematical model for lead-acid batteries," *IEEE Transactions on Energy Conversion*, vol. 7, no. 1, pp. 93–98, Mar. 1992.

[74] L. Gao, S. Liu, and R. A. Dougal, "Dynamic lithium-ion battery model for system simulation," *IEEE Transactions on Components and Packaging Technologies*, vol. 25, no. 3, pp. 495–505, Sep. 2002.

[75] M. Valvo, F. E. Wicks, R. Douglas, and S. Rudiii, "Development and Appliication of an Improved Equivalent Circuit Model of a Lead Acid Blattery," *Proceedings of the 31st Intersociety Energy Conversion Engineering Conference*, 1996.

[76] P. Mauracher and E. Karden, "Dynamic Modeling of lead/acid batteries using impedance spectroscopy for parameter identification," *Journal of Power Sources*, vol. 67, pp. 69–84, 1997.

[77] H. Wiegman and A. Vandenput, "Battery state control techniques for charge sustaining applications," *SAE transactions*, pp. 1–11, 1999.

[78] S. Buller and M. Thele, "Impedance-based simulation models of supercapacitors and Li-ion batteries for power electronic applications," *IEEE Transactions on Industry Applications*, vol. 41, no. 3, pp. 742–747, 2005.

[79] S. Gold, "A PSPICE macromodel for lithium-ion batteries," *The Twelfth Annual Battery Conference on Applications and Advances*, pp. 215–222, 1997.

[80] S. Hageman, "Simple pspice models let you simulate common battery types," *EDN*, vol. 38, pp. 117–117, 1993.

[81] M. Chen and G. Rincon-Mora, "Accurate electrical battery model capable of predicting runtime and IV performance," *IEEE Transactions on Energy Conversion*, vol. 21, no. 2, pp. 504–511, 2006.

[82] R. C. Kroeze and P. T. Krein, "Electrical battery model for use in dynamic electric vehicle simulations," *2008 IEEE Power Electronics Specialists Conference*, pp. 1336–1342, Jun. 2008. [Online]. Available: http://ieeexplore.ieee.org/lpdocs/epic03/wrapper.htm?arnumber=4592119

[83] P. Bauer and E. Kelder, "A practical circuit-based model for Li-ion battery cells in electric vehicle applications," *2011 IEEE 33rd International Telecommunications Energy Conference (INTELEC)*, pp. 1–9, Oct. 2011.

[Online]. Available: http://ieeexplore.ieee.org/lpdocs/epic03/wrapper.htm?arnumber=6099803

[84] B. G. Kim, D. D. Patel, and Z. M. Salameh, "Circuit Model of 100 Ah Lithium Polymer Battery Cell," *Journal of Power and Energy Engineering*, vol. 01, no. 06, pp. 1–8, 2013.

[85] J. Li, M. Mazzola, J. Gafford, and N. Younan, "A new parameter estimation algorithm for an electrical analogue battery model," *2012 Twenty-Seventh Annual IEEE Applied Power Electronics Conference and Exposition (APEC)*, pp. 427–433, Feb. 2012. [Online]. Available: http://ieeexplore.ieee.org/lpdocs/epic03/wrapper.htm?arnumber=6165855

[86] J. Li, M. S. Mazzola, J. Gafford, B. Jia, and M. Xin, "Bandwidth based electrical-analogue battery modeling for battery modules," *Journal of Power Sources*, vol. 218, pp. 331–340, Nov. 2012. [Online]. Available: http://linkinghub.elsevier.com/retrieve/pii/S0378775312011202

[87] B. Schweighofer, K. M. Raab, and G. Brasseur, "Modeling of High Power Automotive Batteries by the Use of an Automated Test System," *IEEE Transactions on Instrumentation and Measurement*, vol. 52, no. 4, pp. 1087–1091, 2003.

[88] S. Abu-Sharkh and D. Doerffel, "Rapid test and non-linear model characterisation of solid-state lithium-ion batteries," *Journal of Power Sources*, vol. 130, no. 1-2, pp. 266–274, May 2004.

[89] X. Han, M. Ouyang, L. Lu, and J. Li, "A comparative study of commercial lithium ion battery cycle life in electric vehicle: Capacity loss estimation," *Journal of Power Sources*, vol. 268, pp. 658–669, Dec. 2014. [Online]. Available: http://linkinghub.elsevier.com/retrieve/pii/S0378775314009756

[90] M. Broussely, P. Biensan, F. Bonhomme, P. Blanchard, S. Herreyre, K. Nechev, and R. Staniewicz, "Main aging mechanisms in Li ion batteries," *Journal of Power Sources*, vol. 146, no. 1-2, pp. 90–96, Aug. 2005. [Online]. Available: http://linkinghub.elsevier.com/retrieve/pii/S0378775305005082

[91] EC Power, *User's Manual - AutoLion-ST: A Thermally Coupled Battery Model for System-level Analysis of Li-ion Battery Packs*, 2nd ed., 2013.

[92] American Electric Power, "Functional Specification For Community Energy Storage (CES) Unit," Tech. Rep., 2009.

[93] D. Rastler and {EPRI}, "Technology Review and Assessment of Distributed Energy Resources - Distributed Energy Storage," {The Electric Power Research Institute}, Tech. Rep. 3, 2006.

[94] P. A. Nelson, K. G. Gallagher, I. Bloom, and D. W. Dees, "Modeling the Performance and Cost of Lithium-Ion Batteries for Electric-Drive Vehicles," Tech. Rep., 2012. [Online]. Available: http://www.cse.anl.gov/batpac/files/BatPaCANL-12_55.pdf

[95] K. G. Gallagher and P. a. Nelson, "Manufacturing Costs of Batteries for Electric Vehicles," in *Lithium-Ion Batteries*. Elsevier, 2014, pp. 97–126. [Online]. Available: http://www.sciencedirect.com/science/article/pii/B9780444595133000066

[96] P. A. Nelson, K. G. Gallagher, and I. Bloom, "BatPaC (Battery Performance and Cost) Software." [Online]. Available: http://www.cse.anl.gov/batpac/

[97] R. Matthe, L. Turner, and H. Mettlach, "VOLTEC Battery System for Electric Vehicle with Extended Range," vol. 4, no. 1, pp. 1944–1962, Apr. 2011.

[Online]. Available: http://www.sae.org/technical/papers/2011-01-1373

[98] R. Parrish, K. Elankumaran, M. Gandhi, B. Nance, P. Meehan, D. Milburn, S. Siddiqui, and A. Brenz, "Voltec Battery Design and Manufacturing," Apr. 2011. [Online]. Available: http://www.sae.org/technical/papers/2011-01-1360

[99] K. Smith and C.-Y. Wang, "Power and thermal characterization of a lithium-ion battery pack for hybrid-electric vehicles," *Journal of Power Sources*, vol. 160, no. 1, pp. 662–673, Sep. 2006. [Online]. Available: http://linkinghub.elsevier.com/retrieve/pii/S0378775306001017

[100] J. Dahn and G. M. Ehrlich, "Lithium-Ion Batteries," in *Linden's Handbook of Batteries*, 4th ed. McGraw Hill, 2011, ch. 26, pp. 26.1—-26.75.

[101] B. Y. Liaw, E. P. Roth, R. G. Jungst, G. Nagasubramanian, H. L. Case, and D. H. Doughty, "Correlation of Arrhenius Behaviors in Power and Capacity Fades with Cell Impedance and Heat Generation in Cylindrical Lithium-Ion Cells," Sandia National Laboratories, Tech. Rep., 2002. [Online]. Available: http://www.sandia.gov/ess/publications/SAND2002-3201j.pdf

[102] M. Ecker, N. Nieto, S. Käbitz, J. Schmalstieg, H. Blanke, A. Warnecke, and D. U. Sauer, "Calendar and cycle life study of Li(NiMnCo)O2-based 18650 lithium-ion batteries," *Journal of Power Sources*, vol. 248, pp. 839–851, Feb. 2014. [Online]. Available: http://linkinghub.elsevier.com/retrieve/pii/S0378775313016510

[103] J. Schmalstieg, S. Käbitz, M. Ecker, and D. U. Sauer, "A holistic aging model for Li(NiMnCo)O2 based 18650 lithium-ion batteries," *Journal of Power Sources*, vol. 257, pp. 325–334, Jul. 2014. [Online]. Available: http://linkinghub.elsevier.com/retrieve/pii/S0378775314001876

[104] S. Käbitz, J. B. Gerschler, M. Ecker, Y. Yurdagel, B. Emmermacher, D. André, T. Mitsch, and D. U. Sauer, "Cycle and calendar life study of a graphite—LiNi1/3Mn1/3Co1/3O2 Li-ion high energy system. Part A: Full cell characterization," *Journal of Power Sources*, vol. 239, pp. 572–583, Oct. 2013. [Online]. Available: http://linkinghub.elsevier.com/retrieve/pii/S0378775313004369

[105] J. Wang, J. Purewal, P. Liu, J. Hicks-Garner, S. Soukazian, E. Sherman, A. Sorenson, L. Vu, H. Tataria, and M. W. Verbrugge, "Degradation of lithium ion batteries employing graphite negatives and nickelcobaltmanganese oxide+spinel manganese oxide positives: Part 1, aging mechanisms and life estimation," *Journal of Power Sources*, vol. 269, pp. 937–948, Dec. 2014. [Online]. Available: http://linkinghub.elsevier.com/retrieve/pii/S037877531401074X

[106] R. P. Ramasamy, R. E. White, and B. N. Popov, "Calendar life performance of pouch lithium-ion cells," *Journal of Power Sources*, vol. 141, no. 2, pp. 298–306, Mar. 2005. [Online]. Available: http://linkinghub.elsevier.com/retrieve/pii/S0378775304010687

[107] C. Forgez, D. Vinh Do, G. Friedrich, M. Morcrette, and C. Delacourt, "Thermal modeling of a cylindrical LiFePO4/graphite lithium-ion battery," *Journal of Power Sources*, vol. 195, pp. 2961–2968, 2010.

[108] S. Chacko and Y. M. Chung, "Thermal modelling of Li-ion polymer battery for electric vehicle drive cycles," *Journal of Power Sources*, vol. 213, pp. 296–303, 2012. [Online]. Available: http://dx.doi.org/10.1016/j.jpowsour.2012.04.015

[109] Benjamin Gully, DNV-GL, Email Correspondence, January 2015.

[110] M. Ecker, J. B. Gerschler, J. Vogel, S. Käbitz, F. Hust, P. Dechent, and D. U. Sauer, "Development of a lifetime prediction model for lithium-ion batteries based on extended accelerated aging test data," *Journal of Power Sources*, vol. 215, pp. 248–257, Oct. 2012. [Online]. Available: http://linkinghub.elsevier.com/retrieve/pii/S0378775312008671

[111] ERCOT. Ercot planning guide, section 5: Generation resource interconnection or change request. [Online]. Available: http://www.ercot.com/mktrules/guides/planning/current

[112] ——. Fast responding regulation service. [Online]. Available: http://www.ercot.com/mktrules/pilots/frrs/index

[113] ERCOT. (2012) Market information. [Online]. Available: http://www.ercot.com/mktinfo/

[114] H. Daneshi and a. K. Srivastava, "ERCOT electricity market: Transition from zonal to nodal market operation," *IEEE Power and Energy Society General Meeting*, pp. 1–7, 2011.

[115] R. E. Rosenthal and GAMS Development Corporation, "GAMS A Users Guide," 2012. [Online]. Available: http://www.gams.com/dd/docs/bigdocs/GAMSUsersGuide.pdf

[116] R Core Team, *R: A Language and Environment for Statistical Computing*, R Foundation for Statistical Computing, Vienna, Austria, 2013. [Online]. Available: http://www.R-project.org

[117] V. Viswanathan, M. Kintner-Meyer, P. Balducci, and C. Jin, "National Assessment of Energy Storage for Grid Balancing and Arbitrage Phase II Volume

2: Cost and Performance Characterization," U.S. Department of Energy, Tech. Rep. September, 2013. [Online]. Available: http://energyenvironment.pnnl.gov/pdf/National_Assessment_Storage_PHASE_II_vol_2_final.pdf

[118] H. Bindner, C. Ekman, O. Gehrke, and F. Isleifsson, "Characterization of Vanadium Flow Battery," Riso DTU National Laboratory for Sustainable Energy, Tech. Rep., 2010.

[119] T. Baumhöfer, M. Brühl, S. Rothgang, and D. U. Sauer, "Production caused variation in capacity aging trend and correlation to initial cell performance," *Journal of Power Sources*, vol. 247, pp. 332–338, 2014. [Online]. Available: http://dx.doi.org/10.1016/j.jpowsour.2013.08.108

[120] Potomac Economics, "2010 State of the Market Report for the ERCOT Wholesale Electricity Markets," Potomac Economics, Tech. Rep. August, 2011. [Online]. Available: https://www.puc.texas.gov/industry/electric/reports/ERCOT_annual_reports/2010annualreport.pdf

[121] ——, "2011 State of the Market Report for the ERCOT Wholesale Electricity Markets," Tech. Rep. July, 2012. [Online]. Available: http://www.potomaceconomics.com/uploads/ercot_documents/2011_ERCOT_SOM_REPORT.pdf

[122] ——, "2012 State of the Market Report for the ERCOT Wholesale Electricity Markets," Potomac Economics, Tech. Rep. June, 2013. [Online]. Available: https://www.puc.texas.gov/industry/electric/reports/ERCOT_annual_reports/2012annualreport.pdf

[123] A. K. Townsend, "A Grid-Level Assessment of Compressed Air Energy Storage in ERCOT," Dissertation, The University of Texas at Austin, 2013.

[124] J. Eyer, "Electric Utility Transmission and Distribution Upgrade Deferral Benefits from Modular Electricity Storage," Sandia National Laboratories, Tech. Rep. June, 2009.

[125] Pecan Street Inc., "Pecan Street Inc." 2013. [Online]. Available: http://www.pecanstreet.org/

[126] ——, "The Pecan Street Project," 2013. [Online]. Available: http://www.pecanstreet.org/projects/smart-grid-demonstration/

[127] J. D. Rhodes, C. R. Upshaw, C. B. Harris, C. M. Meehan, D. A. Walling, P. A. Navrátil, A. L. Beck, K. Nagasawa, R. L. Fares, W. J. Cole, H. Kumar, R. D. Duncan, C. L. Holcomb, T. F. Edgar, A. Kwasinski, and M. E. Webber, "Experimental and data collection methods for a large-scale smart grid deployment: Methods and first results," *Energy*, vol. 65, pp. 462–471, Feb. 2014. [Online]. Available: http://linkinghub.elsevier.com/retrieve/pii/S0360544213009663

[128] J. Song, M. C. Bozchalui, A. Kwasinski, and R. Sharma, "Microgrids availability evaluation using a Markov chain energy storage model: a comparison study in system architectures," in *PES T&D 2012*. IEEE, May 2012, pp. 1–6.

[129] A. Kwasinski, "Technological assessment of distributed generation systems operation during extreme events," *2012 3rd IEEE International Symposium on Power Electronics for Distributed Generation Systems (PEDG)*, pp. 534–541, Jun. 2012. [Online]. Available: http://ieeexplore.ieee.org/lpdocs/epic03/wrapper.htm?arnumber=6254054

[130] IEEE, "Standard for interconnecting distributed resources with electric power systems," *IEEE Std 1547-2003*, pp. 1–16, 2003.

[131] J. H. Eto and K. H. Lacommare, "Tracking the Reliability of the U.S. Electric Power System: An Assessment of Publicly Available Information Reported to State Public Utility Commissions," Lawrence Berkeley National Laboratory, Tech. Rep. October, 2008.

[132] IEEE, "Ieee guide for electric power distribution reliability indices," *IEEE Std 1366-2003 (Revision of IEEE Std 1366-1998)*, pp. 1–50, 2004.

[133] M. J. Sullivan, M. G. Mercurio, J. A. Schellenberg, and Freeman & Sullivan Co., "Estimated Value of Service Reliability for Electric Utility Customers in the United States," Lawrence Berkeley National Laboratory, Tech. Rep. June, 2009. [Online]. Available: http://certs.lbl.gov/pdf/lbnl-2132e.pdf

[134] P. Nelson, D. Santini, and J. Barnes, "Factors Determining the Manufacturing Costs of Lithium- Ion Batteries for PHEVs," in *EVS24 International Battery, Hybrid and Fuel Cell Electric Vehicle Symposium*, 2009, pp. 1–12. [Online]. Available: http://beta.cars21.com/web/assets/link/EVS-24-3550250santini.pdf

[135] J. F. Miller, "Analysis of Current and Projected Battery Manufacturing Costs for Electric, Hybrid, and Plug-in Hybrid Electric Vehicles," *World Electric Vehicle Journal*, vol. 4, pp. 347–350, 2010.

[136] P. Nelson, I. Bloom, K. Amine, and G. Henriksen, "Design modeling of lithium-ion battery performance," *Journal of Power Sources*, vol. 110, no. 2, pp. 437–444, Aug. 2002. [Online]. Available: http://linkinghub.elsevier.com/retrieve/pii/S0378775302002094

[137] P. Nelson, D. Dees, K. Amine, and G. Henriksen, "Modeling thermal management of lithium-ion PNGV batteries," *Journal of Power Sources*, vol. 110, pp.

349–356, 2002.

[138] G. L. Henriksen, K. Amine, J. Liu, and P. A. Nelson, "Materials Cost Evaluation Report for High-Power Li-Ion HEV Batteries," Argonne National Laboratory, Tech. Rep., 2002. [Online]. Available: http://www.ipd.anl.gov/anlpubs/2003/01/45346.pdf

[139] K. G. Gallagher, P. a. Nelson, and D. W. Dees, "Simplified calculation of the area specific impedance for battery design," *Journal of Power Sources*, vol. 196, no. 4, pp. 2289–2297, 2011. [Online]. Available: http://dx.doi.org/10.1016/j.jpowsour.2010.10.020

[140] Tesla Motors, "Gigafactory." [Online]. Available: http://www.teslamotors.com/sites/default/files/blog_attachments/gigafactory.pdf

[141] B. Zakeri and S. Syri, "Electrical energy storage systems: A comparative life cycle cost analysis," *Renewable and Sustainable Energy Reviews*, vol. 42, pp. 569–596, 2015. [Online]. Available: http://dx.doi.org/10.1016/j.rser.2014.10.011

[142] B. Battke, T. S. Schmidt, D. Grosspietsch, and V. H. Hoffmann, "A review and probabilistic model of lifecycle costs of stationary batteries in multiple applications," *Renewable and Sustainable Energy Reviews*, vol. 25, pp. 240–250, Sep. 2013. [Online]. Available: http://linkinghub.elsevier.com/retrieve/pii/S136403211300275X

[143] E. Hittinger, J. F. Whitacre, and J. Apt, "What properties of grid energy storage are most valuable?" *Journal of Power Sources*, vol. 206, pp. 436–449, May 2012. [Online]. Available: http://linkinghub.elsevier.com/retrieve/pii/S0378775311024220

[144] M. Kintner-Meyer, M. Elizondo, P. Balducci, C. Jin, T. Nguyen, F. Tuffner, and X. Guo, "Energy Storage for Power Systems Applications: A Regional Assessment for the Northwest Power Pool (NWPP)," no. April, p. 104, 2010.

[145] S. Schoenung, "Energy Storage Systems Cost Update," Sandia National Laboratories, Tech. Rep. April, 2011. [Online]. Available: http://prod.sandia.gov/techlib/access-control.cgi/2011/112730.pdf

[146] S. M. Schoenung and W. V. Hassenzahl, "Long- vs. Short-Term Energy Storage Technologies Analysis A Life-Cycle Cost Study A Study for the DOE Energy Storage Systems Program," *Power Quality*, vol. SAND2011-2, no. April, p. 84, 2003. [Online]. Available: http://infoserve.sandia.gov/sand_doc/2003/032783.pdf

[147] HDR Engineering Inc., "Update to Energy Storage Screening Study For Integrating Variable Energy Resources within the PacifiCorp System," Tech. Rep., 2014. [Online]. Available: http://www.pacificorp.com/content/dam/pacificorp/doc/Energy_Sources/Integrated_Resource_Plan/2013IRP/Report_Energy-Storage-Screening-Study2012.pdf

[148] S. M. Schoenung and J. Eyer, "Benefit/Cost Framework for Evaluating Modular Energy Storage," Sandia National Laboratories, Tech. Rep. February, 2008. [Online]. Available: http://prod.sandia.gov/techlib/access-control.cgi/2008/080978.pdf

[149] R. L. Fares and M. E. Webber, "A flexible model for economic operational management of grid battery energy storage," *Energy*, vol. 78, pp. 768–776,

2014. [Online]. Available: http://linkinghub.elsevier.com/retrieve/pii/S0360544214012225

[150] E. S. Hittinger and I. M. L. Azevedo, "Bulk Energy Storage Increases United States Electricity System Emissions," *Environmental Science & Technology*, p. 150210161301007, 2015. [Online]. Available: http://pubs.acs.org/doi/abs/10.1021/es505027p

[151] B. Kaun and The Electric Power Research Institute, "Cost-Effectiveness of Energy Storage in California: Application of the EPRI Energy Storage Valuation Tool to Inform the California Public Utility Commission Proceeding R. 10-12-007," Tech. Rep., 2013.

[152] R. L. Fares, "A Dynamic Model-based Estimate of the Potential Value of a Vanadium Redox Flow Battery for Energy Arbitrage and Frequency Regulation in Texas," Master's Thesis, The University of Texas at Austin, 2012. [Online]. Available: http://repositories.lib.utexas.edu/handle/2152/ETD-UT-2012-08-6271